A NON-CONTACT VITAL SIGNS MONITORING APPROACH USING FMCW mmWAVE RADAR

Anuradha Singh

Supervisors

Assoc Prof Sira Yongchareon

Dr. Saeed ur Rehman

Prof Peter Han Joo Chong

Novemeber 2023

School of Engineering, Computer, and Mathematical Science

A Thesis Submitted to

Auckland University of Technology

in (partial) Fulfilment of The Requirements For The Degree of Doctor of Philosophy

Abstract

Vital signs such as heart rate (HR) and respiration rate (RR) are critical for the clinical assessment of an individual's health and have high predictive value in identifying undesired events like cardiac arrest, critical dizziness, arrhythmias, and synchronization with respiration rate. Traditional contact-based methods are limited by their reliance on accessories attached to the body, making continuous monitoring challenging in both clinical and home environments. Moreover, wearable devices may not be suitable for patients with skin allergies, burns, or infants. Microwave radar sensing, which offers superior penetration through materials and clothing, and is less affected by environmental conditions, is posited as a promising alternative for continuous, non-contact monitoring.

However, extracting physiological information from radar signals presents a significant challenge, primarily because the phase changes in the received signal are highly susceptible to environmental noise and interference, particularly when measuring HR in realistic circumstances. Even the individual's body movement can substantially impact HR readings. Skin displacement from heart activity is much smaller than that caused by respiration, leading to a weaker reflected signal from heartbeats compared to respiration. Furthermore, the HR spectrum's entire frequency range contains significant noise from the second and third-order harmonics of the respiration and intermodulation products. Environmental clutter and random body movements also add to the noise in the received reflected signal, posing a considerable challenge in developing an efficient system for HR estimation.

The research focuses on developing an efficient, accurate, and privacy-aware non-contact vital sign (NCVS) monitoring method using mm-wave radar technology and devising a signal processing algorithm to improve the accuracy of heart rate and respiration rate measurements. The research adopts a multi-pronged approach to achieve these goals. This includes analytical modelling of the chest wall motion due to cardiovascular activity, facilitating a nuanced understanding of trade-offs between various radar parameters. Furthermore, the study proposes using a non-linear signal

analysis technique, resonance sparse spectrum decomposition (RSSD), to better capture and analyze the complex dynamics of non-stationary signals. RSSD decomposes the signal into time-varying frequency components using wavelet decomposition and sparse approximation, identifies and isolates resonant frequencies, and constructs a sparse representation of the signal. This approach offers a highly accurate and efficient method for analyzing non-stationary signals with time-varying spectral characteristics. A harmonic-based algorithm is formulated to improve the accuracy of HR measurement.

Additionally, target localization, crucial for the practical deployment of radar-based NCVS systems, becomes even more challenging due to the inevitable positional changes in real-world scenarios. We introduce an automatic, real-time beam steering and beam forming algorithm for identifying target locations, which augments the signal-to-noise ratio (SNR) and enhances vital sign estimation accuracy. The effectiveness of the proposed method is evaluated through a series of experiments carried out in various realistic settings, including artificial clutter and body movements such as reading a book, drinking water, and forward and backward body movements. To mitigate the noise and interference due to these additional attributes, we optimize the Q factor selection for each dataset by modifying the RSSD algorithm parameter selection by leveraging the sub-band energy distribution leading to a more precise extraction of HR. The findings demonstrate that the proposed method effectively mitigates issues caused by unwanted clutter, manages random body motion and harmonic interference, and significantly improves HR estimation accuracy by reducing noise in the phase signal.

Table of Contents

List of Figures

List of Tables

List of Abbreviations

Abbreviation	Definition
ACM	Absolute Value of Cosine Function Model
ADBF	Adaptive Digital Beamforming
ADC	Analog-to-Digital Converter
AMCW	Amplitude Modulation Continuous Wave
ANN	Artificial Neural Network
AoA	Angle-of-Arrival
AR	Auto-Regression
AUTEC	Auckland University of Technology Ethics Committee
AV	Atrial Ventricular
BPM	Beats Per Minute
CAGR	Compound Annual Growth Rate
CM	Cosine Function Model
CMOS	Complementary Metal-Oxide-Semiconductor
CSOMP	Compressed Sensing Orthogonal Matching Pursuit
CW	Continuous Wave
DACM	Differentiate and Cross Multiply
DBF	Digital Beamforming
DC	Direct Current
DDC	Digital Down Converter
DDS	Direct Digital Synthesis
DFT	Digital Fourier Transform
DPSS	Discrete Prolate Spheroidal Sequences
DTW	Dynamic Time Warping
DWT	Dyadic Wavelet Transformation
ECG	Electrocardiogram
EMD	Empirical Mode Decomposition
EPCM	Even Power of Cosine Function
ETSI	European Telecommunications Standards Institute

FCC	Federal Communications Commission
FFT	Fast Fourier Transform
FIR	Finite Impulse Response
FSK	Frequency Shift Keying
FTPR	Frequency-Time Phase Regression
HAPA	Harmonic Path Algorithm
HHT	Hilbert-Huang Transform
HR	Heart Rate
HRV	Heart Rate Variability
HSMM	Hidden Semi-Markov Model
HUA	Harmonic Utilized Algorithm
ICNIRP	International Commission on Non-Ionizing Radiation Protection
IIR	Infinite Impulse Response
ISM	Industrial Scientific and Medical
LM	Levenberg–Marquardt
LNA	Low Noise Amplifier
LO	Local Oscillator
LVDS	Low Voltage Differential Signalling
MAE	Mean Average Error
MFCC	Mel-Frequency Cepstral Coefficient
MIMO	Multiple Input Multiple Output
MIT	Massachusetts Institute of Technology
MTI	Moving Target Indicator
MTM-LWA	Metamaterial Leaky-Wave Antenna
MUSIC	Multiple Signal Classification
NCVS	Non-Contact Vital Sign
NIH	National Institutes of Health
PACM	Power of the Absolute Value of the Cosine Function
PCA	Principal Component Analysis
PLL	Phase Locked Loop
PPG	Photoplethysmography
RADWT	Rational-Dilation Wavelet Transform
RCS	Radar Cross Section

REPA	Regulation Parameter
RF	Radio Frequency
RR	Respiration Rate
RSSD	Resonance Sparse Spectrum Decomposition
Rx	Receiver
SA	Sinoatrial
SALSA	Split Augmented Lagrangian Shrinkage Algorithm
SAR	Specific Absorption Rate
SCSFCW	Single-Conversion Stepped Frequency Continuous-Wave
SFCW	Stepped-Frequency Continuous-Wave Radar
SHAPA	Spectrum Averaged Harmonic Path
SID	Sudden Infant Death
SIL	Self-Injection-Locked
SNR	Signal-to-Noise Ratio
SPA	Switched Phased-Array
SRC	Sampling Rate Conversion
SST	Synchrosqueezing Transform
STFT	Short-Time Fourier Transform
SUID	Sudden Unexpected Infant Deaths
SVM	Support Vector Machine
TI	Texas Instruments
TQWT	Tunable Q-Factor Wavelet Transformation
Tx	Transmitter
UWB	Ultra-Wideband
VCO	Voltage-Controlled Oscillator
VLSI	Very-Large-Scale Integration
VNA	Vector Network Analyzer
XGBoost	Xtreme Gradient Boosting
ZA-SLMS	Zero-Attracting Sign Least Mean Square

Attestation of Authorship

I, Anuradha Singh, hereby declare that this submission is my own work and that, to the best of my knowledge and belief, it contains no material previously published or written by another person (except where explicitly defined in the acknowledgements) nor material that to a substantial extent has been submitted for the award of any other degree or diploma of a university or other institution of higher learning.

Signature	Date
	20/11/2023

Co-Authored Works

All co-authors in the following table have approved these chapters for inclusion in Anuradha Singh's doctoral thesis.

Chapter	**Author %**
Chapter 2: Anuradha Singh, Sira Yongchareon, Saeed ur Rehman, Peter Han Joo Chong. Multi-Resident Non-Contact Vital Sign Monitoring Using Radar: A Review Manuscript accepted in IEEE Sensors Journal	AS = 80 SR = 8 SY = 8 PC = 4
Chapter 3: Anuradha Singh, Sira Yongchareon, Saeed ur Rehman, Peter Han Joo Chong. Modelling of Chest Wall Motion for Cardiorespiratory Activity for Radar-Based NCVS Systems Manuscript accepted in MDPI Sensors Journal	AS = 80 SR = 8 SY = 8 PC = 4
Chapter 4: Anuradha Singh, Sira Yongchareon, Saeed ur Rehman, Peter Han Joo Chong. Human Vital Signs Estimation Using Resonance Sparse Spectrum Decomposition Manuscript submitted to IEEE Transaction on Human Machine Systems	AS = 80 SR = 8 SY = 8 PC = 4
Chapter 5: Anuradha Singh, Sira Yongchareon, Saeed ur Rehman, Yang Yu. Real-time Beam Steering and Accurate Vital Signs Estimation Method in an Indoor Environment Manuscript submitted to IEEE IoT Journal	AS = 80 SR = 8 SY = 8 YY = 2 PC = 2
Anuradha Singh (AS), Sira Yongchareon (SY), Saeed ur Rehman (SR), Peter Han Joo Chong (PC), Yang Yu (YY)	

We, the undersigned, hereby agree to the percentages of participation in the chapters identified above:

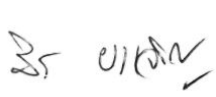

Sira Yongchareon

Saeed ur Rehman

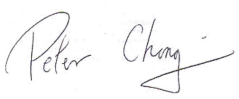

Peter Han Joo Chong

Yang Yu

Anuradha Singh

Acknowledgments

First and foremost, I would like to express my sincere gratitude to my supervisors, Assoc Prof Sira Yongchareon and Dr. Saeed ur Rehman, for their invaluable guidance and unflinching support throughout my research journey. Their immense knowledge and expertise have shaped my understanding of the subject and provided me with the tools and strategies to conduct and present my research with clarity and precision. I extend my heartfelt appreciation for their involvement and commitment to my academic growth. My special thanks to Prof Peter Han Joo Chong for his insightful comments and feedback on the research work, which have significantly contributed to the quality of this research.

I would also like to express my gratitude to Bumjun Kim, Stephen Hartley, and Ramon Lewis for their timely technical assistance, which greatly contributed to the progress of my study.

I sincerely appreciate my colleagues and friends, Sabeeha Mehtab, Dhvani Shah, Gaurav Pathak, Asad Mohammad, Yang Yu, Huiyang Zhang, Alberto Gonzalez Vazquez, Rohit Gade, Danielle Yang, Sidra Shoaib, and Laura Milena Pena Torres, who graciously dedicated their time, support, and invaluable contribution in participating the experiments, enriching the outcomes of this study.

Last but not least, I would like to thank my family for their unconditional love, patience, and unwavering support have been the pillars of strength throughout this challenging journey. I am forever grateful for their constant encouragement and belief in my abilities.

Dedication

To my husband Abhishek and kids Annika, Avika, and Adhiraj

whose unwavering support, patience, and boundless enthusiasm have been the pillars that enabled me to complete this research work

To my parents and parents-in-laws

whose ceaseless prayers and encouragement made the success of this work a reality

Ethics Approval

The study was conducted at Auckland University of Technology, Auckland, from August 2021 to March 2023. The study was approved through Ethics Application **21/228 Non-contact vital signs monitoring system using radar** on 5 July 2021 by the Auckland University of Technology Ethics Committee (AUTEC).

Chapter 1

Introduction

This chapter introduces the research topic and outlines the rationale for undertaking the proposed study. Furthermore, it discusses the gaps in the existing area of research and then presents contributions to bridge those gaps. The chapter concludes by presenting the research methodology and outlining the structure of the thesis.

1. Background

The most frequently measured parameters for clinical assessment of an individual's health include vital signs such as heart rate, breathing rate, body temperature, blood oxygen saturation, and arterial blood pressure [1], [2]. Among these indicators, the respiratory rate (RR) and heart rate (HR) have a high predictive value in identifying undesired events like cardiac arrest, critical dizziness, arrhythmias, cardiac rhythm, temperature regulation, and synchronization with respiration rate, as compared to other parameters like pulse or blood pressure [3], [4]. According to projections, the global population of people aged over 65 is expected to double in 2050 [5]. Sudden infant death (SID) or "crib death" is also a major cause of death in infants, with an estimated 41% of 3400 sudden unexpected infant deaths (SUID) per year reported in the United States [6], [7]. Evidence suggests that physiological defects in breathing control mechanisms can cause crib death. As a result, continuous monitoring of vital signs is crucial for ensuring the well-being of both adults and infants. This system also allows clinicians and caregivers to detect abnormal findings early, monitor disease progression, and assess treatment effectiveness.

Radar technology, bolstered by advancements in integrated circuits that allow for affordable short-range applications, has become a primary choice for diverse uses, including collision avoidance in vehicles, structural monitoring, fall detection, and health monitoring [8]. Renowned research institutes such as the Massachusetts Institute of Technology (MIT), Stanford University, Johns Hopkins University, and the National Institutes of Health (NIH) contribute to advancing radar-based vital signs monitoring technologies through their state-of-art research and development efforts. The vital signs monitoring devices market experienced substantial growth, reaching a value of USD 9.2 billion in 2022. It is projected to maintain a compound annual growth rate (CAGR) of 8.5% from 2023 to 2030 [9]. Continuous innovation in contactless vital signs monitoring devices is fuelling market growth in-home care, as it offers convenient and affordable long-term care and post-surgical recovery options. There is an increasing requirement for accurate and personalized vital sign monitoring, mainly due to the prevalence of

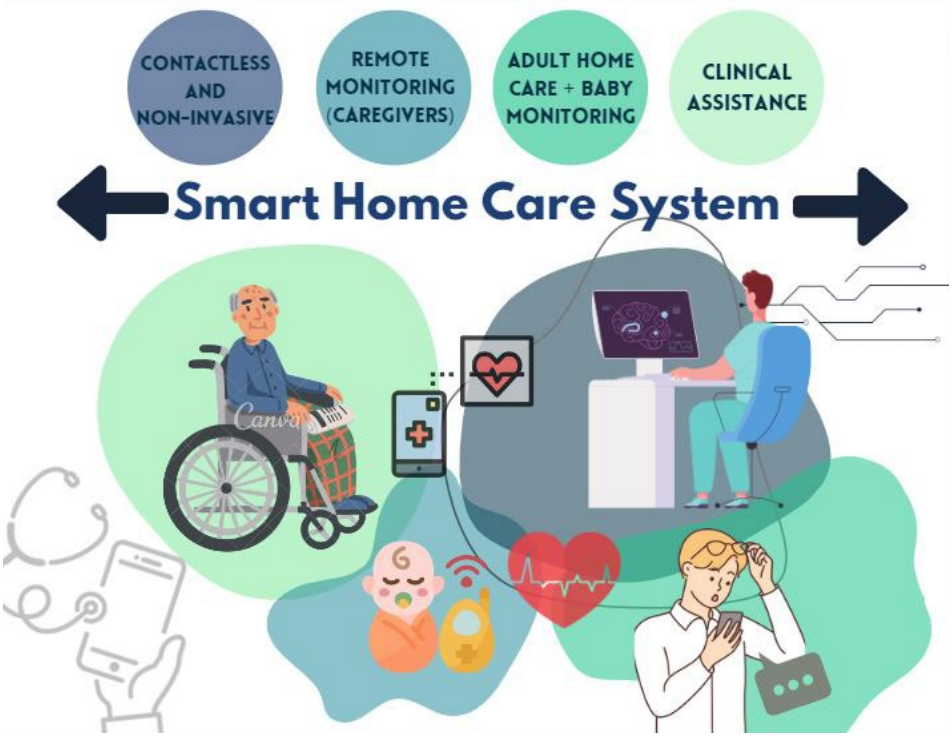

Figure 1: Potential application of radar-based vital sign monitoring in smart home care systems.

lifestyle-related chronic diseases. The COVID-19 pandemic has further boosted the demand, emphasizing the importance of early detection and continuous monitoring. These devices have evolved from individual tools that measure blood pressure, pulse, respiration, and temperature to multifunctional, all-in-one devices. This has attracted the interest of major companies such as Koninklijke Philips N.V., Medtronic, Nihon Kohden Corporation, GE Healthcare, Masimo, Omron Healthcare, Contec Medical Systems Co. Ltd, A&D Company Ltd., Nonin Medical Inc., and SunTech Medical, Inc. These key market players employ strategic initiatives to maintain their competitiveness and introduce innovative products in diverse markets. Fig. 1 depicts the potential application of radar technology in smart home care systems.

1.1 Contactless Vital Sign Monitoring in Healthcare

The conventional method of measuring vital signs, such as electrocardiography (ECG), involves direct contact of electrodes and probes with the skin, which cause discomfort for patients, particularly those with skin allergies, burns, or infants with small limbs, making electrode placement challenging. Moreover, skilled personnel are required for ECG measurement, making it suitable only for clinical settings and resulting in increasing

hospitalization periods and medical costs. Another alternative method, such as photoplethysmography (PPG), also requires accurate and controlled placement of sensors and body contact, which limits its use for continuous monitoring or home healthcare [10]. Therefore, there is a growing need for a robust and precise non-contact approach to vital sign measurement.

Monitoring vital signs non-invasively can have significant benefits in health management, including reducing the time needed to record and maintain patient data logs, improving disease prognosis, and enabling in-home health care for older adults [11]. Non-contact vital sign measurement has the potential to be applied to various areas, such as infant monitoring [12], sleep monitoring [13], home health care [14], and driver safety [15].

A wide range of non-contact methods based on different sensing technologies [16], such as optical vibrocardiography [6], [17], audio signal [18], [19], thermal imaging [20]-[22], RGB camera [23], [24], ultrasound radar [25], and microwave radars [26] have been utilized to design various non-contact vital sign monitoring systems. Despite advancements in sensing technology and signal processing techniques, limitations are still associated with each technology. Although vibrocardiography (VCG) has demonstrated similar accuracy to ECG in resting subjects [6], it requires a retroreflective tape attached to the chest wall to obtain a high-quality reflected signal [18], which restricts user adaptability. Additionally, the VCG signal is heavily distorted by motion artifacts due to its large resolution and the noise in the spectrogram caused by factors such as insufficient respiratory lung volume, background noise, and the presence of multiple people [19]. Furthermore, it cannot be universally applied to patients with heart transplants, speech problems, or irregular lung activity.

Another method uses reflected light to capture volumetric changes in facial vessel walls during cardiac cycles [24]. While this method is accurate, its adaptability is limited by its illumination requirements and invasiveness, and the accuracy can be affected by slight movements or inaccurate face tracking. Some research studied a passive infrared camera to capture the thermal pattern of superficial vessels, modulated by pulsating blood flow during cardiovascular activities [20], [21]. However, this method

requires the subject to be stationary and facing the camera, and the accuracy is limited by manual segmentation of vessels and external temperature variations [22].

Compared to other non-contact sensing methods, such as visible light or infrared, microwave radar sensing exhibits superior penetration through material and clothing and resilience to environmental conditions. This makes it a reliable non-contact method for cardiovascular activity monitoring, even in unilluminated settings. [27]. The Doppler effect allows for the detection of skin displacements induced by physiological movements, such as breathing and heartbeat, by measuring phase shifts of the reflected radar signal. Thus, doppler, specifically frequency-modulated continuous wave (FMCW) radar, has been extensively researched for non-contact measurement of cardiovascular activity. Current research efforts are focused on developing a radar-based, highly accurate, power-efficient, and robust contactless device for practical applications.

However, the radar-based vital signs monitoring of an individual in real-world settings presents a significant challenge due to interference caused by clutter, motion artifacts, intermodulation products, and RR harmonics. This study aims to overcome these challenges by extending the simultaneous monitoring of HR and RR for semi-stationary persons and improving the accuracy of HR detection by suppressing motion artifacts and clutter. The research will enable efficient health management with less supervision and may have applications in home care for adults, sleep apnea, driver's health, and baby monitors.

1.2 FMCW Radar System for Vital Sign Monitoring

A radar system consists of a transmitter that emits the electromagnetic waveform towards the target, usually in the microwave or millimeter band, and senses the reflected echoes back at the receiver. The minute chest wall displacement is measured through the Doppler effect principle, where reflected received signal is phase-modulated by the chest wall's displacement motion [28]. The received signal is phase demodulated, and then fast fourier transform (FFT) and other signal processing techniques are applied to estimate the respiration and heartbeat frequency [29].

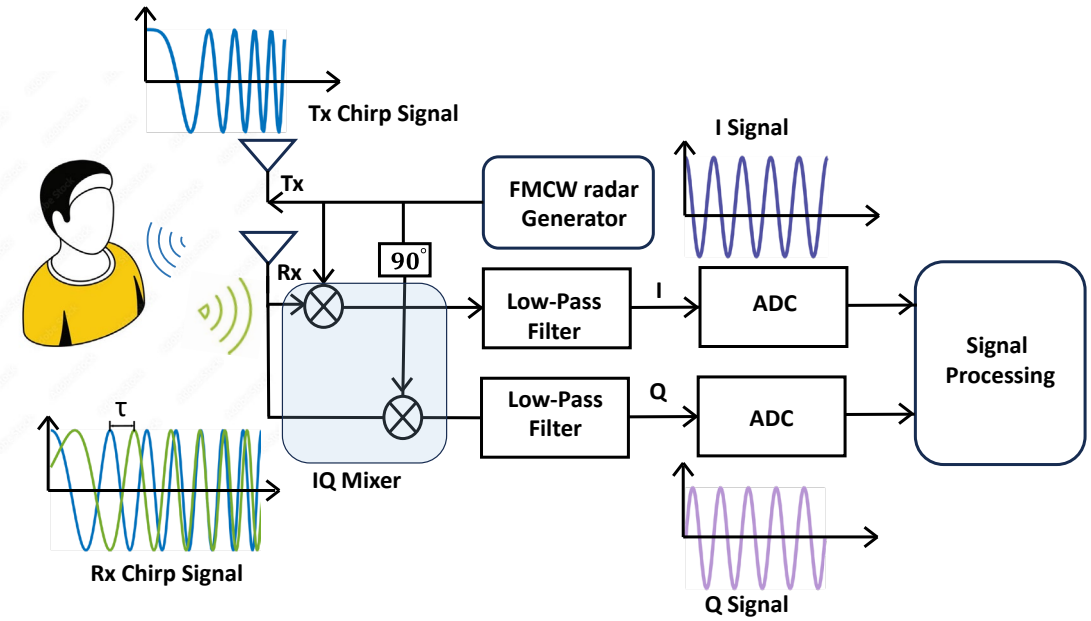

Figure 2:FMCW operation and waveforms at various stages

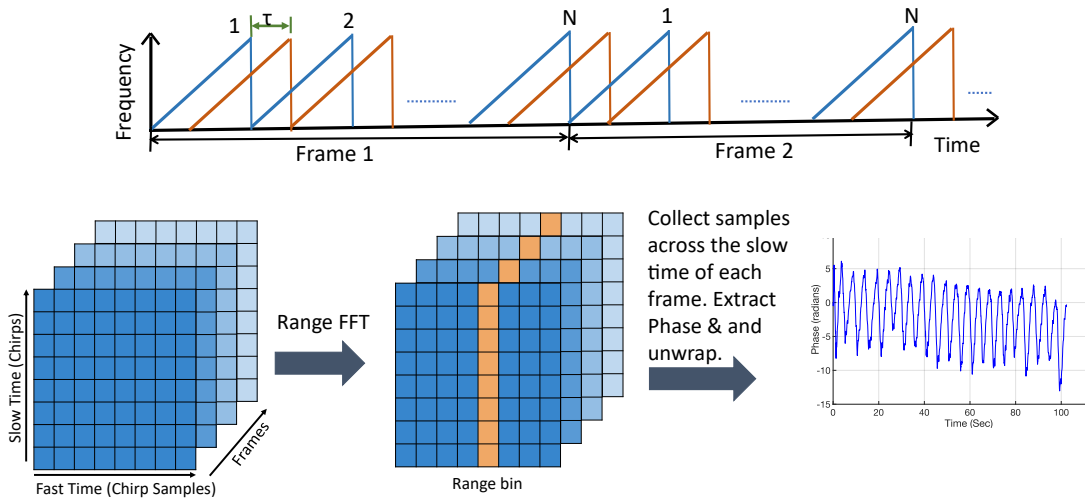

Figure 3: Slow time axis which displays the different chirp frames and the corresponding range-bin

Various radar systems have been explored and analyzed for their operation, covering a wide range of frequencies and different output power related to the system's sensitivity. The standard radar technique used for vital sign measurement includes continuous wave (CW) radars [30]-[37], ultra-wideband pulsed radar (UWB) [38]-[41], frequency modulated continuous wave (FMCW) [42]-[45] and stepped-frequency continuous-wave radar (SFCW) [46] configured either as a single or quadrature channel radar. The CW radars have been extensively used for their simplicity and low cost, but

the CW radar cannot extract the target range because of the lack of time information owing to missing modulation. The need for isolating the transmitter and the receiver is another limitation of the CW radar system. UWB offers several advantages over CW radar, including target range detection and high-range resolution [47]. However, the pulse bandwidth needs to be increased to increase the resolution, shortening the pulse width. Reducing the pulse width to an extent is limited by the technology [48], [49]. UWB radar transmits a wideband waveform, making it very unfavorable if low-power devices should operate in near proximity.

Numerous studies have explored the potential of FMCW radar in contactless vital sign monitoring, such as HR and RR. FMCW radar systems can determine both the distance and velocity of moving objects. The system calculates the distance by measuring the frequency difference (Δf) between the transmitted and received echo signals. The chest wall motion is oscillatory in nature and, therefore, can be estimated through the phase of the radar-received signal. The process of phase extraction in an FMCW radar is explained in Fig. 2, with waveforms at each stage. Collected received chirps are stored in a data cube. Fast time sampling establishes the target range bin, followed by slow time sampling to extract the signal phase, as shown in the Fig. 3. The FMCW radar continuously alters the transmitted signal's frequency using a known rate modulation signal over a set time period. Different modulation techniques can be utilized, such as sawtooth, triangular, sine wave, square wave, and stepped modulation. Sawtooth and triangular wave modulations are the most commonly used [50]. The FMCW can be realized with low power consumption microchips than pulsed radar, better range resolution owing to the wide bandwidth, and therefore presents a better choice. Despite the promising results, several challenges must be addressed before Doppler radar can be widely adopted for contactless vital sign monitoring. These challenges include optimizing the radar system design and developing accurate and reliable signal processing algorithms for complex, realistic scenarios.

The mmWave radar technology, operating at 30 to 300 GHz frequencies, offers a wide range of unexplored spectrums for wireless sensing, imaging, and positioning. The mmWave radar has the advantage of improved range resolution and accuracy compared

to lower-frequency industrial scientific and medical (ISM) band radar systems. However, attenuation in the environment is an important consideration while working with mmWave technology. The current trend is to integrate discrete components of radar systems into a single-chip solution based on complementary metal-oxide-semiconductor (CMOS) technology for long-term monitoring. It provides a wider bandwidth, higher range resolution, smaller antenna size, and reduced number of radars required to cover an area, ultimately reducing costs and installation complexity. This research uses an off-the-shelf mmWave radar, taking advantage of its high-resolution capabilities.

1.3 Radar Signal Processing Techniques

One of the challenges in extracting vital signals is that the signals obtained from radar measurements are affected by noise and other interferences. Therefore, require signal processing techniques to extract relevant physiological information. Some standard signal-processing techniques used in radar-based vital sign detection are time-domain, frequency-domain, and time-frequency, hybrid, each with its own pros and cons. More recently, researchers have been investigating the use of machine learning methods to enhance radar-based vital sign detection.

Time domain analysis is one of the most straightforward approaches to analyzing radar signals. This method analyzes the signal's amplitude, frequency, and phase over time to extract physiological information. Peak amplitude is often used to estimate RR and HR, while SNR and time delay can be used to eliminate noise and artifacts. A time domain analysis [51] used a cross-correlation-based template matching algorithm for HR detection. The time-domain processing of the signal reduces the computational load of the system. However, physiological signals are non-stationary. Due to the time-varying statistical properties, physiological signals are not well-suited for analysis using time-domain techniques that assume that signal properties are constant over time.

Frequency domain analysis is another widely used approach that involves transforming the signal from the time domain to the frequency domain using techniques such as FFT or wavelet transform. The transformed signal can then be analyzed to extract frequency components related to the respiratory and cardiac rates. The most commonly used frequency domain parameters include spectral power, peak frequency, and spectral entropy. The FFT is a simple method to find peaks in the spectrum of a phase signal, but it suffers from performance degradation due to data length limitations. The parametric and cyclic optimization approach called RELAX algorithm employs the synchro squeezing transform (SST) based on continuous wavelet transform to extract time-varying vital signs. However, SST may not be effective for high-frequency and highly variable noise signals [36]. Multiple signal classification (MUSIC) algorithms address FFT smearing and leakage issues [52]. However, they face challenges in selecting signal subspaces and are computationally expensive.

Time-frequency analysis is a more advanced approach that combines time and frequency domain analysis to obtain more detailed information about the signal. This method involves algorithms such as short-time fourier transform (STFT) [47], Gabor transforms [53], and empirical mode decomposition (EMD) [43], to analyze the signal over time and frequency. The resulting spectrogram can then be analyzed to extract respiratory and cardiac rates as well as any temporal changes in the signal. The frequency and time-frequency analysis are more effective on substantially oscillatory or periodic signals. The complex signals, such as cardiac signals produced from the physiological processes, are non-stationary and exhibit a mixture of oscillatory and non-oscillatory transient behaviors due to the effect of noise and close-by clutter. For such signals, linear methods, e.g., frequency and time-frequency analysis, may not be applied effectively. This underscores the importance of developing and utilizing more advanced signal processing techniques, such as non-linear analysis methods, to better capture and analyze the complex dynamics of non-stationary signals.

In recent years, machine learning techniques, including support vector machine (SVM) [54], artificial neural network (ANN) [55], and deep learning [56], have been used for vital sign detection using radar signals by training a model on a set of data and then

analyzing new signals to extract information. However, collecting high-quality radar data and removing noise, artifacts, and interference through preprocessing is crucial for accurate analysis. Extracting important features from radar data for machine learning algorithms can be difficult. The choice of algorithm and parameters may vary depending on the radar data's characteristics and the specific vital signs being monitored. Additionally, the model is sensitive to changes in the measuring environment, requiring relearning the algorithm in case of any environment modification.

This study investigated a non-linear signal analysis technique for non-stationary vital signal extraction. The resonance sparse spectrum decomposition (RSSD) algorithm decomposes the signal into its time-varying frequency components using a combination of wavelet decomposition and sparse approximation [57]. It identifies and isolates the signal's resonant frequencies using a resonance-based frequency estimation technique and constructs a sparse representation of the signal using the identified resonant frequencies. The RSSD algorithm provides a highly accurate and efficient method for analyzing non-stationary signals with time-varying spectral characteristics.

2. Research Problems

One of the major challenges in using radar systems to detect vital signs is that the phase variation of electromagnetic waves is affected by unwanted environmental noise. These small movements related to HR and RR can be easily overshadowed by other sources of noise in the surrounding environment. Despite attempts to eliminate the effects of respiration harmonics, random body motions, and clutter to ensure accurate detection of vital signs, there are still limitations that need to be addressed. Previous research in vital sign monitoring has been performed in a controlled experiment setup and primarily focused on stationary individuals with a known location in close proximity to the sensor. However, in realistic scenarios, individuals may be in motion, accompanied by others, or quasi-stationary state. Research has shown that in certain healthcare applications, patients may always be accompanied by nurses or other healthcare professionals. The presence of another person (nurses/healthcare professionals) can cause interference and pose challenges to accurate vital sign monitoring using radar sensors, particularly in

indoor environments. Therefore, it is crucial to consider this factor when designing non-contact vital sign monitoring systems and developing signal processing algorithms that can effectively separate the signals of interest from interference caused by other individuals in the vicinity. Additionally, indoor settings present challenges such as multipath effects from reflected signals and complex reflections from multiple humans, which make target localization and tracking difficult. Several algorithms have been explored in earlier research, but they have limitations such as increased complexity and instability for long monitoring durations or low signal-to-noise ratios.

To develop a non-invasive and resilient contactless vital sign measuring system, it is essential to consider several critical factors, such as high resolution, a broad detection range, and overcoming challenges associated with RR harmonics, clutter, random body motion artifacts, and target localization. The system's performance must be contingent on accurately measuring heart and breathing rates simultaneously for individual persons under a real-life scenario.

This research aims to achieve these goals primarily through signal processing techniques, leveraging off-the-shelf radar. The research focuses on enhancing the accuracy of HR and RR measurement by implementing a signal-processing method for addressing the challenge associated with RR harmonics, clutter, and moderate body motion for stationary/semi-stationary individuals. Moreover, in real-life scenarios, the location of the subject is unknown. Our method automatically localizes the subject using beam steering to extract vital signs in a real-life indoor environment. Further, the influence of another person in the vicinity of the measurement location is studied. Thus, our research proposed and investigated an efficient, real-time, robust, and computationally efficient non-contact vital sign monitoring method using radar.

3. Research Questions

The primary goal of this study is to develop an efficient and accurate non-contact vital sign monitoring method. The first research question (RQ1) aims to develop a simulation model for chest wall motion caused by cardio-respiratory activities. This model can be used as a reference target to develop and analyze radar-based vital sign detection

methods. RQ2 aims to enhance HR and RR estimation accuracy for stationary and non-stationary subjects by reducing the impact of motion artifacts and clutter. Finally, RQ3 is centered around the approach and factors that can enhance the range and accuracy of HR and RR extraction from stationary targets and mitigate the interference caused by a nearby human on the targeted individual's vital sign detection. The following research questions are addressed to achieve the research objective.

RQ 1: How accurately a mathematical model can be developed to simulate chest wall motion induced by cardiac activities and evaluate its effectiveness in different respiratory scenarios?

Sub-questions:

1a. What approach can be taken to devise a mathematical model to simulate chest wall motion induced by cardiac activities?

1b. Does the proposed model effectively simulate chest wall motion in scenarios like free-breathing and post-exercise breathing?

RQ 2: What signal processing method can be developed to accurately extract the heart and respiratory signals minimizing the impact of noise, random body movements, and other interferences?

Sub-questions:

2a. What method can be developed that leverages the characteristics of a non-stationary radar-received signal to effectively enhance signal extraction from noisy radar data?

2b. Does the proposed method effectively mitigate the effects of random body movements and clutters for vital sign extraction?

2c. Does the proposed method minimize the influence of RR harmonics and intermodulation products on heart rate detection?

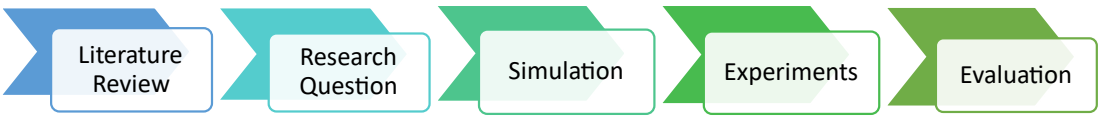

Figure 4: Research Framework

RQ3: What method can be employed to enhance the range and accuracy for stationary/non-stationary targets?

Sub-questions:

3a. Does the proposed method improve the range and accuracy of HR and RR estimation for stationary/non-stationary targets?

3b. What methods can counteract the influence of motion artifacts, clutter, and interference caused by the presence of another human near the target?

4. Research Contributions

The design framework utilized in this research is described in Fig. 4. A systematic literature review has been conducted, and the key findings have been reported. Proposed solutions have been presented to address the identified research gaps. The contributions of this thesis are outlined below.

Contribution 1: An in-depth analysis of NCVS radar systems, examining their varied topologies, architectures, and operational principles, is presented. It explores the health impact of mmWave exposure, environmental attenuation, and the shift towards mmWave frequencies due to their superior bandwidth. The review identifies practical deployment challenges, underlines the system's limited measurement range, and suggests multiple-input-multiple-outputs (MIMO) architecture/beam steering to expand detection reach. It discusses the trade-off between system power, frequency, sensitivity, and resolution and hence partially attributed to RQs, and findings may be leveraged in designing and modelling better approaches. Additionally, the chapter emphasizes the importance of addressing multi-resident scenarios and calls for real-life experiments to evaluate NCVS systems' reliability and robustness in various environments. Finally, the analysis of state-of-the-art schemes is discussed, and the

research challenges in deploying radar-based vital sign monitoring systems in real-life scenarios are highlighted. This contribution is reported in Chapter 2.

Contribution 2: This contribution conceptualizes the mathematical model of chest wall movement due to cardiac activity. A basic system framework is simulated to model the target and a complete NCVS system, and the contribution addresses RQ1. The mathematical modeling of the phase noise, target movement, i.e., the chest wall movement due to the respiration and heart activity and the received signal by Doppler radar, not only provides a deeper understanding of the signal but also makes available all the realistic scenarios through variation of a mathematical parameter only. This chest wall model aids in designing and optimizing radar-based NCVS systems, reduces the need for extensive human testing, and offers valuable insights into chest wall motion and its relation to vital signs. This contribution is presented in Chapter 3.

Contribution 3: This contribution is for RQ2 to minimize the impact of noise, random body movements, and other interferences for vital signs measurement. A method that comprises resonance sparse spectrum decomposition (RSSD) and harmonic utilized algorithm (HUA) for HR/RR extraction is proposed. RSSD utilizes the 'high resonance' part of the signal mitigating the effects of clutter and random body movements from the received phase signal. The efficacy of the proposed method is validated by observing that the HR estimation accuracy is comparable to the RR estimation accuracy, even under heavy clutter and moderate body movement. Comprehensive systematic experiments are conducted to demonstrate and evaluate the performance efficiency of the proposed solution in terms of evaluation metrics, including the degree of similarity and standard deviation error. In this contribution, the performance efficiency of the proposed method is also evaluated with state-of-the-art methods. This contribution is reported in Chapter 4.

Contribution 4: In this contribution, the method successfully demonstrates automatic target localization, angle estimation, and beam steering toward the target. The SNR improvement through beam steering is also achieved. A sub-band energy-based extraction and Q factor optimization solution are proposed to efficiently extract high

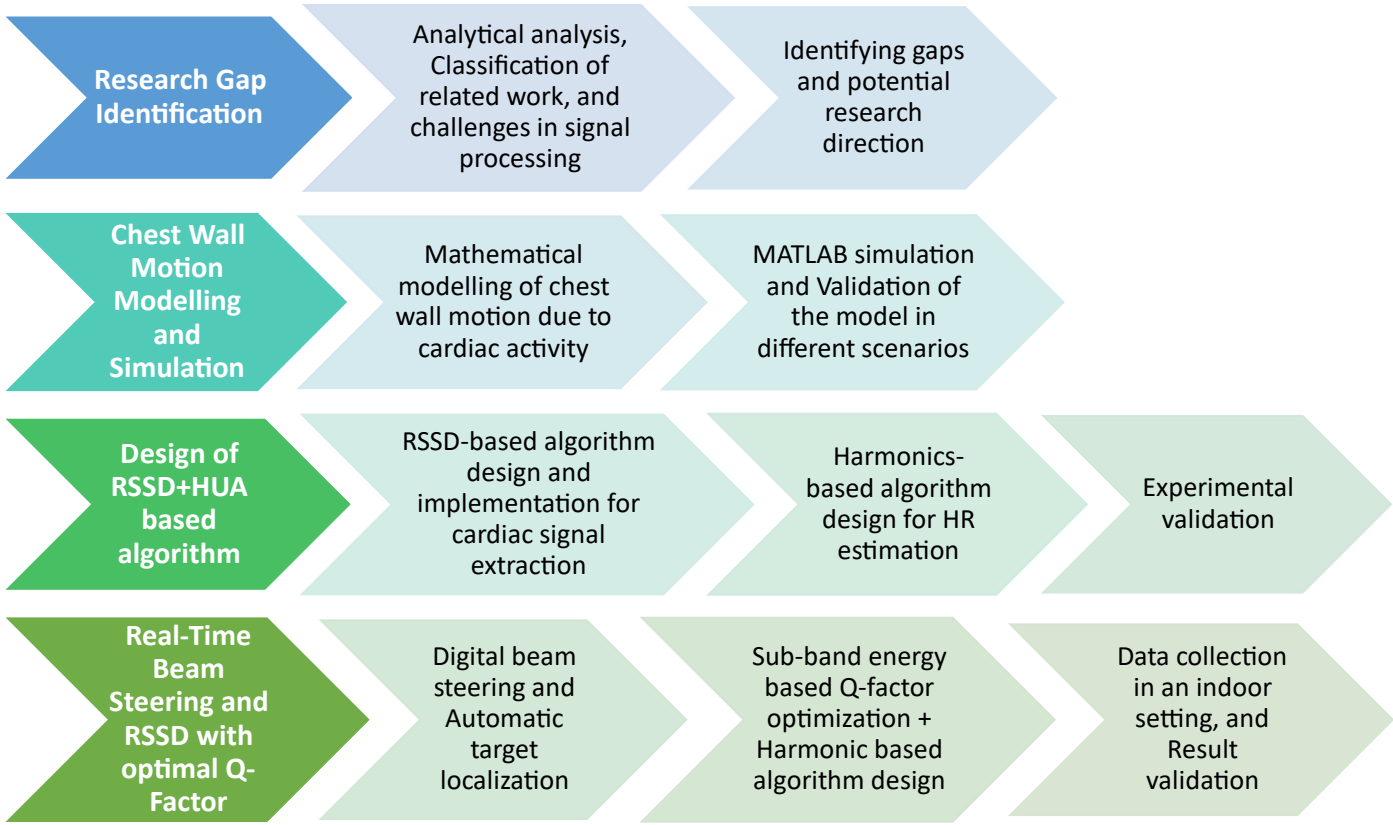

Figure 5: Research methodology

resonance components from the signal and accurately extract the vital signs. The contribution is attributed to RQ3. Analysis of the impact of different radar angles and varying distances from radar on the accurate HR/RR estimation is presented. The effect of heavy clutter and moderate body movement on the HR/RR estimation is also analyzed. The analysis is also performed to assess the impact of another person in the vicinity of the target. This contribution is presented in Chapter 5.

5. Publications

Journal Publication

- A. Singh, S. U. Rehman, S. Yongchareon and P. H. J. Chong, "Multi-Resident Non-Contact Vital Sign Monitoring Using Radar: A Review," in IEEE Sensors Journal, vol. 21, no. 4, pp. 4061-4084, 15 Feb.15, 2021, doi: 10.1109/JSEN.2020.3036039.
- A. Singh, S. U. Rehman, S. Yongchareon, and P. H. J. Chong, “Modelling of Chest Wall Motion for Cardiorespiratory Activity for Radar-Based NCVS Systems,” Sensors, vol. 20, no. 18, p. 5094, Sep. 2020, doi: 10.3390/s20185094.

Under Review Publications

- A. Singh, S. U. Rehman, S. Yongchareon, and P. H. J. Chong, “Human Vital Signs Estimation Using Resonance Sparse Spectrum Decomposition,” submitted in IEEE Transaction on Human Machine Systems.
- A. Singh, S. U. Rehman, S. Yongchareon, Yang Yu and P. H. J. Chong, “Real-time Beam Steering and Accurate Vital Signs Estimation Method in an Indoor Environment,” submitted in IEEE IoT journal.

6. Research Methodology

This thesis adopts a quantitative research methodology and is accomplished using simulation, method design, and experimental validation. The research methodology is depicted in Fig. 5.

An analytical analysis of previous work has been performed to understand the research gap and to identify the potential research direction. Our motivation to undertake this research arises from the challenges experienced in estimating HR and RR in a privacy-aware setting, particularly within signal processing. A mathematical model is employed to simulate the chest wall motion due to cardiac activity to elucidate the range of parameters affecting radar configuration and chest wall behavior for measuring vital signs. A signal processing method is formulated utilizing the RSSD algorithm, an efficient approach for analyzing non-stationary signals with time-varying spectral characteristics. The HR signal is not as strong as respiration, and higher-order RR harmonics can disrupt the fundamental HR frequency range. To address these problems, we designed a harmonic utilized algorithm (HUA) for precise HR extraction. In tackling real-world scenarios where the target individual's position is unknown, adaptive beam steering is incorporated to enhance the signal-to-noise ratio (SNR) and accurately determine heart and respiration rates.

To validate the proposed method, we performed comprehensive experiments using radar sensors. Our radar sensor consists of texas instruments (TI)' millimeter-wave IWR1443EVM and AWR1843EVM, an integrated single-chip FMCW radar sensor operating in the 77 to 81 GHz frequency band. The original raw data from IWR1443 is captured using DCA1000 EVM for further processing. AWR1843 radar is used due to its transmit beam steering feature. A Hexoskin vest is used for ground truth data collection in this study. Hexoskin is an intelligent garment embedded with respiration and Heart sensors. Mathematical modeling is carried out using Simulink software by MathWorks. The collected data is analyzed offline using MATLAB 2020a and 2022a.

Structured experiments are conducted in two stages to simulate different realistic scenarios. Stage one experiments involve four healthy participants (two male and two female) and are conducted in the university staff lounge, simulating a home environment. The setup includes a sofa, table, chairs, PC, refrigerator, and the metal window grid on the room wall, which constitutes the clutter. The second stage experiments are conducted on six healthy participants (three female and three male) in

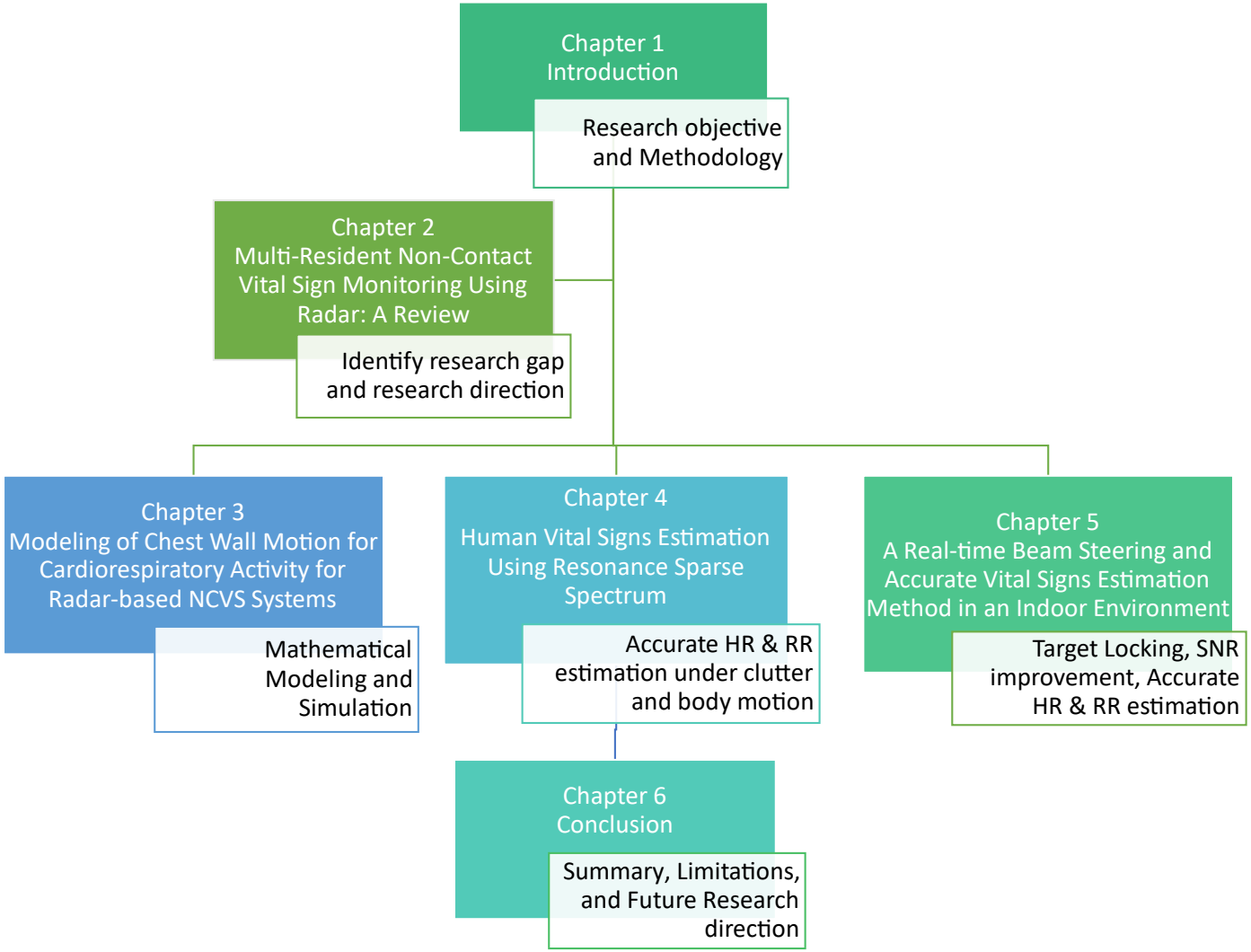

Figure 6: Thesis Structure

a lab environment. The radar was placed at 2.1 m from the ground, inclined at an angle of approximately 20^0 with respect to the ground to depict the realistic indoor setting. The necessary consent is taken from participants, and AUTEC (Auckland University of Technology, New Zealand Ethics Committee) ethics approval is obtained.

Statistical analysis is done to measure the performance of the proposed method using standard evaluation metrics, including mean root square error and correlation coefficient. The performance of a vital sign estimation system is typically evaluated based on its ability to correctly estimate HR/RR within acceptable error with reference to true value measurements. We evaluate the accuracy in terms of error bins (error < = 2 bpm and > 2 bpm) to gauge the performance of the proposed method.

7. Thesis Structure

This thesis is structured into six chapters, with their overall organization represented in Fig. 6. Chapter 1 provides an overview of the research work. Chapter 2 presents a review of relevant literature, highlighting the research gap. Chapter 3 focuses on RQ1 and presents a mathematical model and simulation study of chest wall motion caused by heart and respiration activity. RQ2 is addressed in Chapter 4, which aims to enhance the range and accuracy of vital sign extraction, particularly at greater distances. Chapter 5 presents a real-time method for beam steering and precise estimation of vital signs in an indoor setting, addressing RQ3. Finally, Chapter 6 concludes the research by summarizing the contributions and limitations of the proposed framework and providing recommendations for future research.

Chapter 2

Multi-Resident Non-Contact Vital Sign Monitoring Using Radar: A Review

Abstract

Vital signs are inarguably accepted as important key constituents to improve the health condition. Worldwide medical institutions and clinical observations have emphasized the need for continuous monitoring of vital signs such as heart rate (HR) and respiration rate (RR) for better health management. Radars are investigated as one of the potential technologies for non-contact continuous monitoring of vital signs. This paper provides a comprehensive technological review of the current state-of-art non-contact vital sign (NCVS) measurements using radar. We highlight the need to move towards higher frequency for high accuracy in a multi-resident environment and analyze the implications of mmWave exposure on human health and the effect of environmental attenuation. Significant challenges associated with hardware and signal processing algorithms are discussed in detail. Finally, we conclude the review with future directions and challenges associated with the detection of vital signs in a multi-resident indoor environment.

This contribution has been accepted for publication in IEEE Sensors Journal

1. Introduction

In 1842, CARLO Matteucci demonstrated the measurement of heartbeats through an electrical signal [58]. In 1902, Einthoven produced the first electrocardiogram (ECG) [59], and later, the measurement community introduced a series of methods, devices, and procedures for ECG monitoring. ECG records the electrical activity generated by heart muscle depolarization, which causes pulsating electrical waves to propagate toward the skin [60]. ECG is a contact-based measurement method and is considered to be the gold standard for heart rate measurement. It requires electrodes to be attached to the patient's body through a conductive gel, thus making the measurement suitable only in a supervised clinical environment, as shown in Fig. 7. The conductive gel needs to be applied frequently as it dries rapidly and may create allergies. The requirement for skilled personnel increases the cost of hospitalization and health care. Therefore, ECG becomes inappropriate for continuous monitoring for a prolonged time, either in a clinic or at home, especially for infants and patients suffering from burns or skin allergies. The electrodes may get loose or crumbled due to the infant's tosses and turns.

The continuous monitoring of vital signs such as respiration rate (RR) and heart rate (HR) of patients assists doctors and health professionals in identifying abnormal findings at an early stage and analyzing the disease process's progression and the treatment's effectiveness. Hence, the need arises for non-contact and continuous monitoring of heart rhythm and respiratory reflexes for efficient health monitoring.

Potential applications of non-contact detection and monitoring of vital signs are in infant monitoring [12], home health care, especially for older adults [11], sleep monitoring [13], and patients with skin allergies and burnt cases. The non-contact vital sign (NCVS) systems can provide efficient health management in the clinic and hospitals by reducing the time consumed in recording and maintaining patient data logs.

One such application of NCVS is in sudden infant death (SID) or "crib death." SID is one of the leading death causes in infants, with approximately 10,000 deaths per year in the United States [6]-[7]. A subtle amount of evidence has suggested that

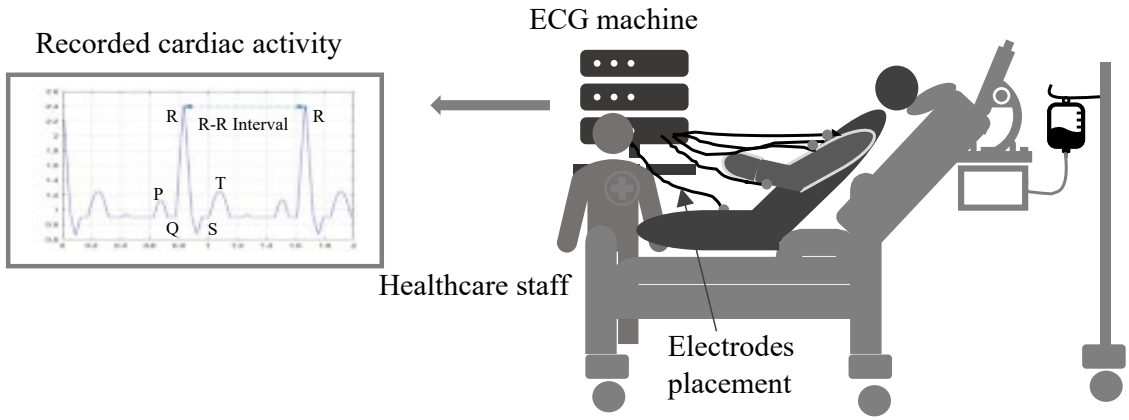

Figure 7: Conventional ECG Method showing the placement of electrodes

physiological defects in breathing control mechanisms cause crib death. The research has indicated that breathing cessation during sleep is the primary cause of crib death.

Different non-contact methods are proposed and experimented for the monitoring and measurement of vital signs. Optical vibro-cardiography [6], audio signal [18], thermal imaging [20], RGB camera [23], ultrasound radar [25], and microwave radars [26] are a few of the technologies used in designing and development of NCVS monitoring system. Advancements in sensing technology and signal processing techniques have improved the accuracy of the systems, yet there exist several limitations associated with each technology. Although optical vibro-cardiography produces comparable accuracy as ECG for the subject at rest, it requires a retroreflective tape to be attached to the chest wall [16]. Further, it requires an optical interface & makes installations complex for long-term monitoring and therefore restricts its use in the home environment. The NCVS measurement through acoustic speech cannot be applied for heart transplant patients with speech problems and irregular lung activities [27].

The RGB camera requires illumination for complete monitoring duration, and the invasiveness of the system makes it impractical and less adaptable for long-term and continuous monitoring. Also, the subject needs to be stationary and facing the camera for better accuracy, and the slight movement introduces blind spots [23]. The thermal imaging method has overcome the problem of an RGB camera being intrusive to some extent. However, even with the application of trackers & multiple cameras, the accuracy is affected by motion artifacts. Issues related to the manual marking of superficial

vessels, i.e. region of interest, accurate peak localization during sweating and external temperature variations, limit the accuracy of the system on the skills of the operator [21].

Compared with another non-contact sensing of vital signs such as visible light or Infra-red, microwave energy has greater penetration capability through material and clothes, less affected by environmental conditions such as illumination, temperature, humidity, etc. This makes Doppler radar being extensively researched in past years for non-contact measurement of cardiovascular activity. In the past, the research was limited due to bulky and expensive waveguide and hardware components. The elevation in microwave technology, hardware integration on a single chip due to advancement in very-large-scale integration (VLSI) technology, advanced signal processing techniques, and machine learning algorithms makes it possible to build compact and portable devices suitable for practical application.

The existing reviews on vital sign measuring systems by Scalise et al. [61] and Kranjec et al. [16] mainly provided a general overview of both the contact-based and non-contact methods for the measurement of vital signs. Bruser et al. [62] presented a study of suitable techniques according to the physiological effect caused by heart or lung activity. The review mainly focused on different attributes offered by body organs while performing the heartbeat and respiration activity. Li et al. [26] studied significant development in the radar sensing for contactless health monitoring mainly in the direction of front-end architecture, baseband signal processing and integration at the system-level. Leonhardt et al. [27] focused on the general review of technology suitable for non-contact sensors for vital sign monitoring systems to be deployed inside the vehicles, cockpits, etc. and Postolache et al. [63] specifically discussed the practical implementation in wheelchairs. Gu et al. [64] examined the advancement in the Doppler radar for healthcare applications. The author discusses the working principle of radar operation by briefly highlighting the issues like random movement and signal distortion and emphasized on the need for hybrid radar systems. Hall et al. [65] presented a brief review of recent advances in NCVS systems and compared them with their own phased-array Doppler radar NCVS biosensor. Gouveia et al. [66] presented a detailed review on

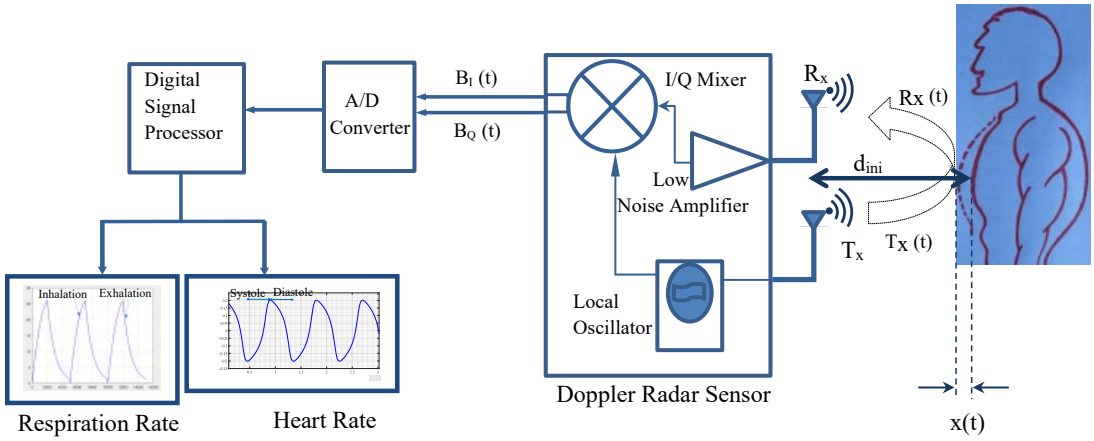

Figure 8: Radar architecture for NCVS measurement system

the already implemented methods for random body movement and compensation for continuous wave (CW) radar. Tran et al. [67] provide a comprehensive review on the challenges associated with the doppler radar specifically for sleep monitoring.

Compared with the existing reviews, our review paper presents a technological review on the current state-of-art of radar technology for vital sign measurement, which would be informative for future research into the multi-resident scenarios. Our study focuses on a multi-resident environment and the research challenges associated with the hardware and signal processing for practical deployment as reported in the literature. Our review briefs relevant mathematical principle and architecture of the radar-based NCVS systems as well as highlights the need for a radar sensor to shift towards higher frequency for bio-medical applications. The implication of mmWave exposure on human health and the effect of environmental attenuation is analyzed and discussed from the NCVS perspective. Finally, we highlight research challenges for a multi-resident scenario.

The rest of the paper is organized as follows. Section 2 gives the basics topologies, architectures of NCVS radar and an overview of the radar operational principle. The effects of operating frequency and transmit power on the basic radar design and human health are discussed in section 3. The challenges associated with practical NCVS and the multi-resident environment is discussed in detail in section 4 and 5, respectively. Summary and future directions are provided in section 6, and the conclusion is presented in section 7.

2. Radar System Topologies and Architecture

The concept of microwave sensing is first successfully experimented and verified by Lin [68] in 1975 by measuring the respiratory movement of the infant rabbit and human. The basic principle of microwave sensing is based on the Doppler shift. A continuous microwave signal is transmitted towards the target, reflected off the human target and is collected back at the receiver. The reflected signal is phase modulated by the time-varying chest wall motion proportional to the periodic breathing and cardiac activities.

A basic radar architecture for NCVS measurement is shown in Fig. 8. The voltage-controlled oscillator (VCO) provides the radio frequency (RF) signal for transmission. One output of the VCO is directly connected to a transmitting antenna, radiating the RF signal towards the target. Another output of the VCO is simultaneously provided to the receiving link for the phase demodulation. The periodic chest motion modulates the electromagnetic wave and scatters the modulated wave towards the receiver of the radar sensor. The receiver antenna receives the backward scattered modulated signal, which is amplified by a low noise amplifier followed by digitization. The received signal consists of phase variation caused by the periodic chest wall movement. The phase of the received signal is extracted, bandpass filtered and signal processing algorithms are applied over this phase signal to determine or estimate the RR and HR, respectively.

CW and ultra-wideband radar (UWB) are the most frequently used topologies for radar-based NCVS systems. The CW radar transmits a continuous wave signal, and the vital sign information is obtained through phase modulation of the reflected signal from the target. The CW radar operates into two modes based on its operation; 1) the unmodulated CW mode transmits an unmodulated signal with a stable amplitude, 2) FMCW mode, which transmits the modulated frequency during the measurement. In UWB radar, the transmitted signal consists of high-frequency short-duration pulses and echoes received during the off-transmission time are analysed for extraction of vital signs. Each of these topologies offers different merits and challenges.

2.1 NCVS Radar Topologies

2.1.1 Continuous-Wave (CW) Radar

In the CW transceiver architecture, narrow bandwidth signal is continuously transmitted and received. The single source of CW radar can be used for both transmitting and receiving. It has the advantages of simplicity, the potential of minimal transmitted spectrum spread, simplification of filters at each stage of the receiver, and the straightforward signal processing. However, the topology has the inability to separate reflections temporally, causing direct current (DC) offsets and low-frequency noise introduction in the received signal [61]. Additionally, due to the missing timing information because of the lack of modulation, target range extraction is not possible with CW radar. Moreover, the need for isolation between the transmitter and the receiver is the major limitation in CW radar system.

2.1.2 Frequency Modulation Continuous Wave (FMCW) Radar

FMCW is frequency-domain radar sensors. FMCW radar is the extension of the CW radar and overcomes the problem of missing time information which prevents the range measurement. As its name suggested, a frequency modulated continuous wave is emitted; however, a timing mark is introduced by changing the transmission frequency over time called frequency sweep or chirp. The reflected signal is received back with a time delay and frequency shift depending on the object's distance and relative speed. The distance from the target to the radar sensor and the range resolution can be estimated applying spectral analysis [69]. However, the implementation of FMCW topology needs addressing of the issues such as Tx-Rx leakage, AC-DC coupling effect, RF nonlinearities and requirement of the high sampling rate.

2.1.3 Pulsed-Wave/Ultra-Wideband (UWB) Radar

Pulse-wave radar can determine the range by measuring the delay between the transmitted pulse and its echo (time information) by observing the Doppler shift on the pulse frequency spectrum. The pulsed radar sensor is typically time-domain radar. The

Table 1: Features of Radar topologies

Features	Radar		
	CW	**FMCW**	**UWB**
Design architecture	Simple	Complex as compared to CW radar	Complex as compared to CW radar
Absolute range detection	Cannot detect	Very high	Better for greater distances and low for short range
Detection of target velocity	Easy without ambiguity	Complex as compared to CW	Complex implementation
Measurement accuracy	High	High but complex processing	High but related to pulse width and rate

pulsed radar sensor sends either impulse train, mono-pulse, or modulated pulse with some pulse repetition interval. The two-way travel time between the transmitted and received pulse determines the range of the target. The pulsed radar offers wider bandwidth. In non-contact vital signs monitoring, where the target is typically at the same range as the nearest clutter, the UWB radar provides the advantage of the elimination of leakage, however, as range measurements do not aid in physiological motions monitoring for single targets, the increased complexity of the architecture over continuous wave architecture does not result in a commensurate increase in benefits [61]. Also, the UWB radar sensors are inappropriate for high-resolution application. For high resolution, the bandwidth of the pulse needs to be increased, which in turn shorten the pulse width. Reducing the pulse width is limited by technology.

Summarizing the different radar topologies in Table 1, CW, FMCW, and UWB radars all are used to detect tiny chest wall movements due to physiological activities. A CW radar is the simplest topology and measures chest wall displacements with accuracy; however, the UWB or FMCW topologies offer the range information which cannot be obtained through CW radar.

2.2 Radar RF-Front End Receiver Architecture

The extraction of vital sign information from the received signal is achieved through a sequence of signal processing methods that involve time and frequency analysis of the signal. The received signal is mixed with a transmitted signal and passed through the

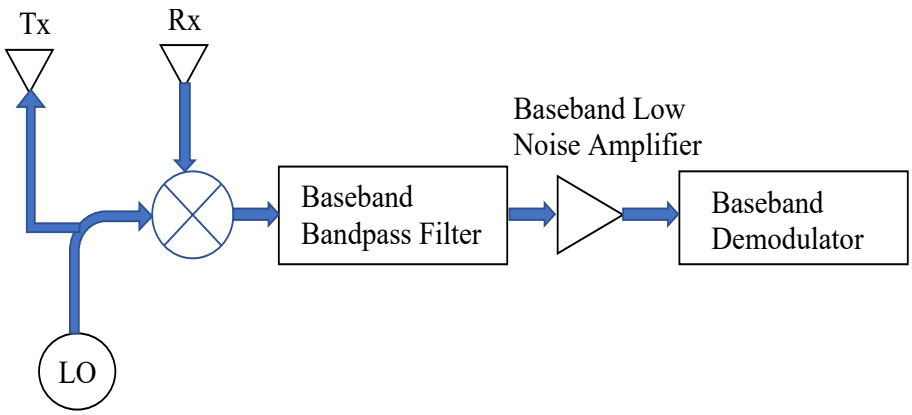

Figure 9: RF front-end Receiver architecture of the homodyne receiver

filters to recover the baseband signal for further processing. Based on the conversion principle, the radar RF front-end architecture is called either heterodyne or homodyne. Further, based on the demodulation scheme, the RF receiver can be a single channel or quadrature channel having different advantages and challenges.

2.2.1 Heterodyne Receiver

The heterodyne transceiver contains a separate local oscillator (LO) in the transmitting and receiving chain. After passing through a band-pass filter, the received signal is mixed with separate LO operating at a different frequency than used in the transmitter stage. Hence the mixed signal is modulated on a non-zero intermediate frequency and not converted directly to baseband. The mixed signal is again filtered by another band-pass filter, amplified through a low noise amplifier (LNA), and then demodulated directly [26], [30]. Heterodyne receiver is robust against the DC offset, compared to homodyne architecture. A major disadvantage is the requirement of large circuit components and related non-linearity.

2.2.2 Homodyne Receiver

As characterized by the name of the direct-conversion receiver or zero-IF receiver, the homodyne architecture directly converts the received signal to baseband. Here the received signal is mixed with the same local oscillator frequency as of the transmitting carrier and converted down to baseband using bandpass filter as shown in Fig. 9. The baseband signal is amplified using a low noise amplifier and then demodulated. The

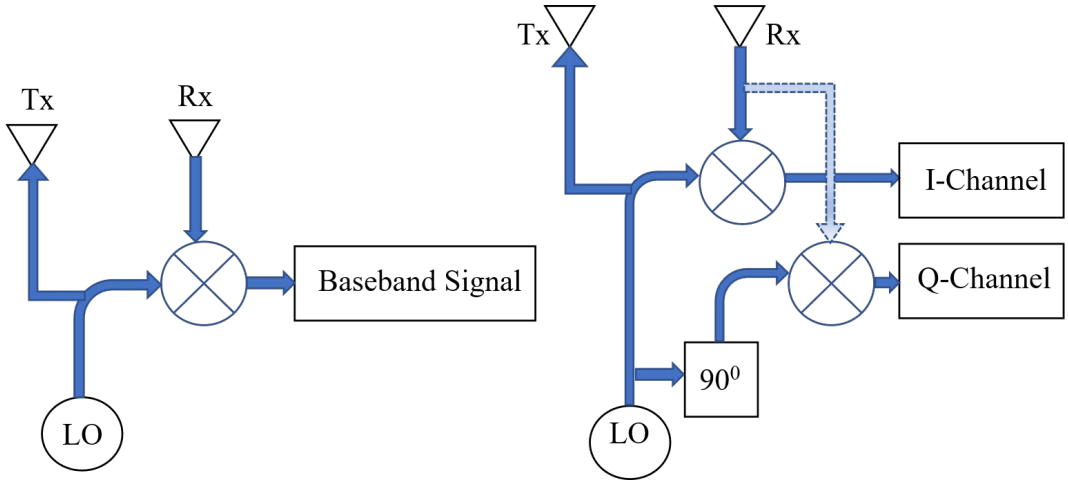

Figure 10: Single and Quadrature Channel Output

homodyne topology has simplified circuitry, but the DC offset introduction by the system causes saturation for the digitization process [26], [30].

2.3 Single or Quadrature Channel Architecture

The Doppler radar transceivers can be designed either as single-channel or in-phase (I) and quadrature (Q) channels, as shown in Fig. 10. The target position and the operating frequency cause a null point problem. Single-channel heterodyne/homodyne receivers are highly sensitive to the null point issue. In the worst scenario, the receiver observes virtually no phase-modulated signal for the estimation of physiological motions. Null point occurs in CW radar when the received signal and local oscillator are either in phase or 180 out of phase, depending on the distance between the target and radar. When a target is at a distance of an integer multiple of λ/4, and phase shift becomes an integer multiple of π, and the baseband signal is no longer proportional to the vital signs movements. Hence, the vital signs frequencies cannot be extracted. Therefore, a quadrature transceiver or frequency tuning on a single channel has been used for optimum signal demodulation. With the quadrature transceiver's in-phase (I) and quadrature (Q) output, there will always be one channel that is not at null point detection [30]. Specifically, the FMCW signals have a complex nature of the received signal, a single channel is sufficient to address the null point issue. The use of complex signals and compression of the FMCW ramp enhances the SNR, and consequently, the maximum unambiguous range is increased.

2.4 Operational Basics of Radar NCVS

A Doppler radar can be described with a signal $T_x(t)$ of frequency f, transmitted towards the target,

$$T_x(t) = A_1 \cos[2\pi f t + \phi(t)] \tag{2.1}$$

Where f: frequency of the signal, $\phi(t)$: phase noise of the local oscillator signal. If the target is at a distance d_{ini} and $x(t)$ is the time-varying chest displacement then, the distance between the transmitter and target at time t, $d(t)$ is as in (2.2),

$$d(t) = d_{ini} + x(t) \tag{2.2}$$

The received signal, $R_x(t)$can be described as in (2.3),

$$R_x(t) = A_2 \cos[2\pi f(t - t_d) + \phi(t - t_d) + \theta_c] \tag{2.3}$$

where A_2 is a received amplitude, t_d is a time delay round trip, and θ_c is a constant phase shift.

The round-trip time delay t_d, for the propagated wave is $2d(t)/c$, where c is a velocity of propagation of the continuous wave. As $d_{ini} \gg x(t)$, hence, $x(t)$/c shall be negligible. Therefore, the received signal may be described as in (2.4),

$$R_x(t) = A_2 \cos\left[2\pi f t - \frac{4\pi d_{ini}}{\lambda} + \phi\left(t - \frac{2d_{ini}}{c}\right) + \theta_c\right] \tag{2.4}$$

$$B_I(t) = \frac{A_2 A_1}{2} \cos\left[\frac{4\pi d_{ini}}{\lambda} - \theta_c + \frac{4\pi x(t)}{\lambda} + \phi_R(t)\right] \tag{2.5}$$

$$B_Q(t) = \frac{A_2 A_1}{2} \sin\left[\frac{4\pi d_{ini}}{\lambda} - \theta_c + \frac{4\pi x(t)}{\lambda} + \phi_R(t)\right] \tag{2.6}$$

$$\tan\left[\frac{4\pi d_{ini}}{\lambda} - \theta_c + \frac{4\pi x(t)}{\lambda} + \phi_R(t)\right] = tan\theta_R \tag{2.7}$$

$$\theta_R = \tan^{-1}\left[\frac{B_Q(t)}{B_I(t)}\right] \tag{2.8}$$

For the quadrature receiver architecture, the received signal is multiplied by two $90°$ phase-shifted local oscillator signals in two separate channels. These two mixed

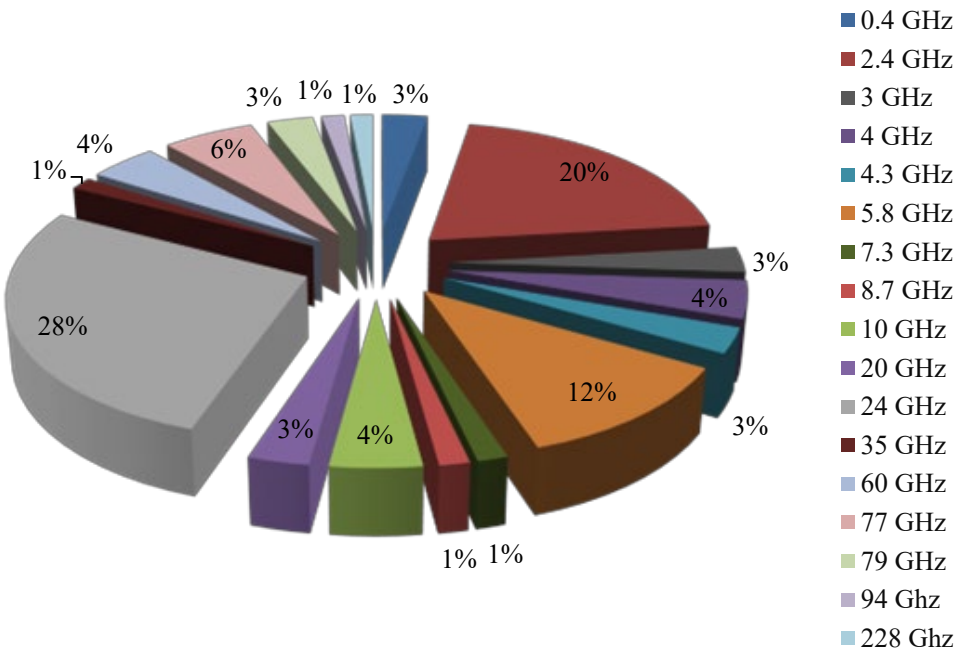

Figure 11: Frequency distribution investigated for NCVS systems

Table 2: Phase variation-chest wall movement at different frequencies [72]

Frequency (GHz)	Wavelength (mm)	Phase difference (degree)
2.4	125	1.7
5.8	51.72	4
10	30	5.7
16	18.75	16

signals are filtered separately to acquire two in-phase and quadrature baseband signals B_I and B_Q, respectively, as in (2.5) and (2.6). The phase variation θ_R, which is linearly proportional to chest wall displacement $x(t)$ is captured as in (2.8).

3. Effects of Transmit Power and Operational Frequency on Basic Radar Design

Major challenges in developing the radar based NCVS measurement include dealing with a feeble signal and extracting information from the dominance of unwanted noise due to clutter and motion artifacts. The received signal strength of a radar system can be calculated using (2.9) [70]

$$S = \frac{P_t.G_t}{4.\pi.R^2}.\frac{\sigma_c}{4.\pi.R^2}.A_e \quad (2.9)$$

where, S is a returned signal power, P_t is a radar transmit power, R is a target range, G_t, A_e are antenna gain & its effective area, respectively, and σ_c is the radar's cross-section area of the target.To have better-received signal strength, the signal-to-noise ratio (SNR) must be maximized by increasing transmit power P_t. However, the transmitting power of electromagnetic fields is limited by the adverse health effects and degradation of biological parameters. As per guidelines of the international commission on non-ionizing radiation protection (ICNIRP) and telecommunication standardization sector of the international telecommunications union (ITU-T) in 2016, the recommended power density of electromagnetic wave in the frequency range of 2-300 GHz should be limited to 10 W/m^2 for the exposure time more than 6 minutes [71]. As per standard, the transmission power cannot be increased beyond suggested limits. Therefore, either the antenna characteristics, the receiver sensitivity or the detection algorithm may be worked upon for better performance for low SNR signals.A target range is also a decisive performance parameter for the system. For the highest sensitive receivers, i.e., $S = S_{min}$ the range of radar depends on $P_t.A_e$. To increase the range, either power or aperture area or both may be increased. However, increasing transmitted power is not a suitable option for achieving a larger detection range. The other factor affecting range is antenna gain and effective aperture area.

These two aspects can be controlled by the size of the antenna and the frequency used. The antenna size cannot be increased due to the application either in the home or nursing care environment. Consequently, it opens a research challenge to evaluate the radar parameters and frequency of operation that resolve these trade-offs in design. Immense research efforts have been deployed in exploring the frequency range most suitable for vital sign monitoring. Most of the research is focused mainly on four bands, namely L band (1-2 GHz), X band (8-12 GHz), Ka-band (26.5-40 GHz), and W (75-110 GHz) band. The radar sensors working in W-band have great potential in medical applications because of its higher bandwidth. The comparative statistical data are given in Fig. 11, indicates that NCVS systems are mainly proposed in frequency bands below 24 GHz.

Table 3: Performance parameter for different frequencies as reported in the literature for different scenarios/applications

Operative frequency (GHz)	Transmission power (mW)				Experimental dataset (no. of subjects)			Maximum measurement range(m)					Radar technology		Accuracy (%)		
	<5	**5-10**	**10-20**	**>20**	**1**	**2-5**	**>5**	**<0.5**	**0.5-1.5**	**1.5-2.5**	**2.5-5**	**>5**	**CW**	**UWB**	**<90**	**90-95**	**>95**
2.4 [30, 31, 32, 34]	✓					✓				✓			✓			✓	
3.3 [47]	✓					✓						✓		✓			✓
4 [38, 40, 41]	✓						✓	✓						✓			✓
4.3 [171, 172]	✓					✓			✓					✓		✓	
5.8 [96, 101,116,126,127, 173, 174]	✓				✓				✓				✓				✓
5.46-7.25 [14]	✓						✓					✓	✓			✓	
8.7 [48]	✓						✓		✓					✓			✓
10 [136]	✓				✓			✓					✓		✓		
10.5[128, 155, 165]				✓	✓				✓				✓		✓		
24 [15, 53, 115, 125, 129, 130, 154, 175, 176]		✓					✓			✓			✓			✓	
77 [33, 453]	✓					✓					✓		✓				✓
79 [121]	✓						✓			✓			✓		✓		
92-96 [177, 178]	✓				✓						✓			✓		✓	

Research [72] has presented a comparative study between different frequencies to find the minimum power required to detect the vital sign. It is found that for a given power with an increase in frequency, wavelength decreases, which tends to increase the phase difference and make the detection process more efficient. The higher frequency has higher sensitivity on small movement detection as compared to lower frequencies, as shown in Table 2. The practical results were in confirmation with the theoretical concept as with an increase in frequency, and with higher bandwidth, the larger range resolution is achieved. Therefore, the researchers have moved from the lower frequency ISM band such as 2.4 GHz or 5.8 GHz to 24 GHz and now further to mmWave range (GHz) as shown in Table 3. Higher frequency range reduces the device size and at the same time, increases the resolution so that micro-doppler effects due to small limb movement can easily be detected.

At present most of the studies have used a 24 GHz frequency band for radar sensors. The 24 GHz system consists of two bands [73]:

- Narrowband includes industrial, scientific, & medical (ISM) applications in the range of 24.0 to 24.25 GHz offering 250 MHz bandwidth to the maximum.
- Ultra-wideband having a bandwidth of 5 GHz and can offer remarkably high range resolution.

The european telecommunications standards institute (ETSI) and federal communications commission (FCC) has regulated and standardized that after 2021, 24 GHz wideband and ultra-wideband radars shall be phased out in Europe, the US and most of the world [74]. Though the narrow-band ISM band shall be available long term, but has the limitation of lower bandwidth and resolution and is already overcrowded [75]. The restrictions and phasing out of wideband 24 GHz and need for high performance in emerging radar application has moved the researcher's interest from 24 GHz to mmWave [76].

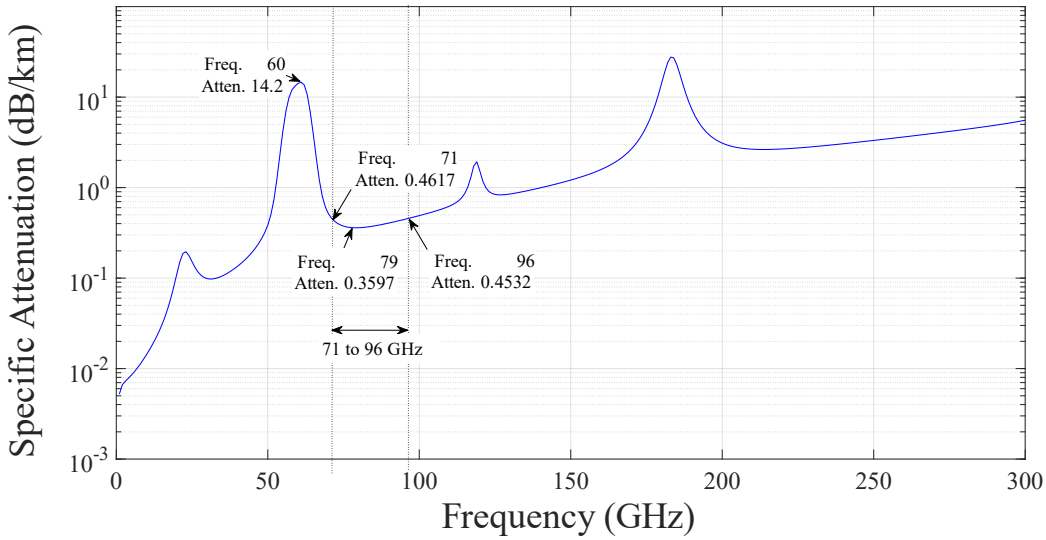

Figure 12: Specific attenuation at mm-wave frequencies. The attenuation at 71 to 96 GHz is about 0.46 to 0.45 dB/km [80]

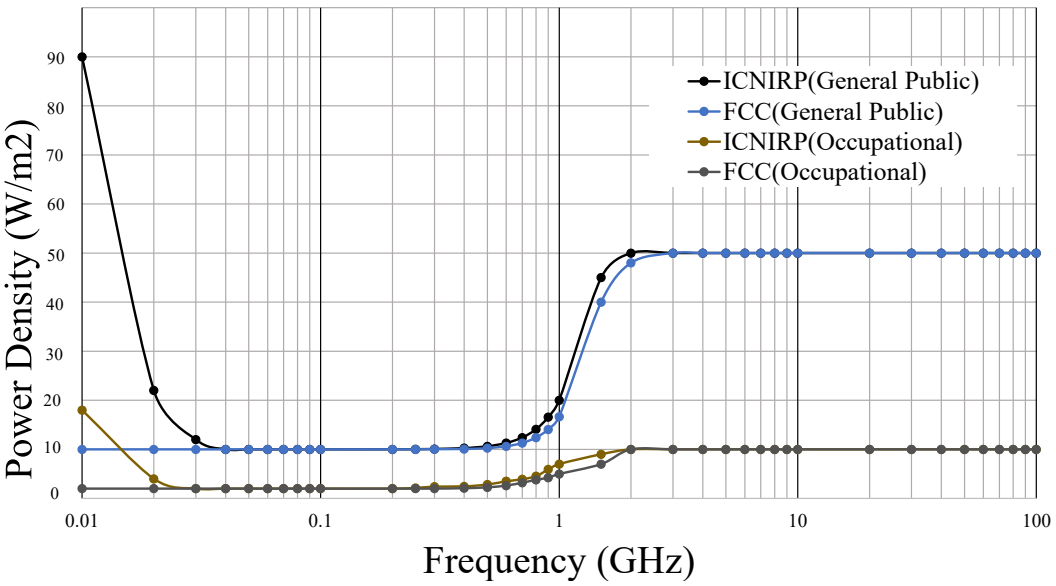

Figure 13: Safe power limits at different frequencies [71]

3.1 Shifting Towards mmWave

The electromagnetic spectrum corresponding to the frequencies band of 30 GHz to 300 GHz is referred to as the mmWave region. The wider bandwidth in mmWave significantly increases range resolution and range accuracy [77]. Compared to the 200 MHz ISM band, which is available at 24 GHz, there is significantly higher bandwidth available at 77 GHz. Specifically, the 77-81 GHz short-range radar band offers up to 4 GHz of sweep bandwidth. Since range resolution and accuracy are inversely proportional to the sweep

bandwidth, a 77 GHz radar sensor can achieve 20 times better range resolution and accuracy performance than a 24 GHz radar. The achievable range resolution (2*C/B) is 4cm as compared to 75cm for 24 GHz radar [78]. High-range resolution drives the better separation of objects and improves environmental modeling and object classification, essential requirements of designing a vital sign monitoring system [79].

The mmWave radar sensing is exceptional in its ability to track the speeds and angles of multiple moving objects, and the sensor's field of view can focus on a narrow angle. Also, 77 GHz sensor improves the velocity resolution and accuracy by a factor of three as compared to the 24 GHz sensors [78]. Another benefit of higher frequency is the small form factor of the device. The antenna size reduces to approximately one third as compared to the one used in a 24 GHz system for the same antenna gain and field of view [78] and offers the advantage of implanting the antenna into a monolithic integrated circuit. Another design aspect of the radar system at mmWave is the beamwidth. For equivalent antenna size, the mmWave frequency offers a small beam angle. Narrow beamwidth increases the directivity and allows measurement at larger distances. The range of detection also depends on received signal strength which is affected by the attenuation in the environment. In general, atmospheric attenuation is lower for low frequencies and higher for higher frequencies as per ITU guidelines [80]. Fig. 12 shows the attenuation for mmWave. Attenuation for 0-30 GHz & 70-100 GHz is within limits (0.15-0.23 dB/km) and does not affect the systems requiring detection range in several meters only. Therefore, considering safe power limits, as in Fig. 13 and attenuation, the range of 0-30 & 70-100 GHz is reliable for industrial application, whereas the band of 71-96 GHz is best suited for mmWave range applications.

The wider bandwidth, higher range resolution, smaller antenna size, and downscaling the requirement of the number of radars to cover an area and consequently the cost, installation complexity is reduced. However, the mmWave associated issues need to be addressed for a robust system. Owing to the high resolution, the clutter caused by multipath reflections interfere with the desired signal. The on-chip integration of radar system components requires critical essentiality of

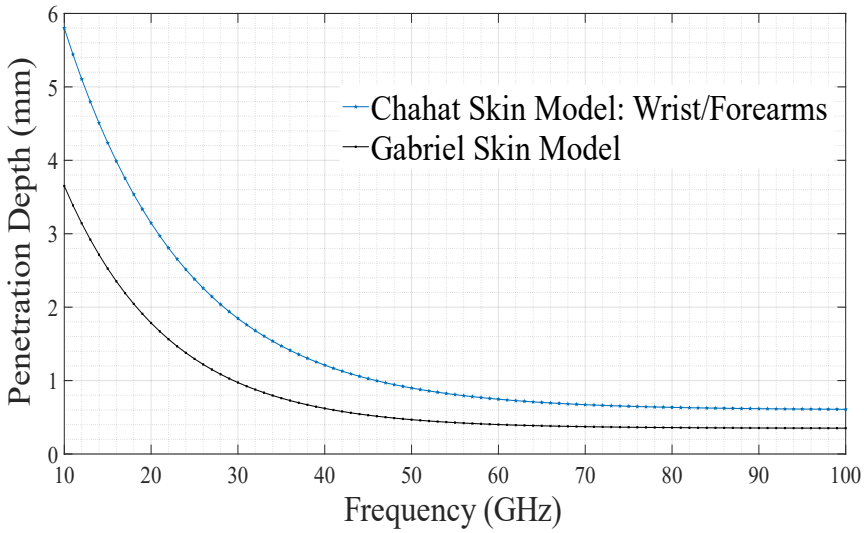

Figure 14: Skin penetration depth over the frequency of operation [83]

electromagnetic interference shielding between the higher RF (mmWave) and the signal processing components [81].

3.2 Effect of Mm-Wave Exposure on Human

The high frequency of mmWaves and their propagation characteristics make them useful for the radar-based application. However, mmWave is always questioned for the health risk in applications where long-term exposure is needed. To answer this, recently, Rappaport et al. [82] have explained that the mmWaves are nonionizing as the photon energy of mmWave is of the order of 0.1 to 1.2 meV. The photon energy of this order is insufficient to dislodge an electron from its atom or a molecule. The photon energy does not result in disruption of molecular bonds (disruption of molecular bonds is linked to cancer), the mmWave radiations are harmless as far as the ionization harms are concerned. The only biological concern can be due to the heating result by the absorption of mmWave energy by tissues and biological fluids. However, these thermal effects must be prevented by keeping the exposure limits as per standards [83].

The effects of RF exposure are measured based on three parameters, namely specific absorption rate (SAR), the steady state or transient temperature, and plane-wave equivalent power density. The steady-state temperature of the tissues is the prime factor in assessing the effect of radiation as it can rapidly heat the skin. The critical detrimental effect of radiations is heating at these mmWave frequencies. As shown in

Fig. 14, the skin penetration depth decreases with the increase in radiation frequencies. Most of the energy due to mmWave exposure is absorbed within the first few millimetres of human skin, and hence heating effects are not on internal deep tissue structure but limited to the upper surface of the skin only [84].

The temperature changes in the range of 1°c in the skin are considered safe [83]. The different body parts such as hands, arms, etc. allow heat to be easily dissipated owing to large blood flow. However, eyes have insufficient blood flow to redistribute the generated heat and hence the thermal effect of radiations over eyes is of much greater importance. Low intensity (< 1 mW/cm^2) for longer duration exposure (at mmWave frequencies) does not have any significant temperature rise and is within the safe exposure limit for the eyes. Moreover, the localized largest peak radiation level is to be maintained as per federal communications commission (FCC) and international commission on non-ionizing radiation protection (ICNIRP) which suggests that up to the range of 100 GHz the distance of the human body to the field source should be greater than 20 cm [82].

Concerning the effect on children or infants, as the mmWave exposure is non-ionizing, the primary focus should be dealt with on the thermal change generated due to the radiation. FCC and ICNIRP have standardized the safe exposure power limits for electromagnetic radiations over different frequency ranges, as shown in Fig. 13. It is advised to keep the exposure level of radiations to a minimum by maintaining the maximum allowed separation from the transmitter so that the nonionizing effect or the temperature variation due to radiation is kept far below 0.1°c [85]. The preliminary results of researches in the biomedical field have highlighted the beneficial effects of mmWave. It is observed that the exposure of mmWave over biological molecules levels results in an increased immunity of tissues. More reproducible results are to be verified for confirming the beneficial effects of mmWave exposure. However, the exposure of mmWave frequencies within safe limits has no detrimental impact over a human body [86] for its application in NCVS systems.

4. Challenges for Practical Non-Contact Vital Sign Monitoring

The general challenges associated with the existing designs need to be addressed amicably. The cardiac signals are small in magnitude and highly sensitive to noise such as clutter, motion artifacts, interference due to respiration harmonics. Moreover, hardware non-idealities, DC offset, and noise, frequency, and phase drift in hardware components over prolonged usage and null-point effect are critical challenges of radar-based vital sign measurement systems. Broadly the challenges offered by the radar-based systems can be classified as related to hardware non-idealities, associated with complexities and computational load of signal processing algorithms.

4.1 Hardware Non-Idealities and Challenges

The accuracy and robustness of the system are affected by hardware related issues. There are different sources of noise either due to hardware nonidealities or the environment. As shown in Fig. 8, the NCVS system comprises VCO, Tx/Rx antennas, amplifiers, mixers, and I/Q demodulators as main hardware modules. The aging effect of hardware, temperature changes, or the non-ideal behaviour of oscillators causes unintended frequency or phase shift from nominal values and is called “drift.” The radar-based NCVS systems work on the phase analysis of the received signal as the heart and lung activity causes phase variations in the radar received signal. The frequency drift and phase variations caused by non-ideal characteristics of hardware block cause error in the detection of vital signs. The drift can cause adjacent channel interference and additional noise introduction in the system.

NCVS systems are to be operated continuously for long duration and hence drift in frequency and phase can severely hamper the performance of NCVS systems. The phase noise of VCO results in residual noise in the demodulated baseband signal, which decreases SNR substantially. As the chest wall displacement and subsequent phase changes are small, the decrease in SNR drastically reduces the efficiency of the system in the detection of RR and HR. The chest wall movements being tiny in amplitude and

being minimal in the area, the directivity of transmission affects the radar received signal strength considerably. As the transmission power is limited due to safety considerations hence for acquiring a good received signal, the transmission needs to be highly directive. Thus, the type of antenna needs to be chosen carefully for the increase directivity.

The preamplifier filter and mixer block apart from being bulky, introduces non-linearity, noise resulting in distortion and degradation of performance. In addition to noise, the performance of a single channel Doppler radar receiver is affected by the relative position of the subject from the radar because of a “null point.” Therefore, quadrature receiver architecture is employed to reduce the effect. However, the non-idealities in I and Q channel hardware produces I/Q channel imbalance and unwanted image frequencies. Phase offset and unwanted image frequencies can be compensated with filters having sharper cutoff. However, it would increase computational load at signal processing stages. The imbalance also introduces amplitude and phase offset in the demodulated baseband signal [87]. This unwanted phase offset affects the performance of a radar-based NCVS system whose efficiency depends on accurate analysis of phase variations of the received signal. Various techniques and methods have been investigated in the literature to overcome these hardware related issues.

4.1.1 Hardware Inaccuracy and RF Nonlinearity

In [81], the mechanical components were replaced with the analog printed circuit board (PCB) to avoid the nonlinear and non-ideal behaviour due to temperature and environmental changes. However, the analog PCB amplifiers become non-linear at high frequency. Another approach to address the VCO related residual phase noise was demonstrated by sharing the VCO between transmitter and receiver. This technique was called a range correlation where the noise was cancelled at the processing stage, and the noise effect was reduced [31], [32]. Guohua et al. [88] also used range correlation along with illumination by a separate transmitter and receiver antenna to reduce the noise effect by VCO and circulators. Further to address the challenge of the bulkiness of filter blocks and noise, Sallen-Key 2nd order low pass and high pass filters were used. Li et al. [29] simplified the circuit of baseband processing, where DC blocking and amplification were done, and all resistors were avoided. The removal of resistance from

the circuitry suppressed all thermal noise. Additionally, an external signal generator was used in place of the wideband oscillator for the high-frequency signal, which reduced the frequency drift issue to some extent. The inaccuracy introduced due to radar movement was addressed with the use of dual-frequency Doppler radar system working at fundamental and harmonic frequency simultaneously [89]. Two signals were transmitted, one fundamental signal towards the target and other its inherent second harmonic towards the fixed reflector. The two received signals were used to cancel the effect of radar movement.

Authors in [90] described that the output frequency of a voltage-controlled oscillator (VCO) has a non-linear dependency on the input voltage. As a result, the beat signal is not a pure sinusoid for FMCW radar system. Furthermore, the spectrum of the beat signal spreads over a wider frequency range with multiple larger side lobes, which causes the difficulties in multitarget detection. Moreover, the phase of the beat signal is not a linear function of time. Toker et al. [90] addressed the issue with a resampling technique. The beat signal is sampled at a non-uniform rate, making the phase a linear function of the sample index. The up-sampling theory was based on fixed structure interpolators optimized/trained for a specific class of functions and achieved nonlinearity correction with improvements in the spectrum, specifically for suppressing the side lobes and sharpening the main lobe.

In [91], [92] the authors have discussed the six-port interferometry, which offers the advantages of a less complicated hardware setup and its extraordinary phase resolution. It is a passive microwave device that uses a network of six ports to measure the phase difference between two signals. The basic concept of a passive microwave device involves splitting an incoming signal into two paths, one of which is delayed by a known amount. The two signals are then combined, and the resulting interference pattern is measured at the output ports. The passive six-port structure generates the I/Q representation directly in the RF domain without noisy circuitry or non-linear processing stages, resulting in strictly linear behavior. The baseband conversion is through a subsequent step by diode detectors, which operate in their square law region and do not spread the signal's energy to harmonic components. However, the six-port

exhibits the drawback of a measurement ambiguity due to the arctan-function. Moreover, calibration of the sensing unit is another challenge for six-port interferometry. To obtain micrometre range resolution, highly linear phase performance over power and frequency is needed. Therefore, blind estimation of the non-idealities to derive linearization coefficients for phase compensation is the most critical requirement for six-port interferometry.

The author in [93] described that the periodic deviations in the frequency ramp are caused by spurious tones, which may result from switching in digital circuits or transient response of the phase locked loop (PLL). As it corresponds to a certain frequency, it results in a sinusoidal nonlinearity in the frequency ramp. Apart from the sinusoidal non-linearity based on the real interference existed in direct digital synthesis (DDS) based signal generation, spurs in the supply voltage or in the DDS-clock also leads to spurious in the DDS output signal. To address the nonlinearity issue, [94] presented a DDS-based FMCW radar front end that generates nonlinear frequency chirps and operates without the commonly used high-frequency DDS reference oscillator. Then the digital post-processing of the de-ramped signal was applied to compensate for such non-linearities.

4.1.2 Null Point

The phase demodulation sensitivity at the receiver is highest when the constant phase shift in received baseband signal is an odd multiple of $\pi/2$. However, base-band signal output becomes non-linear and has minimum information when the phase shift becomes integer multiple of π. For the VCO to be locked at the same frequency for transmitter and receiver, the phase shift largely depends on the target distance from the radar. When a target is at a distance of an integer multiple of $\lambda/4$, phase shift becomes integer multiple of π. This effect is called the null-point effect, which is present at every quarter wavelength distance and severely affects the detection accuracy. The issue was addressed with the use of double-sideband waves for radar operation [95].

The double-sideband transmission provides a null point at larger separation and does not require to generate the quadrature local oscillator signals. The large DC offset

owing to the double-sideband transmission was removed by employing IF-amp using indirect-conversion architecture [96]. However, double-sideband transmission increases the power and bandwidth requirements. Obeid et al. [72] used a vector network analyzer (VNA) to reduce the hardware related noise and to overcome the null point issue. The VNA measures the phase of the forward complex transmission coefficient and correspondingly the displacement of the target. The quadrature architecture was not used for demodulation, and hence related noise and null point issues were avoided. However, the VNA is complex and slow in processing the sweep over the complete signal.

In [97], the null point problem was addressed based on phase and frequency diversity. The phase diversity between a two-channel receiver is introduced either by a phase shift between the channels or by relative displacement between the antennas. This ensures proper detection where one channel is at a null point, and the other detects a maximum. The other method based on frequency diversity uses a variable frequency synthesizer to change its operating frequency so that the null point is shifted, and optimum detection is achieved at the target location. However, tuning of operational frequency to compensate for the target movement is the limitation of the design. In a similar approach, a voltage-controlled tunable phase shifter is introduced to eliminate the null point problem [98]. The phase of the demodulated signal was effectively adjusted, to always lock the radar system to the optimum point using a simple control mechanism. However, manual tuning of the system during each measurement is required once the distance between the antenna and the subject changes which presents limitations for the system design.

The arctangent and complex demodulation techniques are also studied to overcome the null point effect. In [99], arctangent demodulation with DC offset compensation is proposed. However, system calibration is required before each measurement, which brings inconvenience to continuous detection. The arctangent demodulation is sensitive to DC offset thus requires complicated calibration of the DC offset. In the complex signal demodulation method, the complex signal is reconstructed in real-time by in-phase and quadrature component [100]. This eliminates the impact of

residual phase in the frequency domain and applying complex Fourier transform to the signal for spectrum analysis, and the residual phase does not affect the relative strength between the odd and even order frequency components. The desired signal components, i.e., the odd order frequencies, are always present in the spectrum. However, the DC component accumulation in I and Q phase component needs to be addressed separately for measurements. A different approach to avoid null point issues was used by Mercuri et al. [101], where the Doppler radar was designed to operate in the phase-locked loop allowing the architecture to convert received signal to baseband directly.

4.1.3 Amplitude and Gain Error

Owing to the advantage of addressing the null point problem, a quadrature radar topology is used to produce two orthonormal I and Q channel output signals. The reflected data from a periodically and perpendicularly moving chest wall motion forms an arc of a circle followed by the estimation of the distance of the subject through combining the I and Q channel output and using an arctangent function [28]. However, imperfections in the radar components such as the difference between I and Q mixers and signal paths, and inaccuracy of the power splitter causes phase and amplitude imbalance. This causes an undesired linear transform and severely affect the orthonormal properties of I and Q channel outputs [102]. The extent of signal distortion depends on the imbalance between the I and Q channels. It results in the formation of an arc of an ellipse in place of an arc of the circle in the IQ plane.

To avoid signal distortion and accurate displacement estimation, these imbalances need to be measured and compensated before the demodulation with the arctangent function. Therefore, this imbalance compensation needs to be performed prior to the actual measurement of physiological signals. The study in [28] presented a method for measurement of imbalance factors and compensation through Gram-Schmidt procedure, to produce two orthonormal outputs. A voltage controllable phase shifter was introduced in either the LO or RF path. With a linearly increasing control voltage, each channel output becomes a sinusoidal wave at the Doppler frequency with a phase delay corresponding to its path delay. The comparison of sinusoidal and outputs

resulted in the highly accurate estimation of imbalance factors between channels with the advantage of no radar circuit board modification.

In the earlier experiments, the imbalance calibration has been done in a laboratory environment due to the required circuit modifications; however, with ellipse-fitting (geometric or algebraic) imbalance calibration method, the calibration can be performed on-site and periodically. Though the algebraic methods are fast, simple operations and do not require an initial guess, however, [103] owing to the substantial difference between algebraic and geometrical distances, in practical applications it was demonstrated that all algebraic fits, with or without constraints, are statistically inaccurate and biased, in one way or another. Geometric ellipse-fitting methods are iterative and minimize the orthogonal distance from the data points to their projections on the ellipse.

In recent developments [104], the geometric ellipse-fitting method is becoming computationally fast. The efficient levenberg-marquardt (LM) correction of the classical Gauss-Newton method is used in [105], and the method demonstrated that with a large arc length and low noise level, both the algebraic and LM ellipse-fitting methods could be used for imbalance estimation. However, for short arc length and in a noisy environment, the algebraic method results in biased imbalance estimates, whereas the LM method is unbiased and robust for noise. It was concluded that the LM method performs well in the ellipse-fitting problem in physiological sensing applications. However, the LM method provides a good estimation of imbalance, assuming the dominating noise sources in radar physiological sensing to be thermal noise and flicker noise in the receiver chain. However, the performance degrades for artefacts, such as respiration of a nearby person, that are superimposed to the radar signal.

In [106], the signal distortion issue is addressed by applying the artificial neural network (ANN) on raw radar signals eliminating the need for any preprocessing (demodulation, I/Q imbalance, or offset compensation) and avoided any impact of imbalance. The author developed a system for heart rate detection by directly coupling the CW Doppler radar with an ANN stage. The implementation of the shallow ANN within a microprocessor system is quite computationally inexpensive. However, the

experiment is performed in a confined environment with no moving object in the vicinity. Moreover, no exact information on the absolute position of the target could be found. Therefore, the method cannot be used for the estimation of vital sign for multiple people simultaneously.

4.1.4 Antenna Characteristics

The selection of transmitting and receiving antenna and its characteristics play a significant role in estimating the efficiency of the system. Depending on the antenna configuration either single elements or array, using conventional or alternative materials, the overall performance of a system may vary. The antenna performance depends on the infinite gain, lack of side or back lobes. However, in the context of NCVS applications, the due consideration must be given for the system sensitivity to environmental clutter, the small radar cross-section (RCS) and the lowpass signal characteristics.

In a comparative study, it was established that helical antenna because of high directivity and symmetry in H & E plane provided better accuracy as compared to Yagi, log-periodic, and patch antennas [32]. It was concluded that as broader beams are more susceptible to acquire clutter and noise, narrower beamwidth antennas are preferable for NCVS applications as they provide a better signal-to-noise ratio and result in high efficiency. In an extension to the study, a highly directive three helical antenna based phased-array system was designed and compared. It was concluded that the helical antenna could achieve better accuracy as compared to the patch antenna [34]. However, directive antennas lead to the higher power requirement, which again puts a limitation on the design. In another comparison study, to analyze the optimal design of antenna for UWB NCVS systems, different antennas were evaluated [107]. It was concluded that the Vivaldi antenna, which has a medium gain, a directive radiation pattern, and the best co and cross-polarization ratio performed best.

The high frequency increases the sensitivity of bio-signals, detectivity of imperceptible targets and shrinks the antenna size. Planar microstrip antennas tuned at such frequencies enable the low-cost, on-chip integration for portable applications. The

Figure 15: Signal interference due to multi-person, clutter, and motion artefacts

author in [108]-[112], designed the microstrip antenna (patch, horn, dipole) at different frequencies which offer the advantage of increase gain, decreased side-lobe level, and narrow beamwidth. The author [108] also reported that the circularly polarized antenna array in a multi-sensor network provides better isolation against interference than orthogonal linearly polarized antennas. Rabbani et al. [109] demonstrated that the detection range widely varies depending on whether a single antenna or dual antenna is used for transmission and reception. It was shown that their designed single antenna has good accuracy in vital signs' detection, but limited for a short-range of approximately 0.5 cm. However, with the dual antenna system with a separation of 20 cm between Tx and Rx antenna, the vital sign was successfully observed up to 200 cm.

Owing to the small RCS of around 0.5 m^2 for the human chest wall, the proper alignment of transceiver must be ensured to acquire signals with optimal SNR. For a fixed range, fixed-beam antennas require the calibration for every human due to its varying features such as height, body structure. To address the issue and achieve large detection range, an adaptive beamsteering antenna is used which can redirect the beam seeking for the best SNR without increasing the system size [113]. A $2x2$ microstrip patch antenna array and two-phase shifters were embedded on the same board to act as adaptive beamformer.

4.2 Signal Processing, Detection Algorithm, and Associated Challenges

The performance of the NCVS depends on the accurate extraction of HR and RR signals from a composite signal. The displacement in the reflected signal is minimum due to heartbeats as compared to the respiration. The second and third-order harmonics of RR signals are comparable in magnitude to HR fundamental frequency. The RR harmonics and the intermodulation between the heart rate and respiration signal make extraction of HR difficult, increases the complexity of signal processing and detection algorithm. The random body movement and clutter introduce noise in the signal, which is a hurdle in the design of an efficient detection algorithm for low SNR signals. The issue is pictorially represented in Fig. 15, where the red dotted line forms the clutter. It illustrates how high signal strength from these fixed objects diminishes the signal-to-noise ratio (SNR), consequently impacting the accuracy of range calculations. Multipath signals, whether combined constructively or destructively with the received signal, compound the impact on SNR. Given the non-linear nature of real-time signals, attempts to eliminate the influence of static clutter through techniques like frame differencing or background subtraction fall short of complete removal. However, moving clutter impacts differently than static as it creates disruption in phase. Various approaches have been investigated in the literature to address these challenges and to design an efficient and simple detection algorithm to extract RR and HR accurately.

4.2.1 Motion Artifacts Due to Random Body

Motion artifacts are inevitable in certain applications and cannot be ignored, such as baby monitoring or sleep apnea detection where the target may be moving. Since the signal from the random body movement is more substantial or at least comparable to the signal due to respiration and heartbeat, therefore it presents a critical noise source, which should be dealt with in the design of efficient and reliable NCVS detection.

Li et al. [100] suggest that the noise from the random body movement can be eliminated using the techniques based on the complex signal modulation and arctangent modulation using two transceivers. It was observed that the desired

physiological signals presented a phase modulation in the baseband signal and random body movement caused a random frequency drift in the baseband signal for the two-transceiver system. With complex signal demodulation, the two complex signals were multiplied to cancel out the random body effect and enhance the chest wall motion term. In arctangent demodulation, random body effect is cancelled out by adding the angular information from the front and back measurement. The critical issue using arctangent demodulation is the presence of baseband DC offset as it changes with the change in the environment and needs to be calibrated every time. It is observed that complex signal demodulation is more efficient when DC offset cannot be accurately determined and calibrated as this can be easily removed by averaging the signal over each time-domain sliding window. Although, the multiple radar system cancels the random body movement effects but suffers from system complexity and alignment issues of the subject with radar.

The same approach of using two radar is extended for the FMCW mode of operation. The FMCW radar has inherent range-resolution/gating characteristics that help in separating different range bins [114]. The idea is FMCW received signals from various body parts which are more than the radar resolution distance apart from the chest, occupy different range bins and hence can be filtered out [44].

A novel concept of harmonic radar is used where both fundamental (12 GHz) and second harmonic (24 GHz) are transmitted and received to create frequency diversity for vital sign detection and extraction [115]. An FFT algorithm and autocorrelation function are applied on both the received signal to extract the vital signs. Further, they experimentally improved the detection by using selective narrowband antenna than a wideband antenna. In another approach, first, the effect of body motion as a point target in the received signal is analyzed [116]. The baseband frequency spectrum is shifted in a positive or negative frequency axis as the subject moves towards or away from the radar, respectively. The random body movement is determined through a series of short period random time window. Then peak frequency was extracted in these small period time windows, and RR was estimated. Due to heavy interference, HR could not be extracted with accuracy from the designed system. Ye et al. [117] have used

another approach based on the sparse spectrum reconstruction, and zero-attracting sign least mean square (ZA-SLMS) to suppress strong noise and interferences from motion artifacts. The regulation parameter (REPA) was decided adaptively to reduce the effect of small motion artifacts. The moving average filter and background extraction technique were introduced [118]-[120], where the filtered output of the respiratory and body movement signal was subtracted from the original signal to extract the HR signal accurately.

4.2.2 Clutter

At the receiver, the reflected signal from the target is affected by the multipath fading, and reflection from objects, walls, and furniture in the surrounding. The unwanted echoes returned from the objects other than desired are termed as clutter and causes severe degradation of SNR and reduces the detection accuracy. It is required to implement an effective clutter suppression algorithm or technique for the measurement of small chest movement. Researchers have explored a series of approaches to suppress the clutter. In [121], the measurement is carried out from the human head to reduce the multiple reflected signal from the human torso and other body parts. The advantage of the method is that the head is assumed to be a single reflection point, and clutter from other limbs of the body falls in different bins.

In another study, the undesired echoes are also removed by utilizing the time-gating characteristics of the multiple-input and multiple-output (MIMO) configuration of the ultra-wideband radar array [45]. A simple approach to energy thresholding was used. The energy in the vital sign signal was observed over a time window and when the energy within the segment exceeded a threshold, then data from that time window was discarded treating it as a clutter signal. Alternatively, the background subtraction techniques like singular value decomposition, principal component analysis (PCA), and frame differencing are also applied to reduce the clutter significantly [119].

4.2.3 Interference Due to Strong Respiration Harmonics and Intermodulation Products

The heartbeat signal amplitude and frequency are characterized by displacement and the velocity of chest motion, respectively. The chest displacement varies between 4 to 12 mm and 0.2 to 0.5 mm for respiration and heartbeat, respectively. Similarly, 0.2-0.34 Hz & 1-1.34 Hz frequency variation are observed for RR & HR, respectively [122]. The HR signal is smaller in amplitude and slightly higher in frequency than the RR signal. Moreover, the second and third-order harmonics of RR signals are comparable in magnitude to HR fundamental frequency and cause interferences that cannot be filtered. Also, the HR estimation is affected by intermodulation products. When two different frequencies are passed through a nonlinear device, additional frequency tones are generated from a linear combination of these two frequencies. These additional frequency tones are called intermodulation frequencies. Some of the intermodulation products fall within the heartbeat frequency range, and as the level of the heartbeat component is very small, the heartbeat estimation becomes difficult and erroneous. It was emphasized that the impact of the third-order intermodulation product is considerable, especially when the chest wall movement due to respiration is large.

To address the issue, the author in [123], have used a filter for attenuating harmonics and intermodulation product called harmonic canceller or moving target indicator (MTI). The difference between the input signal and its delayed version (by one breathing pulse duration) was observed. As all the harmonic components of the breathing signal are periodic with breathing pulse duration, the harmonics are cancelled by the harmonic canceller. Similarly, a cascade of single delay filters with delay referenced to intermodulation frequencies was used to remove the influence of intermodulation products. However, static clutter could not be separated from Doppler signals with the design.

In another study [124], the author designed the nonlinear smart sensors utilizing the intermodulation frequency generated through a wearable tag. The 3rd-order tone generated by wearable tag along with the fundamental tone is backscattered towards

the receiver. The receiver amplified the desired 3rd-order tone and attenuated the fundamental and undesired 3rd-order intermodulation frequencies. The design was able to increase the relative intensity of the heartbeat signal as compared with the respiration signal along with the successful estimation of respiratory activities.

To avoid the issue of harmonics, the periodic variation of Doppler frequency, which depends on the chest wall movement and less affected by noise, motion artifacts, etc. was used for heartbeat extraction. This finding is utilized by [125] and employed the multi-resolution analysis using continuous wavelet transform. The periodicity in a specific frequency is extracted, and this periodicity infers the heartbeat. The estimation is not affected by the range of displacements and associated noise. In [126], the respiration signal was reconstructed from the spectral analysis of the received signal using the complex signal demodulation technique. The reconstructed respiration signal was subtracted from the original signal in the time domain to have harmonics free HR signal. However, the accuracy of the method governs by the accurate tuning of parameters of the reconstructed respiration signal to match the original respiration signal. Also, the interference due to harmonics becomes significant for an increase in the amplitude of every frequency component $(4.\pi.m_r.\lambda)$ of greater than 0.5. Different frequencies experiences different phase delay, which limits the effectiveness of the technique as the fundamental and higher harmonics cannot be cancelled simultaneously. In [37] double derivative of the signal is considered for the processing in place of taking direct displacement value. The amplitude of the double derivative of a frequency signal is higher by a multiple of ω^2 to the original signal. Then the peaks are obtained through the combined method of derivation and frequency-time phase regression (FTPR). The process resulted in improved detection performance and reduced the effect of respiration harmonics.

The peak detection algorithm was deployed to extract heart rate variability (HRV) from the RR dominated weak HR signals [127]. The high sampling rate reduces the requirement of the steeper cutoff for analog filters and provides a large resolution to address the harmonics issue [53]. Additionally, time-frequency analysis by short-time fourier transform (STFT) with a Gaussian window reduced the effect of RR harmonics

over weak HR signals. Nguyen et al. [40], [41] designed the harmonic path algorithm (HAPA) to find the equidistant three nodes and estimate HR frequency. The amplitude of higher-order RR harmonics is minimal in the range of frequencies of HR harmonics. Hence the HR harmonics are not affected by RR harmonics, and better accuracy was achieved. Further, the spectrum averaged harmonic path (SHAPA) algorithm was introduced to overcome the issues of the HAPA algorithm proposed in their earlier work. Hosseini et al. [47] designed a respiratory motion detection algorithm that utilized both time-varying delay and phase modulation. Finite impulse response (FIR) time-varying filter was used to find out HR, effectively dealing with RR harmonics through the selection of optimum FIR coefficients by discrete prolate spheroidal sequences (DPSS). The HR and RR originated components are separated in the time domain. Further to address the RR harmonics issue instantaneous frequency estimation based on local maxima was used. Hilbert-Huang transform (HHT) and Empirical mode decomposition (EMD) was used for the separation and extraction of HR & RR [43].

Sinharay et al. [128] observed that the larger chest wall displacement causes phase wrapping, which generates RR harmonics. If the wavelength is increased to limit the wrapping, tiny heart movements are missed out. Contrarily, if the wavelength is decreased to enhance sensitivity, phase wrapping introduces RR harmonics in the HR region. Amplitude modulation of a continuous wave (AMCW) was used to address the issue. Through AMCW, phase detection is decoupled from the carrier frequency, and RR harmonics are avoided simultaneously maintaining high sensitivity. However, the major challenge is the leakage power between transmitter and receiver, which produces the error in phase-detection.

4.2.4 Direct Current (DC) Offset and Noise Effects

The low SNR signals observe performance degradation due to DC offset clipping and other non-linearities of an amplifier at the receiving stages. Tan et al. [129] utilized the FIR filtering to address the challenge of low SNR signal. FIR filter with a Hamming window was used for filtering the high-frequency noise. Though the infinite impulse response (IIR) filters have steeper cutoff and better filtering efficiency; however, their use was avoided to reduce the distortion introduced by non-linear group delay. Mogi et al. [130]

applied STFT to the frequency band related to HR. Each frequency spectrum in the selected frequency band was integrated to remove the effect of noise. The peaks and RR intervals in the integrated spectrum were determined based on the threshold-based algorithm, and better efficiency was achieved for low SNR signals. Another approach of processing the signal through a vector subtraction method to remove background noise was deployed [39]. Time-interleaved samples of signal formed the original vector, and the data without transmitting the signal created noise vector. The noise vector was subtracted from the original vector to get a high SNR signal vector. A similar approach of the mean subtraction method was also used for DC offset and noise removal [131].

The Tx-Rx leakage occurs due to inefficient isolation capability of circulators, feeder leakage, mismatch in antenna and spatial paths between antennas [132]. As the leakage power is typically much higher than that of returned signals, LNA can be saturated. Moreover, the dynamic range of FMCW radar is also limited by phase noise leakage. [133] demonstrated use of the down-conversion technique in which the frequency and the constant phase information of the beat signal of the leakage was extracted in the digital IF domain. [134] described that the Tx-Rx leakage is caused by the spectral leakage because of the antenna coupling of FMCW radar causes a DC offset. This DC offset needs to be corrected to obtain error-free phase variations. The efficient gradient descent algorithm is employed to achieve dynamic DC offset tracking and performing DC offset correction [135]. In [89] it was emphasized that prior to the arctangent demodulation, this DC offset must be accurately calibrated, which relies on the accurate estimation of the centre of the arc traced by the detected motion.

The algorithms, such as Levenberg-marquard algorithm [136], L1-norm-based algorithm [137], least squares [138], and gradient descent [139], have been used for the centre tracking. However, for a smaller arc length as compared to the wavelength of the operating frequency challenge still exists to track the centre of the arc accurately. The work [140] demonstrated that the arc length is comparable for higher frequency operation owing to the smaller wavelength even if the chest wall motions are small in magnitude, i.e. target at larger range from radar sensor. If the arc length resulted from

the phase change is relatively short, a linear demodulation method may be a more accurate choice [141].

The source of DC offset at the output of the RF front-end may be due to the direct coupling of the transmitter to receiver and circuit imperfections such as the self-mixing of local oscillators and interferers. This DC offset may cause saturation or limitation of the dynamic range of the following stages of baseband amplifiers. AC coupling is proposed as a solution where the capacitors have been commonly placed between the RF output and baseband amplifiers. However, due to the high-pass characteristics of the coupling capacitor, AC coupling leads to significant signal distortion because the chest wall motion has a very low frequency and amplitude. A high RF-LO isolation mixer [142] was used to employ DC coupling in the system. The approach was complex to implement and was not able to remove DC offsets completely. The authors [143] designed a radar sensor with DC-coupled adaptive tuning architecture which allow the operation of baseband amplifiers with sufficiently high gain. An RF coarse-tuning signal path was added at the RF front end to remove most of the DC offset, and a baseband fine-tuning feedback patch was added to calibrate the remaining DC offset and achieve the largest dynamic range. The fine-tuning baseband architecture adaptively adjusts amplifier bias to a level that allows both high gain amplification and maximum dynamic range.

4.2.5 Influence of Digital Filtering and Sampling Rate

In [144], electrophysiological data were analysed, and it was emphasized that the improvement of the signal-to-noise ratio must be considered at the first stage. At the recording stage of data, it must be ensured to collect higher numbers of trials and reduction of noise. Even after this, in most conditions, filtering will nevertheless be necessary to analyze the data of such electrophysiological signals. Filtering can result in significant distortions of the time course (and amplitude) of a signal. To address the issue, the filter type and parameters must be thoroughly analyzed to minimize filter artifacts. In vital sign NCVS systems, the working principle is based on analyzing phase delay, for which it is necessary to unwrap' the phase response. Any phase distortion introduced by the digital filter during signal processing amounts to the signal distortion.

The bandwidth of the signal must be taken into consideration such that the passband of the digital filter corresponds to the frequency interval over which the phase response is approximately linear. Digital filters are used for the processing of different frequencies within electrophysiological signals. However, the changes are induced in the phases of different frequencies. These phase shifts lead to a disruption of the timing information between different frequencies within the same signal and between different signals. Moreover, the use of high frequency would be beneficial because of the increased phase modulation; however, as the simulations and measurements presented in the paper mentioned some distortion effects also become magnified when increasing the frequency [145]. The phase extraction algorithm must address the issue while using the high-frequency radar for vital sign estimation.

The radar reflected signal contains not only vital sign information but also the clutter from the environment and the static parts of the human body. For removal of the signal part due to unwanted clutter, loopback filter-based technique is used [146]. As the breathing harmonicas may overshadow the heart frequencies, notch filters are utilized to eliminate the breathing harmonics [147]. However, if the breathing harmonics are located very close to the HR, then the notch filter-based solution would suppress HR and would pose a challenge. [134] emphasized that compressive sensing based on orthogonal matching pursuit based processing offered more accuracy than the serially-cascaded Bi-Quad IIR filter based two bandpass filter design. The bandpass filter-based design has low accuracy due to the passband noise and harmonic interference. The use of compressed sensing orthogonal matching pursuit (CS-OMP) improved accuracy by about 7% for HR, and 4% for RR.

The work [148]-[150] described that fast signal processing is a critical issue for the NCVS system based on FMCW radar. As the chest wall motion are very small in amplitude and consequently to get higher SNR, high-speed sampling is required during analog to digital conversion. However, the high sampling rate generates massive data for processing and reduces performance in the real-time. Sampling rate conversion (SRC) along with different digital down converter (DDC) structures have been

implemented to combat the issue. However, designing appropriate filters and structures is a critical design issue for the scheme.

The author [150] presented an efficient demodulation method designed for FMCW, which is a modified DFT (IDFT) algorithm. The algorithm can extract the spectrum segment of interest from the original signal without calculating the whole DFT/FFT. It provides fast demodulation and extraction of desired frequency bands without computation complexity. The desired low sampling rate conversion could be achieved with the combination of forward and backward structure. The digitization of high-frequency carrier signals requires very high sampling rates for ADC and the requirements for ADC clock and aperture jitter become more stringent. Therefore, the frequency translations to lower intermediate frequencies are required for radar received signals for an NCVS system [44]. The issue of group delay introduction by a digital filter during processing was addressed through a digital down-conversion technique which takes a band-limited high-sample-rate digitized signal, shifts the band of interest to a lower frequency and reduces the sample rate while retaining all the information.

In [146], the electrophysiological signals are processed through low pass filtering to temporally smoothing and removing the noise. However, the in-band noise remains intact. These filters have zero phase-lag, thus the issue of the event being smeared out in time appears. It was concluded that raw data should be analyzed directly, without filtering but with artefact rejection if required. The filtering may be avoided for analyzing any temporal dynamics related to the signal.

The authors in [151] demonstrated the heart sound detection using radar systems to measure heart rate variability (HRV). It was described that the heart sounds, caused by muscle contraction and valve closures minimally transit the body as a sound wave. These sounds propagate as a mechanical wave along arteries and vessel walls and generate vibrations of the body surface. Hence a six-port radar system was used to detect both cardio-physiological effects, i.e. heart sounds in addition to the pulse wave component. The detection of heart sounds considerably enhanced radar-based heartbeat detection. As the heart sounds were expected in the range of 16-80 Hz, a

fourth-order Butterworth filter with a passband of 16-80 Hz was used to extract the heart sounds. Subsequently, the logistic regression hidden semi-markov model (HSMM) based algorithm was used to extract heartbeat.

4.2.6 Signal Processing Algorithm

Both the HR and RR need to be extracted from the received data. Various signal processing algorithms are employed, each having its own advantages and limitations. The most straightforward approach to extract the HR and RR was to use FFT over a length of phase signal and find the peaks in the spectrum. However, the detection performance is degraded due to the leakage problem caused by the limited data length of the Fourier transform. The Fourier transform requires the invariability of vital signals over a small duration. If the vital sign varies over time, the FFT algorithms, are invalid and extraction performance degrades substantially.

A parametric and cyclic optimization-based approach called RELAX algorithm was proposed to address the aforementioned problem [152]. The algorithm used the continuous wavelet transform based synchro-squeezing transform (SST) to extract time-varying vital signs. However, the SST is not much beneficial for high frequency and large varying noise signals [131]. In an extension to the earlier study, the auto-correlation and FTPR approach is combined [131]. It was used to extract weak HR from the RR harmonics dominated signal. Lee et al. [15] also addressed FFT smearing and leakage issues by using multiple signal classification (MUSIC) algorithms. The algorithm analyzed the signals using signal subspace and noise space through the use of the Eigenvalues and Eigen matrix from the autocorrelation output matrix. The MUSIC algorithm observes difficulty in selecting an adequate number of signal subspaces and is computationally expensive.

The time-domain processing of the signal reduces the computational load of the system as compared to the frequency-based processing. The authors in [153] used six-port radar with cross-correlation based template matching algorithm for detection of the instantaneous heartbeat. The design offered the detection of a heartbeat without delay and with a very small observation window of 8 to 12 seconds.

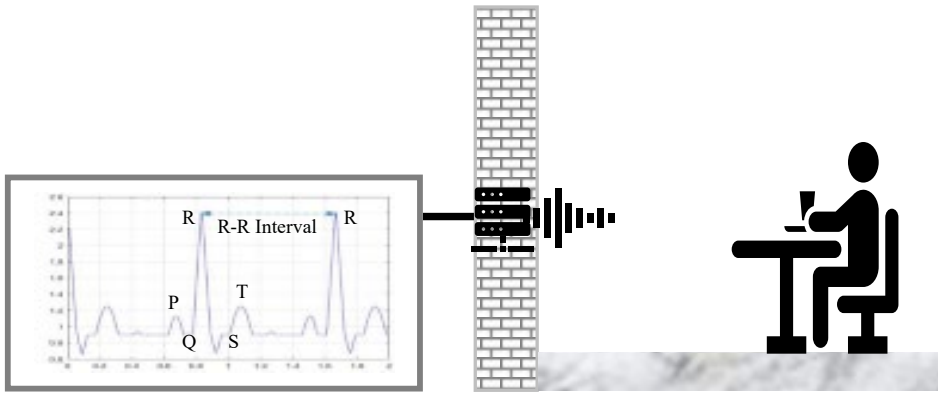

Figure 16: Present state-of-art

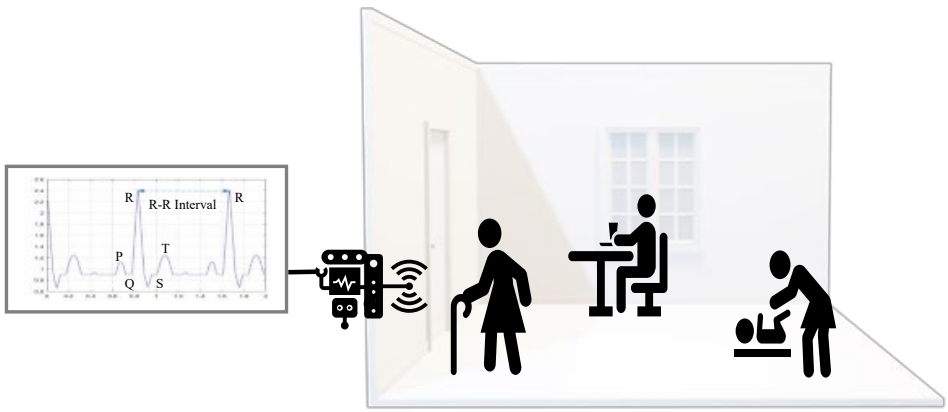

Figure 17: Realistic scenario

However, the tests were conducted with the subjects holding breath and study was limited to detection of heart rate and respiration rate was not analyzed. Moreover, the accuracy of measurements depends on the template of the heartbeat wave through which the matching of a real-time signal is performed. The effect of the physiological behavior of the cardiovascular system, as well as the effects due to the antenna characteristics and filtering on heartbeat template was presented in an extended study [51]. It was concluded that the cardio-physiological effect over different heartbeat wave template was caused due to local pulse waves called sphygmograms which are the depiction of pressure over time in an artery.

It was demonstrated that as a narrow bandpass filter is used to determine the heartbeat from the measured radar signal, the heartbeat templates should be generated through narrow bandpass characteristics and with highly focused narrow-beam antenna characteristics. Yang et al. [154] used a two-stage analog bandpass filter (BPF) for the time-domain peak detection to extract HR and RR.

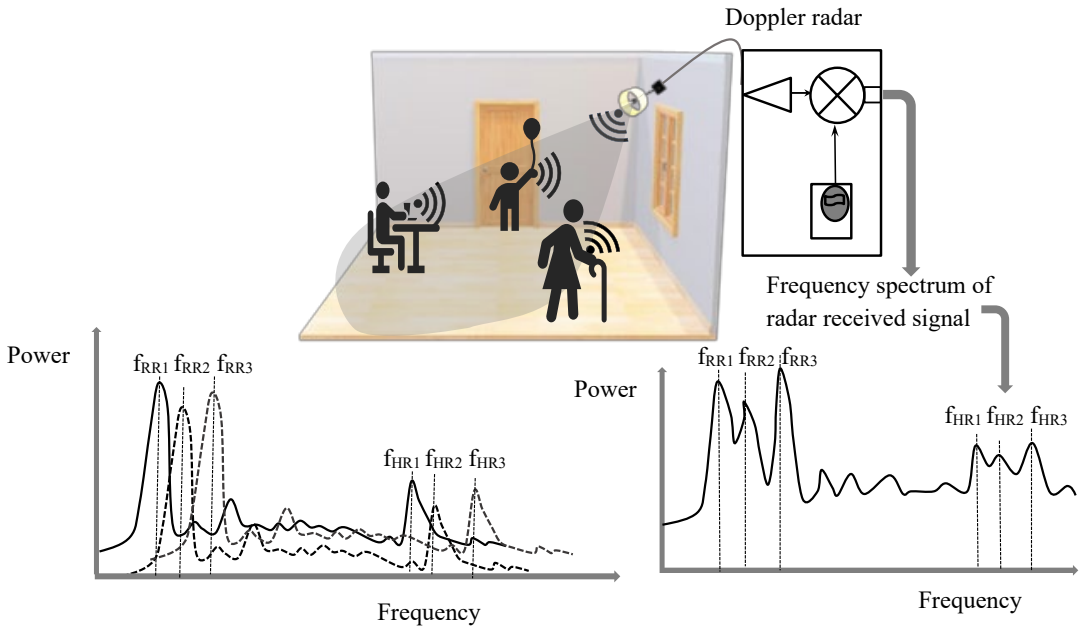

Figure 18: NCVS system for multiple person: visualizing the scenario of without phase collision and with phase collision.

Through the first stage of BPF, the signal was filtered for RR frequencies, and the time interval in the peaks of the signal was used to estimate RR. Similarly, in the second stage of BPF filters, the HR frequencies dominated signal, and the time interval in peaks of the signal determined the HR. Zakrzewski et al. [155] improved the nonlinear demodulation, i.e., arctangent demodulation with centre estimation algorithm using the levenberg-marquardt (LM) method. The park and Yuan-Forg method were also evaluated, but the LM method was proved to be more accurate with the low computational load.

5. Challenges for Multi-Resident Vital Sign Detection

Most of the studies have been conducted in a lab environment with a static target in the proximity of a radar sensor, as shown in Fig. 16. These systems offer good results in a controlled environment, but real scenarios imply new challenges. In a realistic scenario, there is a high probability that the patient may be accompanied by another person such as a nurse or attendants, older adults with caretakers, and babies with the parent, as depicted in Fig. 17. In such a situation, the present proposed vital sign monitoring system ceases to perform. To extend the adaptability of vital sign monitoring systems in all practical scenarios, the design needs to be conceptualized and verified for the multi-

resident environment. Recently, [14], [33], [45], proposed the methods to address the issue, which can be extended further to make the system meaningful and practical, hence bridging the gap between adaptation to the real world and the laboratory setup.

The principle behind the vital sign measurement of multiple people is first to localize the target, and then individual phase information is extracted to retrieve the vital sign information of an individual. The localization of the target means separating the individual in the range-angle plane. High angular resolution is required for localizing the multiple targets to detect the individual's vital signs accurately. A highly directional beam provides a large angle resolution, which is necessary to distinguish the target in different range bins. However, the realization of a highly directional beam and scanning the environment locally requires a large number of antenna structures if steered mechanically or more complex algorithms are needed for digital beam-steering. The increased hardware complexity and requirement of a high computational signal processing algorithm governs the practical realization of the minimum beamwidth antenna structure. Therefore, within a practically realized system, it shall probably be inevitable to have the targets close enough in the same range-angle coordinates.

Moreover, if the targets are close enough (comparable to the theoretical resolution limit), then the vital information for each individual will be in the same steered beam as depicted in Fig. 18, which becomes difficult to separate [156]. In Fig. 18, the first phase spectrum is shown where the targets are at such angular distance apart that no phase collision occurs, and the desired signals are easily distinguishable. The second spectrum shows the situation of the phase collision that occurred in the received signal. Here, the reflection from all the targets collides and distorted the spectrum. Moreover, in most of the situation, the desired signal is masked by the noise and interferences. Another challenge in the vital sign detection is the source separation. Due to the path loss and multipath fading, the signals from the rear target is relatively weak. When the two targets are relatively close within the resolution limit, it becomes difficult to differentiate one from another. Even with the successful extraction of the vital signs, it is computationally expensive to assign the detected vital sign to the correct target. Recent research development in the field has shown that this can be achieved by

either hardware solution where MIMO configuration of sensors is used [45] or by robust signal processing and feature extraction algorithm (multi-person tracking algorithm) that separates the target in different range bin [157].

The choice of the RF carrier signal with modulation schemes like linear FMCW, stepped frequency, frequency shift keying (FSK), etc. makes it possible to obtain absolute range bin for human tracking and localization.

In [158], the phase information is obtained by FFT, and the parametric spectral estimation is applied for the range, which results in high accuracy and resolution. The range information is useful in finding the number of targets in the field of view and calculating their respective distance from the radar sensor. While the phase information determines the change in phase caused by the micro-doppler effect due to each target's cardiac activity. This information is combined to extract the vital sign by using the auto-regression (AR) method. Also, range integration of the signal is performed to reduce mutual interference. The FFT and MUSIC algorithm are applied in conjunction as the conventional FFT method is not enough to extract the beat frequency for multiple targets due to the overlapped main lobes and MUSIC algorithm alone is unable to provide necessary phase information. Although the proposed method gives good results, still some issues must be considered for practical application. The first problem is clutter suppression. Since the MUSIC algorithm is incapable of providing the phase information, therefore, cannot separate the stationary clutter. The standard deviation of phase information can utilize the micro-doppler effects and distinguish the moving targets from a stationary one.

Another issue is the motion artifacts as the signal due to body movement is stronger than the vital sign that makes the detection difficult [67]. The presence of the significant sidelobes in the spectrum creates the target's ghost image, which further degrades the performance. The problem can be overcome with a high gain antenna to suppress the side lobes, and power is concentrated towards the main lobe.

The MIMO technique of wireless communication is utilized to achieve the vital sign monitoring of multiple people [45]. The transmitting antenna array transmits an

FMCW signal in a time-division multiplexing mode. The scattered signal is received over multiple channels that separate the target in the range-azimuth plane. In this manner, the different range bin corresponding to each person is identified. Depending on the relative distance between targets and receiver elements, an additional phase shift occurs. For each Tx-Rx pair, two-step FFT is performed. First, the range FFT is applied to separate the different range bin from each other. Second FFT separates the objects within the same range bin but are at a different angle means mapping different subjects in the range-azimuth plane. Phase values are extracted over the slow-time axis for each range-azimuth range bin, and after performing a sequence of signal processing, the vital signs are estimated. This arrangement worked well under the constraint that the targets should be in the same range-angle bin for the entire experiment time. The requirement of targets to be practically stationary, random body movement, effective cancellation of RR harmonics over HR and robustness of measurements in clutter environment are some research challenges, yet to be addressed.

Recently Marco et al. [33] observed that moving targets affect the transmitting and receiving signals from stationary objects. It generates the phase and amplitude modulations in the reflected signals from stationary objects. This makes target detection difficult in the presence of stationary clutter in an indoor environment, mainly due to the presence of household, tables, etc. An algorithm was designed utilizing the range bin, phase change in range bins, and range speed matrix. A draft path matrix was formed to track the targets. The effect of random body movement was removed by first locating the artifacts using continuous wavelet transform and then suppressing these with moving average filter. The system consists of only one transmitter and one receiver configuration. The experiments were carried out in an office setting with the moderate and vigorous movement of targets. Reasonable results were achieved with the moderate movements of the target, but vital sign signals were lost during vigorous target movement, and subsequently, the system picks up the signal as the target movement reduced and remain locked on the same target.

In most of the studies, the localization of targets was achieved based on the amount of received power from different targets. However, using FMCW as a filter,

multiple targets are isolated into different frequency bins depending on the arrival time of a received signal [14]. The use of filters also isolated some of the body parts' movements as they occupy different frequency bins. Linear regression on the phase of the complex time-domain signal is used in extracting the single dominant frequency of the signal [159]. This concept was used to successfully extracting the breathing and heart rate from the range bins isolated earlier.

Hilbert vibration decomposition method was used to decompose the vibrating components into the lower frequencies in the signal [160]. The algorithm worked on baseband received signal and extracted the largest energy signal around which the signal oscillates [161]. The algorithm extracted the dominant breathing rate with better accuracy. Similarly, the distance spectrum, i.e. the power spectrum of the received signal represented in terms of distance, was calculated through FFT application. Applying the FIR filter over the peak detected in the distance spectrum, the distance and small oscillating displacements are extracted [162]. The sampling rate is limited for practical implementation, and hence the range profiles obtained from FFT/IFFT are limited in range resolution. Moreover, the peak detection algorithm for FFT offers limited performance for multiple targets in close vicinity to each other [163], [164].

Though the range resolution of the MUSIC algorithm is much higher as compared to the conventional IFFT techniques, it is priced with considerable computational complexity [118], [165]. The latest approaches of the Hilbert vibration decomposition algorithm have the advantage of self-adaptation and better ability of decomposition to similar frequencies; however, the performance is limited in the presence of super harmonics in the signal. Moreover, the computational complexity is also very high [160], [166].

Zhang et al. [167] exploit the stepped-frequency continuous-wave (SFCW) radar, which offers the benefits of small size, low power consumption for continuous vital sign monitoring. The different parameters are optimized for high precision and accuracy for multi-target. The results show that to obtain a high range resolution; the SFCW radar system should be designed with high centre frequency, smaller frequency step, large bandwidth, sufficient antenna beamwidth, and a suitable elevation angle. Single-

conversion continuous-wave (SCSFCW) radar which is a combination of SFCW radar and a self-injection-locked (SIL) radar are proposed to obtain high range resolution up to 15 cm [168]. Lee et al. [169] proposed improvement of range resolution through the use of a modified waveform that doubles the bandwidth and subsequently improved the resolution.

The RF waves travel at a speed of light and hence the differences in reflection time are of the order of picoseconds which is very difficult to measure the wavelength, which tends to increase the phase difference and make the detection process more efficient [72]. The higher frequency offers large bandwidth. The bandwidth has a direct consequence on the range precisely for the localization of targets closer than one foot.

The FMCW technique provides the mapping of time differences into corresponding shifts in the carrier frequency. Thus, it makes the measurement simple as the frequency shifts are easy to measure. Another challenge is of multipath effects due to the reflection of the transmitted signal from walls and furniture. The reflections from multiple humans and some static objects are complex and pose a significant challenge in localization of targets in indoor settings. Some recent research works are addressing these challenges, yet the architecture design, the complexity of signal processing algorithm, clutter due to relative movement of target and objects are some of the main areas that need to be dealt for efficient localization and tracking of multiple targets.

6. Summary and Future Direction

Since the early 1970s to date, technological advancements have made it possible to implement the radar sensing on a single chip with low power and low-cost solutions. For NCVS monitoring, the radar-based systems have gained momentum after 2010, and the studies have shown an increasing trend within recent years. Current research efforts are towards producing an NCVS device that is comparable to ECG accuracy, and at the same time power-efficient, smaller in size, robust and reliable for practical applications.

Table 4: Summarized description of methods for addressing the issues in NCVS

Issues in NVCS	Method	Advantage	Limitation
Null Point	1. Double-sideband transmission [95] 2. Vector network analyzer [72] 3. Phase-locked loop (PLL) in VCO [101]	1. Null point at larger separation 2. Simple installation, easy frequency tuning 3. Direct baseband conversion of received signal, avoids IQ unbalance and DC offset	1. Increases the power and bandwidth requirement, require small angle approximation 2. Slow in processing the sweep over complete signal 3. Trade-off between stability of PLL and gain error
Clutter	1. Measurement through Human Head [121] 2. MIMO configuration of radar array + Energy Thresholding [45] 3. Background Subtraction Technique (PCA, Singular Value decomposition, Frame differencing) [119]	1. Single point reflection avoiding reflection from the same range bin 2. High angular resolution, used for multiple people 3. Clutter due to antenna coupling also reduced	1. Limited accuracy, constrained target position 2. Time division multiplexing (TDM) MIMO configuration increases complexity 3. Re-calibration of background signal is required with change dynamics of indoor environment
Motion Artefacts	1. Phase Cancelation using multiple Radar [179] 2. Complex signal demodulation [100] 3. Harmonic Radar [115] 4. Moving Average Filter [175]	1. Remove null point effect 2. Robust against DC offset 3. High sensitivity for HR detection 4. Robust against DC offset	1. System complexity and alignment issue 2. Affected by harmonic and inter-modulation interference 3. Precise frequency stability is required 4. Trade-off between window length, accuracy and processing complexity
RR harmonic interference	1. Periodicity of doppler frequency due to velocity of chest movement [125] 2. Reconstruction and subtraction [126] 3. Double derivative of the signal [180] 4. Time-frequency analysis [53] 5. FIR time varying filter [47] 6. AMCW [128] 7. Signal Processing Algorithm a. Viterbi Algorithm [176] b. Zero-attracting sign least-mean-square (ZA-SLMS) algorithm [117] c. Ensemble empirical mode decomposition (EEMD) [43] d. Adaptive noise cancelation (ANC) [181] e. Variational mode decomposition (VMD) algorithm [171] f. Peak Detection algorithm [127, 175] g. HAPA, SHAPA [40, 41]	1. Limitation in phase variation extraction is avoided 2. Weak higher order BR harmonics can also be removed 3. Requires minimum processing and power consumption 4. Simple, Low computational cost 5. Narrowband processing removes other interferences 6. Antenna size is decoupled from sensitivity 7. Signal Processing Algorithm a. Less processing time b. Large spectral resolution c. Fully adaptive and very simple decomposition algorithm d. Simple and less processing time e. Small computations and can be implemented in embedded systems f. Simplest and fastest processing method g. Low sampling rate and low cost	1. Method is limited for HR detection only; parameter needs to be changed for BR 2. Accuracy depends on reconstructed respiration signal 3. Differentiation introduces numerical instability 4. Requirement to hold the breathing for the measurement duration 5. Complex processing 6. Stability of modulating signal limits the performance 7. Signal processing Algorithm a. Complexity increases manifold if monitoring duration increases b. Trade-off between gradient correction and spectrum sparse penalty affects the accuracy c. Lack of dynamic motion compensation and cannot address the motion artefacts issues. d. Instability for large noise such as motion artefacts e. Large noise affects the accuracy f. Works satisfactorily only for high SNR g. Erroneous results for large heart rate variability cases

Table 5: Current status of the NCVS for multi-person

Author	Frequency	Radar Type	Localization Method	Vital Sign Extraction	Targets	Range	Performance Parameter	Limitations
Ahmed, 2018 [45]	77 GHz	FMCW	Range gating using MIMO radar and Beamforming	Range FFT - range bins Second FFT - separate targets in same range bin	Two targets in same range bin (1m) with angular separation of 60°	1m	-	-Targets should stay in the same angle-range bin for the measurement time -Impact of motion artifacts, clutter, and radar movement
Lee, 2019 [158]	24 GHz	FMCW	Parametric spectral estimation	Auto-regressive algorithm + MUSIC	Two stationary targets in sitting position	Range resolution limited to 40cm Targets' distance varies between 130 to 300 cm from radar	Avg. accuracy more than 98%	-Interference due to clutter and motion artefacts -Insufficient sidelobe suppression generates ghost target
Marco, 2019 [33]	7.3 GHz	FMCW	Tracking algorithm based on range bin and range-speed profile using FFT	Linear demodulation + FFT+ Continuous wavelet transform	Two targets in different walking scenario in a well-setup-controlled environment	Range resolution 20 cm and range 2.6 m and 5.4 m	Avg. accuracy RR: 94 % HR: 88 %	-Subjects to be in quasi-stationary state
Adib, 2015 [14]	5.8 GHz	FMCW	FMCW technique as a filter	FFT	Three quasi-stationary targets	Range 1 m to 8 m	Avg. Accuracy RR:99 % HR:98 %	-Targets are quasi-static - 1-2 m Range resolution required for high accuracy
Sheikh, 2018 [164]	24 GHz	Monopulse	Phase comparison monopulse technique to find DOA	FFT+FIR filter	Two stationary targets	Range 1 m Angular resolution 30°	RR (Normal):78%	-Accuracy decreases drastically for slow and fast breathing case
Lu 2019 [163]	24-27 GHz	CW radar with metamaterial (MTM) leaky wave antennas (LWAs)	Angular space scanning using frequency-space mapping characteristic of MTM LWAs	FFT+ Butterworth High-pass filter	Two stationary targets	-	RR:92% HR:95%	-Stationary targets -Resolution depends on the precise beam angle formation of leaky wave antennas

Various radar topology has been used in the NCVS system. However, FMCW has the advantage of inherent range-gating capability that can separate the multiple targets in different frequency bins. Apart from the radar type, antenna design also has an impact on system performance. High gain antenna improves the SNR of the received signal that increases the sensitivity of the receiver. On the other hand, the highly directive antenna is desired to reduce the effect of clutter.

Other aspects that have a significant impact on system performance are phase noise and offset error, multipath fading, gain, phase error in quadrature demodulation, and non-idealities of ADC dynamic range fitting. Different techniques and robust signal processing algorithms have been studied to address these mentioned issues and for extraction of the HR parameter with better accuracy are summarized in Table 4. The limitation associated with each technique and method opens further research avenue to improve the performance.

Over the evolution period of NCVS, different frequencies have been used to achieve the desired performance. The selection of transmission power and type of radar technology has an impact on the range and accuracy of the system. Table 3 gives an overview of system performance over different frequencies, transmission power, and type of radar technology used in the different scenarios as reported in the literature. We cannot estimate the explicit relation between the operating frequency and the performance of the system as it is highly influenced by the choice of hardware and signal processing algorithm. However, higher frequency gives large bandwidth, resulting in high resolution and hence accurate detection. Therefore, the trend is from lower ISM band to higher frequency and now towards mmWave. Due to the small wavelength, mmWave radar offers the advantage of a smaller footprint which is a crucial factor for implementing a low power single-chip device. Most of the reviewed literature have experimented within a range of 0.5 to 2 m with reference to the target. The measurement accuracy degrades with an increase in the range [14], [33].

Owing to an average floor area per room as 17.7 m^2 [170], for a practical NCVS system, the targets usually are within a distance range of 4 to 5 m. Therefore, the thrust on increasing the measurement range is a critical requirement to deploy the NCVS

system practically. Almost all experiments are performed in a controlled lab environment with a well-defined pathway or distance. In the clinic or home environment, there is the possibility of other persons and objects, causing the clutter interference in the desired vital signal. Even the small body movement or the presence of other moving objects in the room causes the noise comparable or even stronger than the feeble physiological chest wall movement. In such a situation, the present vital sign monitoring system ceases to perform. The vital sign monitoring in a multi-resident environment opens tremendous opportunities in a different application.

The current status of the techniques used for multi-person vital sign detection, performance parameters and associated challenges are summarized in Table 5. To extend the adaptability of vital sign monitoring systems in all practical scenarios, the design needs to be conceptualized and verified for multi-resident environments. Though, various algorithms have been explored for the detection of vital signs for multiple people but are priced with the limitations, as mentioned in Table 4. Referring to Table 4, the experiments are performed in a controlled environment where targets are either static or quasi-static. Also, the multipath effects due to the reflection of transmitted signals from walls and furniture, the complex reflections from multiple humans pose a significant challenge in the localization of targets in an indoor setting. The architecture design and signal processing algorithm are some of the main areas that need to be dealt with for efficient localization and tracking of multiple targets.

The beamforming technique adopted from wireless communications offers the two-fold advantage of improving SNR and provide better angle resolution and hence spatial filtering. The technique may be beneficial to address the challenge of a multi-resident NCVS measurement system. The contribution of this review article towards scientific research society considering radar-based non-contact measuring systems is:

- Different topologies, architectures of NCVS radar and an overview of the radar operational principle to design a non-contact measurement system is presented.
- The implication of mmWave exposure on human health and the effect of environmental attenuation is analyzed and discussed. The review added that there

is a shift towards mmWave frequencies in system design owing to the immense advantages of larger bandwidth of mmWave transmission.

- The review described the research challenges associated with the hardware and signal processing for practical deployment of the NCVS system.
- The review emphasized that the measurement range is limited within 0.5-2 m mainly, and the accuracy decreases drastically if the range is increased further. The detection range can be increased using a high gain antenna.
- The radar system with high power and frequency has higher sensitivity and better resolution. However, the null point problem is enhanced by smaller wavelengths, and high power decreases the safety margin of EM wave radiation.
- Though the power level for transmissions was kept under the safe limits yet to minimize the effects of long-term exposure to the EM wave, a system with minimum power requirement or integration with wi-fi and other daily used devices should be focused on future work.
- The implementation challenges for the multi-resident scenario is discussed in detail. The review emphasized that most of the studies are focussed on detecting vital signs for a single stationary user. However, in a practical scenario, multiple people (mobile or stationary) shall be present in the environment.
- Most of the literature have experimentally verified the design with small datasets in a controlled environment. A vast scope exists for a prolonged trail and with a different group of subjects to check the reliability and robustness of systems while considering device aging and changes in the environment.

7. Conclusion

A technological review on the current state-of-art of radar technology for vital sign measurement is presented, which would be informative for future research into the multi-resident scenarios. The research challenges associated with hardware and signal processing are highlighted for a multi-resident environment. Heart rate and respiration rate measurement through non-contact methods have immense potential in applications such as sleep apnea, sudden infant deaths and the ever-increasing demand for home care. Doppler radar-based NCVS detection systems can be deployed for long

term monitoring with high reliability and accuracy. The recent approaches of designing an NCVS system for multiple persons opens immense possibilities toward the practical realization and adaptation in a realistic scenario. However, motion artifacts, clutter, choice of frequency, efficient detection algorithm to address RR harmonics and noise-related issues are some areas that require extensive investigation for wide commercial applications

Chapter 3

Modelling of Chest Wall Motion for Cardiorespiratory Activity for Radar-Based NCVS Systems

Abstract

Chest wall motion can provide information on critical vital signs, including respiration and heartbeat. Mathematical modelling of chest wall motion can reduce an extensive requirement of human testing in the development of many biomedical applications. In this paper, we propose a mathematical model that simulates a chest wall motion due to cardiorespiratory activity. Chest wall motion due to respiration is simulated based on the optimal chemical–mechanical respiratory control-based mechanics. The theory of relaxation oscillation system is applied to model the motion due to cardiac activity. The proposed mathematical chest wall model can be utilized in designing and optimizing different design parameters for radar-based non-contact vital sign (NCVS) systems.

This contribution has been accepted for publication in Sensors Journal

1. Introduction

Continuous monitoring of vital signs, namely respiration and heartbeat, can provide information in predicting the undesired events like cardiac arrest, critical dizziness, arrhythmias, cardiac rhythm, temperature regulation, synchronization with respiration rate [4]. The continuous monitoring can be achieved either through contact (wearable) sensors or non-contact (radar) sensors. It is not practical to use wearable sensors 24/7 throughout the year. One of the alternative solutions for long term continuous monitoring is using radar-based sensors [14]. The monitoring of surface chest wall motion can provide vital signs information which can be useful in many applications e.g., designing a radar-based non-contact vital sign system for long term home health care and sleep monitoring. Another application of modelling chest wall motion due to respiratory signals is to study the radiotherapy for treating a lung tumor. The main issue in radiotherapy is that a lung tumor may move due to respiration. From existing studies, it is observed that chest wall motion is associated with tumor movements; therefore, it can help in predicting the tumor position [182].

The radar-based system for vital sign detection is developed based on movements of a target, i.e., chest wall motion due to respiration and cardiac activity. Chest wall displacement with respect to time is reflected in the phase variation in the received signals. Subsequently, the modelling accuracy of non-contact vital sign (NCVS) systems depends on the modelling of chest wall motion with respect to time, i.e., the shape of the chest wall motion.

The performance and testing of a robust design depend on the analysis and strength of the experimental dataset available. Though a larger and exhaustive dataset produces an opportunity for the design to be tested and analyzed in all possible scenarios, it would require a considerable number of real-time experiments. It not only consumes time, costs, and power but is also impractical for participating subjects. This can efficiently be managed through simulation and mathematical modelling. In earlier works related to radar-based systems, many researchers conducted exhaustive experiments for analyzing radar-received signals [14]. However, any change in design

parameter or experimental scenarios like change in subject position, movement, and presence of multiple subjects, then reconducting all experiments are required. Additionally, fewer efforts have been made for modelling the chest wall motion due to respiration and heart activity.

In literature, most of the simulation for radar-based NCVS systems to date are based on a simplistic approach of assuming chest wall motion as sinusoidal [16], [61]. The respiration model presented by Fouladi et al. [183] follows the sinusoidal pattern for a periodic breathing activity. The airflow was taken as sinusoidal, and consequently, the time integration of airflow produces the lung volume variation pattern during breathing activity which represents the chest wall movement [184]. However, the main issue is the cusp at the peak after inhalation, which offered a substantial variation of simulation wave with real signals. This inferred that the pure sinusoidal functional model suffers from significant deviation during real-life breathing and modelled breathing pattern. Another model based on the duty cycle, depending on the inhalation and exhalation phases was presented by Li et al. [185]. Primarily three models referenced to duty cycle are designed to model respiratory signals based on cosine function (CM) [186], [187], the absolute value of cosine function (ACM) [188], and even power of cosine function (EPCM) [189]-[191].

The selection of the order of EPCM modelling determines the duty cycle, and there is a significant deviation of a duty cycle from the real signal for different values of the order of EPCM modelling [185]. To address these challenges, the power of the absolute value of the cosine function (PACM) [185] was used to model the breathing signal. Based on the dilation and erosion of sinusoidal PACM base wavelet, the shape of the waveform was adjusted empirically to produce breathing signal with better accuracy. However, the model was realized with a complex algorithm and with very high computational complexity. The mentioned challenges opened the domain of modelling the chest wall motion due to respiration to be simplistic, and computational inexpensive.

The heartbeat signal is complicated and nearly periodic. Almost all simulations to date are based on assuming the chest wall motion due to cardiac activity as sinusoidal

[46], [101], [125], [192], while Morgan et al.'s [193] model is based on heart functioning. A short impulsive action is initiated during the systolic phase when the heart ventricles start emptying. This impulsive motion is filtered by the bone and tissue structure to finally observe the chest wall motion [194], [195]. Morgan et al. [193] chose a second-order Butterworth filter to emulate the bones and tissues structure. Further, the model was slightly simplified to avoid signal processing complexity by Weishaupt et al. [43]. However, as the heart rate variability is observed for cardiac activity, the chest wall displacement varies considerably with respect to time. This implies that the shape of chest wall motion pulse varies considerably and cannot be simplified to a simplistic sinusoidal model [196]-[198] and hence the design performance of the system cannot be analyzed comprehensively through a sinusoidal mathematical model. Addressing the mentioned issue, a mathematical model of chest wall movements due to cardiorespiratory activity is proposed in this paper.

Our proposed model is the first step toward modelling chest wall motion due to cardiorespiratory activity. This would help in customizing it for the various respiratory pattern that arises due to different health conditions/diseases. For example, Kaneko et al., in their study, assess the effect of posture, age, and gender on the breathing movements in healthy subjects [198]. The outcome of the study is helpful in evaluating breathing movement, which is a critical element in a physical therapy assessment. By mapping the simulation parameters for similar observations to study the effect of age, gender, and various disease scenarios, the presented study can be further extended.

The chest wall motion can be used as a critical parameter in assessing patient's health condition during treatment or post-surgery. For example, assessment of the change in chest expansion post-thoracotomy may help in the development of the patient tailored chest physiotherapy [199]. In another study [200], Diaz et al. emphasized an evaluation of the changes in chest wall motion that occur in the patient with the neuromuscular disease during mechanical ventilation. It is demonstrated that measurement of chest wall motion can be useful in the determination of optimal ventilator setting for the children and young adults.

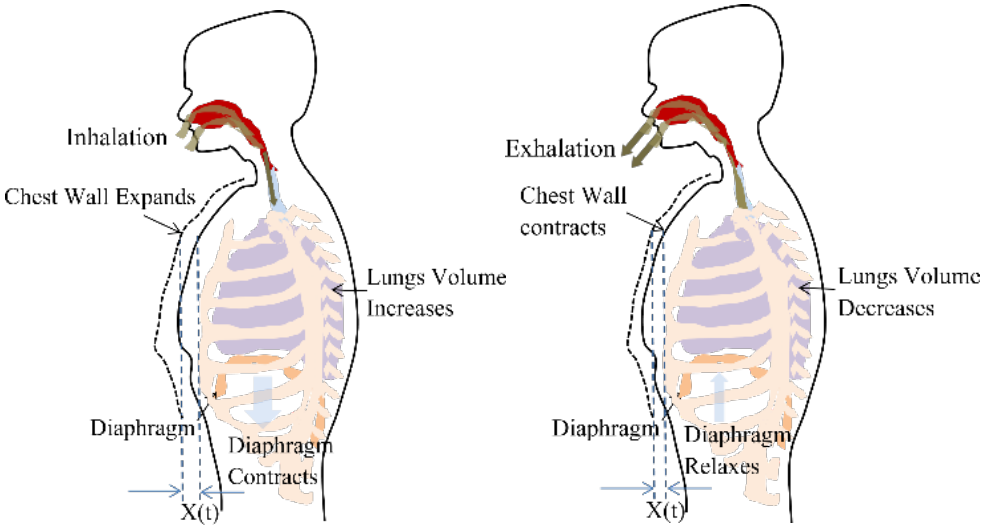

Figure 19: Chest wall motion resultant due to the contraction and relaxation of diaphragm causing the pleural pressure variation.

A recent survey [201] highlights that change in vital sign can be an indicator of the infant's physiology. The continuous analysis of vital sign can help in predicting disease like sepsis, bronchopulmonary dysplasia, brain injury, and mortality by increased vigilance and proactive involvements of the clinical practitioners. Thus, the simulation of chest wall motion can be extended further to be used in designing analytical tools and potential applications as discussed. However, this research work does not explicitly investigate those health conditions, and we will leave it for our future work.

The rest of the paper is organized as follows. The proposed mathematical model for the chest wall motion is described in Section 2. Section 3 presents the experimental analysis and discussion. With summary and future directions, the paper is concluded in Section 4.

2. Proposed Model

2.1 Respiration Signal

Respiration or breathing is a natural periodic activity which involves airflow into and out of lungs, also called pulmonary ventilation. The contraction and relaxation of the diaphragm cause pleural pressure variations and governs the airflow, as shown in Fig. 19. The decrease in lung pressure causes an increase in lung volume. Considering the

ribcage, chest wall, and lungs, forming a rectangular prism shape, the increase in lung volume is accompanied by proportional chest wall movement [32]. Therefore, a chest wall movement x(t) follows the pattern of lung volume variations during a breathing cycle.

In this work, the respiration cycle is simulated based on the optimal chemical–mechanical respiratory control model, which has been utilized earlier to develop a respiratory control simulator [202]. From the physiology viewpoint, it is well known that the instantaneous airflow is controlled by the neural impulses from the respiratory controller. The neuro-mechanical effector that relates a neural respiratory output to a resultant mechanical airflow can be approximated by the electrical RC model based on the lumped parameter mode [203]. The equation of motion can be expressed as

$$P(t) = \dot{V}(t).R_{rs} + V(t).E_{rs} \tag{3.1}$$

where $P(t)$: Isometric respiratory pressure measured at functional residual capacity (FRC), $\dot{V}(t)$: instantaneous airflow, $V(t)$: instantaneous lung volume, R_{rs}: total respiratory system resistance, and E_{rs} represents the elastance of the lungs, chest wall, and airways. The model considers only two phases of the breathing pattern as repeating inhale and exhale phases. The isometric pressure wave shape P(t) is modeled into an inspiratory and expiratory phase in the model. The inspiratory pressure is approximated by a quadratic function, and the expiratory pressure is represented by an exponential discharge function of the form:

$$P(t) = a_0 + a_1 t + a_2 t^2 \quad 0 \leq \mathrm{t} \leq t_1 \tag{3.2}$$

$$P(t) = P(t_1).e^{\frac{t-t_1}{\tau_{rs}}} \quad t_1 \leq \mathrm{t} \leq t_1 + t_2 \tag{3.3}$$

where $P(t_1)$ is the isometric pressure at time t_1. a_0, a_1, and a_2 are pressure pulse shaping parameters and, τ_{rs}, the rate of decline of an inspiratory activity, t_1 and t_2 are inhale and exhale duration, respectively.

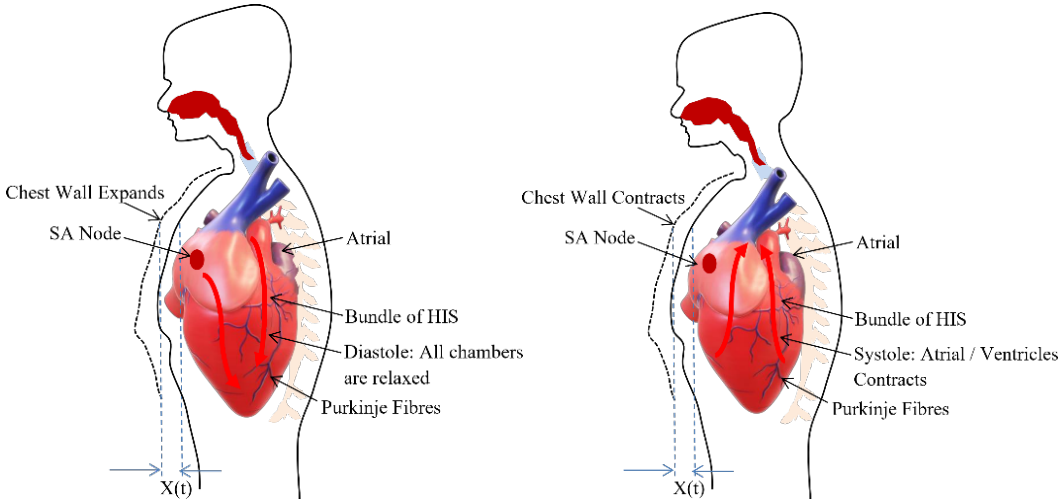

Figure 20: Chest wall motion resultant due to the relaxation (diastole) and contraction (systole) of chambers.

The empirical equations for lung volume variation pattern and, consequently, the chest wall movements for a breathing cycle during inhalation and exhalation periods, can be derived as follows.

$$V(t) = \frac{\tau_{rs}}{R_{rs}}\left[A_1 t^2 + A_2 t + A_3\left(1 - e^{\frac{-t}{\tau_{rs}}}\right)\right] + V_0 e^{\frac{-t}{\tau_{rs}}}, \quad 0 \le t \le t_1 \tag{3.4}$$

$$V(t) = \frac{P(t_1)}{R_{rs}.\left(\frac{1}{\tau_{rs}} - \frac{1}{\tau}\right)}\left[e^{\frac{(t-t_1)}{\tau}} - e^{\frac{-(t-t_1)}{\tau_{rs}}}\right] + V(t_1).e^{\frac{-(t-t_1)}{\tau_{rs}}}, \quad t_1 \le t \le t_1 + t_2 \tag{3.5}$$

$$A_1 = a_2\,,\ A_2 = a_2 - 2a_2\tau_{rs},\ \ \mathrm{A_2 = a_0 - a_1\tau_{rs} + 2a_2{\tau_{rs}}^2},\ \mathrm{\tau_{rs} = R_{rs}.C_{rs}}$$

2.2 Cardiac Signal

The heart is placed in the space called a thoracic cavity. The thoracic cavity is protected by the thoracic wall or, commonly called the chest wall, which consists of a rib cage and associated skin, muscle, and fascia. Inside the thoracic cavity, the heart is located atop the diaphragm having its apex closer to the anterior surface of the thoracic cavity. For every beat, the heart contracts and expands with the apex taping against the chest wall [204].

The heart consists of muscle tissue, commonly called fibers containing contractile elements and coordinate cardiac contraction. The coordination of mechanical activity of the chambers is requisite for the efficient working of the heart. During the systole and diastole, the contraction and expansion of the muscle tissue or

contractile elements govern the thoracic wall or chest wall movement [205] and is described in the Fig. 20. The systole and diastole are a rhythmic activity that describes the heart rate. The heart consists of its own rhythm generator called the sinoatrial (SA) node which comprises of a small strip of modified muscle tissue, about 20-34 mm, on the posterior wall of the atrium [204].

The cardiac impulse generated at the SA node is conducted by the contractile cells or the muscle tissues (myocardial cell) of the heart. Excitation–contraction coupling ties electrical depolarization to the mechanical expansion and shortening of myocardial cells [204]. The different branches derive from the bundle of His and conduct the impulse to the ventricles. This special conduction system consisting of muscle tissues coordinate the contraction of the heart. Through this conducting system, excitation is transferred to the heart muscle to coordinate its contraction from the apex upwards. This ensures the same spontaneous rate of depolarization to the other parts of the heart to have the same spontaneous rhythm [205].

The sinoatrial (SA) node (cardiac pacemaker) rhythmic behavior is represented by a relaxed oscillatory system [206]. It is an oscillatory system having a characteristic of adapting its intrinsic frequency to the frequency of external driving signal without changing its amplitude [207]. The oscillatory behavior of the SA node is defined as

$$\frac{d^2x}{dt^2} - \alpha(1 - x^2)\frac{dx}{dt} + \omega^2 x = 0 \tag{3.6}$$

The rhythm of the SA node cardiac pulse governs the contraction and expansion of contractile cells or muscle tissues. This muscle tissues directly controls the rhythm of thoracic or chest wall activity. The excitation and depolarization cycle of SA node is synchronized with the systole and diastole cycle of cardiac activity. The thoracic wall or chest wall observes expansion and contraction cycle in coordination with the systole and diastole cycle where its rhythmic behavior is synchronously represented by the SA node behavior. Therefore, the heartbeat model used in this study is represented by a relaxed oscillatory system.

Table 6: Design parameter range for respiration wave used in simulation

Pulse Duration ($t_1 + t_2$)	4, 5
Inhale shaping (a_2)	(−1), (−3), (−5), (−7)
Exhale shaping (τ)	3.5, 4.5, 5.5, 6.5, 7.5
Peak amplitude	0.035, 0.045, 0.05, 0.06, 0.07

For an NCVS system the heart rate is extracted from the phase variations in the reflected signal caused by chest wall motion. This chest wall motion has been modeled as linear sinusoidal motion in the earlier literature, assuming the heart rhythm as a simple oscillatory behavior. However, the phase variation of the radar-reflected signal depends on the minute movement of the chest wall, and small variations in movement can result in large variation in the phase or resultant heart rate. Since, heart is treated as a network of elements and these elements show oscillatory behavior that can be modelled as nonlinear van der pol oscillator, therefore, the chest wall motion has been modelled in rhythm to the rhythm of heart network element as novel approach for chest wall movement modelling.

3. Experimental Results and Discussions

We simulate chest wall motion pulse using Simulink, MATLAB 2019b. A sampling rate of 1 kHz is chosen to generate the simulation signals. The simulated waveforms are technically vetted through a separate experimental dataset available for the chest wall motion [208]. The dataset contains different trials obtained from 11 participants recorded in a supine position from a respiratory belt BIOPAC SS5LB attached to the subject's chest in different scenarios such as free-breathing, breath-hold, post-exercise, and irregular breathing. The breath hold is used for cardiac activity and rest dataset for respiration. The dataset contains different trials for each participant (post exercise-5, free breath-16, irregular-11). Each participant's data are compared with total number of generated simulated waves covering entire parameter range. The correlation coefficient of all the simulated wave with each participant is shown in the box plots. The median value for each participant indicates that the better similarity is observed with proposed simulated wave as compared to the sinusoidal model. For the comparison of

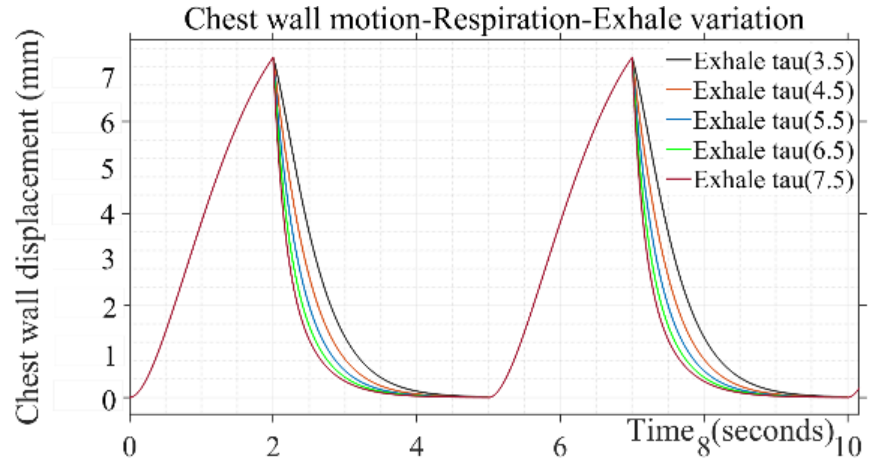

(a)

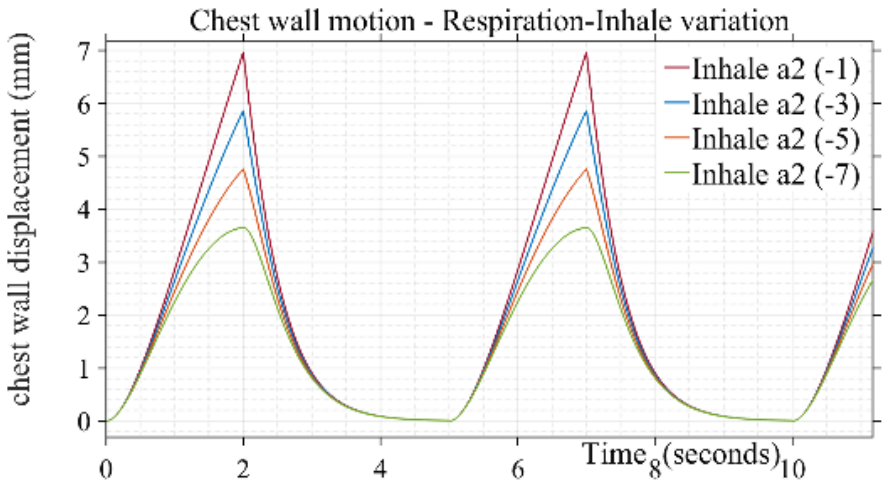

(b)

Figure 21: Variation of inhale parameter on the chest wall motion due to respiration for τ: 4.5 & Variation of exhale parameter on the chest wall motion due to respiration for a_2:-5

our simulated waveforms and the waveforms from the dataset, the simulated waveforms are resampled to 100 Hz, and dataset waveforms are smoothened to arrive at a common comparison platform.

3.1 Simulation Result

3.1.1 Chest Wall Motion—Respiration

Design parameters including pulse duration ($t_1 + t_2$) inhale shaping a_2, exhale shaping τ, and peak amplitude are varied to study their effect on simulated respiration wave shapes. Different values used in presented simulations are given in Table 6.

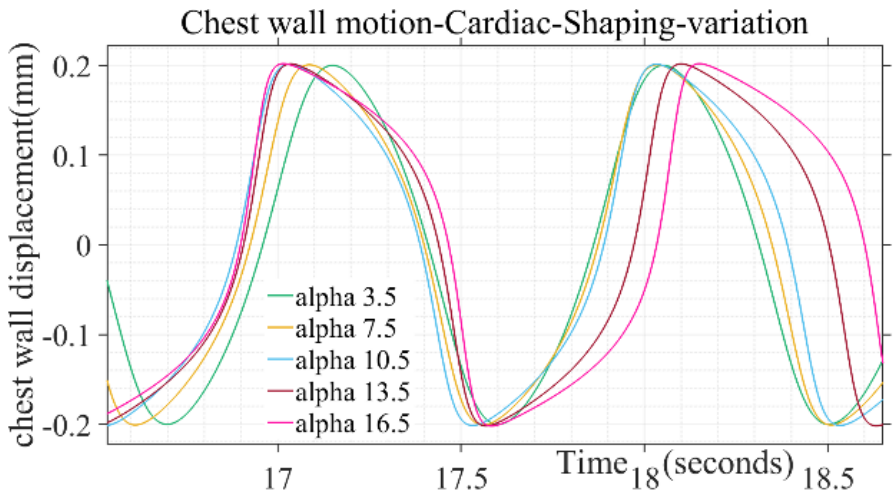

Figure 22: Variation of alpha pulse shape parameter on chest motion due to cardiac activity.

The breathing pulse duration ($t_1 + t_2$) can take a range from 4 to 5 s, which corresponds to the respiration rate of 12 to 16 bpm. Similarly, the peak amplitude parameter can range from 0.035 to 0.11, corresponding to the chest wall displacement from 4 to 12 mm [122]. The values for presented simulation are taken as steps from 0.035 to 0.07 corresponding to 4 to 7 mm of chest wall motion, respectively. The shape defining parameter for inhale (a_2) and exhale (τ) follows the range variation of −1 to −7 and 3.5 to 7.5, respectively.

The inhale shape approaches a straight line resulting in a triangular shape of respiration pulse for inhale parameter (a_2) lower than −1 and starts following a circular pattern with a large duration cusp at the top beyond the parameter value of −7, which is not a realistic scenario [202]. The step increment is taken to generate different simulated shapes covering the entire range for the pulse shaping parameter.

Similarly, air discharge during exhalation follows smooth discharging as a type of exponential decay [203]. Beyond the mentioned parameter range from 3.5 to 7.5, the shape adopts a triangular straight-line decay and discontinuity at the transition stage

Table 7: Design parameter range for cardiac wave used in simulation

Peak amplitude	0.2, 0.5
Pulse Duration (ω^2)	50, 60, 70, 80, 90, 110
Pulse Shaping (α)	3.5, 7.5, 10.5, 13.5, 16.5

from “end of exhale” to “rest” and then “start of inhale” phase for next cycle. Fig. 21 (a) and (b) depicts a variation of inhalation and exhalation-shaping parameters on the chest wall waveshape due to breathing. The shape of the wave during the inspiratory phase is found to be more concave upward indicating the loaded breathing condition through variation of the parameter a_2,. The parametric variation of τ simulates the rate of decline of inspiratory activity, i.e., for the sharper rate of decline with a longer pause between exhale and next inhale instance for the same duty cycle wave represents the breathing pattern of the post-exercise phenomenon.

3.1.2 Chest Wall Motion—Cardiac

Design parameter for simulation of chest wall motion due to cardiac activity is given in Table 7. The parametric variation of α simulates the behavior of atrial sinus (SA) node and atrial ventricular (AV) node during biological rhythms for different human activities such as sleeping, wake cycle etc. Similarly, the pulse duration and maximum chest wall displacement of the wave can be simulated through variation of ω^2 and peak amplitude parameters, respectively.

The shape of the simulated chest wall displacement during heart activity was found to be more bulged out in the middle through higher values of the parameter ($\boldsymbol{\alpha}$) as illustrated in Fig. 22. For chest wall simulation, cardiac pulse duration parameter is taken in the range from 50 to 110 in incremental steps. The parameter range corresponds to the heart rate 60 to 100 beats/min for a healthy adult. Similarly, the peak amplitude parameter ranges from 0.2 to 0.5, corresponding to the chest wall displacement range from 0.2 to 0.5 mm [209]. The shape defining parameter ($\boldsymbol{\alpha}$) for chest wall motion follows the range variation of 3.5 to 16.5, respectively. Beyond the mentioned parameter range the wave shape adopts a trapezoidal form and discontinuity while approaching half of the chest motion amplitude during a beat cycle which is not in tandem with actual chest wall motion where no discontinuity is observed for a beat cycle [122]. Single-step increments are taken to generate different simulated shapes covering the entire range for the pulse shaping parameter.

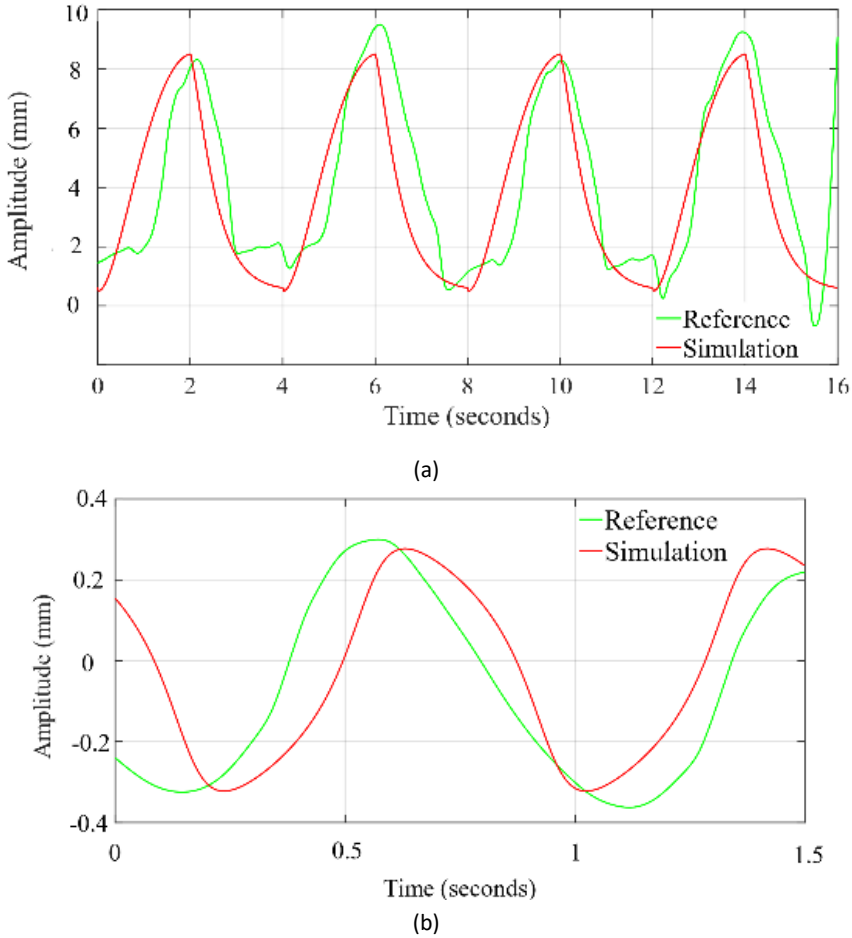

Figure 23: Time profile comparison of chest wall motion due to (a) respiration and (b) heartbeat, with dataset.

3.2 Validation and Comparison Analysis

During a normal breath, chest wall motion comprises of two components, the displacement from respiration activity and second, the displacement due to cardiac activity. However, if a chest wall displacement is captured during a breath-hold condition, the displacement is caused by heart activity only. The motion due to heart activity is too small (0.2–0.5 mm) as compared to the motion due to respiration (3–12 mm). Therefore, a dataset of chest wall motion due to heart activity only is extracted from the breath-hold duration and used to perform the similarity analysis. The time profile of the chest wall movement due to cardiorespiratory activity obtained from the simulation is compared with the human chest wall experimental data [208]. The data at channel 2, where the respiratory belt (SS5LB) is connected to measure the chest motion, are plotted, and zoomed in time axis to visually compare with the simulation waveform.

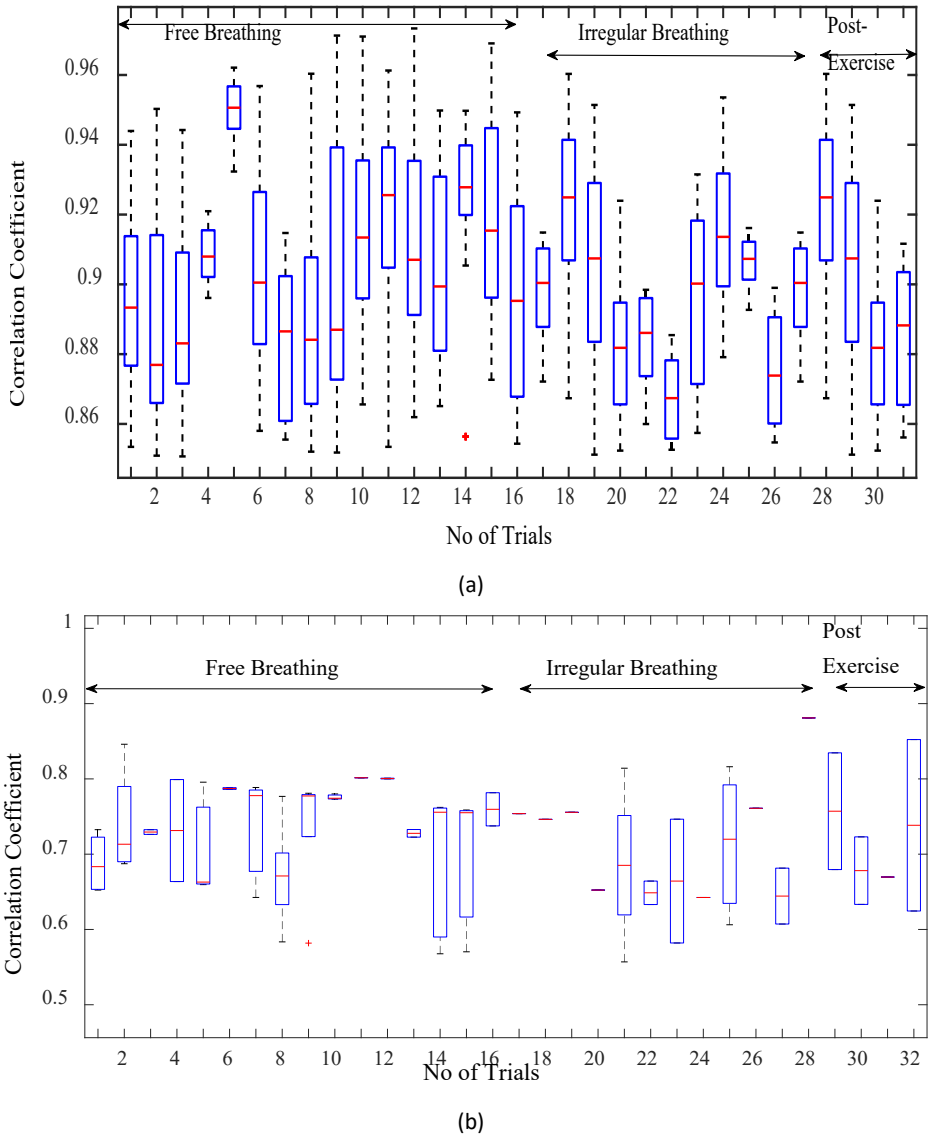

Figure 24: Correlation coefficient for the free breathing, irregular breathing, and post-exercise breathing with (a) simulated wave and (b) sinusoidal wave.

As shown in Fig. 23(a) the exhale-inhale pattern closely follows the experimented dataset wave. The pulse duration and in turn, the respiration rate is the same for both the simulated and referenced signal. As demonstrated in Fig. 23(b), the simulated systole-diastole cycle closely follows the experimented dataset wave. Our proposed model produces accurate matching between the duty cycle of the actual cardiac signal to the model generated wave. The similarity between simulated waves and the signals obtained from the referenced cardiac-respiratory dataset is demonstrated through the Pearson product-moment correlation coefficient and dynamic time warping (DTW). The

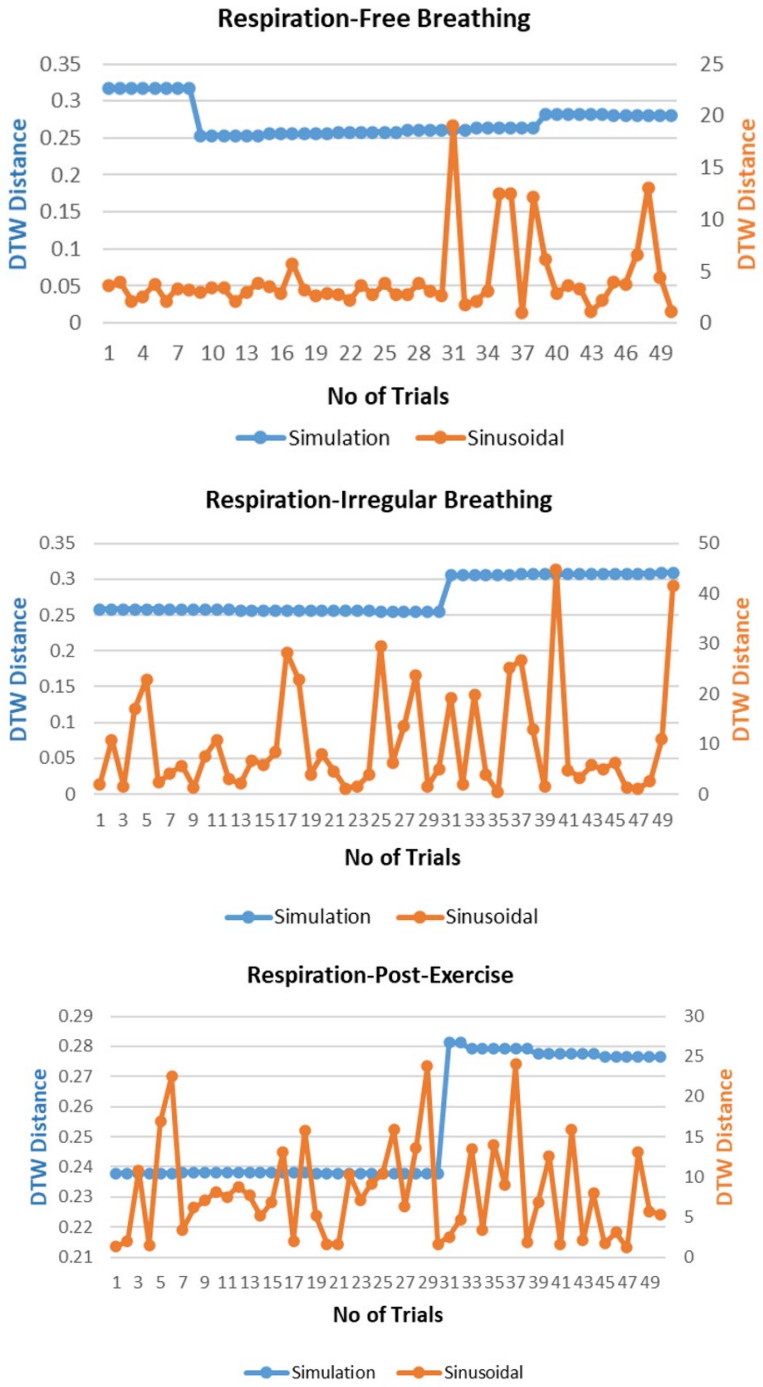

Figure 25: Comparison of dynamic time warping (DTW) between simulation-dataset and sinusoidal-dataset waves.

Pearson product-moment correlation coefficient for two signals A(t) and B(t) is identified as a similarity index and is defined as:

$$\rho(A,B) = \frac{1}{N-1}(A_i - \mu_A\sigma_A)(B_i - \mu_B\sigma_B) \tag{3.5}$$

where μ_A and σ_A are the mean and standard deviation of A, respectively, and μ_B and σ_B are the mean and standard deviation of B, with each variable has N scalar observations.

In time-series analysis, the normalized time-dependent Pearson correlation coefficient is an indicator of similarity index as the cross-correlation coefficient value must lie in the range from −1 to 1, with one indicating perfect correlation [210], [211]. Additionally, in time series analysis, another technique dynamic time warping (DTW) is used for measuring the similarity between two temporal sequences [212]. DTW works on the principle of stretching the vectors to make them similar, and minimum possible distance between vectors is calculated for stretching. This distance is a parameter to measure the similarity of two sequences. We have used this distance to compare the similarity of simulated and sinusoidal chest wall motion with experimental and dataset chest wall motion.

3.2.1 Comparison of Respiration Simulation Signal

Fig. 24(a) displays the correlation coefficient for different breathing scenario for the subjects lying in a supine position. For the free-breathing scenario, it is observed that the maximum correlation coefficient approaches 0.97 with most of the values for coefficient lying between a range of 0.9 and 0.97. The mean cross-correlation coefficient of the simulation-dataset wave is in a range of 0.86-0.94, the 75^{th} percentile reaching above 0.9 on average. A similar pattern can be observed for irregular and post-exercise breathing as well. However, the similarity index between a sinusoid and dataset waveforms lies in the range of 0.68-0.84 with the median lying in the range of 0.65-0.77 correlation coefficient, as shown in Fig. 24(b). This indicates that the chest wall displacement due to respiration is convincingly represented through proposed simulation model in comparison to the assumption of sinusoidal motion.

The respiration waves are nonlinear time series in nature, and hence, revalidation of the simulated model is performed through dynamic time warping, a nonlinear similarity matching technique for two time series. The distance between two waves acquired through DTW analysis is shown in Fig. 25 for different breathing types. The DTW distances between proposed simulation and experimental datasets waves lie at nearly zero between the range of 0.2 and 0.3 while the DTW distance for sinusoidal simulation lies in the range of 2-15. From the results in Fig. 26, the dynamic warping

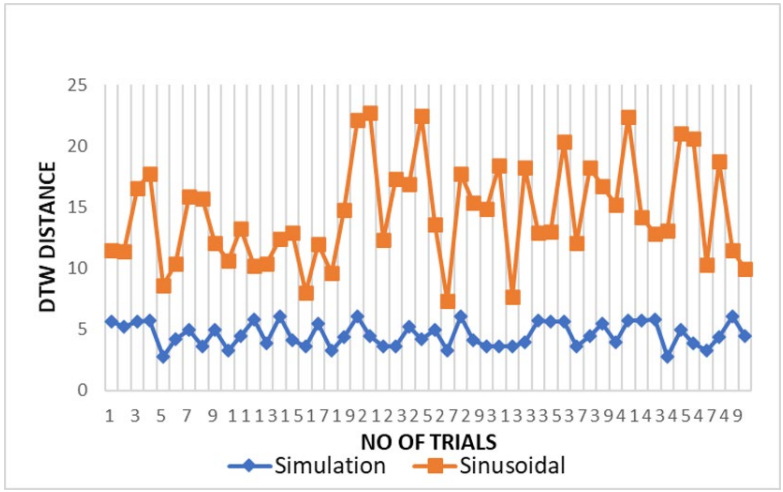

Figure 26: Comparison of DTW between cardiac simulation-dataset and sinusoidal-dataset waves.

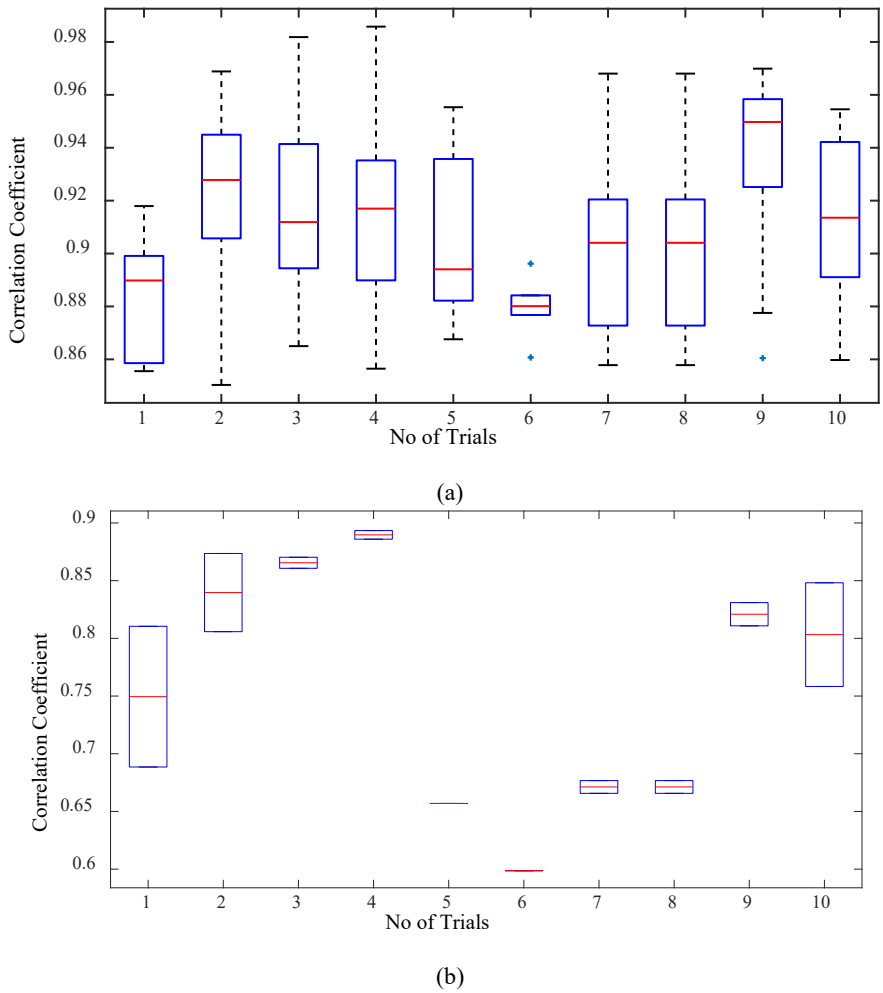

Figure 27: Box-plot representation of correlation coefficient for the chest wall motion due to cardiac activity with (a) simulated wave and (b) sinusoidal wave.

distance between the simulated and experimental wave is consistent and matches closely.

3.2.2 Comparison of Cardiac Simulation Signal

Fig. 27(a) presents the correlation coefficient for cardiac activity (breadth hold condition). It is observed that the median of the correlation coefficient for simulation with reference to the cardiac dataset is around 0.93, the 75th percentile is above 0.9. The maximum correlation coefficient achieved is in a range of 0.9-0.98. The inter-quartile range is also implying that the similarity between the two signal waves is quite high. Whereas the similarity index for sinusoidal wave shape is much lower as compared to simulated wave shape lying in the range of 0.59-0.89 with a median in the range of 0.7-0.84 as given in Fig. 27(b). This infers that simulated shape represents the actual chest wall displacement due to heart activity.

The DTW distance between simulated and experimental dataset waves for cardiac activity acquired through DTW analysis is shown in Fig. 26 for different trials. The threshold distance for DTW similarity match was taken through the experimental cardiac waves match data samples. The DTW distances between proposed simulation and experimental datasets waves closely approach one and lie between range of 2 and 5 with respect to the DTW distance for sinusoidal simulation, which lies in the range of 10-25. From the results in Fig. 26, the dynamic warping distance between simulation and experimented wave is consistent and matches closely.

4. Conclusions

This work contributes to the development of a mathematical model for ubiquitous and nonobtrusive cardio-respiratory vital sign monitoring through radar-based NCVS system. The comparative analysis through cross-correlation demonstrates that the simulated chest wall motion is in close agreement with the real motion and hence validate the applicability of simulated chest motion in cardiac-respiratory applications. The cross-correlation coefficient between the simulated waveform and the experimental dataset approaches to the range of 0.95-0.97, indicating a high degree of similarity of both time sequences.

Our proposed model is not only useful for validating the design parameters through a target modelling for radar-based NCVS system applications but can also be utilized for the development of techniques to evaluate the cardio-respiratory parameters of chest surface motion beneficial in validating the design of artificial cardio-respiratory systems. The proposed model demonstrated the ability to simulate the varying chest wall motion in different scenarios such as free-breathing and post-exercise breathing etc.

The limitation of our study is that it relies on the single experimental dataset available for the chest wall motion. However, in future work, exhaustive experiments with a varying subject profile in terms of age, gender, weight, medical history can be employed for the measurement of chest displacements. This chest wall measurement may be compared with more simulation waveforms to arrive at a conclusion for a shape defining condition of diseases such as lung tumor, sleep apnea or different disease triggering scenarios. In addition, these simulation parameters may be employed for designing a care system to address the diseases or scenarios without exhausting experimentation of the design over real subjects.

Chapter 4

Human Vital Signs Estimation Using Resonance Sparse Spectrum Decomposition

Abstract

The noncontact measurement and monitoring of human vital signs have evolved as a valuable tool for efficient health management. Because of the greater penetration capability through material and clothes, less affected by environmental conditions such as illumination, temperature, humidity, etc., mmWave radar has been extensively researched for human vital sign measurement in the past years. However, interference due to unwanted clutter, random body movement (RBM), and respiration (RR) harmonics make the accurate retrieval of the heart rate (HR) difficult. This paper proposes a resonance sparse spectrum decomposition (RSSD) algorithm and harmonics utilized algorithm (HUA) for accurate HR extraction. RSSD addresses the clutter and random body movement effects from phase signals, while HUA utilizes the harmonics to extract HR accurately. A set of controlled experiments was conducted under different scenarios, and the proposed method is validated against ground truth HR/RR collected by a smart vest. Our results show an accuracy of up to 98-100% for distances up to 2 meters. The method substantially improves the HR estimation accuracy by effectively mitigating the effects of noise in the phase signal, even under heavy clutter and moderate body movement. Our results demonstrate that the proposed method effectively counters harmonic interference for accurate estimation of HR comparable to RR estimation up to 4m of the distance from the radar sensor.

This contribution has been submitted for review in IEEE Transaction on Human Machine Systems Journal

1. Introduction

Radar technology is environmentally robust and is also suitable for working in unilluminated settings. Advancements in Integrated circuits have enabled small, affordable short-range radars. This has made radar a choice for many applications, such as collision avoidance in cars, adaptive control of autonomous vehicles and drones, structural monitoring, gesture recognition, and health monitoring in recent years [213]. Conventional wearable sensors [10], [11], [214], [215] are cumbersome for continuous human monitoring, and people often forget to wear them. Cameras are seen as infringing on privacy [6], particularly in bedrooms and bathrooms. Radar offers remote monitoring without requiring the user to carry any electronic device and addresses privacy issues [216]. The Non-contact measurement and monitoring of human vital signs can be a valuable tool for efficient health management in clinics and hospitals by reducing the time consumed in recording and maintaining the data log for patients, the effective prognosis of many diseases, and inarguably pivotal in-home health care especially for older adults [217]-[219].

The cardio-respiratory system offers a critical attribute of periodic skin displacement, which is utilized to measure vital signs through radar-based systems. The basic radar-based vital sign detection model involves the transmission of microwave signals toward the human target. The reflected signal, which is phase-modulated by the chest wall's displacement motion, is captured by the receiving antenna to be further analyzed. Owing to the skin displacements of 0.6 mm from heart activity as compared to 12 mm displacement from the respiration, the reflected signal due to heartbeats is minimal compared to respiration [122]. Moreover, the strong noise constituted by second and third-order harmonics of RR and intermodulation products is also present in the fundamental frequency range of the HR spectrum [40].

The environmental clutter and random body movement also contribute to noise in the received reflected signal, which presents a challenge in designing an efficient HR estimation system. Therefore, it is much more complex and challenging to accurately extract heart rate than respiration rate under these observations. The challenge is

aggravated for longer distances between the radar and humans. Also, the complexity of the signal processing algorithm is increased. Therefore, the current state-of-art addresses these challenges and investigates an effective and robust heart rate detection algorithm.

Filtering and frequency-based analysis are fundamental tools in signal processing algorithms. The piecewise-smooth signals defined primarily by their transients are analyzed and processed in the time or wavelet domain. In contrast, frequency and time-frequency analysis are more effective on substantially oscillatory or periodic signals. The complex signals such as geophysical (ocean tide-height data) and the HR and RR signals produced from the physiological processes, are non-stationary and exhibit a mixture of oscillatory and non-oscillatory transient behaviors [220]. For such signals, linear methods, e.g., frequency and time-frequency analysis, cannot be applied effectively as these methods are helpful for oscillatory or periodic signals. The non-linear signal analysis method based on signal resonance rather than frequency or amplitude of the signal has achieved much attention. This study proposes a new sparsity-enabled signal analysis method utilizing resonance-based signal decomposition [220] for HR/RR detection.

The method decomposes the signal into the sum of the 'high resonance' and 'low resonance' components. A high resonance component means a signal containing a sustained oscillation sequence, whereas a low resonance component refers to a non-oscillatory transient. The algorithm also produces a residual signal present due to the noise (stochastic) component, whose amplitude can be controlled by the parameters of the decomposition algorithm.

The signal's 'high resonance' component is used further for extraction of the heartbeat and respiration by the proposed harmonic utilized algorithm. Our main contributions are summarized as follows:

- We propose a method that comprises resonance sparse spectrum decomposition (RSSD) and harmonic utilized algorithm (HUA) for HR/RR extraction. RSSD utilizes the 'high resonance' part of the signal mitigating the effects of clutter and random body

movements from the received phase signal. The efficacy of the proposed method is validated by observing that the HR estimation accuracy is comparable to the RR estimation accuracy, even under heavy clutter and moderate body movement.

- We evaluate the effectiveness of the proposed method, and the HR/RR is compared with the reference data obtained through the Hexoskin smart vest. The results show that the proposed method substantially improves HR detection accuracy by effectively mitigating the effects of noise in the phase signal.
- We further evaluate the reliability and robustness of our method based on comprehensive experiments on four participants with various target distances and angles with respect to the radar. It is observed that the detection accuracy remains consistent up to 4 m from the radar device.

The rest of this paper is structured as follows: Section 2 presents the related work. Section 3 discusses the proposed method, including the proposed harmonic utilized algorithm (HUA) for heart rate. Sections 4 and 5 present the experimental results and discussion, respectively. The paper is concluded in Section 6.

2. Related Work

The HR extraction algorithm's chronology starts with the most straightforward approach of using fast fourier transform (FFT) over a phase signal length and finding the spectrum's peaks. However, the detection performance is degraded due to the leakage problem caused by the limited data length of the Fourier transform. The Fourier transform requires the invariability of vital signals over a small duration. Under the time-varying vital sign scenario, the estimation performance of FFT algorithms degrades substantially.

A parametric and cyclic optimization-based approach called the RELAX algorithm was proposed to address the problem but was found computationally demanding [221]. Continuous wavelets transform-based synchro-squeezing transform (SST) was used in the algorithm for estimating the vital signs. However, the SST is not beneficial for high frequency and large varying noise signals caused by body movements [222]. The autocorrelation and frequency-time phase regression (FTPR) approach is combined as

an extension to earlier studies to extract vital signs. Lee et al. [169] also addressed FFT smearing and leakage issues using multiple signal classification (MUSIC) algorithms. The MUSIC algorithm observes difficulty in selecting an adequate number of signal subspaces and is computationally expensive.

The time-domain processing of the signal reduces the computational load of the system compared to frequency-based processing. Yang et al. [223] used a two-stage analog bandpass filter (BPF) to extract HR and RR for the time-domain peak detection. Zakrzewski et al. [155] improved the non-linear demodulation, i.e., arctangent demodulation, with a center estimation algorithm using the levenberg-marquardt (LM) method. For HR estimation, the signal processing algorithm incorporated peak detection through FFT, wavelet, MUSIC, or DCT. However, the problem related to the degradation of HR estimation accuracy due to heavy clutter and body movement persists [224]. Zhao et al. [225] extended the time-domain analysis for multiple target's HR/RR extraction. An algorithm based on energy scaling and sliding window FFT is employed to reduce the effect of random body movement. However, the targets are at a different distance from the radar, and limited accuracy was achieved.

Sekine et al. [125] employed the multi-resolution analysis using continuous wavelet transform to remove the harmonics. The heartbeat is estimated through periodicity in a specific frequency. Tu et al. [126] reconstructed the respiration signal which was subtracted from the original signal in the time domain using the complex signal demodulation technique to have a harmonics-free HR signal. However, the accuracy of the method depends on the quality of the reconstructed respiration signal. Also, different frequencies experience different phase delays, limiting the technique's effectiveness as the fundamental and higher harmonics cannot be canceled simultaneously. Nosrati et al. [37] considered the double derivative of the signal for the processing whose amplitude is higher by a multiple of ω^2 than the original signal. Then frequency-time phase regression (FTPR) is employed to reduce the effect of respiration harmonics.

Additionally, time-frequency analysis by short-time fourier transform (STFT) with a Gaussian window reduced the impact of RR harmonics over weak HR signals. Nguyen

et al. [40], [41] designed the harmonic path algorithm (HAPA), and spectrum averaged harmonic path (SHAPA) algorithm to overcome the issue. Hosseini et al. [47] developed a respiratory motion detection algorithm that utilized both time-varying delay and phase modulation. A finite impulse response (FIR) time-varying filter was used to find out HR, effectively dealing with RR harmonics by selecting optimum FIR coefficients by discrete prolate spheroidal sequences (DPSS). Still, the effect of clutter and body movement persists. The circle fitting-based DC offset calibration technique was used for clutter mitigation, but the body movement effect needed further studies [226].

The HR and RR originated components are separated in the time domain. RR harmonics issue was addressed using instantaneous frequency estimation based on local maxima. Hilbert-huang transform (HHT) and empirical mode decomposition (EMD) were used for the separation and extraction of HR & RR [43]. The accuracy of HR estimation lagged behind the RR estimation accuracy. In [227], the breathing pattern is detected with the xtreme gradient boosting (XGBoost) classification model and adopted mel-frequency cepstral coefficient (MFCC) feature extraction. IIR bandpass filter using cascaded Bi-Quad is implemented for extracting the breathing information from the chest displacement information. Cardillo et al. [228] proposed two methods to distinguish between real target and clutter based on the auto-correlation and cross-correlation applied to phase trails and range doppler bin, respectively. However, there is a trade-off between radar motion extent and computational complexity. The mitigation of clutter and body movement effects, along with accurate HR estimation comparable to RR estimation, were open issues.

Since the respiration magnitude is large compared to the heartbeat signal's magnitude, the proximity of higher-order respiration harmonics and intermodulation products to the HR fundamental component can interfere with the weak HR signal and lead to incorrect peak selection. Advanced filtering methods like adaptive noise cancellation (ANC) [229] and double parameter least mean square (LMS) filter [230] have been developed for HR signal separation. However, despite their computational complexity, these approaches may not effectively handle scenarios where respiration harmonics are closely adjacent to the heartbeat component, especially in low SNR

situations. Khan et al. [231] introduce an HR extraction algorithm based on selecting peak locations using the probability of occurrence over N iterations. However, this method requires long initialization times and may lead to inefficient estimation for fast HR variation.

On the other hand, Morgan et al. [193] have developed a technique to enhance weak heartbeat signals by adaptively canceling respiration harmonics using a mean-square error cost function. However, this method requires precise estimation of the respiration fundamental frequency for higher harmonic cancellation, and it may not effectively retain the heartbeat component when it is close to the respiration harmonics. Furthermore, the adaptive harmonic cancellation method effectively eliminates low-order harmonic components, but the implementation still exhibits relatively large residual high-order harmonic components. Also, if the true HR is the multiple of RR harmonics, then the method may lead to the HR fundamental cancellation itself. The challenges of reliable HR monitoring are further added by random body movement of the subject, which can reduce the small RR and HR signals, making accurate estimation of RR rates difficult and, consequently, reliable HR estimation.

Another method called differential enhancement (DE) [232] is employed for HR monitoring. This approach involves performing differential operations (first- and second-order) on the initially extracted chest wall displacement signal to suppress respiration and enhance the heartbeat components. However, using the differential operation makes the method sensitive to high-frequency noise, often present in the high-frequency region of the phase signal. To mitigate strong noise interference, the phase signal needs to be pre-processed with simple data smoothing techniques, such as moving average or local regression. It is worth noting that employing a second-order differential amplifies more in-band noise, potentially degrading detection performance, especially in low SNR situations. Moreover, a trade-off must always be made between using first- and second-order differentials to achieve accurate estimation and restricting the generality of the approach for all scenarios. Overall, reliable and accurate HR

monitoring remains a challenge due to the potential proximity of high-order respiration harmonics to the weak heartbeat component.

3. Theory and Method

3.1 Resonance-Based Sparse Signal Decomposition (RSSD) and Tunable Q-factor Wavelet Transformation (TQWT)

Resonance is an intrinsic property of a signal defined as resonance index or resonance quality factor Q. We used RSSD to decompose the phase signal comprising of a higher Q signal, which indicates stronger resonance and more oscillation in the time domain, and a low Q signal primarily considered as noise. The center frequency and the frequency bandwidth define the resonance property, and hence signal components with similar center frequency bands but with a different quality factor, Q, can be separated and sparsely represented. RSSD obtains the sparsest representation of each resonance component of the signal. Mathematically, the signal resonance index can be described with the Q-factor, which is the ratio of the center frequency f_c and bandwidth BW in the frequency domain, described in (4.1),

$$\mathrm{Q} = \frac{f_c}{BW} \tag{4.1}$$

We chose the RSSD implementation through TQWT because it specifies the Q-factor, redundancy factor r, and decomposition level J, directly enabling the design of wavelet bases that phenomenally overcome the length limitation of the input signal. TQWT has more flexibility and is most suited for RSSD analysis in physiological signal analysis fields [233]-[235]. We choose the RSSD implementation through TQWT because the common constant-Q transformation method, such as dyadic wavelet transformation (DWT), has a limited application under strict high-frequency resolution requirements [233], [234]. The parameter selection for implementing RSSD through TQWT is controlled through the Q-factor of the phase signal. For a fixed Q factor, an increase in

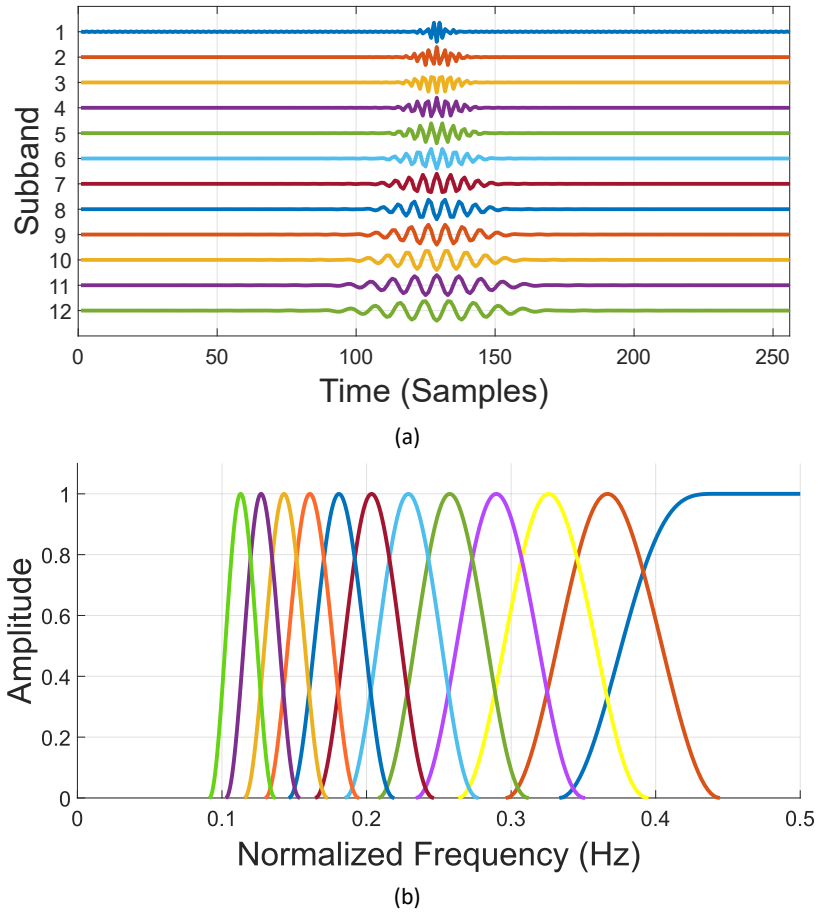

Figure 28: TQWT wavelet bases with Q = 3, r = 3, J = 8. (a) Time-domain waveforms; (b) Frequency responses.

redundancy factor r results in a higher overlapping rate. The value of redundancy factor r should be strictly greater than one, and we have chosen a generally recommended value of three for perfect reconstruction and sparsity. After fixing the Q-factor and redundancy factor r, we have obtained the scaling parameters β and α through (4.2),

$$\beta = \frac{2}{Q+1}, \alpha = 1 - \frac{\beta}{r} \tag{4.2}$$

As a subsequently higher value of the decomposition level, J, covers a broader frequency range and approaches 0 Hz with a trade-off to poor computational efficiency. Specifically, TQWT decomposes an n-point discrete-time signal into J-level sub-bands. The maximum number of levels J_{max} is set according to (4.3),

$$J_{max} = \left\lfloor \frac{\log\left(\beta * \frac{n}{8}\right)}{\log\left(\frac{1}{\alpha}\right)} \right\rfloor \tag{4.3}$$

$$f_c = \alpha^j \frac{2-\beta}{4\alpha} f_s \tag{4.4}$$

$$BW = \frac{1}{2}\beta\alpha^{j-1}\pi \tag{4.5}$$

As shown in Fig. 28, for Q = 3, r = 3, and J = 8, it is described that as the decomposition levels increase, the corresponding center frequency and bandwidth are both decreased, maintaining the Q-factor unchanged. The TQWT sub-bands are no longer flat tops except for the first level sub-band, and each sub-band frequency peak maintains a constant value. Therefore, an explicit Q-factor indicating resonance behavior can be much more conveniently obtained through TQWT.

RSSD separates the different resonance components of a given signal and realizes the sparsest representation of each resonance component. Specifically, for a given signal $x = x_1 + x_2$, through RSSD, the signal is decomposed into the high-resonance component x_1, low-resonance component x_2 and the residual. Considering that x_1 and x_2 can be sparsely represented in bases S_1 and S_2 (obtained through TQWT with high and low Q-factors), respectively. Therefore, the desired optimization problem for estimating coefficient matrixes W_1 and W_2 under S_1 and S_2 is find out according to (4.5) & (4.6),

$$\underset{W_1,W_2}{argmin}\{\| x - S_1W_1 - S_2W_2\|_2^2 + \lambda_1\|W_1\|_1 + \lambda_2\|W_2\|_2\} \tag{4.6}$$

where λ_1, λ_2 are the corresponding weight coefficients. It is pertinent to note that the relative values of λ_1, λ_2 determine the energy distributions of these two resonance components. With a fixed λ_1 increasing λ_2 will increase the energy of x_1, decrease the energy of x_2, and vice versa. Increasing both λ_1 λ_2 will increase the residual energy and reduce that of the resonance components.

Utilizing Split Augmented Lagrangian Shrinkage Algorithm (SALSA) [236], [237], RSSD iteratively updates coefficient matrixes W_1 and W_2 to achieve minimization. After processing all iterations, optimal coefficient matrixes W_1^* and W_2^* and a considerable sparse representation of the resonance components is achieved. Considering the random noise in practical cases based on MCA, the high-and low-resonance components can be estimated as in (4.7),

$$x_1 = S_1W_1^*, x_2 = S_2W_2^* \tag{4.7}$$

The RSSD algorithm steps can be summarized in the following:

- The phase signal x is input to the algorithm;
- Wavelet bases S_1 and S_2 (via TQWT) are constructed using the apriori resonance information, suitable Q -factors Q_1, and Q_2, redundancy factors r_1, and r_2, decomposition levels J_1, and J_2, and suitable weight coefficients λ_1 λ_2;
- The optimal coefficient matrixes W_1^* and W_2^* are estimated to solve the optimization problem with SALSA;
- Finally, the high and low resonance components with $x_1 = S_1 W_1^*, x_2 = S_2 W_2^*$ are obtained using W_1^* and W_2^*.

As the radar returned vital sign phase signal is noisy, the optimization problem can be formulated as the minimization of the following cost function with the RSSD algorithm mentioned above as in (4.8) & (4.9),

$$\underset{W_1,W_2}{argmin}\left\{\| y - \varphi_1 W_1 - \varphi_2 W_2\|_2^2 + \sum_{j=1}^{j_1+1} \lambda_{1,j} \|W_{1,j}\|_1 + \sum_{j=1}^{j_2+1} \lambda_{2,j} \|W_{2,j}\|_1\right\} \quad (4.8)$$

Where $\varphi_1 \, and \, \varphi_2$ represent the inverse TQWT having high and low Q-factors, respectively. The regularization parameters λ_1 and λ_2 are chosen by the user according to the power of the noise. After W_1 and W_2 are obtained, we set,

$$x_1 = TQWT_1^{-1}(W_1), \; x_2 = TQWT_2^{-1}(W_2) \quad (4.9)$$

3.2 Harmonics Utilized Algorithm (HUA)

The respiratory harmonics directly relate to the respiratory amplitude. As the respiratory amplitude increases, the amplitude of respiratory harmonics increases. The second harmonic of respiration is larger for respiration rates on the higher side of the normal range. Sometimes, the third respiratory harmonic has a comparable amplitude to the heartbeat signal in the frequency domain and affects the HR peak in spectrum analysis. The RR harmonics are sustained oscillations, which makes extracting the affected HR beat difficult using RSSD.

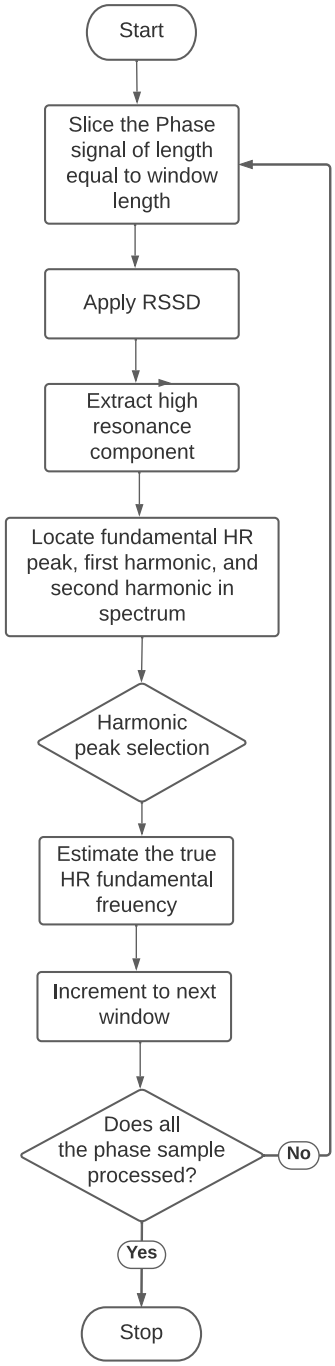

Figure 29: Harmonic utilized algorithm (HUA) for HR Extraction

It is worth noting that higher-order RR harmonics have minimal impact in the second or third HR harmonics range owing to the sufficiently weak amplitude of RR's higher-order harmonics. Therefore, an algorithm is designed using higher-order HR harmonics as described in Fig. 29.

Algorithm 1: Harmonic Utilized Algorithm (HUA) for HR Extraction

INPUT phase signal $X[n],\ 0 \le n \le N-1,\ N * f_s = T,$ Current observation window, C_{obs}
SET RSSD parameters (r, J, Q)
C_{Δ_obs} = number of samples shifted in C_{obs} equivalent to one sec
Number of observation window, $N_{obs} = \frac{X[n]}{C_{\Delta\_obs}}$
WHILE (k <= N_{obs}):
Input current observation signal window, $X_c = X[n], \quad (k-1).C_{obs} \le n \le k.C_{obs} - 1$,
Extract high resonance component x_{c_hreso} through RSSD-TQWT
$X_{c\_hreso}[k] = \sum\left(x_{c_{hreso}}[n] * \exp\left(-\frac{j2\pi kn}{N}\right)\right), 0 \le k \le N_{dft} - 1$
calculate power spectrum Px_{c_hreso}
$Px_{c_{hreso}}(f) = \left|X_{c\_hreso}[k]\right|^2, where\ f = k * f_s/N_{dft}\ ,\ N_{dft} = C_{obs}$
Find largest peak index vector Piv_c in power spectrum $Px_{c_{hreso}}$,

$$Piv_c(m) = \{\text{largest peak index in } Px_{c_{hreso}}(f)\} \begin{cases} 1 \le f \le f_{hr\_max} & m = 1, \\ Piv_c(1) * \frac{f_s}{N_{dft}} \le f \le 2 * f_{hr\_max} & m = 2, \\ (Piv_c(1) + Piv_c(2)) * \frac{f_s}{N_{dft}}) \le f \le 3 * f_{hr\_max} & m = 3, \end{cases}$$

Find pairwise distance vector Dv_c ***for the elements of*** Piv_c
$Dv_c(q) = (|Piv_c(i) - Piv_c(j)|), \forall\ i \ne j, where\ 1 \le i, j, q \le 3$
Select *HR index* hr_{cind} *with a pairwise index distance limit of* Δ_d
$hr_{cind} = avg\left(Piv_c\left((\min\left(Dv_c(q)\right) \le \Delta_d\right)\right)$
Else find minimum of pairwise distance Dv_{min} ***from the previous window estimate*** $hr_{cind}(k-1)$
$Dv_{\min} = min(|Piv_c(i) - hr_{cind}(k-1)|), where\ 1 \le i \le 3$
$hr_{cind} = Piv_c(Dv_{\min})$
Estimate HR in bpm for the current observation window
$hr_{est}(k) = hr_{cind} * f_s * 60/N_{dft}$

The fundamental frequency of RR and HR is estimated through spectral analysis of high resonance components obtained by applying the RSSD algorithm. However, the spectral components (RR harmonics and intermodulation products) close to the HR fundamental may shift the HR fundamental peak from the true location. This shifting depends on the relative interfering amplitude of the above-mentioned spectral components. This phenomenon is called "leakage" and causes an error in the HR estimation as the fundamental HR peak is submerged or completely attenuated by this spectral leakage.

This paper used the harmonics property to deal with the "leakage" issue. The estimation process is described in Algorithm 1. The algorithm processes 512 samples of data in one window (C_{obs}) or iteration with a sampling frequency (f_s) of 20 Hz. Each window overlaps with the previous one by shifting 20 samples (C_{Δ_obs}), which is equivalent to one second. We have taken the HR estimate observed for the observation window as the value of the initial start time. For the observation window, the high

resonance component x_{c_hreso} is extracted through RSSD and power spectrum Px_{c_hreso} is calculated as in (4.10):

$$Px_{c_{hreso}}(f) = \left|X_{c_{hreso}}[k]\right|^2 \tag{4.10}$$

$where\ f = k * \frac{f_s}{N_{dft}}$, f_s is the sampling frequency and N_{dft} is the number of DFT points.

The HR fundamental, second, and third harmonic are located in the power spectrum of the high resonance component of the phase signal. Therefore, the index vector Piv_c is populated with the index of the largest peaks available in the frequency range of HR fundamental, second and third harmonics in the power spectrum $Px_{c_{hreso}}$. The frequency range for the second harmonic is dynamically adapted based on the value of HR fundamentals. Similarly, for the third harmonic, the frequency range is obtained adaptively from the values of the HR fundamental and second harmonic.

To determine the HR index that best represents the HR value, we compare the peak indexes observed in the fundamental, second, and third harmonic ranges. If the peak index in the fundamental range is within a 3 bpm to the second or third harmonic, we primarily rely on the fundamental peak index. This approach ensures the fundamental index is not affected by RR harmonics. However, if the HR fundamental is notably distant from the harmonics, indicating potential RR harmonic interference, we then compare the second and third HR harmonics. If their difference is within 3 bpm, these harmonics are chosen as the representative indexes. The HR value for the current observation window is estimated by averaging these selected indexes. In the event that none of the indexes fall within the 3 bpm range, we compare all three indexes with the previously selected HR index. We chose the closest index to estimate the HR value for the current window in such a worst-case scenario. Thus, the pairwise distance vector Dv_c for the elements of Piv_c can be calculated using (4.11):

$$Dv_c(q) = (|Piv_c(i) - Piv_c(j)|)\ \ \forall\, i \neq j, 1 \leq i, j, q \leq 3 \tag{4.11}$$

The minimum pairwise distance $Dv_c(q)$ is chosen, which is under the limit of Δ_d which corresponds to 3 bpm. Based on the chosen $Dv_c(q)$ the mean of corresponding indexes in Piv_c is taken as hr_{cind}. In the worst case, where none of the distances observed is under the limit of Δ_d then compare the distance between indexes in Piv_c with the estimated HR index of the previous window. The index in Piv_c with minimum distance is taken as hr_{cind} using (4.12) & (4.13).

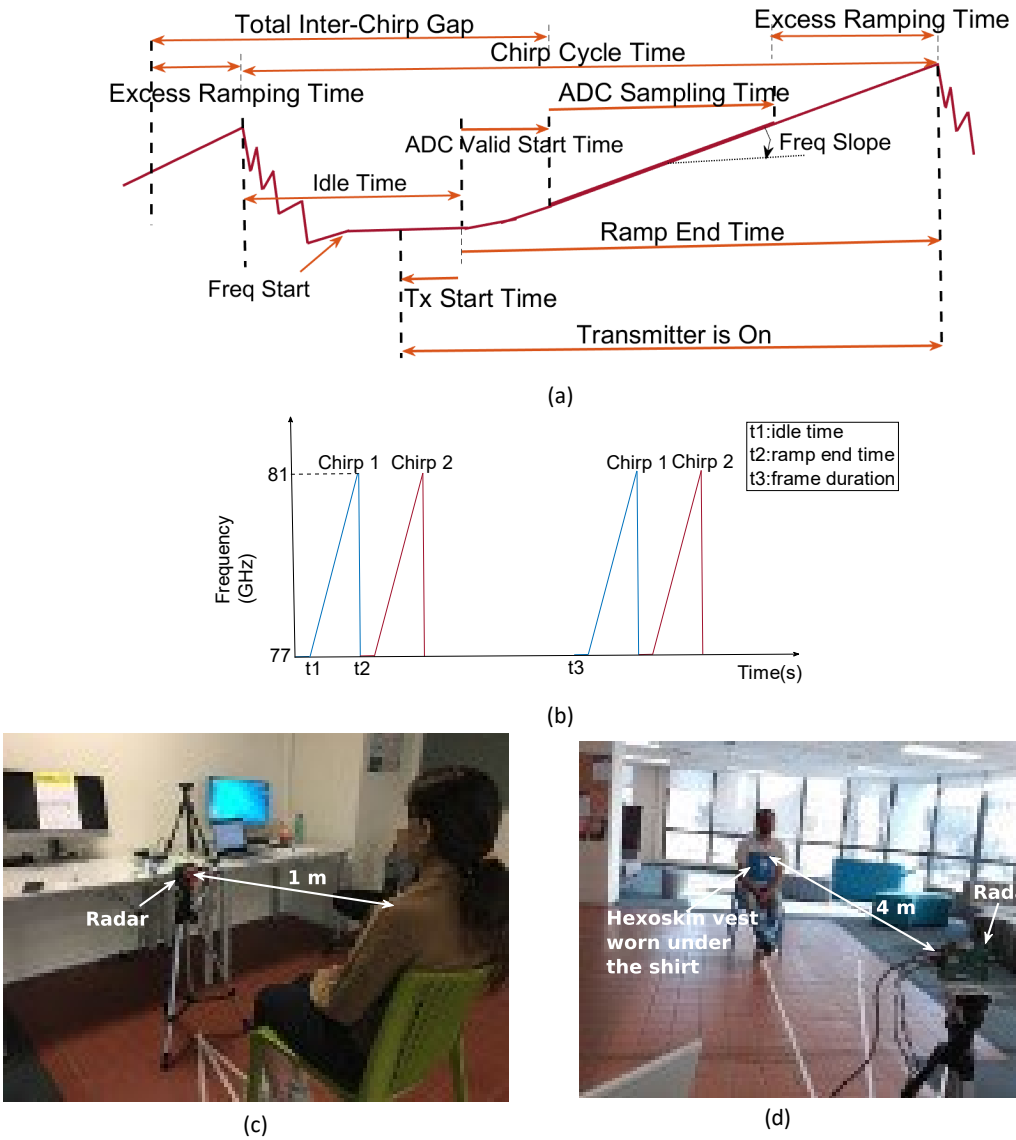

Figure 30: Experimental Platform: (a) Chirp configuration (b) Frame configuration (c) Experimental scene for zero-degree 1 m, and (d) experimental scene for zero-degree 4 m in static position

Table 8: Participants Details

Participant #	Age	Height(cm)	Weight(kg)	Gender
P 1	40	162	67	Female
P 2	30	186	85	Male
P 3	29	182.8	80	Male
P 4	28	152.4	64	Female

$$Dv_{\min} = min(|Piv_c(i) - hr_{cind}(k-1)|) \quad 1 \le i \le 3 \tag{4.12}$$

$$hr_{cind} = Piv_c(Dv_{\min}) \tag{4.13}$$

The heart rate in bpm is estimated using (4.14) as

$$hr_{est}(k) = hr_{cind} * f_s * 60/N_{dft} \tag{4.14}$$

The sliding window approach for estimation makes the non-invasive continuous HR monitoring fast enough for real-time applications.

4. Experimental Results

4.1 Experimental Setup

Four healthy participants (two male and two female) with the demographic parameters mentioned in Table 8 were hired for the data collection. The experimental setup is shown in Fig. 30. The experiments were conducted in the university staff lounge, simulating a home environment. The setup includes a sofa, Table, chairs, PC, refrigerator, wi-fi repeater terminal, and the metal window grid on the room wall, which constitutes the clutter. During data collection, the participants were asked to sit quietly in normal breathing conditions in front of the radar on a chair at a specified marked distance. The experiments were repeated by varying the distance and relative orientation to the radar. Four datasets at different distances (half, one, two, three, and four meters) and at different angles (zero, fifteen, and thirty degrees with respect to radar) were recorded for each participant. A total of 176 datasets of a duration of 105 sec each were recorded.

Our radar sensor consists of texas instruments (TI)' millimeter-wave IWR1443, an integrated single-chip FMCW radar sensor operating in the 77 to 81 GHz frequency band [238]. A Hexoskin vest is used for ground truth data collection in this study. Hexoskin [239] is an intelligent garment embedded with respiration sensors, in the form of two rings present in the chest and abdomen, and heart sensors, in the form of electrodes, can act as an electrocardiogram ECG. Cherif et al. [240] claimed that HR and RR measurement accuracy with Hexoskin is observed between 0.98 and 0.99 for almost all participants compared to the gold-standard laboratory measurement tools.

The original raw data for processing was captured using DCA1000 EVM along with the IWR1443 sensor board. The collected data were analyzed offline using MATLAB 2020a. IWR1443 consists of two transmitting and four receiving one-

dimensional linear array antenna layouts. In our experiment, a combination of $T_{x0} - T_{x2}$ with four receivers implemented to receive a reflected signal from the human body. Figure 30(a) depicts a single chirp and the associated timing parameters. Figure 30(b) shows a frame structure that consists of a series of chirps followed by inter-frame time. This represents fast FMCW modulation, where each chirp is typically 64µs in duration. A train of chirps is generated with chirp interval idle time = 7 µs, the sawtooth frequency modulation slope *S* = 70 MHz/µs, and the frame rate T_m = 5 msec. To better analyze the heartbeat and breathing rate per minute, at least four cycles of breathing or heartbeat signals are required. Therefore, the observation time *T* is kept at 105 sec, and the total number of frames is set to 20480. The data is captured over four low voltage differential signaling (LVDS) lanes of the DCA1000 capture card, and each lane corresponds to each receiver. The idle time setting needs to ensure the LVDS interface transfer is complete before the next chirp data is available. The time available for this data transfer is = "ramp end time" + "idle time". The data is stored in a binary file in an interleaved format.

4.2 Experimental Results

4.2.1 Target Detection and Phase Extraction

The sampled IF signal from the analog-to-digital converter (ADC) is stored in a data cube. The range information is extracted by applying the FFT over the fast time dimension of the data cube, and subsequently, vibration information is obtained by applying the second FFT over the slow time dimension. The circular center tracking algorithm [241] based on levenberg-marquardt-least square (LM) optimization is applied for DC offset correction caused due to micro-movement of the body, low-frequency static clutter, and spectral leakage. After DC correction, the center of the data points has shifted at the red point, as shown in Fig. 31 (a). The peak in the range slow time matrix gives the location

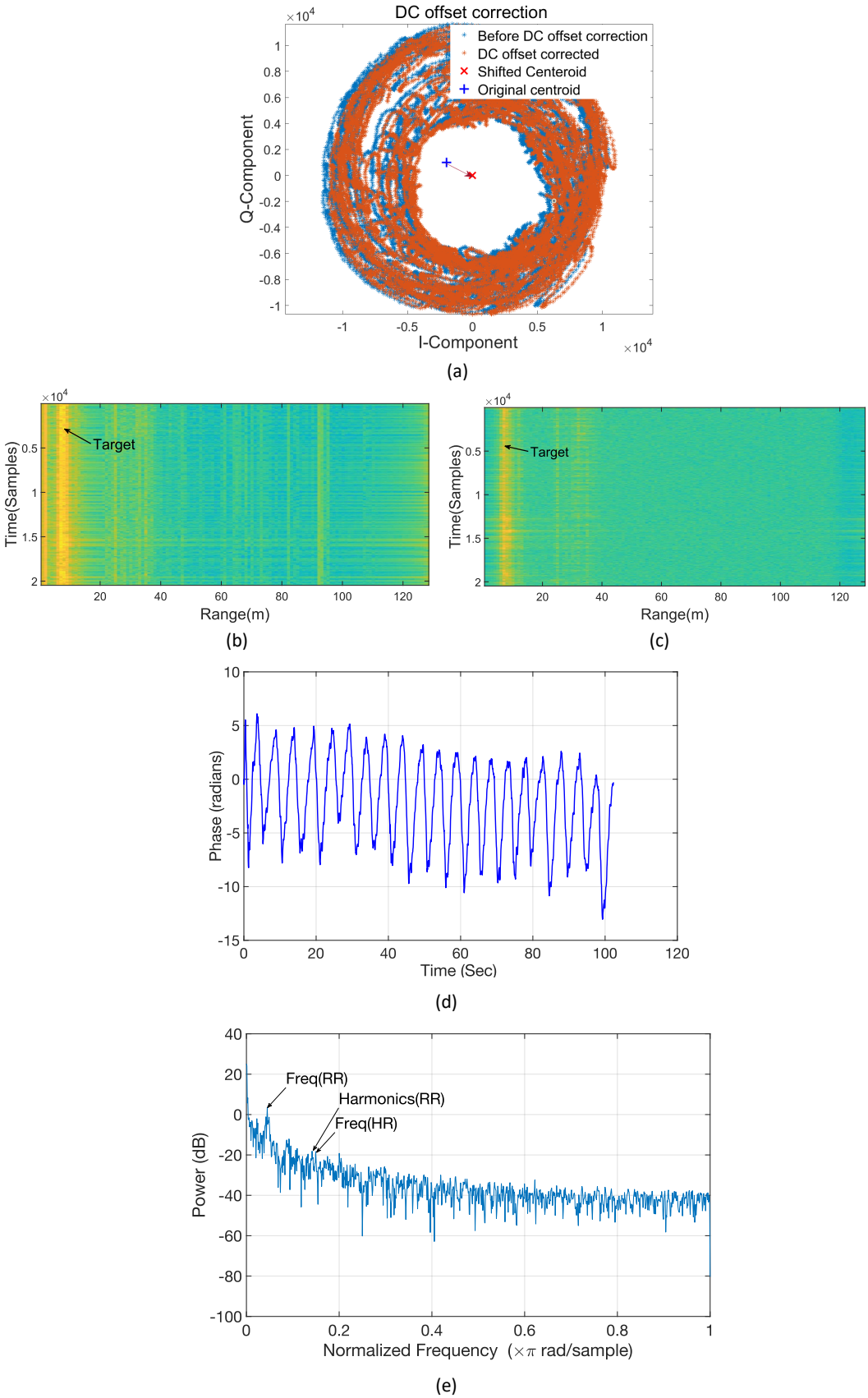

Figure 31: (a) DC offset correction (b), (c) Range profile spectrum before and after background subtraction (d) Phase signal, and (e) Phase spectrum showing RR harmonics close enough to HR in frequency range and amplitude

of the human target. However, in strong static clutter, target detection based on the peak detection technique will be erroneous. Therefore, we used frame differencing, the conventional background subtraction technique [119] as shown in Fig. 31 (b) & (c). After selecting desired range bin in the range-slow time matrix, the phase of the respective column is computed using the differentiate and cross multiply (DACM) method [42]. Fig. 31 (d) & (e) show the phase signal in the time domain and corresponding phase spectrum. DACM eliminates the requirement of phase unwrapping.

4.2.2 Decomposition of High Resonance Signal and Extraction of HR and RR

Decomposing the phase signal into high and low resonance parts requires the signal to be processed through RSSD with two different decomposition parameters (Q_1, r_1, J_1) and (Q_2, r_2, J_2), respectively.

The Q value defines the number of oscillations displayed by the wavelet and should be specified as greater than one. To avoid excessive undesirable ringing of the wavelet and localize it in time, redundancy r is usually taken as greater than or equal to 3 [242]. The extensiveness of information contained by the decomposed sub-signals depends on the number of filter banks, i.e., related to stages J. The number of stages must be maximized and constrained by the length of the input signal N.

We have derived the optimal decomposition parameters by designing and implementing a parameter optimization algorithm based on minimizing reconstruction error (Grid optimization technique). The reconstruction error is calculated using forward and inverse TQWT over the phase signal and for all combinations of parameters from the set.

We are processing phase signal of length 512 samples, and accordingly, the boundary values of stage J_1 are calculated as (27, 91) with redundancy parameter r_1, and r_2 is set as (3, 5) for both. As the low resonance part is characterized by the Q_2 and keeping it minimum with the constraint of localization in time, it is set as (1, 1.2) and the value of J_2 between (8, 10), which is sufficient to represent a low resonance signal [243].

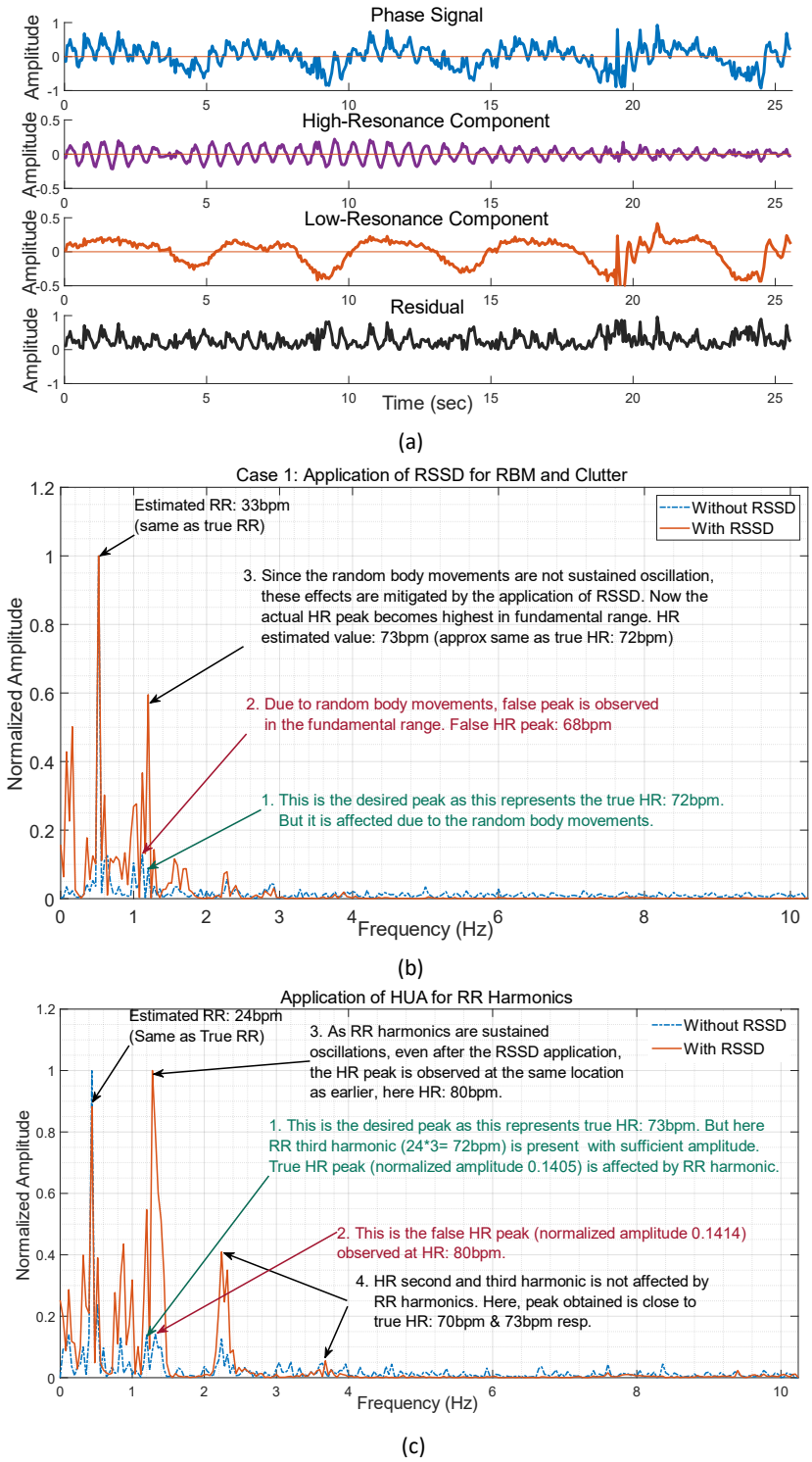

Figure 32: (a). Phase signal, High resonance signal from vital phase signal obtained through RSSD, Low resonance signal, and Residual from the phase signal; Spectrum of phase signal with and without the application of RSSD technique: (b) RBM and clutter mitigation using RSSD indicating sharply identifiable HR peak in the spectrum, (c) RR harmonics mitigation using HUA algorithm utilizing higher-order HR harmonic.

Using these values, Q_1 is calculated as per (4.6), and then iteratively varying all parameter values in step sizes of 0.5, 0.5, 1, and 0.05 for r_1, r_2, J_2, and Q_2, respectively,

the reconstruction error is estimated. Finally, the parameters are optimized for which the reconstruction error is minimum.

Fig. 32 (a) demonstrates the decomposition of the noisy signal. The high resonance signal is an almost ideal periodic signal composed of heartbeat and respiration frequency, and the interference from the clutter or random body movements is minimized. The signal in the topmost window displays the phase signal, which is the input to the RSSD algorithm. The rest three plots are the outputs that constitute the high resonance signal, low resonance signal, and residual from the phase signal. The high resonance contains all the oscillatory signals present in the phase signal, i.e., the high resonance signal contains the RR, HR, their harmonics, intermodulation frequencies, and any other oscillatory frequency if present in the phase signal at that moment.

Fig. 32 (b) shows the spectrum with and without applying the RSSD method. The spectrum of the breathing and heartbeat signal shown in the red line is obtained using a high resonance component of the phase signal. The HR peak obtained after applying RSSD is clearly identifiable at a true location affected by RBM and clutter in the original phase signal. However, RR harmonics and intermodulation products are sustained oscillations and therefore this component appears in high resonance. If the strong RR harmonics fall at or close to the true fundamental HR peak location, then the HR peak is not identified correctly even after the application of RSSD. HUA algorithm utilizes the higher-order HR harmonics for estimation, which are less likely affected by weak higher-order RR harmonics as described in Fig. 32 (c). By utilizing the resilience of higher-order HR harmonics, the HUA algorithm improves the reliability of HR monitoring, particularly when RR harmonics may interfere with the true fundamental HR frequency.

4.2.3 Performance Comparison

To verify the reliability and accuracy of the proposed method, experiments are performed with different participants, radar distance, and radar angles.

To validate the estimation performance, the similarity between two time-series data (radar and hexoskin time series estimation data) is measured based on similarity

measure parameters such as mean similarity, root mean square similarity, cosine angle between two series, and Pearson Correlation Coefficient [244]. The common interval [0, 1] maps the similarity, where 1 indicates the maximum similarity. Considering two vectors x and y of dimension n, the similarity between the two can be measured as,

$$sim_{xy(x,y)} = 1 - \frac{|x-y|}{|x|+|y|} \tag{4.15}$$

The mean similarity and root mean square similarity can be defined as,

$$mean_{sim_{xy(x,y)}} = \frac{1}{n}\sum_{i=1}^{n} sim_{xy(x_i,y_i)} \tag{4.16}$$

$$Rt_{mean_{sqr_{sim_{xy(x,y)}}}} = \sqrt{\frac{1}{n}\sum_{i=1}^{n} sim_{xy(x_i,y_i)}{}^2} \tag{4.17}$$

Another way is to evaluate the cosine of the angle between the two vectors x and y, which can be given as,

$$sim_{\cos\theta = \frac{X.Y}{|X||Y|}} = \frac{\sum_{i=1}^{n} x_i.y_i}{\sqrt{\frac{1}{n}\sum_{i=1}^{n} x_i{}^2}.\sqrt{\frac{1}{n}\sum_{i=1}^{n} y_i{}^2}} \tag{4.18}$$

The cosine similarity provides the range boundary [-1, 1]. The lower boundary value indicates that x and y are opposite, the upper boundary value shows both are the same, and the 0 indicates independence.

Similarity measure , the Pearson Correlation Coefficient C_{pcc} is also used to measure the linear correlation between two series . The Pearson correlation coefficient is a statistical measure that assesses the linear relationship between two continuous variables. This coefficient ranges from -1 to 1, with -1 indicating a perfect negative linear correlation, 1 indicating a perfect positive linear correlation, and 0 indicating no linear correlation. It is calculated by dividing the covariance of the two variables by the product of their standard deviations. Widely employed in scientific research, the Pearson correlation coefficient provides insights into the degree and direction of association

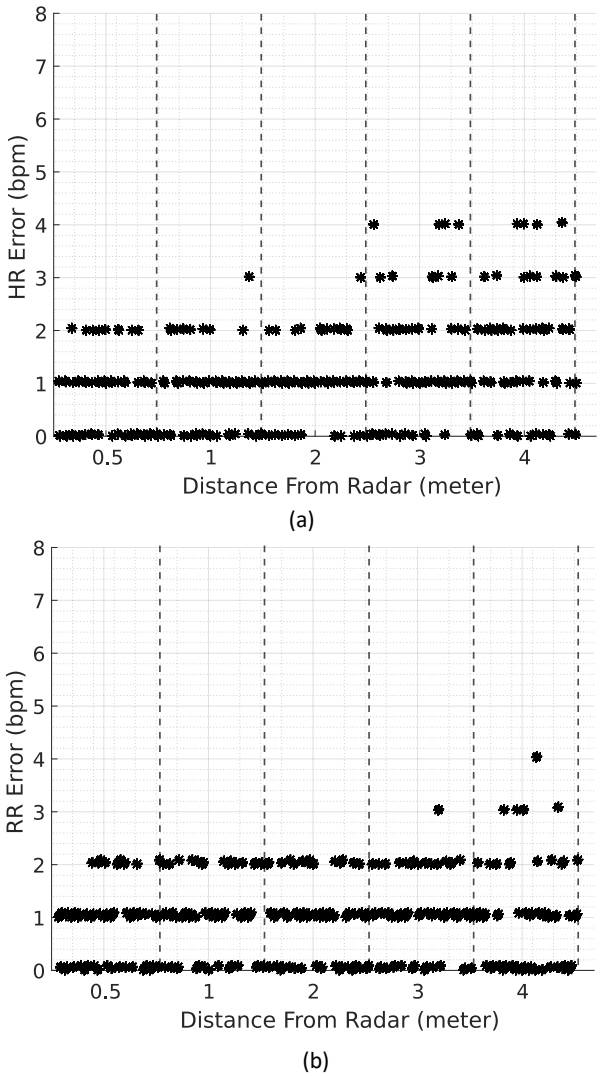

Figure 33: The error rate for (a) HR and (b) RR estimation for increasing distance between target and radar from half meters to four meters for all four participants

between two time series variables. The Pearson product-moment correlation coefficient for two series X and Y is identified as a similarity index and is defined as,

$$\rho(X,Y) = \frac{1}{(n-1)} \sum \left(\frac{\mathrm{Xi}-\mu\mathrm{X}}{\sigma\mathrm{X}}\right)\left(\frac{\mathrm{Yi}-\mu\mathrm{Y}}{\sigma\mathrm{Y}}\right) \tag{4.19}$$

where $\mu\mathrm{X}$, $\sigma\mathrm{X}$ and $\mu\mathrm{Y}$, $\sigma\mathrm{Y}$ are the mean and standard deviation of X and Y, respectively, with each variable having n scalar observations. In time series analysis, the normalized time-dependent Pearson correlation coefficient (PCC) is an indicator of similarity index as the cross-correlation coefficient value must lie in the range from −1 to 1, with one indicating perfect correlation.

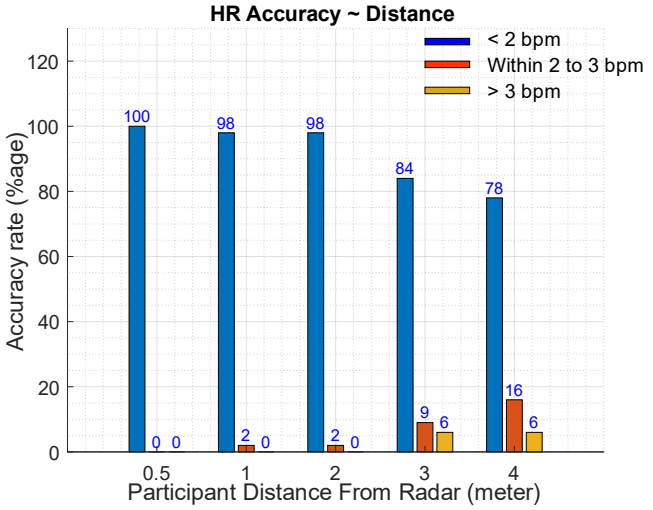

(a)

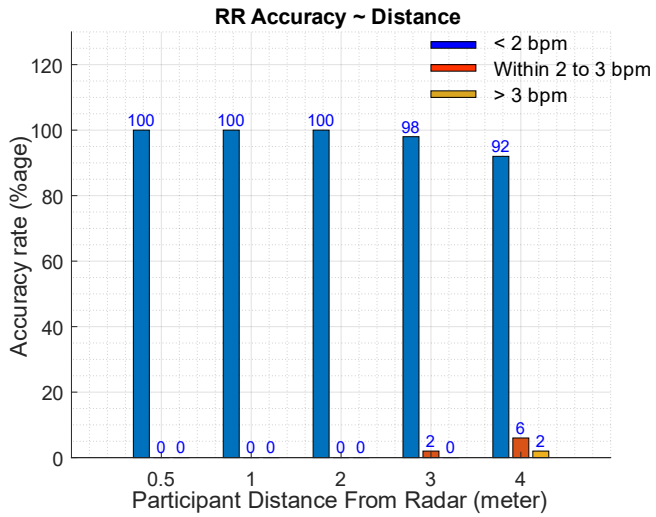

(b)

Figure 34: Accuracy rate indicating the percentage of time experimental value is same as the reference at varying distance, (a) HR accuracy rate, and (b) RR accuracy rate at half, one, two, three, and four meters.

Additionally, accuracy is evaluated in breaths/beats per minute. Classification of accuracy rate is defined for the values <2 bpm, between 2 and 3 bpm, and >3 bpm compared with respect to the referenced wearable sensor values.

A. Impact of Distance

The distance between the radar and the subject's chest is approximately 0.5 m for the first set of experiments (Fig. 30 (c)). Then distance was varied up to 4 m (Fig. 30 (d)). The median of similarity measures, i.e., the similarity index for RR for all datasets, lies in the range of 0.95 to 0.99. The PCC is in the range of 0.8-0.9. The similarity decreases slightly for the larger distance between the radar and the target. Similar behavior is exhibited for HR, but the drop in similarity for larger distances is slightly higher than the drop in

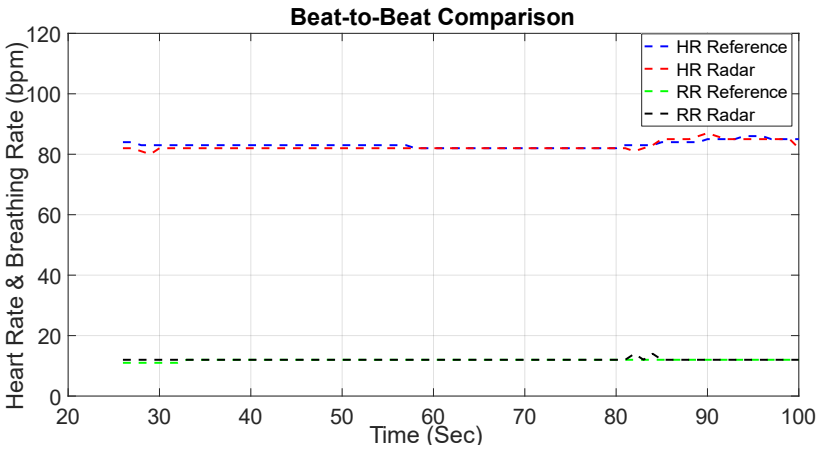

Figure 35: Heart Rate and Breathing Rate beat to beat comparison for the duration of 75s measurement data.

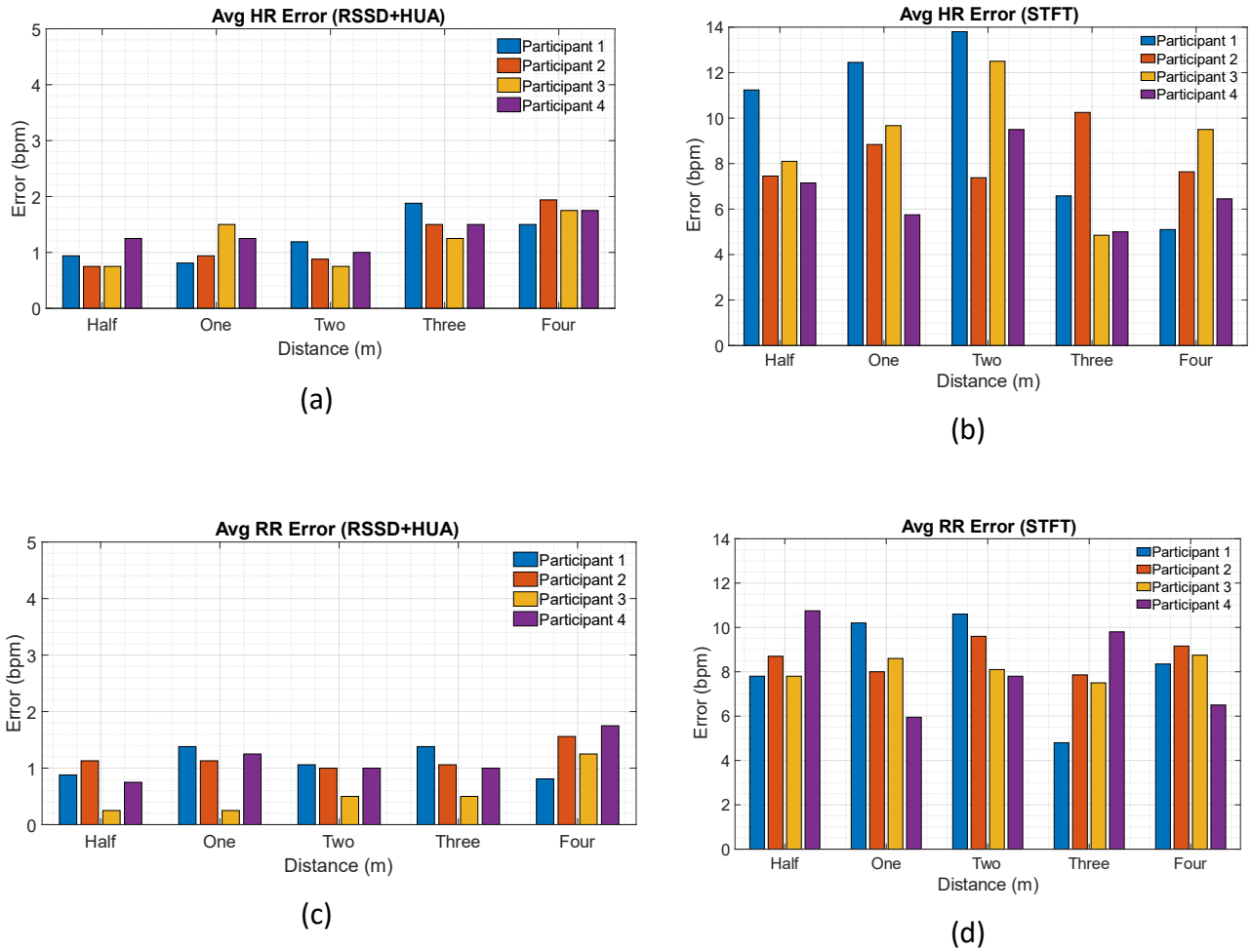

Figure 36: The average error rate using RSSD+HUA and STFT for (a), (b) HR (c), and (d) RR respectively for increasing distances between target and radar from half meters to four meters for all four participants.

RR similarity indexes. The overall average similarity indexes for HR are in the range of 0.98-0.99, and the PCC lies between 0.8-0.9. The similarity measure parameters are

consistent with the error rate in breaths per minute shown in Fig. 33. and it demonstrates the average accuracy rates for all participants with respect to the distances for HR and RR, respectively.

The overall accuracy rate of the method is defined as the difference from the referenced within two bpm. It is evident from Fig. 34 that the HR and RR accuracy rate is 98-100% between true and experimental values even up to 2 m distance. As the overall accuracy rate of the method is defined as the difference from the referenced within two bpm. It is evident from Fig. 34 that the HR and RR accuracy rate shown in Fig. 34 (a), the difference between the reference and experimental values is within 2 bpm for 2 m and within 3 bpm for 4 m. The performance is not affected much at a distance up to 2 m, and the error difference of up to 3 bpm is observed for more considerable distances. The accuracy rate decreases as the distance increases, and the rate of decline in accuracy is lesser in RR estimation as compared to HR estimation. Fig. 35 shows the beat-to-beat comparison of heart and breathing rates obtained by the proposed method using the radar sensor and Hexoskin vest for one data set for participant 3. The graph shows that experimental values closely follow the true values after an initialization period of 26 sec.

A short time-frequency transform is used for analyzing signal characteristics in the time-frequency domain. The vital signal being time-varying, these can be analyzed in the time-frequency domain with a carefully chosen STFT window length. To better ascertain the efficacy of the proposed algorithm, we analyzed the results obtained with the STFT method and our proposed RSSD-based HUA algorithm. These results are shown in Fig. 36. The average HR and RR estimation error for all participants with respect to the distances ranges between 4 to 11 bpm for STFT. The average HR and RR error rates of less than 2 bpm are observed for the proposed algorithm, emphasizing the advantage of the RSSD-based HUA algorithm.

B. Impact of Artificial Clutter and Body Movement

To observe the performance under heavy clutter and moderate body movement, we conducted experiments on two subjects in a home environment that included

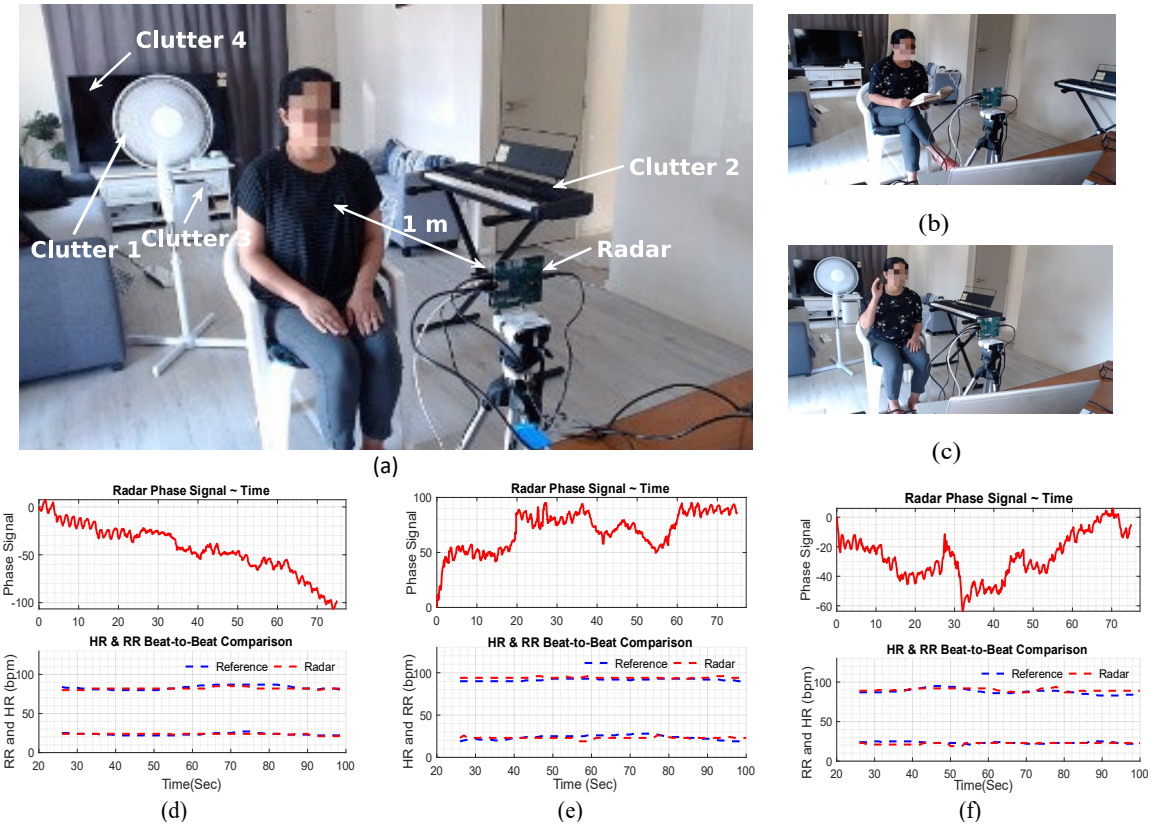

Figure 37: Experimental set up (a, b, c) for different clutter and body movement scenario, phase signal, and HR and RR beat-to-beat comparison for (d) additional clutter only (e) body movement only, and (f) additional clutter with body movement.

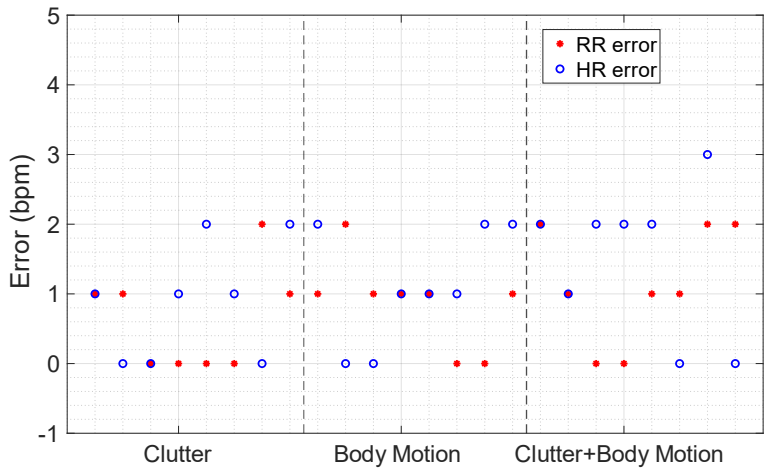

Figure 38: RR and HR error estimation in different scenario of clutter and body movement.

household items to constitute the additional clutter. The TV was at 4 m; the dehumidifier was placed at 3.5 m, the keyboard was beside the subject at the same distance, and the running fan was just behind the subject at 2 m. The subject was seated on a chair at 1 m from the radar. The experiments were conducted in three different scenarios of clutter and body motion. In the first case, only additional clutter was introduced. The subject was asked to sit static in a comfortable position without any body movement. In this

case, clutter such as a running table fan, dehumidifier, and a keyboard with an iron stand was placed near the subject, as shown in Fig. 37 (a). The running fan frequency differs from the RR and HR frequency bands. However, any artificial clutter having a frequency within the band of RR and HR frequency will affect the measurement. As the frequency of the respiration and heartbeats is a maximum of 1 Hz to 2 Hz, any signal with the same frequency clutter will affect the heartbeat and respiration rate as it shall also be a high resonating signal in the same frequency range. The scenario is not tested in this study and is left for future work. The perturbations due to clutter can be seen in the phase signal. The high resonance signal obtained after applying the RSSD algorithm is resonating, and the zero crossings are clearly distinguishable. This facilitates the HUA algorithm to extract the HR quite accurately. The beat-to-beat comparison of the true and estimated value of HR and RR, as shown in Fig. 37 (d), shows that the algorithm effectively addresses the clutter issue.

The additional clutter close to the subject was removed in the second scenario. The subject was asked to do a moderate activity like changing the position of arms, moving a hand up and down, crossing the legs, turning the pages while reading a book, to-and-fro body movements in the direction of radar, etc., as shown in Fig. 37 (b) & (c). The subject performed three to four times small activities to cause moderate body movement during 75-sec of measurement time. The abrupt change in phase can be seen in Fig. 37 (e). However, the HR value is estimated satisfactorily at these abrupt phase transitions. The maximum error is 4 bpm at the starting point where the abrupt phase occurs, and the minimum error for the complete observation duration of the scenario is 1 bpm. The estimation approaches the true value more rapidly as soon as the body movement/activity burst phase is over.

In the third case, additional clutter was introduced again, similar to the first case, shown in Fig. 37 (e). The variation due to clutter and body movement can be seen in the phase signal. During the body movement, the error observed between the true and estimated value is up to 2 bpm. However, the estimation performances become comparable to the true value after the body movement phase is over. The performance comparison for all three cases mentioned above is shown in Fig. 38, which shows that

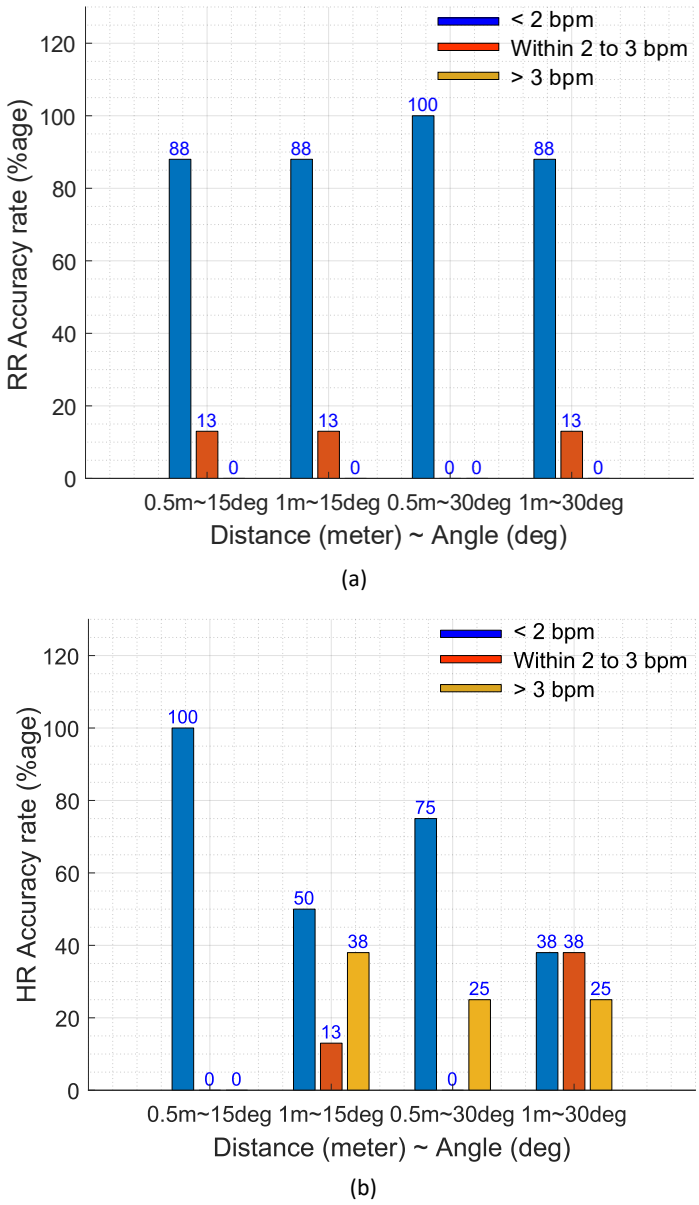

Figure 39: Accuracy rate represents the percentage of agreement with reference at varying distance and incidence angle (a) RR, and (b) HR.

the HR estimation is carried out as accurately as the RR estimation. The proposed method exhibits clutter and moderate body movement mitigation within the average HR and RR error of 2 and 1 bpm in all cases mentioned above. In addition, we find that the proposed method performs robustly with an average HR and RR error of 1 bpm under cases I and II. The average HR error is slightly higher to 2 bpm for case III, in which both additional clutter and moderate body movement were introduced. However, the average RR error is still under 1 bpm for case III.

C. Impact of Radar Angles

The impact of the radar angle on the estimation of RR and HR is also studied. We used two additional radar angles [15^0, 30^0] other than zero to evaluate participants breathing and heart rates. The deployed radar is TI IWR1443 EVM which consists of onboard etched antennas for the four receivers and three transmitters. The antenna peak gain is > 10.5 dBi across the frequency band of 76 to 81 GHz. At 78 GHz, based on a 3 dB drop in the gain as compared to bore sight, the horizontal 3dB-beamwidth of the antenna is approximately $\pm 28^0$, and the elevation 3 dB-beamwidth of the antenna is approximately $\pm 14^0$ [238]. We have used two transmitters and four receiver combinations in our experiments.

The experiments are performed at a half and one-meter distance. The overall accuracy for all the participants for RR and HR with different radar angles is shown in Fig. 39 (a) and (b), respectively. It is observed that the accuracy decreases with the increment in the radar angle for both RR and HR estimation. Even at lower radar angles, the accuracy decreases substantially if the distance has increased from a half meter to one meter. The reason is that the reflection loss depends on the radar angle, and an increment in the angle increases the reflection loss, rendering poor SNR of the reflected signal.

Similarly, the increased distance for the same radar angle decreases the radar cross-section (RCS) observed as the target area goes out of the beam span. However, since the SNR of the breathing signal is much higher than the heartbeat signal, the performance degradation of RR estimation is not as severe as HR estimation.

5. Discussions

After applying the circular center dynamic tracking algorithm to correct the DC offset, the extended DACM allows us to obtain heartbeat and breathing-related phase information. RSSD and the estimation algorithm are proposed to process the extracted differential phase signal. The high resonance signal obtained by the RSSD, and its corresponding spectral function observes periodicity. The proposed method reduces the

Table 9: Summarized analysis of different algorithms (stationary target) for (a) HR and (b) RR estimation

Paper	Radar System	Distance	Position	Method/Algorithm	Dataset	Measurement	RR Error (bpm)	HR Error (bpm)
[41]	UWB	15cm	sitting	Spectrum-Averaged Harmonic Path (SHAPA)	8 participants	Stationary HR	-	1.43%
[43]	LFMCW MIMO	~1m	sitting	EMD	-	stationary	-	4.4bpm
[44]	FMCW	1.7m	sleep	Advanced phase unwrapping manipulation	-	RR/HR	94%	80%
[118]	CW	40 cm	sleep	Peak detection algo	6	Stationary HR	-	96.78%
[134]	FMCW	0.6-0.9m	sitting	Compressive sensing based on orthogonal matching pursuit (CS-OMP) algorithm and Rigrsure adaptive soft threshold noise reduction based on discrete wavelet transform (RA-DWT)	10	RR/HR	93%	93%
[245]	FMCW	1-2m	sitting	wavelet packet transformation & spectral frequency estimation	8	RR/HR	1.21 bpm	3.138 bpm
[246]	IR-UWB	30 cm	sitting	Quadrature Demodulation IR-UWB radar	1	HR	-	4 bpm
[247]	SFCW-UWB	2m	sleep	Empirical wavelet transform (EWT)	10	RR/HR	0.3 bpm	2 bpm
[248]	FMCW	2m on ceiling	sleep	Fast Fourier transform based cepstral and autocorrelation analyses	11 participants	RR/HR	96.5%	96.3%
[249]	FMCW	1m	sitting	Adaptive peak detection, and Band pass filter	10	RR/HR	91.08	87.2
[250]	CW	1.5m	sitting	Adaptive noise cancellation (ANC) with polynomial fitting and new-type discrete cosine transforms (N-DCT)-based spectrum extractor	-	RR/HR	4.86	1.25
[251]	CW	1m	sitting	Fast Fourier transform (FFT)	16 participants	Stationary HR/RR	Error rate: 5%	Error rate: 5%
[252]	IR-UWB	1m	sitting	Fast Fourier transform (FFT)	7 participants	Stationary HR/RR	RR: 0.3 bpm	HR: 8 bpm
[253]	UWB	0.2-5m	sitting	Ensemble empirical mode decomposition (EEMD) and Continuous wavelet transforms (CWT)	3 participants	Stationary RR	0.3bpm	-

Table 10: Summarized analysis of different algorithms (stationary target) for (a) HR and (b) RR estimation (cont.…)

Paper	Radar System	Distance	Position	Method/Algorithm	Dataset	Measurement	RR Error (bpm)	HR Error (bpm)
[254]	UWB	3m	sitting	Ensemble empirical mode decomposition (EEMD)	5 participants	Stationary HR	-	Error rate: 1.5–3.75%
[255]	UWB	0.64m	sitting	Harmonic Multiple Loop Detection (HMLD)	10 participants	Stationary HR/RR	Error rate (RR): 4.95%	Error rate (HR): 5.06%
[258]	IR-UWB	1.25m	sitting	Time Domain Processing Algorithm	5 participants	Stationary HR	-	Error rate: 1.01%–4.32%
[259]	UWB	1m	sitting	Time series analysis	-	Stationary HR	-	Error rate: 1.26%
[This Paper]	**FMCW (Proposed method)**	**0.5-4m**	**Sitting/Minor Body movements**	**RSSD using TQWT**	**4 participants/ 64 dataset per participant**	**Stationary**	**Less than 2 bpm for distances up to 3 m**	**Less than 3 bpm for distances up to 3 m**

Table 10: Summarized analysis of different algorithms (with Body Motion) for (a) HR and (b) RR estimation

[33]	FMCW	5.4m	Sitting and walking	FFT, Continuous Wavelet Transform (CWT)	8 participants	Non-Stationary HR/RR	RR: 94%	HR: 89%
[231]	IR-UWB	1-2m	Sitting and minor body movements	Kalman filter, auto-correlation-based technique is applied for detecting random body movements	30/	Body movement	6bpm	8-19bpm
[256]	IR-UWB	4.5m	Standing and minor moving body	Wavelet, Kalman filter	4 participants	Non-Stationary HR	-	Error rate: 2.25%–4.6%
[257]	UWB	0.7m	Sitting and minor hands movements	FFT	1 participant	Non-Stationary RR	SNR (handwriting): 16 dB	-
[This Paper]	**FMCW (Proposed method)**	**1m**	**Sitting/Minor Body movements**	**RSSD using TQWT**	**1 participant/ 12 dataset**	**moderate body movements**	**Less than 2 bpm**	**Less than 2 bpm**

irregular waveform phenomenon and effectively reduces the noise and harmonic interference while retaining the time-frequency characteristics of the original phase signal.

Prior researchers have deployed different algorithms for vital sign extraction from the radar signal. The summary of the previous work is given in Table 10 to present the comparison with the proposed algorithm. Though most researchers have presented the works for the stationary human subject, being perfectly stationary for a long time is not feasible for humans, and some body movement always happens after a time. We have also included the works which presented vital sign extraction for body movement scenarios separately and are summarized in Table 11. Compared with the algorithms deployed in earlier works, the proposed algorithm shows an accuracy of up to 98-100% for distances up to 2 m. However, the performance of the RSSD algorithm relies not only on the signal intrinsic characteristics but also on the selection of ideal parameters to a great extent. The selection of high and low resonance quality factors and optimized weight factors is challenging.

Among the various signal processing and analysis techniques, the resonance sparse spectrum decomposition based on tuneable Q-factor wavelet transform (RSSD-TQWT) is more feasible due to its relatively high computational efficiency. Empirical wavelet analysis (EWA), stationary wavelet transforms (SWT), and undecimated wavelet transform (UWT) share comparable computational costs of O (N log N) depending on factors like the chosen wavelet, number of decomposition levels, and signal length [59]. While empirical mode decomposition (EMD) and variational mode decomposition (VMD) are computationally expensive with a cost of O(N2) or higher due to the signal length and the number of iterations required for convergence [60]. However, RSSD-TQWT exhibits a significantly lower cost of O (r N log N), where N represents the signal length and r denotes the redundancy factor [28]. Moreover, its implementation is optimal, ensuring a linear relationship with r. Additionally, the computational cost as a function of N remains low, benefiting from its reliance on the discrete Fourier transform (DFT).

Our research would greatly help in an application where contact is to be avoided, such as burnt patients and neonates. The proposed system was tested for four subjects over multiple distances, and their heart and respiration rates were accurately estimated. The contribution of this work to the community is that it provides:

- Detailed analysis and application of RSSD and harmonic-based signal processing in HR/RR estimation
- Our proposed method verifies reliable HR estimation up to four meters.
- The efficacy of the proposed method is validated on HR/RR estimation by varying the target's distance.
- The effect of heavy clutter and moderate body movement on the HR/RR estimation is analyzed.
- Analysis of the impact of different radar angles on the accurate HR/RR estimation detection rate.

Although the proposed method observes HR detection as accurately as RR detection under a daily ambulant environment, a few limitations deserve further research. Impacts of daily objects on measurements:

- The Texas Instruments millimeter-wave IWR1443 radar system possesses range and angular discrimination capabilities. The proposed algorithm is designed for a single human participant, and there exists an opportunity for future enhancement. However, the proposed method can be extended to accommodate monitoring multiple individuals by employing a minor modification in the phase signal selection part of the algorithm.
- As the chest wall motion and, consequently, the phase signal shall be different for a static person having hyper/hypoventilation conditions, it would be beneficial to investigate how the algorithm performs under hyper/hypoventilation conditions in future works.

6. Conclusion

In this paper, the resonance property of a non-stationary vital signal is utilized to extract the heart and breathing signal from a noisy radar signal. This paper systematically introduced the signal processing flow and parameter configuration for an FMCW radar. The RSSD algorithm is applied to the extracted phase signal to efficiently decompose the HR signal to remove the effect of random body movements and clutters. Then, the HUA algorithm is used based on the higher-order harmonics to suppress the influence of RR harmonics and intermodulation products on HR value. The detection accuracy rate of heart rate and respiration rates are comparable to reference even up to a considerable distance of 4 m from the radar, proving the feasibility and effectiveness of RSSD in remote HR/RR monitoring. The implementation of transmitter beam steering and digital beamforming on the receiving end would complement this work. The advantages include an increased SNR and improved target localization, which we have left for future work.

Chapter 5

A Real-time Beam Steering and Accurate Vital Signs Estimation Method in an Indoor Environment

Abstract

An accurate heart rate (HR) estimation using a radar sensor is challenging in a real-life situation due to interference from unwanted clutter, respiration (RR) harmonics, body movement, and especially variations in the target's position. To address these challenges, this paper presents a real-time beam steering algorithm that dynamically determines the target's position at the beginning of each measurement cycle while simultaneously calculating the range-angle values of the target during the scanning phase. We propose a novel method based on resonance sparse spectrum decomposition (RSSD) that leverages sub-band energy distribution for optimizing the quality factor (Q) and the subsequent extraction of HR using harmonics. The Q factor defines the resonance property of an oscillatory signal, and hence, signal components with similar center frequencies band but with a different quality factor, Q, can be separated and sparsely represented. This RSSD-based algorithm mitigates the effects of clutter and random body motion from the phase signal while optimizing the Q factor through sub-band energy distribution, ensures accurate extraction of the high-resonance segment of the signal, and significantly enhances HR estimation accuracy. Comprehensive experiments performed under various realistic conditions were utilized to evaluate the efficacy of the proposed method. The results demonstrate that with the proposed method, coupled with beam steering, the HR accuracy remains consistently high at 98.72% within a 4m range across all azimuth angles.

This contribution has been submitted for review in IEEE IoT Journal

1. Introduction

Monitoring human vitals like heart rate (HR) and respiration rate (RR) can lead to suggestions for changes in indoor lifestyle activities, reducing the likelihood of disease, which is a crucial aspect of healthcare. Radar-based physiological state monitoring is a promising approach to the long-term measurement of vital signs and is helpful in many applications [217], [260], [261]. Home health care and monitoring systems have triggered potential public interest as real-time monitoring of physiological parameters can avoid many health emergency conditions [248], [262].

Heartbeat and respiration generate periodic micro-movements of the human chest, producing a periodic vibration collected by the radar sensor. Due to considerable interest, several methodologies and techniques exist for human vital sign extraction. Radars have directional beam patterns, and the detection performance degrades substantially if the person is not directly facing the radar at a fixed distance. In literature, most radar-based vital sign estimation systems require individuals to be placed at a specific distance and zero-degree angle-of-arrival (AoA) directly in front of the radar. However, in reality, people tend to change their sitting or sleeping position frequently, making this approach challenging to implement. In addition, the reflected radar signal strength, and the accuracy of estimating vital signs can be influenced by each individual's unique physical body structure and sitting or sleeping posture. The radar cross section (RCS) of the human body is approximately between 0.5 m^2 to 3 m^2 [263], and more specifically, the real cardio-pulmonary reflections have an RCS of less than 0.5 m^2 [264].

The accuracy of estimating vital signs can be enhanced by localizing and directing the radar transmission toward the human target, which can increase the strength of the reflected signal. A beam steering phased array can be used to steer the beam transmission angle toward the human subject. However, as manual steering is not feasible in real-life scenarios, a real-time beam steering solution is required to improve estimation accuracy. In a multiple input and multiple outputs (MIMO) radar system with multiple transmitters (Tx) and receivers (Rx), the phase values across the system can be adaptively altered for a specific angle of arrival. This enables the beam-steered signal to

be directed toward the human target and improves the signal-to-noise ratio (SNR). Thus, in real-life situations, steering the radar beam toward human participants can be beneficial for accurate vital sign estimation.

In some of the studies, the effect of receiver beamforming is studied where the methods included conventional or adaptive digital beamforming [265], portable FMCW radar transceivers with beamforming arrays [266], and ultra-wideband array radar with the Capon adaptive beamforming technique [267]. These methods mainly focused on estimating respiration signals for stationary targets with limited angular resolution. There is a tradeoff between resolution and antenna array size.

Beam steering is used scarcely for localization and vital sign extraction of targets [268]-[270]. Real-time beam-steering for vital sign measurement is a novel approach yet to be widely explored. The primary challenge lies in the real-time processing of the radar device, which includes configuring phase delays in transmitter antennas, handling hardware limitations, and addressing beamforming errors. Hardware constraints can impact the efficiency and precision of beam steering, influenced by factors like antenna quantity and arrangement. Achieving precise calibration and synchronization is crucial for accuracy, but hardware or timing alignment errors can introduce inaccuracies, particularly in dynamic environments or with multiple radar systems in play. Components like the antenna array, phase shifters, and control system are pivotal, and maintaining phase signal quality is essential. Selecting appropriate parameters, such as radar frame duration and scanning time, is critical to minimize frame loss and ensure efficient performance during real-time processing.

Several algorithms have been developed for vital sign estimation to address the issues of noisy and weak HR signals. Traditional spectrum-based algorithms such as the short-time Fourier transform (STFT), empirical mode decomposition (EMD), ensemble empirical mode decomposition (EEMD), and variable mode decomposition (VMD) only focus on the HR and RR fundamental peaks but ignore their harmonics. It is difficult to accurately estimate the HR, due to the fact that the RR harmonics and intermodulation components also have a similar frequency range to the HR, so they may mask the HR fundamental frequency. In this paper, we employ resonance-based sparse signal

decomposition (RSSD) alongside an optimal Q selection method and leverage HR harmonic components to enhance the heartbeat frequency estimation accuracy.

Our research focuses on empirically evaluating beam steering's efficacy in human localization and beamforming across non-zero angles of arrival. The main contributions of this work are as follows:

- We propose a real-time scanning algorithm based on beam steering, which utilizes a range-angle map to accurately locate the human target's position. This method demonstrates a high accuracy of 98.72% within a 4 m range across all azimuth angles in the HR/RR estimation, owing to a substantial signal strength increase of approximately three-to-fourfold, resulting from an SNR boost of about 4-5 dB.
- We propose a resonance-based sparse signal decomposition (RSSD) method, which combines optimum quality factor selection with sub-band energy distribution relative to total signal energy. This enables high resonance signal extraction under heavy noise conditions with a mean estimation error reduced from 10 bpm to 1 bpm.
- We devise an experimental strategy to mimic real-world scenarios for stationary/non-stationary targets at unknown locations. We evaluate the reliability and robustness of the proposed method through comprehensive experiments with six participants in various scenarios.

The rest of the manuscript is organized as follows. Section 2 delves into a review of previous studies, while Section 3 elaborates on the research's theoretical framework and methodologies, focusing on beam steering, beamforming techniques, and the signal processing algorithm essential for vital sign measurement. The experimental procedures and their corresponding results are detailed in Section 4. Finally, Sections 5 and 6, respectively, present a comprehensive discussion of the research findings and conclusion.

2. Related Work

In most previous studies, human subjects are located at zero angles of arrival during the vital sign measurements. However, it is unlikely that the subject will be directly in front

of the radar for most practical applications. Beam steering and beamforming can be used to increase SNR locate and measure the vital signs of human participants present other than at the zero angles of arrival.

Xiong et al. [265] proposed a single-input–multiple-output (SIMO) radar system with an adaptive digital beamforming (ADBF) technique to estimate only the respiration of multiple stationary human subjects at unknown positions. In their work, Peng et al. [266] presented a novel method by implementing a portable K-band FMCW radar transceiver with a beamforming array realized on a printed circuit board. The approach demonstrated the application of vector controllers and a six-port circuit for short-range target localization. Muragki et al. [267] utilized ultra-wideband array radar and the Capon adaptive beamforming technique with different diagonal loading factor values for the angle of arrival estimation for stationary targets. Only respiration displacement was extracted.

In [269], the static beam steering technique was used to isolate the respiratory signatures for individual subjects from radar signals reflected simultaneously from multiple subjects separated by a 30° angular discrimination limit. However, the two subject's position was fixed at a pre-defined angle. In [270], the authors developed a 2x2 microstrip patch antenna and two phase shifters on a single board to achieve an adaptive beam-steering range from -22° to 22° in the H-plane to measure vital signs. However, HR estimation was conducted while holding the respiration, limiting the application in a realistic scenario as it does not mimic the normal physiological condition where heart rate and respiration occur simultaneously. The author in [271] designed and implemented a time-division multiplexing (TDM) phased-MIMO radar sensing scheme for high-precision vital sign monitoring of multiple humans at the same radial distance to the radar at a known position.

Some contributions are made in designing a self-injection locked (SIL) metamaterial leaky wave antenna. The dual-beam radiation leverages space diversity and addresses the phase collision problem. In [272], Wu introduced two types of radar sensor architecture integrated with a metamaterial (MTM) leaky-wave antenna (LWA) to detect multi-target vital signs and locations simultaneously. However, the beam

scanning was frequency-dependent, and the measurement distance was from 0.5 to 1m, limiting its application in real-life scenarios. In [273], Rabbani et al. designed a beam-scanning Fabry–Perot LWA for remote vital sign monitoring (RVSM) in a dynamic environment for patients during sleep. Su et al. [274] presented a switched phased-array (SPA) radar using SIL and digital beamforming (DBF) technologies for estimating the vital sign detection of a single stationary person. The system was efficient compared to the conventional phased array radar in terms of complexity and target localization, but the clutter and random body movement due to non-stationary subjects were not addressed.

Combining multi-beam and phased-array designs enabled multi-beam radiation to scan in different directions; authors in [156], [275] addressed the phase collision issue of the target's signatures. The design was capable of detecting multi-person respiration signals with a limited measurement range of 2-3m. Ahmed et al. [276] provided an experimental comparison of vital sign extraction with and without beamforming. The preliminary results suggested that as the observation angle increases, the effectiveness of beamforming increases. Conventional beamforming was employed. However, adaptive and complex beamforming was left for future work. The authors primarily worked on applying conventional beamforming to improve SNR for stationary targets. The signal processing issues related to clutter and random body movements for non-stationary targets were unaddressed. In [277], Dai used MIMO configuration to improve the SNR level by leveraging its channel diversity. Vital sign information was extracted using arctangent demodulation (AD) and maximal ratio combining (MRC) with an adapted wavelet continuous wavelet transform (CWT). The improvement of HR estimation accuracy was observed by addressing the stationary and moving clutter issue. However, non-stationary targets and moving clutter close to the respiration rate were unaddressed.

Recently, various novel signal processing algorithms have been used to address the challenges related to non-stationary targets, moving clutter, and enhancing the accuracy of vital sign measurements. The Hilbert-Huang transform (HHT) is utilized to identify respiration characteristics and cardiac signatures, as demonstrated in [278]. HHT effectively separates the characteristics of breathing and heartbeat in the time-

frequency domain. Zhang et al. [279] applied empirical mode decomposition (EMD) to detect vital signals in multiple individuals. Ensemble EMD (EEMD) has gained significant popularity as an enhancement to EMD. Hu et al. [280] introduced an EEMD-based noise reduction approach and a CWT-based method for precisely separating respiratory and heartbeat frequencies using radar sensors.

Variational mode decomposition (VMD) has been introduced as an alternative to EMD as the EMD lacks a robust mathematical foundation. VMD effectively separates the original signal into sub-signals of distinct frequency bands by solving an optimization problem [281], [282]. For instance, Shen et al. [171] employed VMD to separate HR and RR after determining the target location through the autocorrelation method. Li et al. [283] combined UWB-MIMO radar with the VMD algorithm to achieve multi-subject localization and vital sign detection through walls to address the clutter and noise issue. The mode decomposition-based algorithms have the limitation of specifying the number of modes, and efforts have been made to enhance the optimization objective to emphasize the narrow-band characteristics of the decomposition outcomes. Also, mode mixing remains a concern, affecting the decomposition results.

Another method, called differential enhancement (DE) [284], is employed for heart rate (HR) monitoring. It uses first and second-order differential operations on the chest wall displacement signal to suppress respiration and enhance heartbeat components. However, this approach is sensitive to high-frequency noise in the phase signal's high-frequency region, and potential degradation in detection performance can be observed, especially in low signal-to-noise ratio (SNR) scenarios.

All the above algorithms estimate the heartbeat frequency by excluding respiratory harmonics or using heartbeat harmonics. Jing et al. presented a harmonics and intermodulation products-based fuzzy logic (HIPBFL) algorithm for vital sign estimation [285]. However, the measurement range was limited to 0.8m, and estimation accuracies are still to be improved. Another study proposes employing the Spectral Unmixing Successive Variational Mode Decomposition (SUSVMD) algorithm [286] to overcome the issue of RR component mixing with HR. The proposed method involves

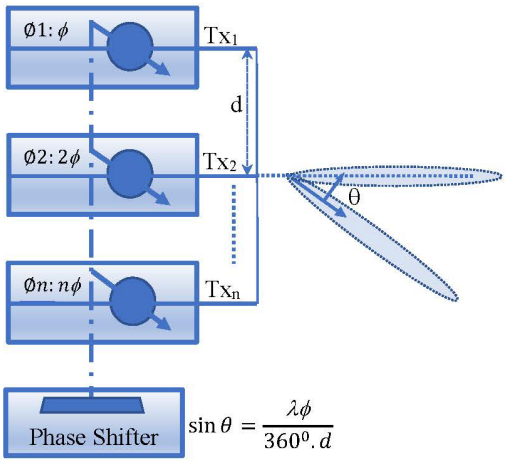

Figure 40: Digital Beam steering through a Phase shifter

the extraction of band-limited modes through back projection and spectral unmixing optimization.

Thus, signal processing algorithms used in real-life situations need to address the interference infused due to clutter and body movements. Additionally, humans are non-stationary and do not always stay in the same place or position in an indoor environment. Therefore, the system must adaptively locate the person and steer the beam direction to improve the SNR and achieve accurate vital sign measurements.

3. Theory and Method

This section focuses on key aspects of the vital sign measurement method, such as SNR improvement through beam steering and beam forming and the vital sign estimation algorithm. We discuss the theoretical principles and challenges involved in RSSD algorithms to analyze data from radar and extract information about the vital signs of the target.

3.1 Beam Steering and Beam Forming

The beam steering technique adjusts the antenna pattern in real-time by altering the signal phase. Alternatively, digital beamforming techniques create radiation patterns by combining and cancelling signals in particular directions. Fig. 40 shows the phase shifter

modifying the signal phase for each transmitting antenna, allowing control of the beam direction.

If the signal beam is to be directed at the θ angle to the radar, the phase difference of the signal phase shifter can be obtained from,

$$\sin\theta = \frac{\lambda\phi}{360^0 d} \tag{5.1}$$

where, d = antenna distance, λ = wavelength, ϕ = phase difference, and θ = direction of subject or electromagnetic beam from the radar.

To achieve the adaptive scanning and localization for non-contact vital sign monitoring, the phase difference at T_{x1} and T_{x2} is determined through (5.1), and the transmitting beam is steered towards a specific direction (θ) from the radar. Furthermore, since noise is a stochastic process, each receiver channel has its own unique noise profile, and two receivers are unlikely to experience the same noise peaks [287]. Combining the receive channels in-phase component enhances the echo signal, and the noise can be decorrelated, resulting in an improved SNR and higher radar sensitivity. A significant advantage of this proposed solution is that the array pattern can be tailored to force the interferences to be placed in the pattern's nulls while amplifying the receiver signal and suppressing noise. This significantly enhances the system's detection accuracy in real-life environments heavily intruded by clutters.

There are two categories of beamformers: data-independent and statistically optimum, which are determined by the method used to select the beamformer's weights. The data-independent beamformer's weights are selected to achieve a specific response for all signal and interference scenarios and are not dependent on the array data. In contrast, the statistically-optimum beamformer's weights are determined based on the statistics of the array data in order to optimize the array's response. This research utilized statistically optimum beamformers such as capon beamforming which offers better performance due to their adaptive ability to suppress directional interferences. Unlike the other method, it does not require knowledge of the desired signal and interference directions. The 4-dimensional sensor array shown in Fig. 41 forms the

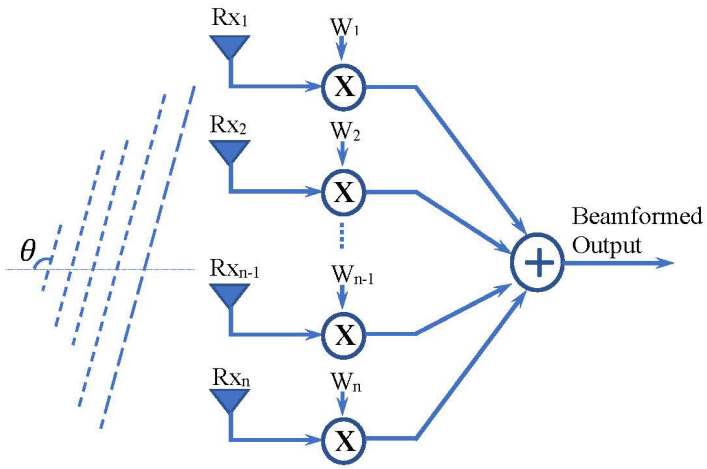

Figure 41: Receiver digital beamforming

beamformed signal at the receiver. The 4-dimensional antenna array is characterized by the use of time modulation in one or more antenna parameters, which enhances system information capacity and enables advanced radiation pattern characteristics, addressing the need for an additional degree of freedom beyond the traditional three spatial dimensions. Suppose that $a(\theta)$ represents the array's response to a plane wave with unit amplitude arriving from the direction(θ).

We assume that a narrow-band source $s(t)$ is targeting the array from an angle (θ) and is situated in the far field of the array. The resulting vector array output y(t) can be expressed as:

$$y(t) = a(\theta)s(t) + v(t) \tag{5.2}$$

where $a(\theta)$ takes into account the impact of various factors, such as coupling between elements and resulting amplification, while $v(t)$ represents the vector of additive noise, including unwanted signals like thermal noise or interference. We use $y(k)$ to represent the sampled array output, and the combined beamformer output can be defined as:

$$y_c(k) = w^* y(k) = w^* a(\theta)s(k) + w^* v(k) \tag{5.3}$$

where w is a vector of weights, and $(\cdot)*$ mentions the conjugate transpose. If we can make $w^* a(\theta) \approx 1$ and $w^* v(k)$ too small, then the receiver signal can effectively recover the transmitted signal i.e., $s(k)$. The expected impact of noise and interference

at the combined output is represented by $w^* R_v w$, where $R_v = E_{vv^*}$ and E is the expected value. Minimum variance beamforming, which is commonly referred to as Capon Beamforming, in which R_v is substituted with an estimate of the covariance of the received signal derived from the latest samples of the array output. Additionally, the optimization process for extracting the weight coefficient w, through minimizing the power expression, which includes the effect of the desired signal plus noise. Moreover, the constraint $w^* a(\theta) \approx 1$ prevents a reduction in gain in the direction of the signal, and the solution can be obtained for n number of receiver antennas by:

$$R_y = \frac{1}{n} \sum_{i=k-n+1}^{k} y(i) y(i)^* \tag{5.4}$$

3.2 Vital Sign Measurement

In this section, we discuss the theoretical principles behind the proposed method and its implementation in the signal processing chain, which involves pre-processing, phase extraction, and vital sign extraction. We aim to develop an optimal Q-factor selection algorithm in reference to the RSSD and tunable Q-factor wavelet transformation (TQWT) method.

3.2.1 Resonance-Based Sparse Signal Decomposition (RSSD) and Tunable Q -factor Wavelet Transformation (TQWT)

Selesnick [57] introduced a new approach to signal processing, i.e., resonance-based sparse signal decomposition (RSSD) for non-stationary signals. Resonance is a signal characteristic that can be measured by its resonance quality factor Q, with a higher Q indicating stronger resonance and more oscillations in a given time frame. Resonance property can be defined by its center frequency and frequency bandwidth. The RSSD technique utilizes the resonance property of a signal to separate and sparsely represent signal components with similar center frequencies but different Q values. The most efficient representation of each resonance component of the signal can be obtained using RSSD.

In the traditional RSSD approach, values are typically assigned to the Q-factors, such as $Q_1: 3\sim9$ and $Q_2\sim1$. However, the decomposition quality strongly depends on the optimum selection of the Q-factor. Therefore, the adaptive selection of quality factors is critical in the RSSD method. It should be noted that non-integer Q-factors may be required in real-life vital sign extraction applications. In a high background noise working environment, the high and low resonance components of the chest reflected radar signal that RSSD decomposes might have a high degree of overlapping due to noise interference, which can affect the extraction of high resonance components. Nonetheless, the extraction method only accumulated sub-band components from high to low frequencies based on the filtering characteristics of the Q-factors. Hence, some sub-bands may introduce noise into the extracted phase signal.

The proportions of sub-band frequencies and their contributions to the signal energy are not considered conventionally. Suppose the signal carrying the vital sign information is to be decomposed into components with specific resonance attributes, a wavelet-based function library must be created that matches the oscillation characteristics of the vital resonance signal. In this research, the sub-bands proportion of the total energy is considered when selecting the Q factor from the library. This Q factor library is designed based on the total energy of the signal and the energy distribution within the frequency sub-bands of interest. The frequencies of interest for the vital sign are taken as 1-2 Hz for heart rate and 0.1 to 0.5 Hz for respiration rate signals. The detailed process is described as follows:

- Apply TQWT on the input signal to obtain the sub-bands energy distribution and center frequencies. Calculate the energy E_j of $J_1 + 1$ sub-band signals using (5.5) and (5.6).

$$E_j = \sum_i^{N_j} \left|W_{ji}\right|^2 \tag{5.5}$$

where W_{ji} represents the ith wavelet coefficient belonging to the j^{th} level, and N_j is the length of the j^{th} level wavelet coefficient.

$$E_h = \sum_{j=f_{ci}}^{f_{ch}} E_j \tag{5.6}$$

where E_h represents the total energy in the signal in the heartbeat range. f_{ci}, f_{ch} the initial and end frequency range for heart rate.

- Make four bands in the frequency range of interest. Distribute the total energy in these sub-bands. Calculate the energy percentage e_j corresponds to energy distribution in four sub-band, as shown in (5.7).

$$e_{jn} = \frac{\sum_{j=f_{cjn}}^{f_{chn}} E_j}{E_h} * 100 \tag{5.7}$$

where f_{cjn}, f_{chn} the initial and end frequency range for the respective sub-band.

- Optimize Q for the signal by comparing the Euclidean distance of each e_{jn}, $n = 1, 2, 3, 4$ with the values in the library. The Q is selected for which the Euclidean distance is minimum.

With the selection of optimum Q and using RSSD, a signal like $x = x_1 + x_2$ can be decomposed into its high-resonance (x_1), low-resonance (x_2), and residual components. The RSSD algorithm steps can be summarized as follows:

- The signal x is used as input to the algorithm.
- Wavelet bases S_1 and S_2 (via TQWT) are constructed leveraging the apriori resonance information.

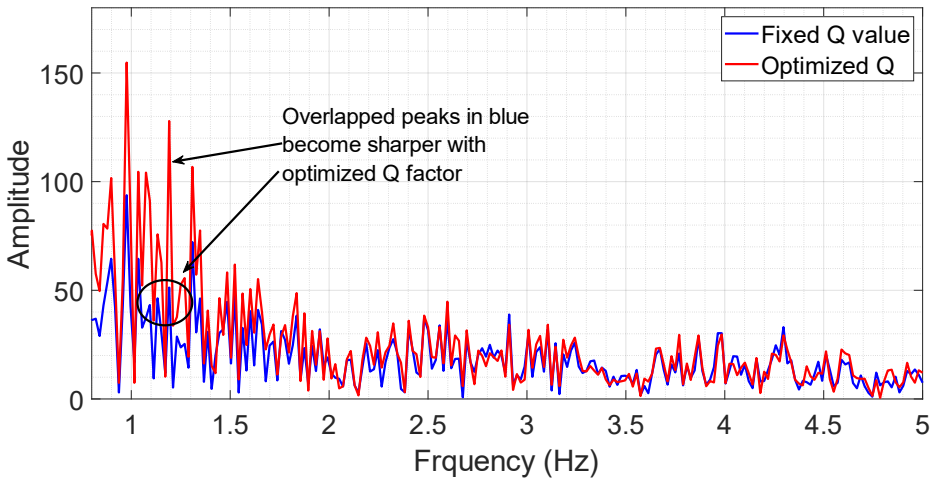

Figure 42: Frequency spectrum of High resonance component with optimized Q and with fixed Q value.

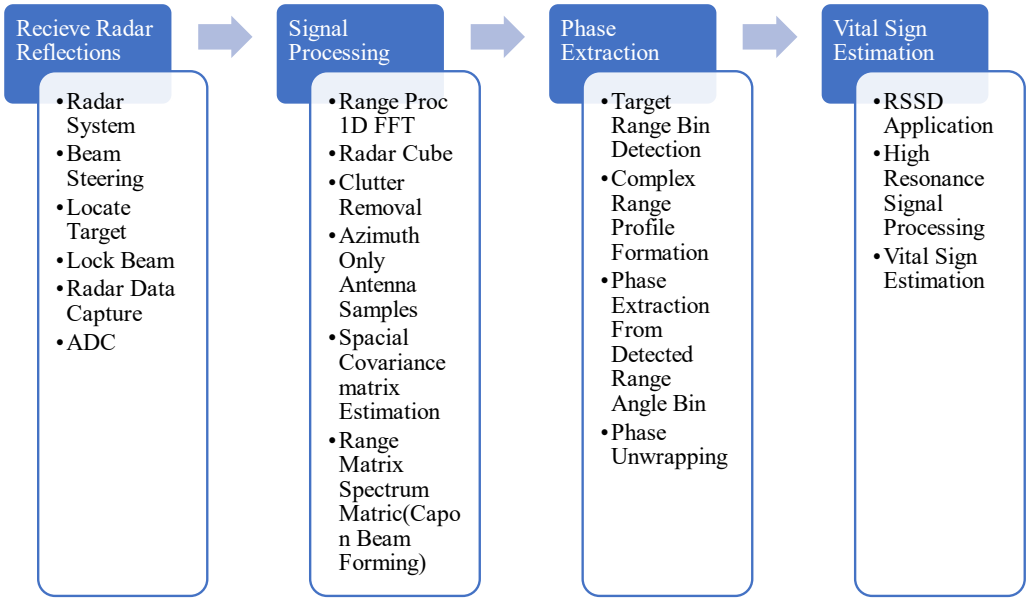

Figure 43: Signal Processing chain for Vital Sign Estimation

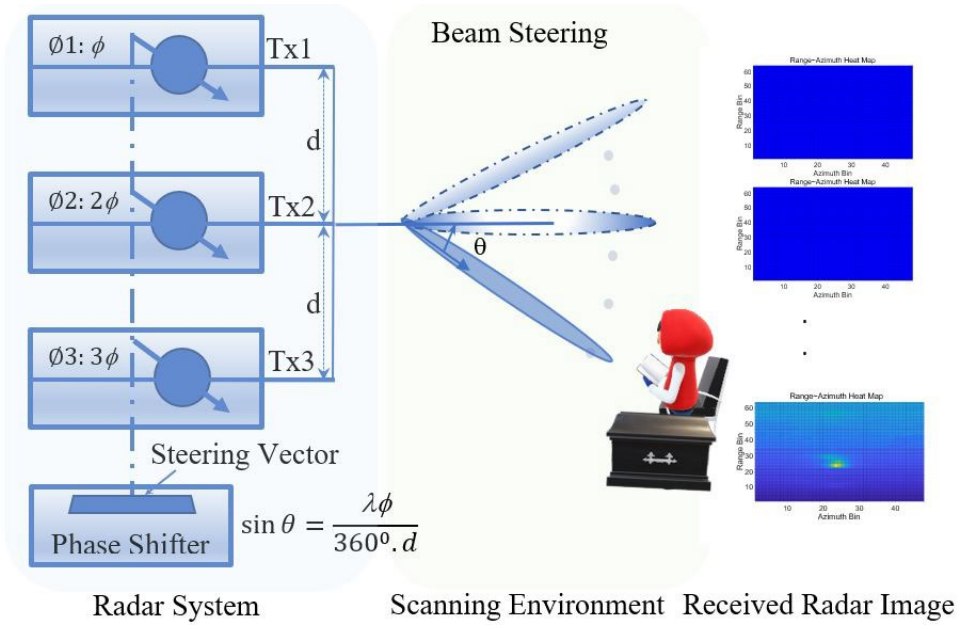

Figure 44: Beam Steering technique used in the experiments using phase shifter which adds phase difference in transmitting antennas dynamically.

- Split Augmented Lagrangian Shrinkage Algorithm (SALSA) is used to estimate the coefficient matrixes optimally W_1^*, and W_2^* [231].
- Using W_1^*, W_2^*, high and low resonance components with $x_1 = S_1 W_1^*, x_2 = S_2 W_2^*$ are derived.

The effectiveness of Q-factor optimization can be observed in Fig. 42, which shows the frequency spectrum of the high resonance component extracted from the phase signal with an optimized Q-factor and a fixed Q value. It's evident from the graph that the peaks are narrower and sharper compared to those obtained with a fixed Q value. This is because peaks that merged due to overlapping with noise interference have been segregated, addressing the challenge in peak selection for heart rate estimation.

3.2.2 Signal Processing Chain

The vital sign estimation is carried out through several signal-processing steps implemented through the FMCW radar system, as shown in Fig. 43. The Tx beam steering involves multiple Tx channels to transmit synchronously. To steer the beam at the desired angle, each Tx channel is controlled through a 6-bit phase shifter that can be programmed with a steering resolution of 5.625^0, as shown in Fig. 44. The value programmed to each channel is determined based on where the main beam should be focused. This coherent gain achieved in the Tx beam steered and formed leads to a much stronger signal in the specific direction being targeted. Next, the amount of phase value programmed to each Tx channel is calculated based on the array factor and target angle. Finally, the allowed phase step size of 5.625^0 is used to determine the integer value to be programmed to the phase shifters for optimal performance as in (5.8).

$$\emptyset_{integer} = \left[\frac{[\emptyset_1\ \emptyset_2\ \emptyset_3]}{5.625}\right] \tag{5.8}$$

where $\emptyset_1, \emptyset_2, \text{and}\ \emptyset_3$ are phase shift values corresponding to transmitting antennas.

In this paper, we have used TI EVM AWR1843 [288], where three azimuth Tx antennas can be used for beam steering. The Tx beam steering supports the per-chirp-based and frame-based beam steering. We utilized frame-based steering with three steps between angles of -60^0 to $+60^0$ to cover the entire scene in front of the radar. The process involves configuring the phase shifter with the values corresponding to -60^0 for all chirps used in the frame, followed by applying phase values corresponding to -30^0,

Algorithm 1: Phase Shifter Integer Value

```
// Set values for start frequency, number of antennas,
// antenna spacing, and desired phase shift theta
// Calculate wavelength based on start frequency
lambda = (3*10^8)/(startfreq*10^9);
// Store the calculated phase shift for each antenna
antennaPhase = zeros(1, numAntennas);
// Loop through each antenna and calculate the
// corresponding phase shift
for i = 1:numAntennas
  antennaPhase(1, i) = rad2deg((2pi/lambda)(i-1) *dsin(deg2rad(theta)));
end
// Convert the calculated phase shift values to bits
// for programming the phase shifter
antennaPhaseBits = antennaPhase/5.625
```

Algorithm 2: Automatic Target Localization Algorithm

```
// Initialize variables
theta = [0, 30, 60]  // degrees
rangeAngleBin = []

// Iterate through scanning angles
For i = 1 to 3
   // Calculate the phase shifter value in bits
   For j = 1 to 3
      antennaPhase(1, j) = rad2deg((2*pi/lambda)*(j-1)*sin(deg2rad(theta(i))))
   End For
   phaseShifterValues(i) = antennaPhase(1, j)/5.625

   // Update the profileCfg command with new phase shifter bits
   varPhase = 'profileCfg 0 77 30 7 62 0 x 60 1 64 2500 0 0 40'
   cliCfg = stringReplace(varPhase, 'x', phaseShifterValues(i))
   sendConfigToRadar(cliCfg)

    // Estimate the range and angle for the corresponding transmitting beam angle
   rangeAzimuthMatrix = getRangeAzimuthMatrix(rxSignalDataCube)
   maxStrength = max(rangeAzimuthMatrix)
   [rangeBin, angleBin] = find(rangeAzimuthMatrix = maxStrength)
   rangeAngleBin(i) = [rangeBin, angleBin]
End For

// Estimate the final range and angle values from the three scannings
[estimatedRange, estimatedAngle] = mode(rangeAngleBin)
finalAntennaPhase = 2*pi*([0, 1, 2]*sinInverse(estimatedAngle)*180/pi)/lambda
phaseShifter = round(finalAntennaPhase / 5.625) .* [0, 2^8, 2^16]' * 4

varPhase = 'profileCfg 0 77 30 7 62 0 x 60 1 64 2500 0 0 40'
cliCfg = stringReplace(varPhase, 'x', phaseShifter)

// Send the config file to the radar and lock the beam toward the target and lock beam
sendConfigToRadar(cliCfg)
```

0^0, 30^0, and $+60^0$. This approach allows us to effectively scan the entire scene as the 3db beamwidth for AWR1843 is $\pm 28^0$.

Algorithm 1 and Algorithm 2 describe the phase shifter calculation for steering vector and target localization. Algorithm 1 computes the desired phase shifts for an array of transmitting antennas which are $\lambda/2$ apart. The algorithm loops over each antenna and calculates its corresponding phase shift based on its position in the array and the desired phase shift using (5.1). The calculated phase shift values are then converted to bits suitable for programming the phase shifter using (5.8).

Algorithm 2, designed to automate target localization for a phased-array radar system, iteratively scans the environment with different beam angles (0, 30, and 60 deg). The radar returns a Range-Azimuth matrix for each scan. This matrix is processed to estimate the range and angle of the detected targets for the corresponding transmission beam angle using a specified number of frames. After completing the three-step scanning process, the algorithm uses the accumulated results to estimate the target's final range and angle values. These estimated values are then used to calculate a final phase shifter value, representing the optimal target beam angle. With this updated configuration, the radar locks the beam towards the target, effectively focusing its scanning capability on the detected target, resulting in enhanced SNR.

The raw data received from the front end of the radar is converted into a digital format using an analog-to-digital converter (ADC). The digital data is then subjected to a 1-D FFT (range FFT) and processed further to remove any unwanted signals (static clutter removal). The 1D FFT data is averaged across all chirps for a single virtual Rx antenna to remove static information from the signal. This average is then subtracted from each chirp from the Virtual Rx antenna. This process ensures that only the signals returned from moving objects remain. Next, Capon BF is applied to obtain a range-azimuth heatmap. The Capon BF algorithm consists of the computation of the spatial covariance matrix and the generation of the Range-Azimuth Heatmap. Finally, the chirps in the frame are averaged to estimate the spatial covariance matrix, $R_{xx,n}$ as in (5.9).

$$R_{xx,n} = \frac{1}{N_c}[X_{nc}1, X_{nc}2 \dots \dots \dots \dots X_{nc}N_r] \tag{5.9}$$

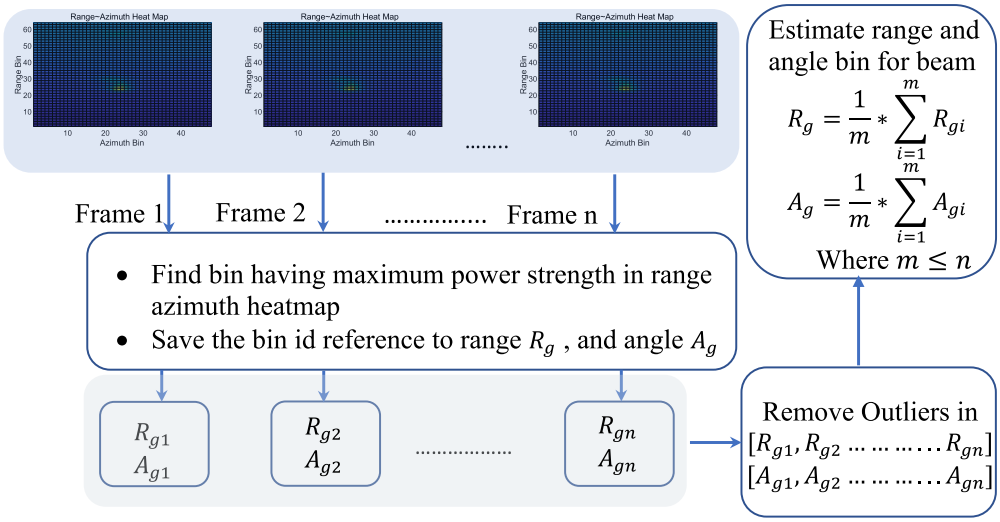

Figure 45: Range-Azimuth Estimation

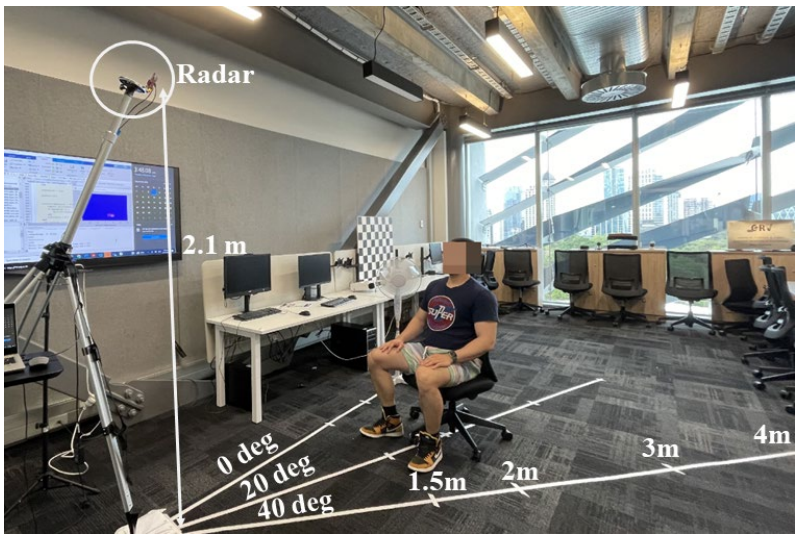

(a)

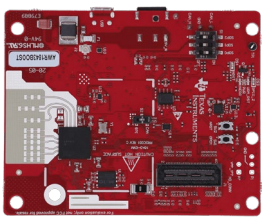

(b)

(c)

Figure 46: (a) Experiment setup (b) AWR1843 EVM [288] and (c) Hexoskin device [238]

Where N_c are the number of chirps in a frame, X_{nc} is range-azimuth heatmap matrix, and N_r is the number of virtual receiver antennas. To begin with, the Range-Azimuth Heatmap is calculated for each azimuth bin. This heatmap is then used as input for the constant false alarm rate (CFAR) algorithm, which is used to detect target points

in the Range-Azimuth spectrum. The process is illustrated in Fig. 45. A two-pass CFAR is applied to detect objects on the range azimuth heat map. The first pass is for per angle bin along the range domain. The second pass in the angle domain is used to confirm the first pass's detection. The phase value of the selected range bin is computed from the complex range profile data, and these phase values are measured over time. Phase values are between [-π, π] and need to be unwrapped to obtain the actual displacement profiles. Phase unwrapping is performed by adding/subtracting 2π from the phase whenever the phase difference between consecutive values is greater/less than ± π.

To estimate the vital signs from the unwrapped phase, the signal RSSD algorithm is applied. The noise in a realistic environment has a different degree of impact on the phase signal; therefore, the Q factor is optimized for each dataset. First, collect 1024 samples of phase signals, each of approximately 100 seconds in duration. These signals are then decomposed using the TQWT into four sub-bands in the HR frequency range, with the energy in each sub-band calculated. The high resonance quality factor Q_1 is then estimated based on the sub-band energy distribution. The estimated Q_1 is used to decompose the phase signal into high and low resonance components. Next, the phase signal is sliced into 1-second segments, and each segment is decomposed into high and low resonance components using RSSD. The process identifies the three sub-bands with the highest energy in the HR range, and finally, the most dominant and sustained frequency within these sub-bands across the signal duration is identified.

4. Experiment Design

This section presents the experimental analysis and results of a radar-based vital sign estimation system using AWR1843 [288]. The collected data is analyzed offline using MATLAB 2022a. The accuracy and reliability of the system are evaluated by comparing it with the ground truth data collected using a Hexoskin vest [238]. Hexoskin is an intelligent garment embedded with respiration and Heart sensors. The respiration sensor is in the form of two rings in the chest and abdomen. Heart sensors are in the form of electrodes that act as an electrocardiogram ECG. The experiments are conducted on six healthy participants in a lab environment with the necessary ethical

Table 11: Participants Details

Participant #	Age	Height(cm)	Weight(kg)
P 1 (F)	40	162	67
P 2 (M)	30	186	85
P 3 (F)	29	182.8	80
P 4 (F)	28	152.4	64
P 5 (M)	29	188	106
P 6 (M)	28	180	78

approval and consent obtained. The demographic details are given in Table 12. The ethics approval is obtained from AUTEC (Auckland University of Technology, New Zealand Ethics Committee).

To ensure synchronization between the ground truth and radar data, a time-stamping approach is performed by matching the time intervals of both data sources. The phase signal received from the radar is processed in batches of 512 samples, with a sampling rate of 10 Hz. These batches are processed in consecutive segments, where each segment involves shifting the window of 512 samples by 20 samples, equivalent to a one-second interval. This shifting process ensures that the algorithm generates estimation outputs for each second, aligning with the timing of available hexoskin ground truth data.

4.1 Experimental Setup

We used a millimeter-wave AWR1843 radar, an integrated single-chip FMCW radar sensor operating in the 77 to 81 GHz frequency band. Transmit beam steering feature is available in the AWR1843. The phase shifters allow all transmitters to focus on a desired direction with a steering resolution of 5.6°. AWR1843 consists of three transmitting and four receiving one-dimensional linear array antenna layouts. In our experiment, a combination of $T_{x0} - T_{x1}$ with four receivers is configured. A train of chirps is generated with chirp duration time, T_c= 62 µs, the chirp interval idle time = 30 µs, the sawtooth frequency modulation slope S = 60 MHz/µs, and the frame rate T_m = 100 msec.

The radar is placed at 2.1 m from the ground, inclined at an angle of approximately 20^0 w.r.t. the ground to depict the realistic scenario. Unlike other

research work, e.g., [270], [275], [276] where radar was placed at the same torso level. This inclination angle is calculated depending on the beam width of the main lobe of the radar antenna and the range of interest from the radar. For the elevation 6 dB-beamwidth of approximately ±20 deg, the radar's inclination angle is calculated as 20 deg considering the target's distance from the radar between 1.2 to 4 m.

The experimental setup is shown in Fig. 46. The setup consists of desktop computers, chairs, and tables which constitute a good amount of clutter, emulating a more realistic environment. Each data collection is performed for a total duration of 162 sec, including the time required for beam steering and target localizing. The angles are marked on the ground with the tape at -40^0, -20^0, 0^0, 20^0, and 40^0. The data is captured at various distances from radar at 1.5, 2, 3, and 4 m.

4.2 Observation Scenarios

This study elucidates the specifics of the diverse experimental scenarios employed. Our experiments are tailored to achieve several objectives, such as studying the improvement in SNR attributable to beam steering, assessing the accuracy of HR/RR measurements, examining the impact of body motion and clutter such as reading books, drinking water, evaluating the effect of the presence of a second person, and analyzing the effects of body orientation. Each scenario is described in detail:

Case 1- SNR improvement and HR/RR accuracy: During the data collection, the participants were asked to sit quietly in normal breathing conditions in front of the radar (radar not at the same level) on a chair at a specified marked distance and angle. Two datasets are recorded at each combination of angles. The experiment is repeated to record multiple combinations of angles and distances.

Case 2- Effect of Body Orientation: The experiments are performed to study the effect of body orientation for the given radar setup. The two datasets are collected from each participant at 2 m and zero deg from the radar. The signal is captured from the target's front, back, left, and right sides of the body.

Table 12: Comparison analysis of HR estimation for Participant 1 dataset with and without Q-factor optimization

Participant 1 Dataset	Q1		Q1opt	
	Mean Error	Std Dev	Mean Error	Std Dev
0 deg	11.25	7.838	1.5	0.866
20 deg	14.625	8.601	2.25	1.56
40 deg	3.875	3.689	1.5	0.866
neg 20 deg	7.75	6.359	3.125	2.803
neg 40 deg	7.25	4.323	2.875	1.536
Body orientation	6.875	6.936	4	1.871
Clutter+BM	10.5	10.712	1	0.707

Case 3- Effect of Clutter and Body Movements: We conducted further experiments to assess performance in conditions with heavy clutter and moderate body movement. The setup incorporated clutter like desktop computers, tables, and chairs. A running fan is placed close to the target to simulate interference from periodic signals. The experiments are carried out on all participants, with varying scenarios for body movements introduced by performing different activities in a controlled manner. Each subject is asked to sit still for the first 30 sec, followed by a specified activity for the next 20 sec, and this cycle is repeated throughout the observation period. The time for body movements and static positions is closely monitored, and the researcher signals the subject when to start the movement. The experiments are designed to study the participant's movement's impact on the radar system's accuracy and reliability. This whole series of activities constitute a realistic scenario for moderate body movement.

Scenario 1: Only additional clutter is introduced. During the experiment, the subject is requested to maintain a stable and relaxed posture without making any bodily movements at a distance of 2 m-0^0.

Scenario 2: The subject is positioned at 2 m-20^0 and asked to do backward and forward body movements.

Scenario 3: The subject is reading a book at a distance of 2 m-0^0.

Scenario 4: The subject is asked to grab the bottle from the side table, drink the water, and put it back. The subject is at 2 m-20^0.

Case 4- Effect of Second Person in the Vicinity: We further extended the complexity of the experiments and the effect on the vital sign analysis due to the second person in the vicinity of the subject being analyzed. Again, different scenarios are simulated as follows:

Scenario 1: The Second person walks and crosses from the back after 30sec from the measurement start time and returns.

Scenario 2: The Second person walks and crosses from the front after 30sec from the measurement start time and returns.

Scenario 3: Second person is walking and standing at 2 m-20^0, 3 m-20^0, and 3 m-0^0, respectively.

Scenario 4: Second person is standing at 2 m-20^0 for the whole measurement duration.

5. RESULTS ANALYSIS

The performance of a vital sign estimation system is typically evaluated based on its ability to correctly estimate HR/RR within acceptable error with reference to ground truth values. We use evaluation metrics such as R2 value and accuracy in terms of error bins (error < = 2 bpm and > 2 bpm) to measure the performance of the proposed method. These metrics are widely used in radar-based vital sign measurement systems and comprehensively assess the system's performance [269].

5.1 SNR and Target Angle

We initially analyze the advantage of beam steering by evaluating SNR improvement and target angle accuracy.

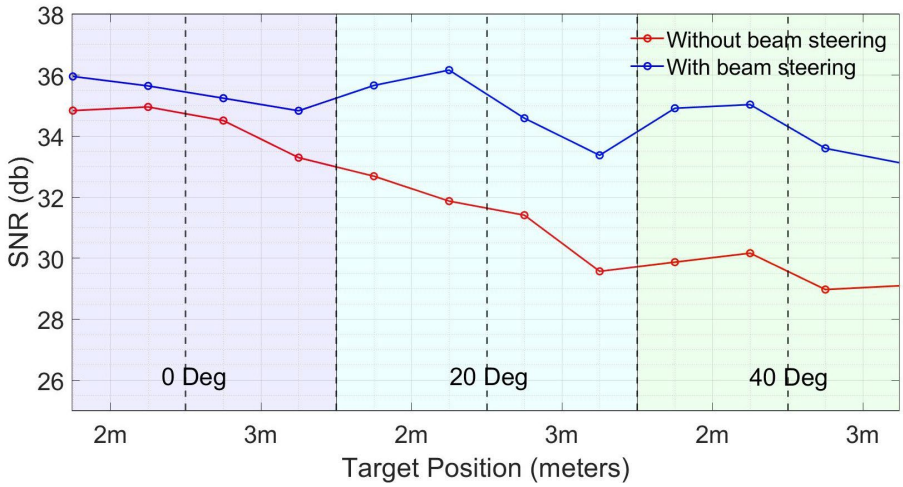

Figure 47: Comparison analysis of SNR with and without Beam Steering at various radar angles

5.1.1 SNR with and without Beam Steering

Fig. 47. demonstrates the comparison of SNR versus azimuth angle with and without beam steering. For the single-person measurements, the subject is asked to position at 2 & 3 m for different azimuth angles (0, 20, and 40 deg). Without beam steering, the SNR is maximum at zero deg and drops to half for each 20 deg increment due to reduced H plane beam coverage at larger distances and angles. Conversely, employing beam steering improves SNR, equating it to zero-degree value. The SNR boost of about 4-5 dB at 40 deg and 2-3 m implies a three-to-fourfold signal strength increase. This confirms the beam steering technique's effectiveness, yielding enhanced SNR at varying angular positions.

5.1.2 Target Angle Estimation

The angle estimation is verified with the case 1 dataset. The participants are seated at different marked locations. The location is marked at -40^0, -20^0, 0^0, 20^0, and $40^{0,}$ and various distances from radar are 1.5, 2, 3, and 4 m for each angle. Each data collection step includes environmental scanning. Due to the space restriction in the lab, the environment is scanned in zone I (positive angles) and zone II (negative angles). The beam is steered in three steps in each zone from 600, 300, and 00 (and -600 and -300 for zone II).

The Azimuth static heatmap, a 64x48 matrix of intensities that represent different ranges and angle bins, is generated from the received radar image, as shown

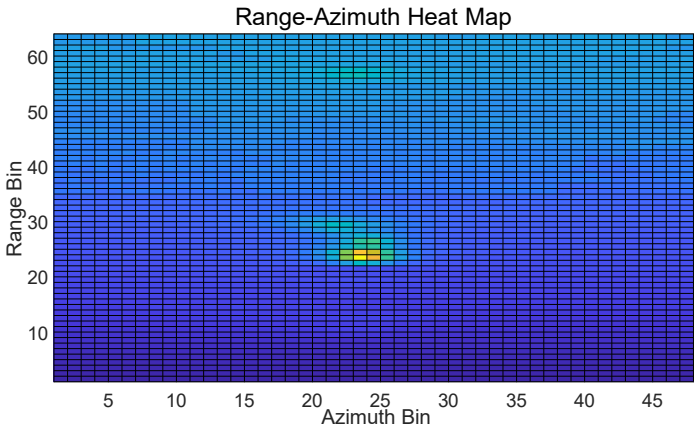

Figure 48: Range-Angle Heat Map

in Fig. 48. Since no other significant object is placed between the radar and the human target, we can conclude that the reflection from the human target produces the highest intensity on the heat map. Therefore, the target's location (angle and range) is estimated at the coordinates of the highest intensity on the heat map. The angle and range estimated in each scan are verified with the Range-Angle heat map at the time of data collection. The beam is then locked at the estimated location by radar, and data is collected.

The result of target angle estimation is compared with the true values, and the results show strong agreement. This results in accurate beam locking at various unknown locations with a deviation of one angle bin corresponding to 2.5 deg, mainly at shorter distances. The reason for deviation may be attributed to the fact that the human target is not a point target. At short distances, the radar with 3db beam width of 28 deg, the target reflection is obtained from the RCS of around 0.5-3 m2 [267] and hence the angle bin (maximum strength signal bin) may get shifted one to two bins around the actual angle bin.

5.2 Vital Sign Estimation

To initiate the estimation of vital signs, we initially examined how the RSSD algorithm's performance is affected by carefully selecting an optimal Q-factor, which is determined based on the energy distribution within sub-bands. Table 13 presents a comparison of error estimations, highlighting the differences with and without Q optimization. A mean error ranging from 3.8 to 14.6 bpm and a high error standard deviation is observed when the Q-factor is fixed. In contrast, we consistently observe a mean error under 3 bpm

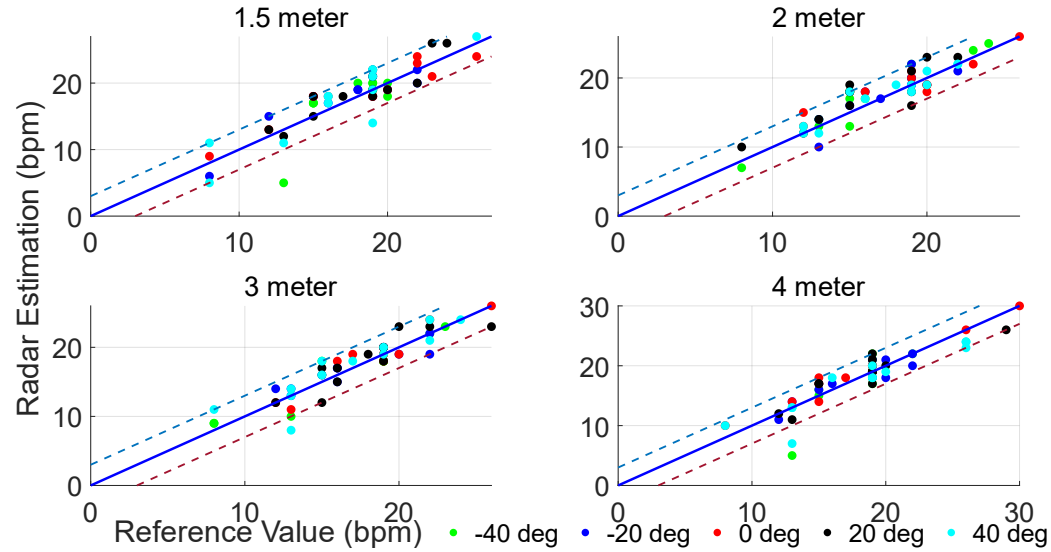

(a)

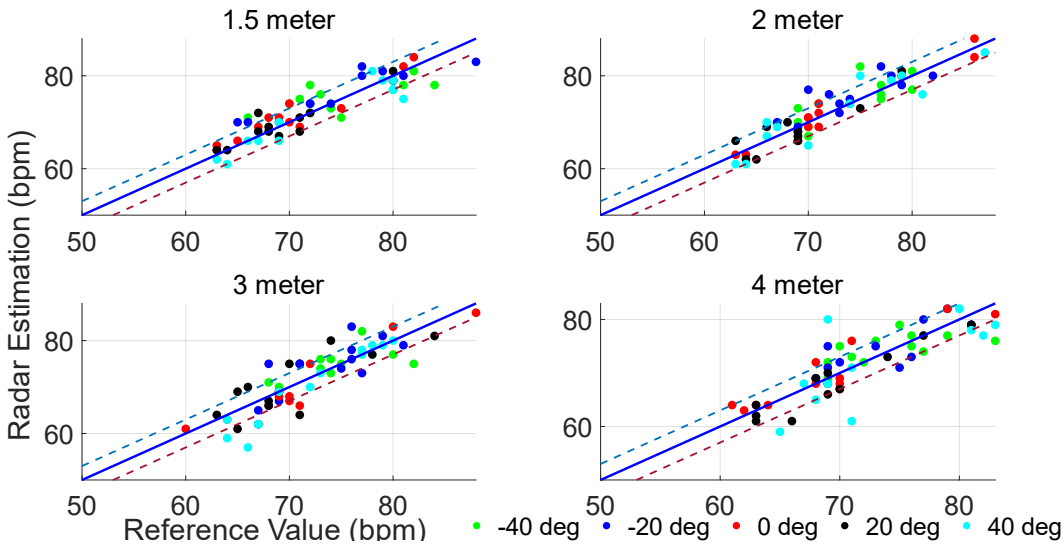

(b)

Figure 49: (a): Scatter plot showing the relation between RR reference values and radar estimation with R-Squared values 0.77, 0.83, 0.85, 0.813 at 1.5, 2, 3, and 4 m respectively (b) Scatter plot showing the relation between HR reference values and radar estimation with R-Squared values 0.81, 0.832, 0.743, 0.716 at 1.5, 2, 3, and 4 m respectively.

post-optimization with a significantly reduced standard deviation. The Q-factors optimization enhances high resonance component extraction, thereby improving HR/RR estimation.

5.2.1 Effect of angular position and range

The HR and RR accuracy results for each participant at varying distances are validated using the dataset from case 1. In the first round of experiments, the distance between the radar and the participant's chest is approximately 1.5 m. This distance is progressively increased in the following experimental rounds, with measurements taken at 2, 3, and 4 m. Fig. 49 gives a comparison of the estimated and actual RR/HR. The reference values are on the x-axis, and the estimated values are on the y-axis. The solid blue line represents the 100% match between reference and estimation. The dotted lines show the 2 bpm deviation band.

RR estimation at all azimuth angles, the difference between the reference and experimental values is well within 2 bpm and exhibits an average accuracy of 99% up to a distance of 4 m. For the experiment at 40^0, the Hexoskin vest for Participant 5 lost its proper fit around the abdomen. As a result, the respiratory sensor was misplaced, leading to a noticeable effect on the RR estimation. Consequently, when measured at 40^0, the RR estimation accuracy degrades to 96.27%. Across all azimuth angles up to 4 m, HR estimation accuracy maintains a significant 98.72%. Notably, the peak performance is observed at 2 m, attaining an accuracy of 99.12%. The impact of the target's angle on RR and HR estimation is observed. Importantly, it should be highlighted that the accuracy of HR remains consistent regardless of variations in the target angle, maintaining a fairly good accuracy of 98.72% even at distances up to 4 m. This confirms the effectiveness of the beam-steering and estimation method.

5.2.2 Effect of Body Orientation

During the experiment, data were gathered from four distinct human subject orientations positioned 2 m from the radar, as depicted in Fig. 50. When the radar is situated at torso level; the radar detects a smaller radar cross-section (RCS) when the subject's orientation is either left or right profile, compared to the 'back' or 'front' profile. As a result, the target chest area is not visible to radar when the subject's body side (left or right) faces the radar, complicating the detection of necessary skin vibrations for precise RR and HR estimation. However, in our experiments, the radar is

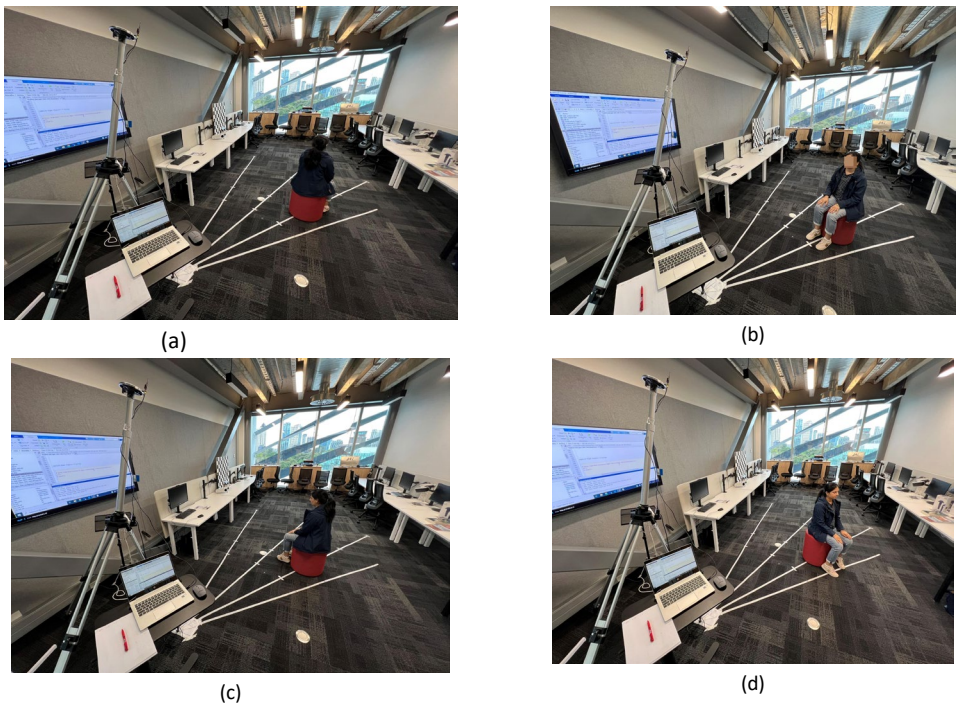

Figure 50: Experimental Setup showing different Body Orientation (a) Back (b) Front (c) Left (d) Right

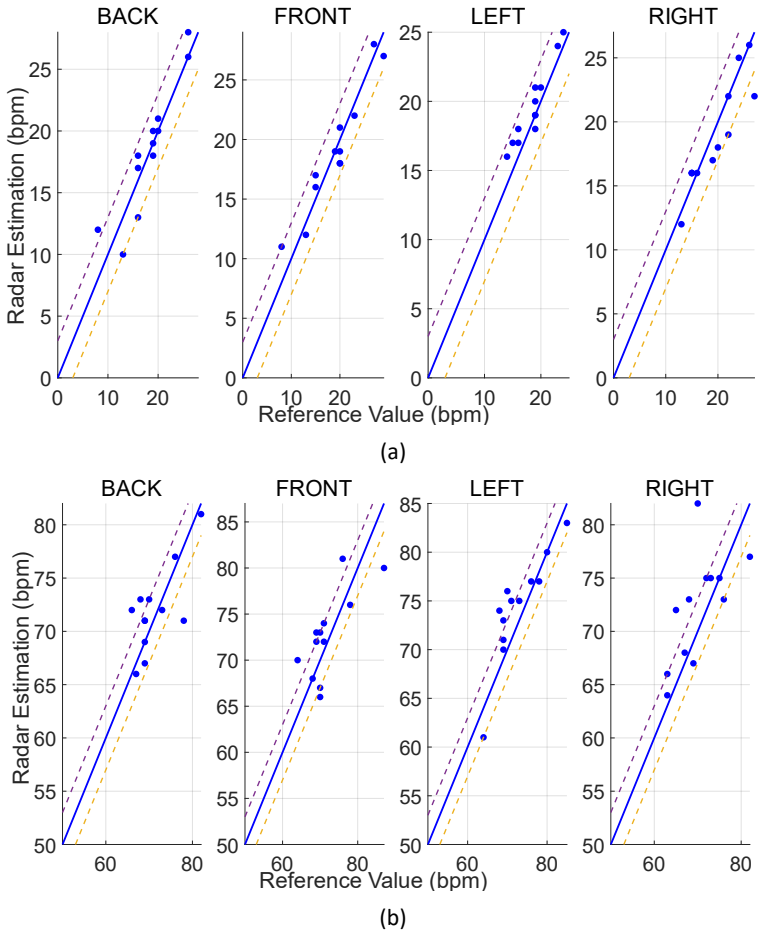

Figure 51: Different Postures (a): Scatter plot showing the relation between RR reference values and radar estimation with R-Squared values 0.854, 0.924, 0.899, 0.838 at 1.5, 2, 3, and 4 m (b) Scatter plot showing the relation between HR reference values and radar estimation with R-Squared values 0.517, 0.549, 0.76, 0.416 at 1.5, 2, 3, and 4 m.

placed at a higher level, providing the radar transmission beam with a significant view of the chest area. This leads to relatively accurate HR/RR estimations under various body orientation scenarios.

The experimental results are depicted in Fig. 51 (a) and (b), with the dotted lines illustrating a deviation band of 2 bpm. The average HR accuracy for the front, back, left, and right orientations are noted as 97.75%, 98.49%, 98.52%, and 97.39%, respectively. The four orientations (front, right, left, and back) do not seem to affect RR estimation as well. For an acceptable deviation within 2 bpm from the actual value, RR estimation accuracy is around 99.24%, 97.14%, 100%, and 98.43% for the front, back, left, and right orientations, respectively.

5.2.3 Effect Clutter and Body Motion

We conducted experiments on six subjects in an experimental setup, as shown in Fig. 52, to test the performance of our proposed method under heavy clutter and moderate body movement. The environment included items to create additional clutter, such as a desktop, monitor, CPU, keyboard, furniture, and running fan placed at various distances from the subject. The experiments are conducted in four different scenarios, with varying levels of body movement.

In the initial setup, the subject is stationary, with no body movement, and only clutter is present. The clutter here refers to a running fan that operates at a frequency distinct from the respiration and heart rate frequency bands. Introducing any artificial clutter within these bands could potentially disrupt the measurements. Nevertheless, the RSSD algorithm is capable of accurately separating the high resonance signal from the clutter and moderate body movements, like reading, drinking water, changing arm positions, head movement, allowing the estimation algorithm to accurately derive the heart rate with errors mostly below 2 bpm, as presented in Table 14. The average RR accuracy ranges from 98.2% to 100% in all scenarios. As depicted in Fig. 53, our proposed method demonstrates strong performance and closely follows the actual value for most of the observation period under all circumstances.

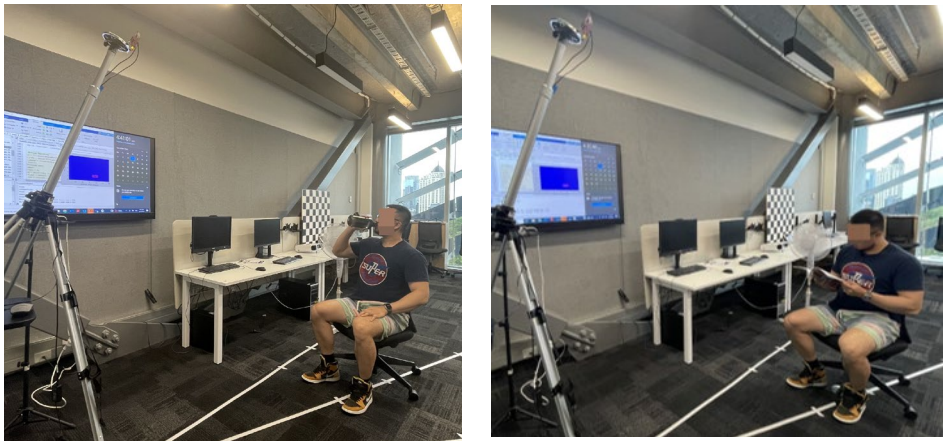

(a) (b)

Figure 52: Experimental Setup showing different scenarios of Clutter and Body Motion (a) Drinking water (b) Reading.

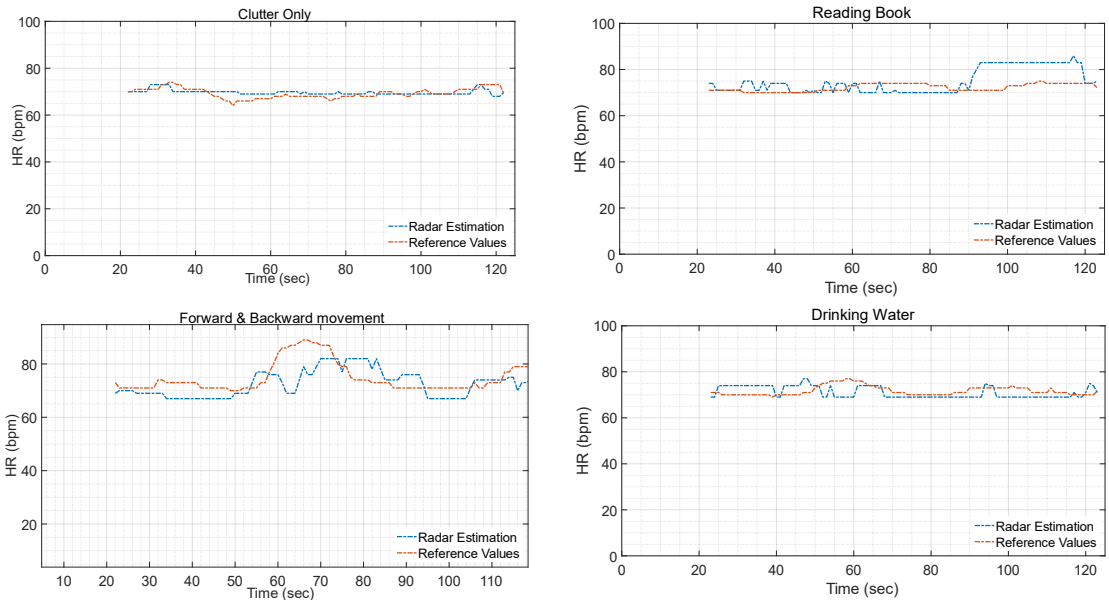

Figure 53: Beat-to-beat comparison for vital sign estimation under the effect of clutter and body motion (a) Clutter only b) Clutter+Forward/Backward movement (c) Clutter+Reading book and (d) Clutter+Drinking water.

Table 13: Average HR accuracy for different scenarios

Scenarios	HR Average Accuracy (%)
Clutter Only	99.14
Forward/Backward movement	100.00
Reading	98.51
Drinking Water	99.43
Crossing from Back	100.00
Crossing from Front	99.44
Walking and standing close to target	98.28
Standing at back	96.57

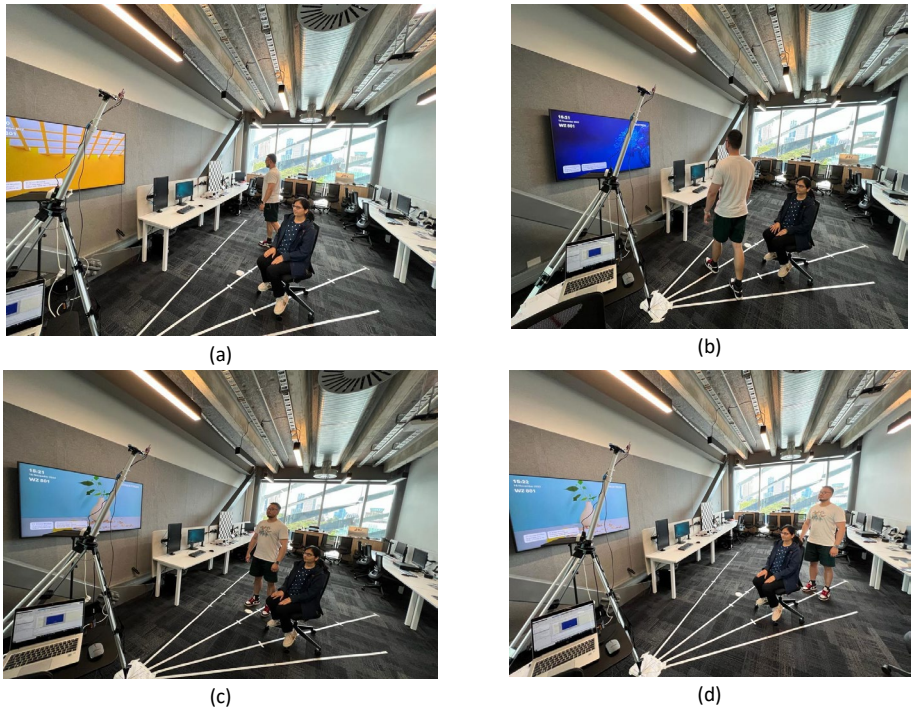

Figure 54: Experimental Setup: another person in the vicinity (a) Crossing from the Back, (b) Crossing from Front, (c) Walking and standing close to the target, and (d) Standing at back.

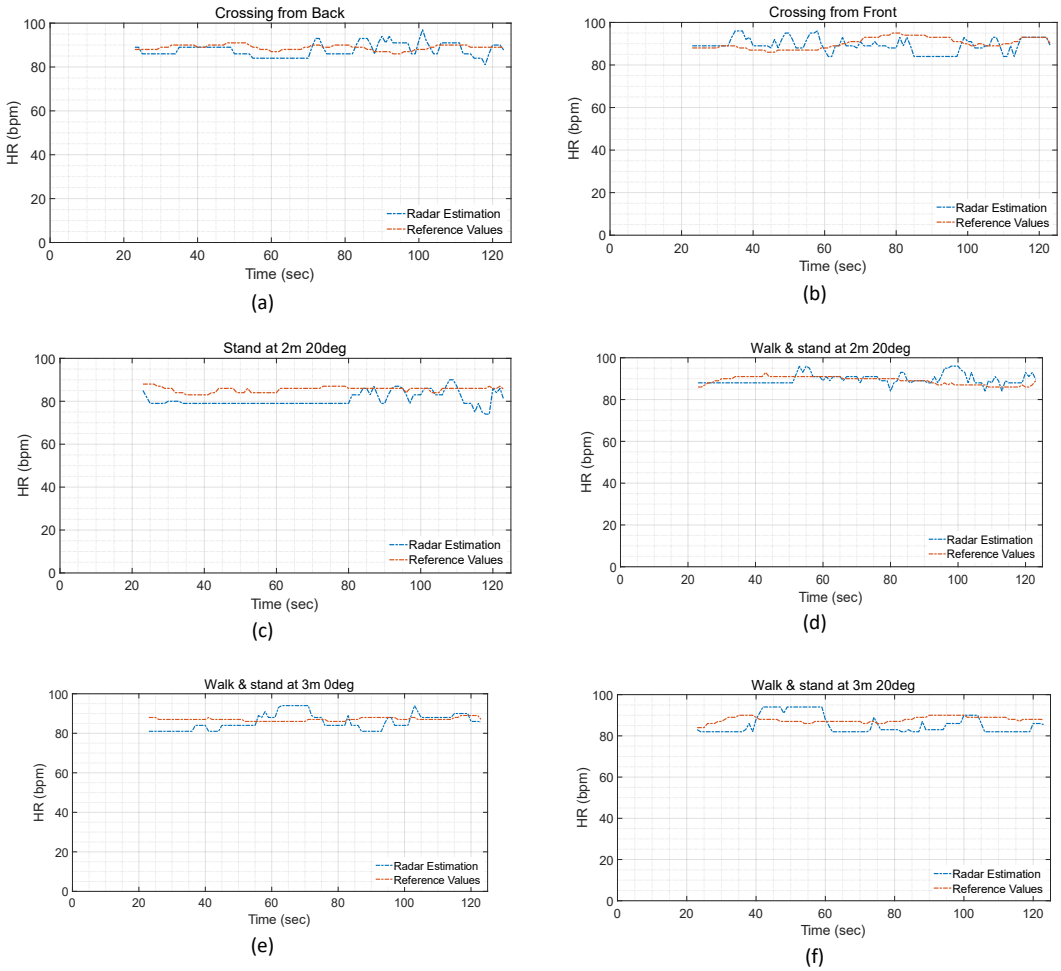

Figure 55: Beat-to-beat comparison for the two-person scenario in the vicinity (a) Crossing from the Back, (b) Crossing from the Front, (c) Standing at the back, and (d), (e), and (f) Walking and standing close to target.

5.2.4 Effect of Another Person in the Vicinity

This research investigates a crucial scenario that focuses on how the presence of a second person near the target affects vital sign estimation. This scenario introduces complexity, making it more reflective of a real-life environment. The experimental configuration is displayed in Fig. 54, which involves a second individual instructed to cross the target's path from the front and back before standing next to the target, aligned with the radar. Table 14 presents the findings demonstrating the negligible impact of crossing a person from the front and back on vital sign estimation, as the HR estimation accuracy remains around 99.4% for error within ±2 bpm.

However, accuracy degrades when the person stands close to the subject. Specifically, when the person stands close behind the subject, the HR estimation accuracy degrades to 96.57% while the RR estimation accuracy maintains around 100% except for when the person walks and stands near the target, which is 99.24%. The proposed method demonstrates promising performance and follows the actual value for most of the observation duration under all scenarios, as shown in Fig. 55.

6. Discussion

This research focused on addressing the challenges associated with the contactless measurement of vital signs using radar in a realistic environment. Experiments were conducted under intricate, realistic scenarios with the radar placed at a height of 2.1 m, contrary to typical research setups where the radar aligns directly with the torso level. The paper presents a novel approach for extracting vital signs such as heartbeat and breathing-related phase information from radar signals in complex, realistic scenarios using the RSSD algorithm. The proposed method effectively addresses the challenges posed by noise and harmonic interference while preserving the time-frequency characteristics of the original phase signal. However, the effectiveness of the RSSD algorithm is significantly affected by the choice of high and low resonance quality factors. The Q-factor is optimally selected through sub-band energy distribution to address this challenge. The optimum Q factor selection reduces the mean error ranging

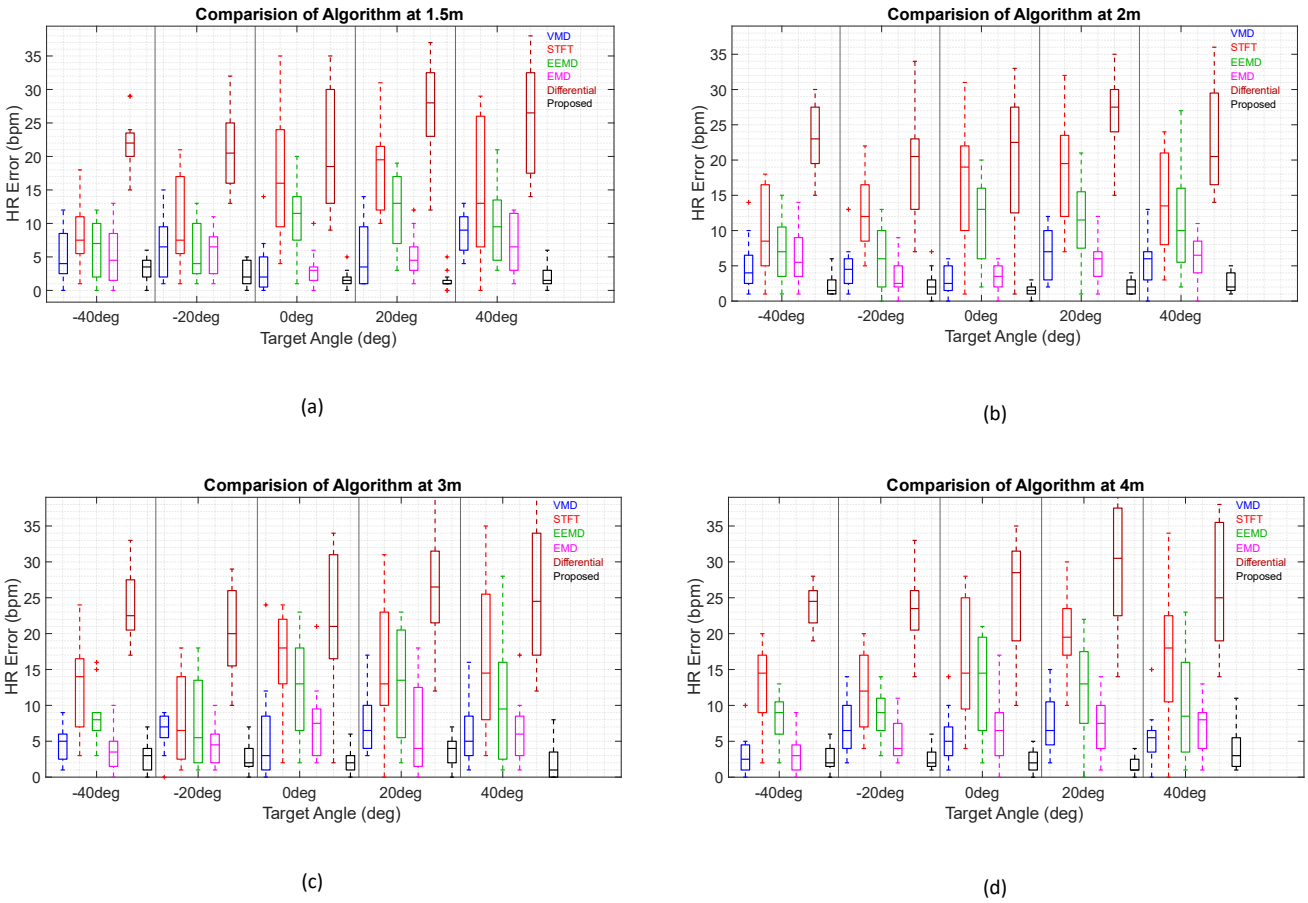

Figure 56: Comparative analysis of the proposed method with the state-of-art techniques. HR estimation error with target angle at different distances from radar.

from 3.8 to 14.6 bpm for fixed Q value to the mean error within 3 bpm, paired with a considerably lower error standard deviation.

Table 15 describes the comparative analysis of the experimental setup and scenarios for the works related to target localization with beamforming or beam steering. It is evident from the table that this study incurred the stationary and non-stationary subjects to cater to the problem of random body movement. Additionally, different level of complexity is added to the non-stationary scenarios. We conduct a comparison of the proposed method with state-of-the-art HR estimation techniques, as presented in Fig. 56. Different signal processing algorithms are applied to our dataset to facilitate a more comprehensive comparative analysis. Among the other algorithms, STFT and differential tend to exhibit higher errors, particularly when dealing with more distant target ranges. In contrast, the VMD algorithm displays varying heart rate measurement errors at a target range of 1.5 meters, with a mean average error of roughly 6.25 and a variance of about 14.97. Meanwhile, the EEMD algorithm ,

Table 14: Comparison of related works with this study

Ref#	Radar Type	Radar Configuration	Radar at torso level	Target Location	Scenario	Additional Clutter & Body Motion	Target Localization Technique	Measured Parameter
[265]	CW	SIMO (1Tx8R)	✓	2m, Two people at ±30, ±15 deg	Stationary sitting at a known location	×	ADBF	RR
[267]	UWB	SIMO (1Tx4R)	Subject in lying position	0.5m	Stationary sleep posture	×	Capon DBF	RR
[269]	FMCW	MIMO (4Tx4R)	✓	0.5m, Two targets at ±35 deg	Stationary sitting at a known location	×	Beam Steering	HR & RR
[270]	-	Phased array	Subject in lying position	1.5m, -13.3-14.1deg	Stationary sleep posture	-	Beam Steering	HR
[271]	FMCW	Single Phased-MIMO (3Tx4R)	✓	4m, Two people at 15 & 30 deg	Stationary sitting at a known location	-	TDM-MIMO	HR & RR
[275]	IF-CW	MIMO (6Tx6R)	✓	1.8m, Two targets at ±15 deg	Stationary sitting & sleeping at a known location	×	DBF	HR & RR
[156]	CW	MIMO (4Tx4R)	✓	3m	Stationary sitting at a known location	×	Hybrid DBF	RR
[276]	FMCW	MIMO (3Tx4R)	✓	0.9m, 1.2 & 1.5m at ±20, ±40 deg	Stationary sitting at a known location	-	DBF	HR & RR
[289]	-	MIMO (2Tx8R)	✓	1.8m, 2.3m	Stationary sitting at a known location	-	-	HR & RR
[This Paper]	FMCW	MIMO (2Tx4R)	× (at the height of 2.1m)	1.5, 2, 3, 4m at 0, ±20, ±40 deg	Stationary/non-stationary at an unknown location.	✓ + Second person in the vicinity	Automatic Beam Steering	HR & RR

demonstrates HR measurement errors spanning from 0 to 20, with a mean average error of approximately 7.14 and a variance of roughly 26.48. Particularly, performance degrades at greater target ranges. In contrast, the proposed algorithm consistently demonstrates the lowest HR measurement errors across the entire dataset, encompassing different transmitter angles and target ranges.

The study demonstrated that the HR accuracy has improved at different distances and angles compared to a previous study [289]. In our work mean average error (MAE) for HR measurement at 1.5 m and 0^0, 20^0, 40^0, -20^0 is 2, 1.5, 2.25, 2.25 bpm, where the MAE in [289] is 3.71, 2.47, 3.26, 3.20 bpm, respectively. While at -40^0, the results are comparable. An overall improvement of 48% is observed. The results suggest that the methodology used in this study offer a more precise way to measure vital signs, suggesting potential improvements in various experimental settings. The proposed method demonstrated high HR accuracy of up to 98.7% at all distances and angles combinations. The paper presents a novel approach for extracting vital signs such as heartbeat and breathing-related phase information from radar signals in complex, realistic scenarios using the RSSD algorithm.

While previous research mainly focused on stationary human subjects or required apriori knowledge of target location for multi-person detection, this research demonstrates the feasibility of accurate vital sign extraction in realistic situations where body movement and positional changes are inevitable. These findings have significant implications for developing of radar-based vital sign monitoring systems with potential applications in clinical and home care settings. The contribution of this work is summarized as follows:

- **Automatic target localization and SNR Improvement:** Our method successfully achieved automatic target localization, angle estimation, and beam steering toward the localized target for vital sign measurement in realistic scenarios, which has not been quantified. The study demonstrated the SNR improvement achieved through beam steering.

- **Accurate Vital Sign Estimation:** The study demonstrated the effectiveness of the HR/RR extraction method based on RSSD combined with optimal quality factor selection using subband energy distribution even under heavy noise conditions.
- **Comprehensive Experimentation:** The efficacy of the proposed method is validated on HR/RR estimation by conducting various realistic scenarios such as the unknown location of the target, radar at different elevation levels with the target, adding heavy clutter and moderate body movement, and another person in the vicinity of the target person.

Though the proposed method accurately estimates the HR and RR under a realistic, complex emulated environment, yet a few limitations worth noting.

- The frequency of operation in mm-wave radar systems makes them vulnerable to random body movements, and target distance significantly impacts their ability to detect vital signs, reducing their accuracy. However, improving the system's performance is challenging as it already operates at the maximum permitted radiation power limits. Nonetheless, a potential solution could involve combining chips and antenna arrays to enhance the MIMO capabilities, improving hardware performance and being a helpful direction for future research.
- This study focuses on analyzing the impact of a second person's presence near the target on the accuracy of vital sign measurements for a single person. Potential future work could explore estimating vital signs for multiple individuals.

7. Conclusion

This research paper presents a method for extracting vital heart and breathing signals from noisy radar signals, leveraging the resonance property of these vital signs. It provides an in-depth look into the signal processing flow and parameter configuration for FMCW radar and demonstrates automatic target localization and beam steering's effect on SNR enhancement. The RSSD algorithm, integrating optimal Q-factor selection and subband energy distribution, is used for phase signal extraction and HR signal decomposition, effectively mitigating random body movement and clutter effects. The subband energy-based vital sign estimation algorithm suppresses the influence of RR

harmonics and intermodulation products on HR value. The proposed method successfully suppresses noise and RR harmonic interference even at increased angles and distances from the radar. Also, it explores the effect of substantial clutter, moderate body movement, and the presence of another individual in the target's vicinity on HR/RR estimation. Overall, this research provides a novel and effective HR/RR monitoring technique, which could potentially have significant applications in healthcare and other fields such as sports and wellness.

Chapter 6

Conclusion and Future Work

This chapter presents a comprehensive overview of the thesis, drawing a conclusion, discussing limitations and future directions. Section 6.1 offers a detailed summary of the thesis contributions, highlighting the key findings and outcomes. Subsequently, in Section 6.2, the limitations of the thesis work are discussed, along with recommendations for future research in non-contact vital signs monitoring.

1. Summary

Accurate monitoring of vital signs, including heart and respiration rates, is crucial for effective health management. In recent years, the utilization of mmWave radar for non-contact vital sign monitoring has gained prominence due to its exceptional penetration capabilities and resilience to environmental factors. This has led to extensive research and exploration in leveraging mmWave radar for reliable and convenient vital sign measurements. Extracting physiological information from radar signals faces significant challenges due to environmental noise, interference, and the impact of body movements. The weak reflected signal from heartbeats compared to respiration, along with noise from respiration harmonics and intermodulation products, further complicates accurate estimation. Additionally, environmental clutter and random body movements contribute to the complexity of developing an efficient system for heart rate estimation.

This research focuses on developing an efficient, accurate, non-contact vital sign (NCVS) monitoring method using mm-wave radar technology. The research incorporates analytical modeling of chest wall motion resulting from cardiovascular activity. This modeling helps in understanding the trade-offs associated with various radar parameters, enabling the optimization of the monitoring system for accurate vital sign measurements. A signal processing method is devised to enhance the accuracy of heart rate and respiration rate measurements. This method utilizes resonance sparse spectrum decomposition (RSSD), which allows for the precise analysis of complex, non-stationary signals. A more accurate representation of the vital sign signals is obtained by decomposing the signal into time-varying frequency components and identifying resonant frequencies. An automatic beam steering and beam forming algorithm are introduced to address the challenge of target localization in realistic scenarios. It enables the radar system to identify target locations in real time. It enhances the signal-to-noise ratio (SNR) and improves the accuracy of vital sign estimation.

The proposed method is thoroughly evaluated through experiments conducted in various realistic settings. These settings include scenarios with artificial clutter and

body movements like reading a book, drinking water, and forward/backward body motion. A critical scenario involving the impact of a second person near the target on vital sign estimation is also examined. The results demonstrate the effectiveness of the method in mitigating issues caused by unwanted clutter, random body motion, and harmonic interference. The proposed method significantly improves heart rate estimation accuracy by reducing noise in the phase signal.

Chapter 2 of the thesis presents a comprehensive overview of various aspects related to NCVS radar systems. It covers different topologies and architectures of NCVS radar and provides an operational and principal overview for designing a non-contact measurement system. The implications of mmWave exposure on human health and the effect of environmental attenuation are analyzed, highlighting the shift towards mmWave frequencies in system design due to their larger bandwidth advantages. The review identifies research challenges associated with hardware and signal processing for the practical deployment of NCVS systems. It emphasizes the limited measurement range of 0.5-2 m and the decrease in accuracy beyond this range, suggesting the use of high-gain antennas to extend the detection range. The trade-off between radar system power, frequency, sensitivity, resolution, and the null point problem is discussed, highlighting the need to consider the safety margins of EM wave radiation. To minimize the effects of long-term exposure, the focus must be on developing systems with minimum power requirements or integrating them with commonly used devices. The implementation challenges for multi-resident scenarios are highlighted, emphasizing the need to address vital sign detection for multiple people in realistic environments. The review also highlights the need for extensive real-life experiments with different subject groups to assess the reliability and robustness of NCVS systems, considering environmental changes.

Chapter 3 contributes to developing a mathematical model for simulating chest wall motion in the context of cardiorespiratory activity, which maps to RQ1. In literature, most of the simulations for radar-based NCVS systems to date are based on a simplistic approach of assuming chest wall motion as sinusoidal. The proposed model incorporates optimal chemical-mechanical respiratory control-based mechanics to simulate

respiration-induced chest wall motion and applies the theory of relaxation oscillation system to model motion caused by cardiac activity. This mathematical chest wall model offers a valuable tool for designing and optimizing various parameters in radar-based NCVS systems and can aid in evaluating cardio-respiratory parameters for artificial systems. The cross-correlation analysis validates the accuracy of the simulated chest wall motion, with a high degree of similarity between the simulated waveform and experimental data (cross-correlation coefficient of 0.95-0.97). It successfully simulates varying chest wall motion in different scenarios, such as free-breathing and post-exercise breathing. Using this model reduces the need for extensive human testing in the development of biomedical applications, as it provides insights into chest wall motion and its relationship to vital signs such as respiration and heartbeat.

We propose a method that combines resonance sparse spectrum decomposition (RSSD) and harmonic utilized algorithm (HUA) for accurate heart and respiration rate extraction in Chapter 4 that address the RQ2. The RSSD algorithm decomposes the signal into its time-varying frequency components using a combination of wavelet decomposition and sparse approximation. It identifies and isolates the signal's resonant frequencies using a resonance-based frequency estimation technique and constructs a sparse representation of the signal using the identified resonant frequencies. The RSSD algorithm provides a highly accurate and efficient method for analyzing non-stationary signals with time-varying spectral characteristics. It effectively mitigates the effects of clutter and random body movements in the received phase signal.

Further, the second harmonic of respiration is more prominent at higher respiratory rates, while the third harmonic has a comparable amplitude to the heartbeat signal in the fundamental frequency range. Extracting the HR beat becomes challenging due to these respiratory harmonics, necessitating to mitigate the effect of RR harmonics before HR estimation. Leveraging the fact that RR harmonics and intermodulation products have a lesser or no impact on HR harmonics due to their weak amplitudes and the fact that the heart rate does not change abruptly, an algorithm is designed and proposed for HR estimation. This algorithm effectively estimates HR even in cases where

the HR fundamental is missing or influenced by neighboring RR harmonics and intermodulation products.

The efficacy of the proposed method is validated by demonstrating comparable HR estimation accuracy to RR estimation accuracy, even in the presence of heavy clutter and moderate body movement. The proposed method is validated against ground truth HR/RR data collected using a Hexoskin vest. To evaluate the reliability and robustness of our method, comprehensive experiments were conducted involving four participants at varying distances and angles with respect to the radar device. The findings indicate an accuracy range of 98-100% within a distance of 2 m, and the detection accuracy remains consistent up to 4 m from the radar device. The results demonstrate that the proposed method significantly improves HR detection accuracy even in the presence of noise, clutter, and moderate body movement by effectively reducing the impact of noise and harmonic interference in the phase signal.

Chapter 5 addresses the challenges of monitoring individuals in real-life situations where their positions are unknown. This contribution maps to RQ3. Adaptive steering of radar beams towards the target was identified as crucial for achieving a satisfactory signal-to-noise ratio (SNR) and accurately extracting heart and respiration rates. Interference from other individuals, self-body motion, and clutter present additional challenges by obscuring vital signals. To overcome these issues, a signal processing method combining the RSSD algorithm with optimal quality factor leveraging sub-band energy distribution is proposed. Sub-band energy distribution optimizes the Q factor for precise extraction of high resonance components, and subsequently, RSSD effectively mitigates clutter and random body motion effects from the phase signal.

This study encompasses a range of diverse experimental scenarios to achieve multiple objectives. The study was conducted at Auckland University of Technology, Auckland, and ethics approval was obtained from the Auckland University of Technology Ethics Committee (AUTEC) before commencing the experiments. These experiments aim to assess the improvement in SNR)resulting from beam steering, evaluate the accuracy of HR and RR measurements, investigate the impact of body motion and clutter (e.g., reading books, drinking water), examine the effects of the presence of a second person,

and analyze the influence of body orientation. The proposed method is extensively validated through these experiments conducted in various real-life scenarios. The findings demonstrate an accuracy rate of up to 97.6% within a 4 m range, even in challenging conditions. The results of this research hold promise for various fields, such as adult home care, sleep apnea monitoring, driver health monitoring, and infant monitoring.

2. Thesis Limitations and Recommendations for Future Research

This section provides a brief overview of the limitations of the proposed framework and outlines some potential areas for future research. It is important to note that these limitations and future directions do not detract from the value of the research contributions made in this thesis. Instead, they highlight areas that can be further explored to improve the proposed framework and facilitate the deployment of mm-wave radar-based non-contact vital sign monitoring systems in practical applications.

The mathematical model presented in this research for evaluating cardiopulmonary characteristics based on the chest surface motion mimics chest wall movement patterns across various scenarios, including natural and post-exercise breathing. A limitation of our simulation is that it relies on a limited experimental dataset regarding chest wall motion. However, future research could include comprehensive experiments involving subjects of diverse ages, gender, weight, and medical history to quantify chest displacements. A potential extension of this simulation could involve incorporating clutter and environmental noise to simulate realistic experimental conditions for evaluating radar-based NCVS systems.

The signal processing method proposed in this research to accurately extract HR and RR values from radar-received signals in a noisy environment validates the method through various experiments carried out under varying indoor settings for a single stationary and non-stationary human target. In our experiments, all participants wear everyday clothing and do not carry personal belongings such as mobile phones,

handbags, or exercise equipment. These large objects could temporarily inflate the estimated weights during movement power detection, leading to a noisy phase signal. The data was collected with limited participants and for a limited time duration in a controlled environment. More experiments will help to validate the robustness of the method. This research work with an off-the-shelf radar device with limited hardware capabilities, specifically Tx-Rx antennas and electronic beam steering. More Tx-Rx antennas would help in improving the resilience against noise through beamforming.

Further, the performance of the algorithm under hyper or hypoventilation conditions for a stationary person experiencing such conditions is worth exploring. This investigation could provide valuable insights for future research as these conditions alter chest wall motion and, consequently, the phase signal quality.

This study primarily delves into the influence of an additional person's presence near the target on the precision of vital sign measurements for a single individual. Future research could evaluate how the algorithm performs when several individuals are near the target person. Building upon these findings, future research could also focus on simultaneously estimating vital signs for multiple persons. To make the system more scalable, the signal processing algorithm needs to be modified for simultaneous multi-person monitoring. Also advanced beamforming and tracking algorithms would help in improving SNR and range resolution.

References

1. T. Ahrens, “The most important vital signs are not being measured,” in Australian critical care: official journal of the Confederation of Australian Critical Care Nurses, vol. 21, no. 1, pp. 3–5. 2008, doi: 10.1016/j.aucc.2007.12.061.
2. M. Elliott, and A. Coventry, “Critical care: the eight vital signs of patient monitoring,” in British Journal of Nursing (Mark Allen Publishing), vol. 21, no. 10, pp. 621–625, 2012, doi: 10.12968/bjon.2012.21.10.621.
3. S. Ridley, “Cardiac scoring systems--what is their value?,” in Anaesthesia, vol. 58, no. 10, pp. 985-991, 2003, doi: 10.1046/j.1365-2044.2003.03342.x
4. L. Scalise, and U. Morbiducci, “Non-contact cardiac monitoring from carotid artery using optical vibrocardiography,” in Medical engineering & physics, vol. 30, no. 4, pp. 490-497, 2008, doi: 10.1016/j.medengphy.2007.05.008.
5. United Nations, Department of Economic and Social Affairs, Population Division (2019), “World Population Ageing 2019: Highlights,” (ST/ESA/SER.A/430), Available: https://www.un.org/en/development/desa/population/publications/pdf/ageing/WorldPopulationAgeing2019-Highlights.pdf, (accessed Oct 2019).
6. J. R. Duncan, and R. W. Byard, “Sudden Infant Death Syndrome: An Overview” in SIDS Sudden Infant and Early Childhood Death: The Past, the Present and the Future, University of Adelaide Press, May 2018, ch. 1-2, Available from: https://www.ncbi.nlm.nih.gov/books/NBK513399/.
7. Division of Reproductive Health, National Center for Chronic Disease Prevention and Health Promotion, “Sudden Unexpected Infant Death and Sudden Infant Death Syndrome,” cdc.gov, https://www.cdc.gov/sids/data.htm (accessed March 2023).
8. A. Singh, S. U. Rehman, S. Yongchareon and P. H. J. Chong, "Sensor Technologies for Fall Detection Systems: A Review," in IEEE Sensors Journal, vol. 20, no. 13, pp. 6889-6919, July 1, 2020, doi: 10.1109/JSEN.2020.2976554.
9. “Contactless Vital Signs Monitoring Market 2023 - Detailed Analysis of Industry, Potential Growth, Attractive Valuation and Growth Forecast Up to 2029,” MarketsandResearch.biz, Mar 22, 2023. Available from: https://www.marketwatch.com/press-release/contactless-vital-signs-monitoring-market-2023---detailed-analysis-of-industry-potential-growth-attractive-valuation-and-growth-forecast-up-to-2029-2023-03-22
10. G. Lu, and F. Yang, “Limitations of oximetry to measure heart rate variability measures,” Cardiovascular engineering (Dordrecht, Netherlands), vol. 9, no. 3, pp. 119-125. 2009, doi: 10.1007/s10558-009-9082-3.
11. Md. Uddin, W. Khaksar, and J. Torresen, “Ambient Sensors for Elderly Care and Independent Living: A Survey,” in Sensors, vol. 18, no. 7, pp. 2027, Jun. 2018, doi: 10.3390/s18072027.
12. C. B. Pereira et al., "Noncontact Monitoring of Respiratory Rate in Newborn Infants Using Thermal Imaging," in IEEE Transactions on Biomedical Engineering, vol. 66, no. 4, pp. 1105-1114, April 2019, doi: 10.1109/TBME.2018.2866878.
13. F. Lin et al., "SleepSense: A Noncontact and Cost-Effective Sleep Monitoring System," in IEEE Transactions on Biomedical Circuits and Systems, vol. 11, no. 1, pp. 189-202, Feb. 2017, doi: 10.1109/TBCAS.2016.2541680.
14. F. Adib, H. Mao, Z. Kabelac, D. Katabi, and R. C. Miller, “Smart Homes that Monitor Breathing and Heart Rate,” in Proceedings of the 33rd Annual ACM Conference on Human Factors in Computing Systems (CHI '15), ACM, pp. 837–846, April 2015, doi: 10.1145/2702123.2702200

15. K. J. Lee, C. Park, and B. Lee, “Tracking driver's heart rate by continuous-wave Doppler radar,” in Annual International Conference of the IEEE Engineering in Medicine and Biology Society, EMBC, vol. 2016, pp. 5417-5420, 2016, doi: 10.1109/EMBC.2016.7591952.
16. J. Kranjec, S. Beguš, G. Geršak, and J. Drnovšek, “Non-contact heart rate and heart rate variability measurements: A review,” in Biomedical Signal Processing and Control, vol. 13, pp. 102-112, 2014, doi: 10.1016/j.bspc.2014.03.004.
17. U. Morbiducci, L. Scalise, M. De Melis, and M. Grigoni, “Optical Vibrocardiography: A Novel Tool for the Optical Monitoring of Cardiac Activity,” Annals of Biomedical Engineering, vol. 35, pp. 45–58, 2007, doi: 10.1007/s10439-006-9202-9
18. A. Mesleh, D. Skopin, S. Baglikov, and A. Quteishat, “Heart Rate Extraction from Vowel Speech Signals,” Journal of Computer Science and Technology, vol. 27, pp. 1243–1251, 2012, doi: 10.1007/s11390-012-1300-6.
19. M. de Melis, G. Mauro, M. Umberto, and L. Scalise, “Optical monitoring of the heart beat,” in Biomedicine, vol. 8, pp. 181-190, 2005, doi: 10.2495/BIO050181.
20. M. Garbey, N. Sun, A. Merla and I. Pavlidis, "Contact-Free Measurement of Cardiac Pulse Based on the Analysis of Thermal Imagery," in IEEE Transactions on Biomedical Engineering, vol. 54, no. 8, pp. 1418-1426, Aug. 2007, doi: 10.1109/TBME.2007.891930.
21. S. Y. Chekmenev, A. A. Farag and E. A. Essock, "Multiresolution Approach for Non-Contact Measurements of Arterial Pulse using Thermal Imaging," 2006 Conference on Computer Vision and Pattern Recognition Workshop (CVPRW'06), New York, NY, USA, 2006, pp. 129-129, doi: 10.1109/CVPRW.2006.139.
22. T. R. Gault and A. A. Farag, "A Fully Automatic Method to Extract the Heart Rate from Thermal Video," 2013 IEEE Conference on Computer Vision and Pattern Recognition Workshops, Portland, OR, USA, 2013, pp. 336-341, doi: 10.1109/CVPRW.2013.57.
23. M. Poh, D. J. McDuff, and R. W. Picard, “Non-contact, automated cardiac pulse measurements using video imaging and blind source separation,” in Optics express, vol. 18, no. 10, pp. 10762-10774, 2010, doi: 10.1364/OE.18.010762.
24. C. H. Antink et al., “A Broader Look: Camera-Based Vital Sign Estimation across the Spectrum,” Yearbook of medical informatics, vol. 28, no. 1, pp. 102-111, 2019, doi: 10.1055/s-0039-1677914.
25. L. Ge, J. Zhang, and J. Wei, “Single-Frequency Ultrasound-Based Respiration Rate Estimation with Smartphones,” in Computational and mathematical methods in medicine, vol. 2018, pp. 3675974, May 2018, doi: 10.1155/2018/3675974.
26. C. Li, V. M. Lubecke, O. Boric-Lubecke, and J. Lin, "A Review on Recent Advances in Doppler Radar Sensors for Noncontact Healthcare Monitoring," in IEEE Transactions on Microwave Theory and Techniques, vol. 61, no. 5, pp. 2046-2060, May 2013, doi: 10.1109/TMTT.2013.2256924.
27. S. Leonhardt, L. Leicht, and D. Teichmann, “Unobtrusive Vital Sign Monitoring in Automotive Environments-A Review,” Sensors, vol. 18, no. 9, pp. 3080, Sep. 2018, doi: 10.3390/s18093080.
28. A. D. Droitcour, “Non-contact measurement of heart and respiration rates with single chip microwave Doppler radar,” Ph.D. dissertation, StanfordUniversity, USA, 2006.
29. C. Li, J. Lin, and Y. Xiao, "Robust Overnight Monitoring of Human Vital Signs by a Non-contact Respiration and Heartbeat Detector," 2006 International Conference of the IEEE Engineering in Medicine and Biology Society, New York, NY, USA, 2006, pp. 2235-2238, doi: 10.1109/IEMBS.2006.260148.
30. R. Ichapurapu, S. Jain, M. U. Kakade, D. Y. C. Lie and R. E. Banister, "A 2.4GHz non-contact biosensor system for continuous vital-signs monitoring on a single PCB," 2009

IEEE 8th International Conference on ASIC, Changsha, China, 2009, pp. 925-928, doi: 10.1109/ASICON.2009.5351542.
31. W. Hu et al., "An intelligent non-contact wireless monitoring system for vital signs and motion detection," 2010 International Conference on System Science and Engineering, Taipei, Taiwan, 2010, pp. 190-194, doi: 10.1109/ICSSE.2010.5551795.
32. V. Das, A. Boothby, R. Hwang, T. Nguyen, J. Lopez, and D. Y. C. Lie, "Antenna evaluation of a non-contact vital signs sensor for continuous heart and respiration rate monitoring," 2012 IEEE Topical Conference on Biomedical Wireless Technologies, Networks, and Sensing Systems (BioWireleSS), Santa Clara, CA, USA, 2012, pp. 13-16, doi: 10.1109/BioWireless.2012.6172730.
33. M. Mercuri, "Vital-sign monitoring and spatial tracking of multiple people using a contactless radar-based sensor," Nature Electron, vol. 2, no. 6, pp. 252–262, Jun 2019, doi: 10.1038/s41928-019-0258-6.
34. T. Hall et al., "Extending the range of phased array non-contact vital signs monitoring in an office cubicle setting," Texas Symposium on Wireless and Microwave Circuits and Systems, Waco, TX, USA, 2014, pp. 1-4, doi: 10.1109/WMCaS.2014.7015870.
35. Zhijian Li, L. P. Ligthart, Peikang Huang, Weining Lu and W. F. van der Zwan, "Trade-off between sensitivity and dynamic range in designing digital radar receivers," 2008 International Conference on Microwave and Millimeter Wave Technology, Nanjing, China, 2008, pp. 1368-1371, doi: 10.1109/ICMMT.2008.4540695.
36. H. Zhao, H. Hong, L. Sun, Y. Li, C. Li and X. Zhu, "Noncontact Physiological Dynamics Detection Using Low-power Digital-IF Doppler Radar," in IEEE Transactions on Instrumentation and Measurement, vol. 66, no. 7, pp. 1780-1788, July 2017, doi: 10.1109/TIM.2017.2669699.
37. M. Nosrati and N. Tavassolian, "Accuracy Enhancement of Doppler Radar-Based Heartbeat Rate Detection Using Chest-Wall Acceleration," 2018 IEEE International Microwave Biomedical Conference (IMBioC), Philadelphia, PA, USA, 2018, pp. 139-141, doi: 10.1109/IMBIOC.2018.8428898.
38. B. Gupta, E. Cianca, M. Ruggieri and R. Prasad, "A novel FM-UWB system for vital sign monitoring and its comparison with IR-UWB," 2009 2nd International Symposium on Applied Sciences in Biomedical and Communication Technologies, Bratislava, Slovakia, 2009, pp. 1-4, doi: 10.1109/ISABEL.2009.5373708.
39. C. -H. Hong et al., "Fast selection of time-interleaved samples for wireless healthcare monitoring with pulse radar," 2012 IEEE Biomedical Circuits and Systems Conference (BioCAS), Hsinchu, Taiwan, 2012, pp. 45-48, doi: 10.1109/BioCAS.2012.6418473.
40. V. Nguyen, A. Q. Javaid and M. A. Weitnauer, "Harmonic Path (HAPA) algorithm for non-contact vital signs monitoring with IR-UWB radar," 2013 IEEE Biomedical Circuits and Systems Conference (BioCAS), Rotterdam, Netherlands, 2013, pp. 146-149, doi: 10.1109/BioCAS.2013.6679660.
41. V. Nguyen, A. Q. Javaid and M. A. Weitnauer, "Spectrum-averaged Harmonic Path (SHAPA) algorithm for non-contact vital sign monitoring with ultra-wideband (UWB) radar," 2014 36th Annual International Conference of the IEEE Engineering in Medicine and Biology Society, Chicago, IL, USA, 2014, pp. 2241-2244, doi: 10.1109/EMBC.2014.6944065.
42. J. Wang, X. Wang, L. Chen, J. Huangfu, C. Li and L. Ran, "Noncontact Distance and Amplitude-Independent Vibration Measurement Based on an Extended DACM Algorithm," in IEEE Transactions on Instrumentation and Measurement, vol. 63, no. 1, pp. 145-153, Jan. 2014, doi: 10.1109/TIM.2013.2277530.
43. F. Weishaupt, I. Walterscheid, O. Biallawons and J. Klare, "Vital Sign Localization and Measurement Using an LFMCW MIMO Radar," 2018 19th International Radar Symposium (IRS), Bonn, Germany, 2018, pp. 1-8, doi: 10.23919/IRS.2018.8448229.

44. M. Alizadeh, G. Shaker, J. C. M. D. Almeida, P. P. Morita and S. Safavi-Naeini, "Remote Monitoring of Human Vital Signs Using mm-Wave FMCW Radar," in IEEE Access, vol. 7, pp. 54958-54968, 2019, doi: 10.1109/ACCESS.2019.2912956.
45. A. Ahmad, J. C. Roh, D. Wang and A. Dubey, "Vital signs monitoring of multiple people using a FMCW millimeter-wave sensor," 2018 IEEE Radar Conference (RadarConf18), Oklahoma City, OK, USA, 2018, pp. 1450-1455, doi: 10.1109/RADAR.2018.8378778.
46. S. Nahar, T. Phan, F. Quaiyum, L. Ren, A. E. Fathy and O. Kilic, "An Electromagnetic Model of Human Vital Signs Detection and Its Experimental Validation," in IEEE Journal on Emerging and Selected Topics in Circuits and Systems, vol. 8, no. 2, pp. 338-349, June 2018, doi: 10.1109/JETCAS.2018.2811339.
47. S. M. A. Tayaranian Hosseini and H. Amindavar, "UWB radar signal processing in measurement of heartbeat features," 2017 IEEE International Conference on Acoustics, Speech and Signal Processing (ICASSP), New Orleans, LA, USA, 2017, pp. 1004-1007, doi: 10.1109/ICASSP.2017.7952307.
48. Y. Lee et al., "A novel non-contact heart rate monitor using impulse radio ultra-wideband (IR-UWB) radar technology," Sci. Rep., vol. 8, Article number: 13053, pp. 1–10, Dec. 2018.
49. M. Leib, W. Menzel, B. Schleicher and H. Schumacher, "Vital signs monitoring with a UWB radar based on a correlation receiver," Proceedings of the Fourth European Conference on Antennas and Propagation, Barcelona, Spain, 2010, pp. 1-5.
50. B. R. Mahafza, Radar Systems Analysis and Design Using MATLAB (3rd ed.). Chapman and Hall/CRC, 2013, doi: 10.1201/b14904.
51. C. Will et al., "Local Pulse Wave Detection Using Continuous Wave Radar Systems," in IEEE Journal of Electromagnetics, RF and Microwaves in Medicine and Biology, vol. 1, no. 2, pp. 81-89, Dec. 2017, doi: 10.1109/JERM.2017.2766567.
52. B.-S. Kim, Y. Jin, J. Lee, and S. Kim, "Low-Complexity MUSIC-Based Direction-of-Arrival Detection Algorithm for Frequency-Modulated Continuous-Wave Vital Radar," Sensors (Basel, Switzerland), vol. 20, no. 15, pp. 4295, Jul 2020, doi:10.3390/s20154295.
53. N. Birsan and D. -P. Munteanu, "Non-contact cardiopulmonary monitoring algorithm for a 24 GHz Doppler radar," 2012 Annual International Conference of the IEEE Engineering in Medicine and Biology Society, San Diego, CA, USA, 2012, pp. 3227-3230, doi: 10.1109/EMBC.2012.6346652.
54. J. J. Saluja, J. Lin and J. Casanova, "A Supervised Learning Approach for Real Time Vital Sign Radar Harmonics Cancellation," 2018 IEEE International Microwave Biomedical Conference (IMBioC), Philadelphia, PA, USA, 2018, pp. 67-69, doi: 10.1109/IMBIOC.2018.8428911.
55. V. Rajagopal, A. -K. Moadi, A. E. Fathy and M. A. Abidi, "Portable Real-Time System for Multi-Subject Localization and Vital Sign Estimation," 2023 IEEE Radio and Wireless Symposium (RWS), Las Vegas, NV, USA, 2023, pp. 40-43, doi: 10.1109/RWS55624.2023.10046315.
56. P. E. Numan, H. Park, J. Lee and S. Kim, "Machine Learning-Based Joint Vital Signs and Occupancy Detection With IR-UWB Sensor," in IEEE Sensors Journal, vol. 23, no. 7, pp. 7475-7482, April 1, 2023, doi: 10.1109/JSEN.2023.3247728.
57. I.W. Selesnick, "Resonance-based signal decomposition: a new sparsity-enabled signal analysis method," in Signal Process, vol. 91, no. 12, pp. 2793–2809, Dec 2011, doi: 10.1016/j.sigpro.2010.10.018.
58. C. Matteucci, "Sur un phenomene physiologique produit par les muscles en contraction," Ann Chim Phys., vol. 6, pp. 339–341, Nov. 1842.
59. W. Einthoven, "Un nouveau galvanometre," Soc. Holl. Sci., vol. 6, pp. 625–33, Series 2, 1901.

60. B. J. Drew et al., “Practice standards for electrocardiographic monitoring in hospital settings: an American Heart Association scientific statement from the Councils on Cardiovascular Nursing, Clinical Cardiology, and Cardiovascular Disease in the Young: endorsed by the International Society of Computerized Electrocardiology and the American Association of Critical-Care Nurses,” Circulation vol. 110, no. 17, pp. 2721-2746, 2004, doi: 10.1161/01.CIR.0000145144.56673.59
61. L. Scalise, “Non contact heart monitoring,” in Adv. Electrocardiogram Methods Anal., vol. 2012, no. 4, pp. 80–106, Jan 2012, doi: 10.5772/22937.
62. C. Brüser, C. H. Antink, T. Wartzek, M. Walter and S. Leonhardt, "Ambient and Unobtrusive Cardiorespiratory Monitoring Techniques," in IEEE Reviews in Biomedical Engineering, vol. 8, pp. 30-43, 2015, doi: 10.1109/RBME.2015.2414661.
63. O. Postolache, P. S. Girao, J. Mendes and G. Postolache, "Unobstrusive heart rate and respiratory rate monitor embedded on a wheelchair," 2009 IEEE International Workshop on Medical Measurements and Applications, Cetraro, Italy, 2009, pp. 83-88, doi: 10.1109/MEMEA.2009.5167960.
64. C. Gu, “Short-Range Noncontact Sensors for Healthcare and Other Emerging Applications: A Review,” Sensors, vol. 16, no. 8, pp. 1169, Jul. 2016, doi: 10.3390/s16081169.
65. T. Hall et al., “Non-Contact Sensor for Long-Term Continuous Vital Signs Monitoring: A Review on Intelligent Phased-Array Doppler Sensor Design,” Sensors (Basel, Switzerland), vol. 17, no. 11, pp. 2632, Nov 2017, doi: 10.3390/s17112632.
66. C. Gouveia, J. Vieira, and P. Pinho, “A Review on Methods for Random Motion Detection and Compensation in Bio-Radar Systems,” Sensors, vol. 19, no. 3, pp. 604, Jan. 2019, doi: 10.3390/s19030604.
67. V. P. Tran, A. A. Al-Jumaily, and S. M. S. Islam, “Doppler Radar-Based Non-Contact Health Monitoring for Obstructive Sleep Apnea Diagnosis: A Comprehensive Review,” Big Data and Cognitive Computing, vol. 3, no. 1, pp. 3, Jan. 2019, doi: 10.3390/bdcc3010003.
68. J. C. Lin, "Noninvasive microwave measurement of respiration," in Proceedings of the IEEE, vol. 63, no. 10, pp. 1530-1530, Oct. 1975, doi: 10.1109/PROC.1975.9992.
69. D. Zhang, M. Kurata, and T. Inaba, “FMCW radar for small displacement detection of vital signal using projection matrix method,” in International Journal of Antennas and Propagation, vol. 2013, pp. 1-5, Nov. 2013, doi: 10.1155/2013/571986.
70. M. I. Skolnik, Radar Handbook. 3rd ed. New York, NY, USA: McGraw-Hill, 2008. https://www.accessengineeringlibrary.com/content/book/9780071485470
71. Guidance on Complying With Limits for Human Exposure to Electromagnetic Fields, document ITU-T K.52 (01/2018), 2018. [Online]. Available: https://www.itu.int/rec/T-REC-K.52-201801-I/en
72. D. Obeid, G. Issa, S. Sadek, G. Zaharia and G. El Zein, "Low power microwave systems for heartbeat rate detection at 2.4, 5.8, 10 and 16 GHz," 2008 First International Symposium on Applied Sciences on Biomedical and Communication Technologies, Aalborg, Denmark, 2008, pp. 1-5, doi: 10.1109/ISABEL.2008.4712623.
73. F. Series, Fixed Service Use and Future Trends. Accessed: 2015. [Online]. Available: https://www.itu.int/dms_pub/itu-r/opb/rep/R-REPF.2323-1-2017-PDF-E.pdf
74. FCC 47 CFR 15.256—Operation of Level Probing Radars Within the Bands 5.925-7.250 GHz, and A.-G. 29.00 GHz. [Online]. Available: https://www.law.cornell.edu/cfr/text/47/15.256
75. FCC 47 IFCC Report and Order-Radar Services in the 76–81 GHz Band ET Docket no 15-26. Accessed: Jun. 22, 2017. [Online]. Available: https://www.fcc.gov/document/radar-services-76-81-ghz-band

76. Attenuation by Atmospheric Gases, document, Sep. 2016, [online] Available: https://www.itu.int/rec/R-REC-P.676-11-201609-I
77. S. Narnakaje, “TI’s smart sensors ideal for automated driving applications,” Texas Instrum., Dallas, TX, USA, Tech. Rep. spyy009, 2017. [Online]. Available: http://www.ti.com/lit/wp/spyy009/spyy009.pdf
78. K. R. K. Ramasubramanian and A. Aginskiy, “Moving from legacy 24 GHz to state-of-the-art 77-GHz radar,” Texas Instrum., Dallas, TX, USA, Tech. Rep. spry312, Oct. 2017. [Online]. Available: http://www.ti.com/lit/wp/spry312/spry312.pdf
79. R. Jacobi, “Choosing 60-GHz mmWave sensors over 24-GHz to enable smarter industrial applications,” Texas Instrum., Dallas, TX, USA, Tech. Rep. spry328, Nov. 2018. [Online]. Available: http://www.ti.com/lit/wp/spry328/spry328.pdf
80. ITU-R,SM.2153-2,2011. [Online]. Available: https://www.itu.int/dms_pub/itu-r/opb/rep/R-REP-SM.2153-2-2011-PDF-E.pdf
81. J. H. Yu, “Millimeter-wave system-on-chip advancement for fusion plasma diagnostics,” The Review of scientific instruments, vol. 89, no. 10, 2018, doi:10.1063/1.5035559.
82. T. S. Rappaport et al., "Wireless Communications and Applications Above 100 GHz: Opportunities and Challenges for 6G and Beyond," in IEEE Access, vol. 7, pp. 78729-78757, 2019, doi: 10.1109/ACCESS.2019.2921522.
83. T. Wu, T. S. Rappaport and C. M. Collins, "Safe for Generations to Come: Considerations of Safety for Millimeter Waves in Wireless Communications," in IEEE Microwave Magazine, vol. 16, no. 2, pp. 65-84, March 2015, doi: 10.1109/MMM.2014.2377587.
84. International Commission on Non-Ionizing Radiation Protection (ICNIRP). “ICNIRP statement on the "Guidelines for limiting exposure to time-varying electric, magnetic, and electromagnetic fields (up to 300 GHz)".” Health Physics vol. 97, no. 3, pp. 257-258, 2009, doi:10.1097/HP.0b013e3181aff9db.
85. L. Kheifets, “The sensitivity of children to electromagnetic fields,” Pediatrics, vol. 116, no. 2, pp. e303–e313, Aug. 2005, doi: 10.1542/peds.2004-2541.
86. L. Gherardini, G. Ciuti, S. Tognarelli, and C. Cinti, “Searching for the perfect wave: The effect of radiofrequency electromagnetic fields on cells,” International Journal of Molecular Sciences, vol. 15, no. 4, pp. 5366–5387, Mar. 2014, doi: 10.3390/ijms15045366.
87. G. Vallant, M. Epp, W. Schlecker, U. Schneider, L. Anttila and M. Valkama, "Analog IQ impairments in Zero-IF radar receivers: Analysis, measurements and digital compensation," 2012 IEEE International Instrumentation and Measurement Technology Conference Proceedings, Graz, Austria, 2012, pp. 1703-1707, doi: 10.1109/I2MTC.2012.6229222.
88. Lu Guohua, W. Jianqi, Y. Yu and J. Xijing, "Study of the Ballistocardiogram signal in life detection system based on radar," 2007 29th Annual International Conference of the IEEE Engineering in Medicine and Biology Society, Lyon, France, 2007, pp. 2191-2194, doi: 10.1109/IEMBS.2007.4352758.
89. F. Zhu, K. Wang and K. Wu, "A Fundamental-and-Harmonic Dual-Frequency Doppler Radar System for Vital Signs Detection Enabling Radar Movement Self-Cancellation," in IEEE Transactions on Microwave Theory and Techniques, vol. 66, no. 11, pp. 5106-5118, Nov. 2018, doi: 10.1109/TMTT.2018.2869591.
90. O. Toker and M. Brinkmann, “A Novel Nonlinearity Correction Algorithm for FMCW Radar Systems for Optimal Range Accuracy and Improved Multitarget Detection Capability,” Electronics, vol. 8, no. 11, p. 1290, Nov. 2019, doi: 10.3390/electronics8111290.

91. A. Koelpin, F. Lurz, S. Linz, S. Mann, C. Will, and S. Lindner, “Six-port based interferometry for precise radar and sensing applications,” Sensors, vol. 16, no. 10, pp. 1556, Sep. 2016, doi: 10.3390/s16101556.
92. S. Lindner, F. Barbon, S. Mann, G. Vinci, R. Weigel and A. Koelpin, "Dual tone approach for unambiguous six-port based interferometric distance measurements," 2013 IEEE MTT-S International Microwave Symposium Digest (MTT), Seattle, WA, USA, 2013, pp. 1-4, doi: 10.1109/MWSYM.2013.6697581.
93. S. Ayhan, S. Scherr, A. Bhutani, B. Fischbach, M. Pauli and T. Zwick, "Impact of Frequency Ramp Nonlinearity, Phase Noise, and SNR on FMCW Radar Accuracy," in IEEE Transactions on Microwave Theory and Techniques, vol. 64, no. 10, pp. 3290-3301, Oct. 2016, doi: 10.1109/TMTT.2016.2599165.
94. S. Scheiblhofer, S. Schuster and A. Stelzer, "Signal model and linearization for nonlinear chirps in FMCW Radar SAW-ID tag request," in IEEE Transactions on Microwave Theory and Techniques, vol. 54, no. 4, pp. 1477-1483, June 2006, doi: 10.1109/TMTT.2006.871361.
95. Yanming Xiao, J. Lin, O. Boric-Lubecke and M. Lubecke, "Frequency-tuning technique for remote detection of heartbeat and respiration using low-power double-sideband transmission in the ka-band," in IEEE Transactions on Microwave Theory and Techniques, vol. 54, no. 5, pp. 2023-2032, May 2006, doi: 10.1109/TMTT.2006.873625.
96. C. Li, J. Cummings, J. Lam, E. Graves and W. Wu, "Radar remote monitoring of vital signs," in IEEE Microwave Magazine, vol. 10, no. 1, pp. 47-56, February 2009, doi: 10.1109/MMM.2008.930675.
97. D. Girbau, A. Lazaro, Á. Ramos, and R. Villarino, “Remote sensing of vital signs using a Doppler radar and diversity to overcome null detection,” IEEE Sensors Journal, vol. 12, no. 3, pp. 512–518, Mar. 2012, doi: 10.1109/JSEN.2011.2107736.
98. W. Pan, J. Wang, J. Huangfu, C. Li, and L. Ran, “Null point elimination using RF phase shifter in continuous-wave Doppler radar system,” Electronics Letters, vol. 47, no. 21, pp. 1196–1198, Nov 2011, doi: 10.1049/el.2011.2419.
99. B. -K. Park, O. Boric-Lubecke and V. M. Lubecke, "Arctangent Demodulation With DC Offset Compensation in Quadrature Doppler Radar Receiver Systems," in IEEE Transactions on Microwave Theory and Techniques, vol. 55, no. 5, pp. 1073-1079, May 2007, doi: 10.1109/TMTT.2007.895653.
100. Changzhi Li and Jenshan Lin, "Complex signal demodulation and random body movement cancellation techniques for non-contact vital sign detection," 2008 IEEE MTT-S International Microwave Symposium Digest, Atlanta, GA, USA, 2008, pp. 567-570, doi: 10.1109/MWSYM.2008.4633229.
101. M. Mercuri et al., "A Direct Phase-Tracking Doppler Radar Using Wavelet Independent Component Analysis for Non-Contact Respiratory and Heart Rate Monitoring," in IEEE Transactions on Biomedical Circuits and Systems, vol. 12, no. 3, pp. 632-643, June 2018, doi: 10.1109/TBCAS.2018.2813013.
102. B. -K. Park, S. Yamada and V. Lubecke, "Measurement Method for Imbalance Factors in Direct-Conversion Quadrature Radar Systems," in IEEE Microwave and Wireless Components Letters, vol. 17, no. 5, pp. 403-405, May 2007, doi: 10.1109/LMWC.2007.895742.
103. N. Chernov and H. Ma, “Least squares fitting of quadratic curves and surfaces,” in Computer Vision, vol., 2011, pp. 287-302, Jan 2011.
104. D. Eberly, 3D Game Engine Design, 2nd ed. San Francisco, CA, USA: Morgan Kaufmann, 2007, pp. 639–679, doi: 10.1016/B978-0-12-229063-3.50005-4.
105. M. Zakrzewski et al., "Quadrature Imbalance Compensation With Ellipse-Fitting Methods for Microwave Radar Physiological Sensing," in IEEE Transactions on

Microwave Theory and Techniques, vol. 62, no. 6, pp. 1400-1408, June 2014, doi: 10.1109/TMTT.2014.2321738.
106. N. Malešević, V. Petrović, M. Belić, C. Antfolk, V. Mihajlović, and M. Janković, “Contactless Real-Time Heartbeat Detection via 24 GHz Continuous-Wave Doppler Radar Using Artificial Neural Networks,” Sensors, vol. 20, no. 8, p. 2351, Apr. 2020, doi: 10.3390/s20082351.
107. A. Alemaryeen, S. Noghanian and R. Fazel-Rezai, "Antenna Effects on Respiratory Rate Measurement Using a UWB Radar System," in IEEE Journal of Electromagnetics, RF and Microwaves in Medicine and Biology, vol. 2, no. 2, pp. 87-93, June 2018, doi: 10.1109/JERM.2018.2813534.
108. T. -M. Shen, T. -Y. J. Kao, T. -Y. Huang, J. Tu, J. Lin and R. -B. Wu, "Antenna Design of 60-GHz Micro-Radar System-In-Package for Noncontact Vital Sign Detection," in IEEE Antennas and Wireless Propagation Letters, vol. 11, pp. 1702-1705, 2012, doi: 10.1109/LAWP.2013.2239957.
109. M. S. Rabbani and H. Ghafouri-Shiraz, “Ultra-wide patch antenna array design at 60 GHz band for remote vital sign monitoring with Doppler radar principle,” J Infrared Milli Terahz Waves, vol. 38, pp. 548–566, May 2017, doi: 10.1007/s10762-016-0344-z.
110. N. T. P. Van, L. Tang, N. D. Minh, F. Hasan, and S. Mukhopadhyay, “Extra wide band 3D patch antennae system design for remote vital sign Doppler radar sensor detection,” in Proc. 11th International Conference on Sensing Technology (ICST), Sydney, NSW, Australia, pp. 1–5, Dec. 2017, doi: 10.1109/ICSensT.2017.8304418.
111. Q. Liang, R. S. Mpanda, X. Wang, J. Shi and L. Xu, "A Printed Dipole Array Antenna for Non-contact Monitoring System," 2018 Cross Strait Quad-Regional Radio Science and Wireless Technology Conference (CSQRWC), Xuzhou, China, 2018, pp. 1-3, doi: 10.1109/CSQRWC.2018.8455428.
112. X. Ma, Y. Wang, W. Song, X. You, J. Lin and L. Li, "A 100-GHz Double-Sideband Low-IF CW Doppler Radar in 65-nm CMOS for Mechanical Vibration and Biological Vital Sign Detections," 2019 IEEE MTT-S International Microwave Symposium (IMS), Boston, MA, USA, 2019, pp. 136-139, doi: 10.1109/MWSYM.2019.8701067.
113. C. -M. Nieh and J. Lin, "Adaptive beam-steering antenna for improved coverage of non-contact vital sign radar detection," 2014 IEEE MTT-S International Microwave Symposium (IMS2014), Tampa, FL, USA, 2014, pp. 1-3, doi: 10.1109/MWSYM.2014.6848388.
114. J. -M. Muñoz-Ferreras, Z. Peng, J. Wang, C. Li and R. Gómez-García, "Coherent Deramping-Based Multi-FMCW Radar Architecture," 2019 IEEE Topical Conference on Wireless Sensors and Sensor Networks (WiSNet), Orlando, FL, USA, 2019, pp. 1-4, doi: 10.1109/WISNET.2019.8711795.
115. L. Chioukh, H. Boutayeb, K. Wu and D. Deslandes, "Monitoring vital signs using remote harmonic radar concept," 2011 8th European Radar Conference, Manchester, UK, 2011, pp. 381-384.
116. J. Tu, T. Hwang and J. Lin, "Respiration Rate Measurement Under 1-D Body Motion Using Single Continuous-Wave Doppler Radar Vital Sign Detection System," in IEEE Transactions on Microwave Theory and Techniques, vol. 64, no. 6, pp. 1937-1946, June 2016, doi: 10.1109/TMTT.2016.2560159.
117. C. Ye, K. Toyoda and T. Ohtsuki, "A Stochastic Gradient Approach for Robust Heartbeat Detection With Doppler Radar Using Time-Window-Variation Technique," in IEEE Transactions on Biomedical Engineering, vol. 66, no. 6, pp. 1730-1741, June 2019, doi: 10.1109/TBME.2018.2878881.
118. J.-Y. Kim, J.-H. Park, S.-Y. Jang, and J.-R. Yang, “Peak Detection Algorithm for Vital Sign Detection Using Doppler Radar Sensors,” Sensors, vol. 19, no. 7, p. 1575, Apr. 2019, doi: 10.3390/s19071575.

119. C. Eren et al., “Background subtraction techniques to detect human vital signs using UWB GPR,” in International Conference on Advanced Technology & Sciences (ICAT’17), pp. 743–747, May 2017.
120. S. Costanzo, “Software-Defined Doppler Radar Sensor for Human Breathing Detection,” Sensors, vol. 19, no. 14, pp. 3085, Jul. 2019, doi: 10.3390/s19143085.
121. T. Sakamoto et al., “Measurement of instantaneous heart rate using radar echoes from the human head,” Electron. Lett., vol. 54, no. 14, pp. 864–866, Jul. 2018, doi: 10.1049/el.2018.0811.
122. A. De Groote et al., “Chest wall motion during tidal breathing,” Journal of applied physiology (Bethesda, Md.: 1985), vol. 83, no. 5, pp. 1531-1537, Nov 1997, doi:10.1152/jappl.1997.83.5.1531.
123. A. Mishra and C. Li, "A Low Power 5.8-GHz ISM-Band Intermodulation Radar System for Target Motion Discrimination," in IEEE Sensors Journal, vol. 19, no. 20, pp. 9206-9214, 15 Oct.15, 2019, doi: 10.1109/JSEN.2019.2926189.
124. A. Mishra, W. McDonnell, J. Wang, D. Rodriguez and C. Li, "Intermodulation-Based Nonlinear Smart Health Sensing of Human Vital Signs and Location," in IEEE Access, vol. 7, pp. 158284-158295, 2019, doi: 10.1109/ACCESS.2019.2950347.
125. M. Sekine and K. Maeno, "Non-contact heart rate detection using periodic variation in Doppler frequency," 2011 IEEE Sensors Applications Symposium, San Antonio, TX, USA, 2011, pp. 318-322, doi: 10.1109/SAS.2011.5739803.
126. J. Tu and J. Lin, "Respiration harmonics cancellation for Accurate Heart Rate measurement in non-contact vital sign detection," 2013 IEEE MTT-S International Microwave Symposium Digest (MTT), Seattle, WA, USA, 2013, pp. 1-3, doi: 10.1109/MWSYM.2013.6697732.
127. V. Vasu, C. Heneghan, T. Arumugam and S. Sezer, "Signal processing methods for non-contact cardiac detection using Doppler radar," 2010 IEEE Workshop On Signal Processing Systems, San Francisco, CA, USA, 2010, pp. 368-373, doi: 10.1109/SIPS.2010.5624817.
128. A. Sinharay, R. Das and S. Seth, "A Novel Microwave Measurement Technique for Non-Contact Vital Sign Monitoring," 2018 IEEE SENSORS, New Delhi, India, 2018, pp. 1-4, doi: 10.1109/ICSENS.2018.8589769.
129. H. Tan, D. Qiao and Y. Li, "Non-contact heart rate tracking using Doppler radar," 2012 International Conference on Systems and Informatics (ICSAI2012), Yantai, China, 2012, pp. 1711-1714, doi: 10.1109/ICSAI.2012.6223372.
130. E. Mogi and T. Ohtsuki, "Heartbeat detection with Doppler radar based on spectrogram," 2017 IEEE International Conference on Communications (ICC), Paris, France, 2017, pp. 1-6, doi: 10.1109/ICC.2017.7996378.
131. H. Zhao, X. Gu, H. Hong, Y. Li, X. Zhu and C. Li, "Non-contact Beat-to-beat Blood Pressure Measurement Using Continuous Wave Doppler Radar," 2018 IEEE/MTT-S International Microwave Symposium - IMS, Philadelphia, PA, USA, 2018, pp. 1413-1415, doi: 10.1109/MWSYM.2018.8439354.
132. K. Lin, Y. E. Wang, C. -K. Pao and Y. -C. Shih, "A Ka-Band FMCW Radar Front-End With Adaptive Leakage Cancellation," in IEEE Transactions on Microwave Theory and Techniques, vol. 54, no. 12, pp. 4041-4048, Dec. 2006, doi: 10.1109/TMTT.2006.885882.
133. J. Park, S. Park, D. -H. Kim and S. -O. Park, "Leakage Mitigation in Heterodyne FMCW Radar for Small Drone Detection With Stationary Point Concentration Technique," in IEEE Transactions on Microwave Theory and Techniques, vol. 67, no. 3, pp. 1221-1232, March 2019, doi: 10.1109/TMTT.2018.2889045.

134. Y. Wang, W. Wang, M. Zhou, A. Ren, and Z. Tian, “Remote Monitoring of Human Vital Signs Based on 77-GHz mm-Wave FMCW Radar,” Sensors, vol. 20, no. 10, p. 2999, May 2020, doi: 10.3390/s20102999.
135. Q. Lv et al., "High Dynamic-Range Motion Imaging Based on Linearized Doppler Radar Sensor," in IEEE Transactions on Microwave Theory and Techniques, vol. 62, no. 9, pp. 1837-1846, Sept. 2014, doi: 10.1109/TMTT.2014.2342663.
136. M. Zakrzewski, H. Raittinen and J. Vanhala, "Comparison of Center Estimation Algorithms for Heart and Respiration Monitoring With Microwave Doppler Radar," in IEEE Sensors Journal, vol. 12, no. 3, pp. 627-634, March 2012, doi: 10.1109/JSEN.2011.2119299.
137. W. Xu, C. Gu, C. Li, and M. Sarrafzadeh, “Robust Doppler radar demodulation via compressed sensing,” Electronics Letters, vol. 48, no. 22, pp. 1428–1430, Oct 2012, doi: 10.1049/el.2012.3130.
138. S. Guan, J. A. Rice, C. Li and C. Gu, "Automated DC Offset Calibration Strategy for Structural Health Monitoring Based on Portable CW Radar Sensor," in IEEE Transactions on Instrumentation and Measurement, vol. 63, no. 12, pp. 3111-3118, Dec. 2014, doi: 10.1109/TIM.2014.2317298.
139. Q. Lv, T. Hu, S. Qiao, Y. Sun, J. Huangfu and L. Ran, "Non-contact detection of Doppler bio-signals based on gradient decent and extended DACM algorithms," 2013 IEEE MTT-S International Microwave Workshop Series on RF and Wireless Technologies for Biomedical and Healthcare Applications (IMWS-BIO), Singapore, 2013, pp. 1-3, doi: 10.1109/IMWS-BIO.2013.6756174.
140. X. Gao and O. Boric-Lubecke, "Radius Correction Technique for Doppler Radar Noncontact Periodic Displacement Measurement," in IEEE Transactions on Microwave Theory and Techniques, vol. 65, no. 2, pp. 621-631, Feb. 2017, doi: 10.1109/TMTT.2016.2625796.
141. W. Massagram, V. M. Lubecke, A. HØst-Madsen and O. Boric-Lubecke, "Assessment of Heart Rate Variability and Respiratory Sinus Arrhythmia via Doppler Radar," in IEEE Transactions on Microwave Theory and Techniques, vol. 57, no. 10, pp. 2542-2549, Oct. 2009, doi: 10.1109/TMTT.2009.2029716.
142. X. Zhao, C. Song, V. Lubecke and O. Boric-Lubecke, "DC coupled Doppler radar physiological monitor," 2011 Annual International Conference of the IEEE Engineering in Medicine and Biology Society, Boston, MA, USA, 2011, pp. 1909-1912, doi: 10.1109/IEMBS.2011.6090540.
143. C. Gu et al., "Accurate Respiration Measurement Using DC-Coupled Continuous-Wave Radar Sensor for Motion-Adaptive Cancer Radiotherapy," in IEEE Transactions on Biomedical Engineering, vol. 59, no. 11, pp. 3117-3123, Nov. 2012, doi: 10.1109/TBME.2012.2206591.
144. A. Widmann and E. Schröger, “Filter effects and filter artifacts in the analysis of electrophysiological data,” Frontiers in psychology, vol. 3, pp. 233, Jul. 2012, doi:10.3389/fpsyg.2012.00233.
145. O. Aardal, S. Brovoll, T. Berger, I. Balasingham and S. -E. Hamran, "Phase distortions in radar respiration monitoring," 2017 First IEEE MTT-S International Microwave Bio Conference (IMBIOC), Gothenburg, Sweden, 2017, pp. 1-4, doi: 10.1109/IMBIOC.2017.7965778.
146. D. H. Yim and S. H. Cho, “An equidistance multi-human detection algorithm based on noise level using mono-static IR-UWB radar system,” in Proceedings of the 2014 International Conference on Future Communication, Information and Computer Science (FCICS 2014), Beijing, China, pp. 131–134, May 2014, doi: 10.1201/b18049-31.

147. A. Lazaro, D. Girbau, and R. Villarino, “Analysis of vital signs monitoring using an IR-UWB radar,” Progress In Electromagnetics Research, vol. 100, pp. 265–284, Feb. 2010, doi: 10.2528/PIER09120302.
148. M. Burgos-Garcia, C. Castillo, S. Llorente, J. M. Pardo, and J. C. Crespo, “Digital on-line compensation of errors induced by linear distortion in broadband LFM radars,” Electronics Letters, vol. 39, no. 1, pp. 116–118, Jan. 2003, doi: 10.1049/el:20030012.
149. A. Meta, P. Hoogeboom and L. P. Ligthart, "Signal Processing for FMCW SAR," in IEEE Transactions on Geoscience and Remote Sensing, vol. 45, no. 11, pp. 3519-3532, Nov. 2007, doi: 10.1109/TGRS.2007.906140.
150. W. Shen and B. Wen, “A new demodulation and modulation method designed for FMCW radar,” Journal of Electrical and Computer Engineering, vol. 2010, pp. 1–6, Jan 2010, doi: 10.1155/2010/897429.
151. C. Will et al., “Radar-based heart sound detection,” Scientific Reports 8, Article number: 11551, pp. 1–4, Dec. 2018, doi: 10.1038/s41598-018-29984-5.
152. H. Zhao, H. Hong, Y. Li, L. Sun and X. Zhu, "Low-power digital-IF noncontact instantaneous vital sign detection based on synchrosqueezing transform," 2016 IEEE Topical Conference on Biomedical Wireless Technologies, Networks, and Sensing Systems (BioWireleSS), Austin, TX, USA, 2016, pp. 91-93, doi: 10.1109/BIOWIRELESS.2016.7445571.
153. C. Will, K. Shi, F. Lurz, R. Weigel and A. Koelpin, "Instantaneous heartbeat detection using a cross-correlation based template matching for continuous wave radar systems," 2016 IEEE Topical Conference on Wireless Sensors and Sensor Networks (WiSNet), Austin, TX, USA, 2016, pp. 31-34, doi: 10.1109/WISNET.2016.7444314.
154. X. Yang, G. Sun and K. Ishibashi, "Non-contact acquisition of respiration and heart rates using Doppler radar with time domain peak-detection algorithm," 2017 39th Annual International Conference of the IEEE Engineering in Medicine and Biology Society (EMBC), Jeju, Korea (South), 2017, pp. 2847-2850, doi: 10.1109/EMBC.2017.8037450.
155. M. Zakrzewski, A. Kolinummi and J. Vanhala, "Contactless and Unobtrusive Measurement of Heart Rate in Home Environment," 2006 International Conference of the IEEE Engineering in Medicine and Biology Society, New York, NY, USA, 2006, pp. 2060-2063, doi: 10.1109/IEMBS.2006.260714.
156. M. Nosrati, S. Shahsavari, S. Lee, H. Wang and N. Tavassolian, "A Concurrent Dual-Beam Phased-Array Doppler Radar Using MIMO Beamforming Techniques for Short-Range Vital-Signs Monitoring," in IEEE Transactions on Antennas and Propagation, vol. 67, no. 4, pp. 2390-2404, April 2019, doi: 10.1109/TAP.2019.2893337.
157. Z. Peng and C. Li, “Portable Microwave Radar Systems for Short-Range Localization and Life Tracking: A Review,” Sensors, vol. 19, no. 5, p. 1136, Mar. 2019, doi: 10.3390/s19051136.
158. H. Lee, B.-H. Kim, J.-K. Park, and J.-G. Yook, “A Novel Vital-Sign Sensing Algorithm for Multiple Subjects Based on 24-GHz FMCW Doppler Radar,” Remote Sensing, vol. 11, no. 10, p. 1237, May 2019, doi: 10.3390/rs11101237.
159. S. B. Oppenheim, “Sampling of Continuous-Time Signals,” *Discrete-Time Signal Processing*, 2nd ed. Upper Saddle River, NJ, USA: Prentice-Hall, 1999, Ch. 4, pp. 140-214.
160. S. Braun, “Hilbert transform applications in mechanical vibration,” in *Mechanical Systems and Signal Processing*, M. Feldman, Ed. Hoboken, NJ, USA: Wiley, 2011, ch. 6, pp. 73-126.
161. H. Dalal, A. Basu, M. P. Abegaonkar, and S. K. Koul, “Through the wall respiration rate detection of multiple human subjects using Hilbert vibrational decomposition,” Progress In Electromagnetics Research M, vol. 80, pp. 83–91, Apr. 2019, doi: 10.2528/PIERM19020103.

162. K. Yamaguchi, M. Saito, T. Akiyama, T. Kobayashi, N. Ginoza, and H. Matsue, “A 24 GHz FM-CW radar system for detecting closed multiple targets and its applications in actual scenes,” Open J. Internet Things, vol. 2, no. 1, pp. 1–15, 2016.
163. C. Lu, Y. Yuan, C. -H. Tseng and C. -T. Michael Wu, "Multi-Target Continuous-Wave Vital Sign Radar using 24 GHz Metamaterial Leaky Wave Antennas," 2019 IEEE MTT-S International Microwave Biomedical Conference (IMBioC), Nanjing, China, 2019, pp. 1-4, doi: 10.1109/IMBIOC.2019.8777736.
164. S. M. M. Islam, E. Yavari, A. Rahman, V. M. Lubecke and O. Boric-Lubecke, "Multiple Subject Respiratory Pattern Recognition and Estimation of Direction of Arrival using Phase-Comparison Monopulse Radar," 2019 IEEE Radio and Wireless Symposium (RWS), Orlando, FL, USA, 2019, pp. 1-4, doi: 10.1109/RWS.2019.8714272.
165. N. A. Baig and A. Hussain, "RADAR signal processing for target range, Doppler and DoA estimation," 2017 14th International Bhurban Conference on Applied Sciences and Technology (IBCAST), Islamabad, Pakistan, 2017, pp. 820-825, doi: 10.1109/IBCAST.2017.7868151.
166. X. Zhu, Y. Yuan, P. Zhou, B. Xu, and Z. Han, “An improved Hilbert vibration decomposition method for analysis of rotor fault signals,” J. Brazilian Soc. Mech. Sci. Eng., vol. 39, no. 12, pp. 4921–4927, Dec. 2017, doi: 10.1007/s40430-017-0886-6.
167. Z. Zhang, Y. Nian, J. Chen and M. He, "An Experimental Study to Optimize the Stepped-Frequency Continuous-Wave Radar Parameters for Noncontact Multi-target Vital Sign Monitoring," 2019 IEEE International Conference on Computational Electromagnetics (ICCEM), Shanghai, China, 2019, pp. 1-4, doi: 10.1109/COMPEM.2019.8779202.
168. W. -C. Su, M. -C. Tang, R. E. Arif, T. -S. Horng and F. -K. Wang, "Stepped-Frequency Continuous-Wave Radar With Self-Injection-Locking Technology for Monitoring Multiple Human Vital Signs," in IEEE Transactions on Microwave Theory and Techniques, vol. 67, no. 12, pp. 5396-5405, Dec. 2019, doi: 10.1109/TMTT.2019.2933199.
169. H. Lee, B. -H. Kim, J. -K. Park, S. W. Kim and J. -G. Yook, "A Resolution Enhancement Technique for Remote Monitoring of the Vital Signs of Multiple Subjects Using a 24 Ghz Bandwidth-Limited FMCW Radar," in IEEE Access, vol. 8, pp. 1240-1248, 2020, doi: 10.1109/ACCESS.2019.2961130.
170. I. Khajehzadeh and B. Vale, “Large housing in New Zealand: Are bedroom and room standards still good definitions of New Zealand house size,” in Proc. 9th Australas. Housing Researchers Conf. Auckland, New Zealand: At Univ. of Auckland, 2016.
171. H. Shen et al., "Respiration and Heartbeat Rates Measurement Based on Autocorrelation Using IR-UWB Radar," in IEEE Transactions on Circuits and Systems II: Express Briefs, vol. 65, no. 10, pp. 1470-1474, Oct. 2018, doi: 10.1109/TCSII.2018.2860015.
172. K. -K. Shyu, L. -J. Chiu, P. -L. Lee, T. -H. Tung and S. -H. Yang, "Detection of Breathing and Heart Rates in UWB Radar Sensor Data Using FVPIEF-Based Two-Layer EEMD," in IEEE Sensors Journal, vol. 19, no. 2, pp. 774-784, 15 Jan.15, 2019, doi: 10.1109/JSEN.2018.2878607.
173. M. A. Othman et al., "5.8 GHz microwave Doppler radar for heartbeat detection," 2013 23rd International Conference Radioelektronika (RADIOELEKTRONIKA), Pardubice, Czech Republic, 2013, pp. 367-370, doi: 10.1109/RadioElek.2013.6530947.
174. J. -K. Huang and C. -H. Tseng, "A 5.8-GHz radar sensor chip in 0.18-µm CMOS for non-contact vital sign detection," 2016 IEEE International Symposium on Radio-Frequency Integration Technology (RFIT), Taipei, Taiwan, 2016, pp. 1-3, doi: 10.1109/RFIT.2016.7578187.
175. M. Kagawa and K. T. S. Matsui, “Sleep stage classification by noncontact vital signs indices using Doppler radar sensors,” in Annual International Conference of the IEEE

Engineering in Medicine and Biology Society (EMBC), vol. 2016, pp. 4913–4916, Aug. 2016, doi: 10.1109/EMBC.2016.7591829.
176. T. Ohtsuki and E. Mogi, "Heartbeat detection with Doppler radar based on estimation of average R-R interval using Viterbi algorithm," 2016 IEEE 27th Annual International Symposium on Personal, Indoor, and Mobile Radio Communications (PIMRC), Valencia, Spain, 2016, pp. 1-5, doi: 10.1109/PIMRC.2016.7794965.
177. I. Walterscheid and G. E. Smith, "Respiration and heartbeat monitoring using a distributed pulsed MIMO radar," 2017 39th Annual International Conference of the IEEE Engineering in Medicine and Biology Society (EMBC), Jeju, Korea (South), 2017, pp. 3449-3452, doi: 10.1109/EMBC.2017.8037598.
178. S. Bakhtiari et al., "Compact Millimeter-Wave Sensor for Remote Monitoring of Vital Signs," in IEEE Transactions on Instrumentation and Measurement, vol. 61, no. 3, pp. 830-841, March 2012, doi: 10.1109/TIM.2011.2171589.
179. D. Novák, M. Švecová, and D. Kocur, “Multiple person localization based on their vital sign detection using UWB sensor,” in Microwave Systems and Applications, Rijeka, Croatia: InTech, Jan. 2017, ch. 17, pp. 399–422.
180. M. Nosrati and N. Tavassolian, "Accurate Doppler Radar-Based Cardiopulmonary Sensing Using Chest-Wall Acceleration," in IEEE Journal of Electromagnetics, RF and Microwaves in Medicine and Biology, vol. 3, no. 1, pp. 41-47, March 2019, doi: 10.1109/JERM.2018.2879452.
181. C. Li, G. Lu, F. Chen, F. Qi and J. Wang, "Contact-free detection of respiration signal from continuously moving-object noise via a Doppler radar using adaptive line enhancer," 2015 IEEE 28th Canadian Conference on Electrical and Computer Engineering (CCECE), Halifax, NS, Canada, 2015, pp. 801-805, doi: 10.1109/CCECE.2015.7129377.
182. Y. Wang et al., “Assessment of respiration-induced motion and its impact on treatment outcome for lung cancer,” BioMed research international, vol. 2013, doi:10.1155/2013/872739.
183. R. F. Fouladi and A. Oncu, "Vital signs modeling for Doppler radar cardiorespiratory monitoring," 2013 36th International Conference on Telecommunications and Signal Processing (TSP), Rome, Italy, 2013, pp. 363-366, doi: 10.1109/TSP.2013.6613953.
184. F. T. Tehrani, "Mathematical analysis and computer simulation of the respiratory system in the newborn infant," in IEEE Transactions on Biomedical Engineering, vol. 40, no. 5, pp. 475-481, May 1993, doi: 10.1109/10.243414.
185. X. Li, D. Qiao, and Y. Li, “An analytical model for regular respiratory signal,” Annual International Conference of the IEEE Engineering in Medicine and Biology Society, vol. 2014, pp. 102-105, doi:10.1109/EMBC.2014.6943539.
186. Y. Xu, S. Wu, C. Chen, J. Chen and G. Fang, "A Novel Method for Automatic Detection of Trapped Victims by Ultrawideband Radar," in IEEE Transactions on Geoscience and Remote Sensing, vol. 50, no. 8, pp. 3132-3142, Aug. 2012, doi: 10.1109/TGRS.2011.2178248.
187. S. S. Vedam et al. “Predicting respiratory motion for four-dimensional radiotherapy,” Medical Physics, vol. 31, no. 8, pp. 2274-2283, Aug 2004, doi: 10.1118/1.1771931.
188. A. Nezirovic, A. G. Yarovoy and L. P. Ligthart, "Experimental study on human being detection using UWB radar," 2006 International Radar Symposium, Krakow, Poland, 2006, pp. 1-4, doi: 10.1109/IRS.2006.4338133.
189. X. Li, D. Qiao, Y. Li and H. Dai, "A novel through-wall respiration detection algorithm using UWB radar," 2013 35th Annual International Conference of the IEEE Engineering in Medicine and Biology Society (EMBC), Osaka, Japan, 2013, pp. 1013-1016, doi: 10.1109/EMBC.2013.6609675.

190. A. E. Lujan, E. W. Larsen, J. M. Balter, and R. K. Ten Haken, “A method for incorporating organ motion due to breathing into 3D dose calculations,” in Medical Physics, vol. 26, no. 5, pp. 715-720, May 1999, doi: 10.1118/1.598577.
191. Y. Seppenwoolde et al., “Precise and real-time measurement of 3D tumor motion in lung due to breathing and heartbeat, measured during radiotherapy,” International Journal of Radiation Oncology, Biology, Physics, vol. 53, no. 4, July 2002, pp. 822-834, doi: 10.1016/s0360-3016(02)02803-1.
192. J. Kranjec et al., “Design and Clinical Evaluation of a Non-Contact Heart Rate Variability Measuring Device,” Sensors (Basel, Switzerland), vol. 17, no. 11, pp. 2637, Nov 2017, doi: 10.3390/s17112637.
193. D. R. Morgan, and M. G. Zierdt, “Novel signal processing techniques for Doppler radar cardiopulmonary sensing,” in Signal Processing, vol. 89, no. 1, pp. 45–66, Jan 2009, doi: 10.1016/j.sigpro.2008.07.008.
194. S.-M. Ko, Y-J Kim, J-H Park, and N-M Choi, “Assessment of left ventricular ejection fraction and regional wall motion with 64-slice multidetector CT: a comparison with two-dimensional transthoracic echocardiography,” in British Journal of Radiology, vol. 83, no. 985, pp. 28-34, Jan 2010, doi:10.1259/bjr/38829806.
195. N. Ranganathan, V. Sivaciyan, and F. B. Saksena, “Precordial Pulsations,” in *The Art and Science of Cardiac Physical Examination,* Contemporary Cardiology. Humana Press, Totowa, NJ, 2006, Ch. 5, pp. 113-139. doi: 10.1007/978-1-59745-023-2_5.
196. I. V. Mikhelson, S. Bakhtiari, T. W. Elmer, II and A. V. Sahakian, "Remote Sensing of Heart Rate and Patterns of Respiration on a Stationary Subject Using 94-GHz Millimeter-Wave Interferometry," in IEEE Transactions on Biomedical Engineering, vol. 58, no. 6, pp. 1671-1677, June 2011, doi: 10.1109/TBME.2011.2111371.
197. D. Obeid, S. Samad, S. Sadek, G. Zaharia and G. E. Zein, Position-Free Vital Sign Monitoring: Measurements and Processing, Rijeka, Croatia:InTech, 2016.
198. H. Kaneko, and J. Horie. “Breathing movements of the chest and abdominal wall in healthy subjects,” Respiratory Care, vol. 57, no. 9, pp. 1442-1451, Sep 2012, doi: 10.4187/respcare.01655.
199. K. Tukanova et al., “Assessment of chest wall movement following thoracotomy: a systematic review,” Journal of Thoracic Disease, vol. 12, no. 3, pp. 1031-1040, Mar 2020, doi: 10.21037/jtd.2019.12.93.
200. C. E. Diaz, K. S. Deoras, and J. L. Allen, “Chest wall motion before and during mechanical ventilation in children with neuromuscular disease,” in Pediatric Pulmonology, vol. 16, no. 2, pp. 89-95, Aug 1993, doi: 10.1002/ppul.1950160203.
201. N. Kumar, G. Akangire, B. Sullivan, K. Fairchild, and V. Sampath, “Continuous vital sign analysis for predicting and preventing neonatal diseases in the twenty-first century: big data to the forefront,” Pediatric Research, vol. 87, no. 2, pp. 210-220, Jan 2020, doi:10.1038/s41390-019-0527-0.
202. S. Lin, N.-R. Guo, and C. Chiu, “Modeling and simulation of respiratory control with labview.” Journal of Medical and Biological Engineering, vol. 32, no. 1, pp. 51–60, Jan 2012, doi: 10.5405/jmbe.829.
203. W. Riddle, and M. Younes, “A model for the relation between respiratory neural and mechanical outputs. II. Methods,” in Journal of Applied Physiology: Respiratory, Environmental and Exercise Physiology, vol. 51, no. 4 pp. 979-89, Oct 1981, doi: 10.1152/jappl.1981.51.4.979.
204. J. Feher, “The Cardiovascular System,” in *Quantitative Human Physiology,* 2nd ed., Elsevier Science Publishing Co Inc.: San Diego, CA, USA, 2016, Ch. 5, pp. 446–454.
205. R. Carroll, “The Heart,” in *Elsevier's Integrated Physiology*, 1st ed., Mosby Elsevier: Philadelphia, PA, USA, Nov 2006; Ch. 7, pp. 65–75.

206. B. Van Der Pol, J. Van Der Mark, “LXXII. The heartbeat considered as a relaxation oscillation, and an electrical model of the heart,” Lond. Edinb. Dubl. Phil. Mag., Vol. 6(38), pp. 763–775, 1928, doi: 10.1080/14786441108564652.
207. S.R.F.S.M. Gois, and M.A. Savi, “An analysis of heart rhythm dynamics using a three-coupled oscillator model Chaos,” Solitons Fractals, vol. 41(5), pp. 2553-2565, Sep 2009, doi: 10.1016/j.chaos.2008.09.040.
208. G. Shafiq, and K. C. Veluvolu, “Multimodal chest surface motion data for respiratory and cardiovascular monitoring applications,” in Scientific Data, vol. 4, Article no. 170052, Apr 2017, doi: 10.1038/sdata.2017.52.
209. G. Ramachandran, and M. Singh, “Three-dimensional reconstruction of cardiac displacement patterns on the chest wall during the P, QRS and T-segments of the ECG by laser speckle interferometry,” in Medical & biological engineering & computing, vol. 27, no. 5, pp. 525-30, Sep 1989, doi: 10.1007/BF02441473.
210. A. Kaur, L. Kaur, and S. Gupta, “Image Recognition using Coefficient of Correlation and Structural SIMilarity Index in Uncontrolled Environment,” in International Journal of Computer Applications, vol. 59, no. 5, pp. 32-39, doi: 10.5120/9546-3999.
211. V. Starovoitov, E. E. Eldarova, and K.T. Iskakov, “Comparative analysis of the SSIM index and the Pearson coefficient as a criterion for image similarity,” Eurasian Journal of Mathematical and Computer Application, vol. 8., pp. 76-90, Jan 2020, doi: 10.32523/2306-6172-2020-8-1-76-90.
212. Y. Li, C. Huiguo, and W. Zheqian, “Dynamic Time Warping Distance Method for Similarity Test of Multipoint Ground Motion Field,” in Mathematical Problems in Engineering, Jan 2010, doi: 10.1155/2010/749517.
213. A. Ștefania Ghiță and A. M. Florea, "Real-Time People Re-Identification and Tracking for Autonomous Platforms Using a Trajectory Prediction-Based Approach," Sensors, vol. 22, no. 15, p. 5856, Aug. 2022, doi: 10.3390/s22155856.
214. M. A. F. Pimentel et al., "Toward a Robust Estimation of Respiratory Rate From Pulse Oximeters," in IEEE Transactions on Biomedical Engineering, vol. 64, no. 8, pp. 1914-1923, Aug. 2017, doi: 10.1109/TBME.2016.2613124.
215. H. N. Ingabire et al., "Analysis of ECG Signals by Dynamic Mode Decomposition," IEEE Journal of Biomedical and Health Informatics, vol. 26, no. 5, pp. 2124-2135, May. 2022, doi: 10.1109/JBHI.2021.3130275.
216. J. D. Cardenas, C. A. Gutierrez, and R. Aguilar-Ponce, “Deep Learning Multi-Class Approach for Human Fall Detection Based on Doppler Signatures,” International Journal of Environmental Research and Public Health, vol. 20, no. 2, p. 1123, Jan. 2023, doi: 10.3390/ijerph20021123.
217. A. Singh, S. U. Rehman, S. Yongchareon and P. H. J. Chong, "Multi-Resident Non-Contact Vital Sign Monitoring Using Radar: A Review,"IEEE Sensors Journal, vol. 21, no. 4, pp. 4061-4084, Feb. 2021, doi: 10.1109/JSEN.2020.3036039.
218. K. Fujiwara et al., "Heart Rate Variability-Based Driver Drowsiness Detection and Its Validation With EEG," in IEEE Transactions on Biomedical Engineering, vol. 66, no. 6, pp. 1769-1778, June 2019, doi: 10.1109/TBME.2018.2879346.
219. D. -M. Chian, C. -K. Wen, C. -J. Wang, M. -H. Hsu and F. -K. Wang, "Vital Signs Identification System With Doppler Radars and Thermal Camera," in IEEE Transactions on Biomedical Circuits and Systems, vol. 16, no. 1, pp. 153-167, Feb. 2022, doi: 10.1109/TBCAS.2022.3147827.
220. W. Huang, H. Sun, and W. Wang, “Resonance-Based Sparse Signal Decomposition and its Application in Mechanical Fault Diagnosis: A Review,” Sensors, vol. 17, no. 6, pp. 1279, Jun. 2017, doi: 10.3390/s17061279.
221. C. Li, J. Ling, J. Li, and J. Lin, "Accurate Doppler Radar Noncontact Vital Sign Detection Using the RELAX Algorithm," in IEEE Transactions on Instrumentation and

Measurement, vol. 59, no. 3, pp. 687-695, March 2010, doi: 10.1109/TIM.2009.2025986.
222. G. Thakur, E. Brevdo, N. S. Fučkar, and H.-T. Wu, "The Synchrosqueezing algorithm: a robust analysis tool for signals with the time-varying spectrum," Signal Processing, Elsevier, vol. 93, no. 5, pp. 1079-1094, May. 2013, doi: 10.1016/j.sigpro.2012.11.029.
223. Y. Zi-Kai, S. Zhao, X.-D. Huang, and W. Lv, "Accurate Doppler Radar-Based Heart Rate Measurement Using Matched Filter," IEICE Electron. Express, vol. 17, pp. 1–6, Mar. 2020, doi: 10.1587/elex.17.20200062.
224. T. Kitagawa, K. Yamamoto, K. Endo and T. Ohtsuki, "Multibeam Doppler Sensor-Based Non-Contact Heartbeat Detection Using Beam Diversity," in IEEE Access, vol. 10, pp. 16242-16253, 2022, doi: 10.1109/ACCESS.2022.3148426.
225. Y. Zhao, V. Sark, M. Krstic and E. Grass, "Multi-Target Vital Signs Remote Monitoring Using mmWave FMCW Radar," 2021 IEEE Microwave Theory and Techniques in Wireless Communications (MTTW), Riga, Latvia, 2021, pp. 290-295, doi: 10.1109/MTTW53539.2021.9607087.
226. J. Liu, Y. Li, C. Li, C. Gu and J. -F. Mao, "Accurate Measurement of Human Vital Signs With Linear FMCW Radars Under Proximity Stationary Clutters," in IEEE Transactions on Biomedical Circuits and Systems, vol. 15, no. 6, pp. 1393-1404, Dec. 2021, doi: 10.1109/TBCAS.2021.3123830.
227. A. T. Purnomo, D.-B. Lin, T. Adiprabowo, and W. F. Hendria, “Non-Contact Monitoring and Classification of Breathing Pattern for the Supervision of People Infected by COVID-19,” Sensors, vol. 21, no. 9, p. 3172, May 2021, doi: 10.3390/s21093172.
228. E. Cardillo, C. Li and A. Caddemi, "Vital Sign Detection and Radar Self-Motion Cancellation Through Clutter Identification," in IEEE Transactions on Microwave Theory and Techniques, vol. 69, no. 3, pp. 1932-1942, March 2021, doi: 10.1109/TMTT.2021.3049514.
229. G. Lu, F. Yang, X. Jing, and J. Wang, "Contact-free measurement of heartbeat signal via a Doppler radar using adaptive filtering," Int. Conf. Image Anal. Signal Process., pp. 89-92, Apr. 2010.
230. M. He, Y. Nian, and Y. Gong, "Novel signal processing method for vital sign monitoring using FMCW radar," Biomed. Signal Process. Control, vol. 33, pp. 335-345, 2017.
231. F. Khan and S. Cho, “A Detailed Algorithm for Vital Sign Monitoring of a stationary/Non-Stationary Human through IR-UWB Radar,” Sensors, vol. 17, no. 2, p. 290, Feb. 2017, doi: 10.3390/s17020290.
232. Y. Xiong, Z. Peng, C. Gu, S. Li, D. Wang, and W. Zhang, "Differential Enhancement Method for Robust and Accurate Heart Rate Monitoring via Microwave Vital Sign Sensing," in IEEE Transactions on Instrumentation and Measurement, vol. 69, no. 9, pp. 7108-7118, Sept. 2020, doi: 10.1109/TIM.2020.2978347.
233. I. Bayram and I. W. Selesnick, "Overcomplete Discrete Wavelet Transforms With Rational Dilation Factors," in IEEE Transactions on Signal Processing, vol. 57, no. 1, pp. 131-145, Jan. 2009, doi: 10.1109/TSP.2008.2007097.
234. I. Bayram and I. W. Selesnick, "Frequency-Domain Design of Overcomplete Rational-Dilation Wavelet Transforms," in IEEE Transactions on Signal Processing, vol. 57, no. 8, pp. 2957-2972, Aug. 2009, doi: 10.1109/TSP.2009.2020756.
235. I. W. Selesnick, "Wavelet Transform With Tunable Q-Factor," in IEEE Transactions on Signal Processing, vol. 59, no. 8, pp. 3560-3575, Aug. 2011, doi: 10.1109/TSP.2011.2143711.
236. M. V. Afonso, J. M. Bioucas-Dias and M. A. T. Figueiredo, "An Augmented Lagrangian Approach to the Constrained Optimization Formulation of Imaging Inverse Problems," in IEEE Transactions on Image Processing, vol. 20, no. 3, pp. 681-695, March 2011, doi: 10.1109/TIP.2010.2076294.

237. J. S. Bendal and A. C. Piersol, “Nonstationary Data Analysis,” in *Random data: Analysis and nteasurelnenz procedures*, Los Angeles, New York: Wiley, Measurement Analysis Corp. Digitek Corp., and Dept. Engineering, Univ. Southern California, Ch. 12, pp. 417-467.
238. Texas Instruments, "Mmwave Radar Device ADC Raw Data Capture," Available at: https://www.ti.com/lit/an/swra581b/swra581b.pdf?ts=1630131969704
239. Hexoskin, "Key metrics Delivered by Hexoskin," Available at: https://www.hexoskin.com/pages/key-metrics
240. N. Cherif et al., "Physical activity classification using a smart textile," IEEE Life Sci. Conf. (LSC), 2018, pp. 175-178, doi:10.1109/LSC.2018.8572280.
241. S. Bellavia, S. Gratton, and E. Riccietti, "A Levenberg-Marquardt method for large non-linear least-squares problems with dynamic accuracy in functions and gradients," Numerische Mathematik, Springer Verlag, vol. 140, no. 3, pp. 791-825, June 2018, doi:10.1007/s00211-018-0977-z.
242. X.-M. Chen, Y. Dejie, J.-S. Luo, "Envelope demodulation method based on resonance-based sparse signal decomposition and its application in roller bearing fault diagnosis," in Journal of Vibration Engineering., vol. 25, no. 6, pp. 628-636, Dec. 2012.
243. Y. Lu, J. Du, and X. Tao, “Fault diagnosis of rolling bearing based on resonance-based sparse signal decomposition with optimal Q-factor,” in Measurement and Control, vol. 52, no. 7-8, pp. 1111-1121, June 2019, doi: 10.1177/0020294019858181.
244. C. Cassisi, P. Montalto, M. Aliotta, A. Cannata, and A. Pulvirenti, "Similarity Measures and Dimensionality Reduction Techniques for Time Series Data Mining," Advances in Data Mining Knowledge Discovery and Applications, Sep. 2012, doi: 10.5772/49941.
245. L. J. Dirksmeyer, A. Marnach, D. Schmiech, and A. R. Diewald, “Developing of Algorithms Monitoring Heartbeat and Respiration Rate of a Seated Person with an FMCW Radar,” Adv. Radio Sci., vol.19, pp.195–206, Dec. 2021, doi: 10.5194/ars-19-195-2021.
246. L. Beidian et al," A new method for vital sign monitoring using IR-UWB radar," IOP Conference Series Earth and Environmental Science, vol. 512, no. 1, June 2020, doi: 10.1088/1755-1315/512/1/012158.
247. M. He, Y. Nian, L. Xu, L. Qiao, and W. Wang, "Adaptive Separation of Respiratory and Heartbeat Signals among Multiple People Based on Empirical Wavelet Transform Using UWB Radar," Sensors, vol. 20, no. 17, pp. 4913, Aug 2020, doi: 10.3390/s20174913.
248. E. Turppa, J. M. Kortelainen, O. Antropov, and T. Kiuru, "Vital Sign Monitoring Using FMCW Radar in Various Sleeping Scenarios," Sensors, vol. 20, no. 22, pp. 6505, Nov. 2020, doi: 10.3390/s20226505.
249. S. Wang et al., "A novel ultra-wideband 80 GHz FMCW radar system for contactless monitoring of vital signs," 2015 37th Annual International Conference of the IEEE Engineering in Medicine and Biology Society (EMBC), Milan, Italy, 2015, pp. 4978-4981, doi: 10.1109/EMBC.2015.7319509.
250. Z.-K. Yang, H. Shi, S. Zhao, and X.-D. Huang, "Vital Sign Detection during Large-Scale and Fast Body Movements Based on an Adaptive Noise Cancellation Algorithm Using a Single Doppler Radar Sensor," Sensors, vol. 20, no. 15, pp. 4183, Jul. 2020, doi: 10.3390/s20154183.
251. G. Sun et al., "Vital-CUBE: A Non-Contact Vital Sign Monitoring System Using Medical Radar for Ubiquitous Home Healthcare." Journal of Medical Imaging and Health Informatics 4, vol. 4, no. 6, pp. 863-867, Dec. 2014, doi:10.1166/JMIHI.2014.1334.
252. R. El-Bardan, D. Malaviya and A. Di Rienzo, "On the estimation of respiration and heart rates via an IR-UWB radar: An algorithmic perspective," 2017 IEEE International Conference on Microwaves, Antennas, Communications and Electronic Systems (COMCAS), Tel-Aviv, Israel, 2017, pp. 1-5, doi: 10.1109/COMCAS.2017.8244781.

253. C. Gouveia, D. Albuquerque, J. Vieira, and P. Pinho, “Dynamic Digital Signal Processing Algorithm for Vital Signs Extraction in Continuous-Wave Radars,” Remote Sensing, vol. 13, no. 20, p. 4079, Oct. 2021, doi: 10.3390/rs13204079.
254. X. Liang, H. Zhang, S. Ye, G. Fang, and T. A. Gulliver, "Improved denoising method for through-wall vital sign detection using UWB impulse radar," Digital Signal Processing, vol. 74, pp. 72-93, March 2018, doi: 10.1016/j.dsp.2017.12.004.
255. Y. Zhang, X. Li, R. Qi, Z. Qi and H. Zhu, "Harmonic Multiple Loop Detection (HMLD) Algorithm for Not-Contact Vital Sign Monitoring Based on Ultra-Wideband (UWB) Radar," in IEEE Access, vol. 8, pp. 38786-38793, 2020, doi: 10.1109/ACCESS.2020.2976104.
256. W. Yin, X. Yang, L. Li, L. Zhang, N. Kitsuwan, and E. Oki, “HEAR: Approach for Heartbeat Monitoring with Body Movement Compensation by IR-UWB Radar,” Sensors, vol. 18, no. 9, p. 3077, Sep. 2018, doi: 10.3390/s18093077.
257. C. Eren, S. Karamzadeh and M. Kartal, "The artifacts of human physical motions on vital signs monitoring," 2019 Scientific Meeting on Electrical-Electronics & Biomedical Engineering and Computer Science (EBBT), Istanbul, Turkey, 2019, pp. 1-5, doi: 10.1109/EBBT.2019.8741668.
258. S. Leem, F. Khan, and S. Cho, “Vital Sign Monitoring and Mobile Phone Usage Detection Using IR-UWB Radar for Intended Use in Car Crash Prevention,” Sensors, vol. 17, no. 6, p. 1240, May 2017, doi: 10.3390/s17061240.
259. L. Ren, H. Wang, K. Naishadham, O. Kilic and A. E. Fathy, "Phase-Based Methods for Heart Rate Detection Using UWB Impulse Doppler Radar," in IEEE Transactions on Microwave Theory and Techniques, vol. 64, no. 10, pp. 3319-3331, Oct. 2016, doi: 10.1109/TMTT.2016.2597824.
260. F. -K. Wang et al., "Review of Self-Injection-Locked Radar Systems for Noncontact Detection of Vital Signs," in IEEE Journal of Electromagnetics, RF and Microwaves in Medicine and Biology, vol. 4, no. 4, pp. 294-307, Dec. 2020, doi: 10.1109/JERM.2020.2994821.
261. C. Gu, G. Wang, Y. Li, T. Inoue and C. Li, "A Hybrid Radar-Camera Sensing System With Phase Compensation for Random Body Movement Cancellation in Doppler Vital Sign Detection," in IEEE Transactions on Microwave Theory and Techniques, vol. 61, no. 12, pp. 4678-4688, Dec. 2013, doi: 10.1109/TMTT.2013.2288226.
262. J. Li, L. Liu, Z. Zeng and F. Liu, "Advanced Signal Processing for Vital Sign Extraction With Applications in UWB Radar Detection of Trapped Victims in Complex Environments," in IEEE Journal of Selected Topics in Applied Earth Observations and Remote Sensing, vol. 7, no. 3, pp. 783-791, March 2014, doi: 10.1109/JSTARS.2013.2259801.
263. E. Piuzzi, S. Pisa, P. D'Atanasio and A. Zambotti, "Radar cross section measurements of the human body for UWB radar applications," 2012 IEEE International Instrumentation and Measurement Technology Conference Proceedings, Graz, Austria, 2012, pp. 1290-1293, doi: 10.1109/I2MTC.2012.6229134.
264. J. E. Kiriazi, O. Boric-Lubecke and V. M. Lubecke, "Radar cross section of human cardiopulmonary activity for recumbent subject," 2009 Annual International Conference of the IEEE Engineering in Medicine and Biology Society, Minneapolis, MN, USA, 2009, pp. 4808-4811, doi: 10.1109/IEMBS.2009.5332634.
265. J. Xiong, H. Hong, H. Zhang, N. Wang, H. Chu and X. Zhu, "Multi-target Respiration Detection With Adaptive Digital Beamforming Technique Based on SIMO Radar," in IEEE Transactions on Microwave Theory and Techniques, vol. 68, no. 11, pp. 4814-4824, Nov. 2020, doi: 10.1109/TMTT.2020.3020082.
266. Z. Peng, L. Ran and C. Li, "A K -Band Portable FMCW Radar With Beamforming Array for Short-Range Localization and Vital-Doppler Targets Discrimination," in IEEE

Transactions on Microwave Theory and Techniques, vol. 65, no. 9, pp. 3443-3452, Sept. 2017, doi: 10.1109/TMTT.2017.2662680.
267. M. Muragaki et al., "Noncontact respiration monitoring of multiple closely positioned patients using ultra-wideband array radar with adaptive beamforming technique," 2017 IEEE International Conference on Acoustics, Speech and Signal Processing (ICASSP), New Orleans, LA, USA, 2017, pp. 1118-1122, doi: 10.1109/ICASSP.2017.7952330.
268. T. Hall et al., "A phased array non-contact vital signs sensor with automatic beam steering," 2015 IEEE MTT-S International Microwave Symposium, Phoenix, AZ, USA, 2015, pp. 1-4, doi: 10.1109/MWSYM.2015.7166973.
269. S. M. M. Islam, N. Motoyama, S. Pacheco and V. M. Lubecke, "Non-Contact Vital Signs Monitoring for Multiple Subjects Using a Millimeter Wave FMCW Automotive Radar," 2020 IEEE/MTT-S International Microwave Symposium (IMS), Los Angeles, CA, USA, 2020, pp. 783-786, doi: 10.1109/IMS30576.2020.9223838.
270. C. -M. Nieh, C. Wei and J. Lin, "Concurrent Detection of Vibration and Distance Using Unmodulated CW Doppler Vibration Radar With An Adaptive Beam-Steering Antenna," in IEEE Transactions on Microwave Theory and Techniques, vol. 63, no. 6, pp. 2069-2078, June 2015, doi: 10.1109/TMTT.2015.2422692.
271. Z. Xu et al., "Simultaneous Monitoring of Multiple People's Vital Sign Leveraging a Single Phased-MIMO Radar," in IEEE Journal of Electromagnetics, RF and Microwaves in Medicine and Biology, vol. 6, no. 3, pp. 311-320, Sept. 2022, doi: 10.1109/JERM.2022.3143431.
272. Y. Yuan, C. Lu, A. Y. -K. Chen, C. -H. Tseng and C. -T. M. Wu, "Multi-Target Concurrent Vital Sign and Location Detection Using Metamaterial-Integrated Self-Injection-Locked Quadrature Radar Sensor," in IEEE Transactions on Microwave Theory and Techniques, vol. 67, no. 12, pp. 5429-5437, Dec. 2019, doi: 10.1109/TMTT.2019.2931834.
273. M. S. Rabbani, J. Churm and A. P. Feresidis, "Fabry–Perot Beam Scanning Antenna for Remote Vital Sign Detection at 60 GHz," in IEEE Transactions on Antennas and Propagation, vol. 69, no. 6, pp. 3115-3124, June 2021, doi: 10.1109/TAP.2021.3049233.
274. W. -C. Su, P. -H. Juan, D. -M. Chian, T. -S. Horng, C. -K. Wen and F. -K. Wang, "Human Tracking and Vital Sign Monitoring with a Switched Phased-Array Self-Injection-Locked Radar," 2020 IEEE/MTT-S International Microwave Symposium (IMS), Los Angeles, CA, USA, 2020, pp. 659-662, doi: 10.1109/IMS30576.2020.9223889.
275. C. Feng et al., "Multi-target Vital Signs Measurement With Chest Motion Imaging Based on MIMO Radar," in IEEE Transactions on Microwave Theory and Techniques, vol. 69, no. 11, pp. 4735-4747, Nov. 2021, doi: 10.1109/TMTT.2021.3076239.
276. S. Ahmed, J. Park, and S. H. Cho, "Effects of Receiver Beamforming for Vital Sign Measurements Using FMCW Radar at Various Distances and Angles," Sensors, vol. 22, no. 18, pp. 6877, Sep. 2022, doi: 10.3390/s22186877.
277. T. K. V. Dai et al., "Enhancement of Remote Vital Sign Monitoring Detection Accuracy Using Multiple-Input Multiple-Output 77 GHz FMCW Radar," in IEEE Journal of Electromagnetics, RF and Microwaves in Medicine and Biology, vol. 6, no. 1, pp. 111-122, March 2022, doi: 10.1109/JERM.2021.3082807.
278. Z. Duan and J. Liang, "Non-Contact Detection of Vital Signs Using a UWB Radar Sensor," in IEEE Access, vol. 7, pp. 36888-36895, 2019, doi: 10.1109/ACCESS.2018.2886825.
279. C. Zhang, C. Zhang, and Q. Zhang, "Applications of EEMD in vital signal detection for UWB radar," Electron. Meas. Technol., vol. 35, no. 4, pp. 76–80, 2012.
280. X. Hu and T. Jin, "Short-range vital signs sensing based on EEMD and CWT using IR-UWB radar," Sensors, vol. 16, no. 12, p. 2025, Nov. 2016.

281. K. Dragomiretskiy and D. Zosso, "Variational mode decomposition," IEEE Trans. Signal Process., vol. 62, no. 3, pp. 531–544, Feb. 2014.
282. Y. Wang, R. Markert, J. Xiang, and W. Zheng, "Research on variational mode decomposition and its application in detecting rub-impact fault of the rotor system," Mech. Syst. Signal Process., vols. 60–61, pp. 243–251, Aug. 2015.
283. Z. Li, T. Jin, Y. Dai, and Y. Song, "Through-wall multi-subject localization and vital signs monitoring using UWB MIMO imaging radar," Remote Sens., vol. 13, no. 15, p. 2905, Jul. 2021.
284. Y. Xiong, Z. Peng, C. Gu, S. Li, D. Wang, and W. Zhang, "Differential Enhancement Method for Robust and Accurate Heart Rate Monitoring via Microwave Vital Sign Sensing," in IEEE Transactions on Instrumentation and Measurement, vol. 69, no. 9, pp. 7108-7118, Sept. 2020, doi: 10.1109/TIM.2020.2978347.
285. F. Jing, J. Liang, Y. Wang, and P. Chen, "Harmonics and Intermodulation Products-Based Fuzzy Logic(Hipbfl) Algorithm for Vital Sign Frequency Estimation Using a Uwb Radar,". In Expert Syst. Appl. 228, C (Oct 2023), doi: 10.2139/ssrn.4188732.
286. L. Qiao et al., "Spectral Unmixing Successive Variational Mode Decomposition for Robust Vital Signs Detection Using UWB Radar," in IEEE Transactions on Instrumentation and Measurement, vol. 72, pp. 1-13, 2023, Art no. 8502813, doi: 10.1109/TIM.2023.3274171.
287. B. Friedlander, "On Transmit Beamforming for MIMO Radar," in IEEE Transactions on Aerospace and Electronic Systems, vol. 48, no. 4, pp. 3376-3388, October 2012, doi: 10.1109/TAES.2012.6324717.
288. Texas Instruments, "xWR1843 Evaluation Module (xWR1843BOOST) Single-Chip mmWave Sensing Solution," https://www.ti.com/lit/ug/spruim4b/spruim4b.pdf?ts=1678056281212&ref_url=https%253A%252F%252Fwww.ti.com%252Ftool%252FAWR1843BOOST (accessed: Oct 1, 2022).
289. S. Wang, S. Kueppers, H. Cetinkaya, and R. Herschel, "3D Localization and Vital Sign Detection of Human Subjects with a 120 GHz MIMO Radar," 2019 20th International Radar Symposium (IRS), Ulm, Germany, 2019, pp. 1-6, doi: 10.23919/IRS.2019.8768192